KEM-19 - Evaluation of post-abandonment fluid migration and ground motion risks in subsurface exploitation operations in the Netherlands

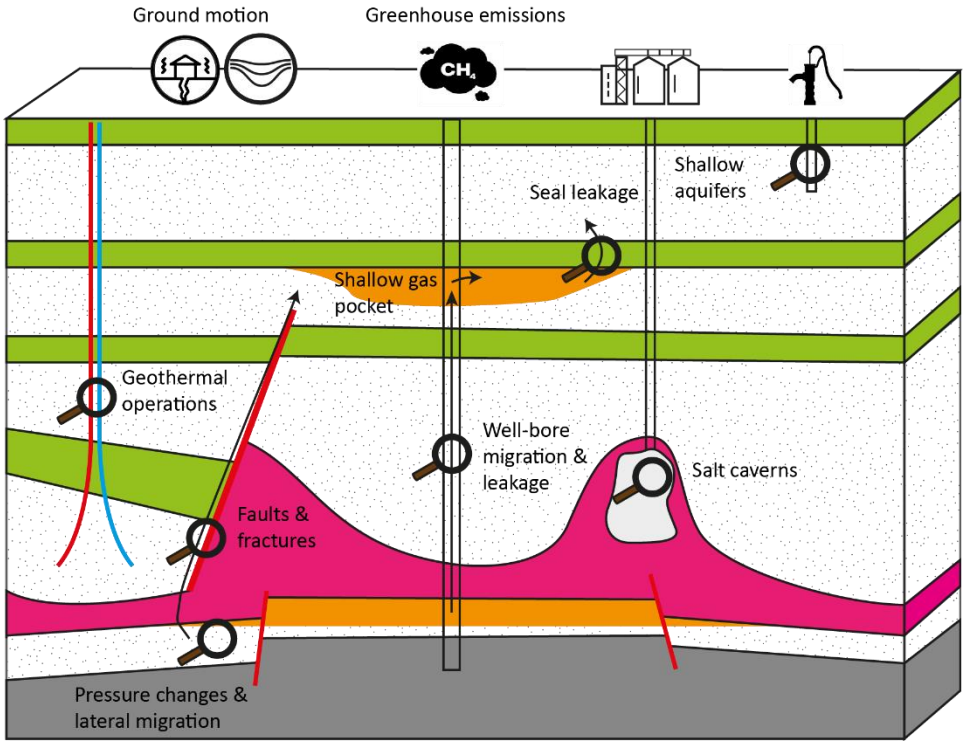

Final Report - Phase 2

Client	Ministry of Economic Affairs and Climate Policy
Client reference	KEM 19 / 202003118
Client Contact	van Thienen - Visser K.
Prepared by	Wildenborg T., Peters L., Moghadam A., Fokker P., Geel K., Nelskamp S., Bottero S., (TNO); Wiersma A., Marsman A., (Deltares);
Date	Final Report: 1 July 2022

Contents

Executive summary 7
Background 7
Objective 7
Approach 8
Main outcomes of the hazard analysis 8
Long-term evolution of pressure redistribution 8
Subsidence and uplift 9
Induced seismicity 9
Fluid migration along wells 9
Fluid migration along geological pathways 9
Interference with subsurface activities 10
Recommendations for quantitative assessment and monitoring 10
1 Introduction 12
2 Risk management framework for gas fields after abandonment 15
2.1 Establishment of the context 18
2.2 Risk identification and screening 19
2.3 Quantitative hazard and risk assessment 20
2.4 Monitoring and risk treatment 22
2.5 Stakeholders communication and risk review 23
3 Establishment of the context 24
3.1 Objectives, assessment parameters and resources 24
3.2 Groningen setting 25
4 Hazard and risk identification, screening and measures 28
4.1 Pressure redistribution and lateral migration 28
4.2 Fluid migration to shallow freshwater aquifers and the atmosphere and biosphere 29
4.2.1 Fluid migration along geological pathways 29
4.2.2 Fluid migration along well pathways 31
4.3 Subsidence and uplift 34

4.4 Induced seismicity ... 35
4.5 Interference with subsurface activities ... 37
5 Quantitative hazard and risk analysis and evaluation ... 38
5.1 Pressure redistribution and lateral migration ... 38
5.1.1 Modelling approach ... 38
5.1.2 Input data ... 39
5.1.3 Sensitivity analysis results ... 41
5.1.4 Conclusions ... 44
5.2 Subsidence and uplift ... 44
5.2.1 Modelling approach ... 45
5.2.2 Input data ... 45
5.2.3 Sensitivity analysis results ... 45
5.2.4 Conclusion ... 47
5.3 Induced seismicity ... 47
5.3.1 Modelling approach ... 47
5.3.2 Input data ... 50
5.3.3 Sensitivity analysis results ... 50
5.3.4 Conclusion ... 54
5.4 Fluid migration along wells to biosphere ... 55
5.4.1 Modelling approach ... 56
5.4.2 Input data ... 57
5.4.3 Sensitivity analysis results ... 58
5.4.4 Conclusions ... 60
6 Recommendations for quantitative hazard & risk assessment and monitoring ... 62
6.1 Pressure redistribution and lateral migration ... 63
6.2 Fluid migration to biosphere ... 65
6.2.1 Fluid migration along geological pathways to biosphere ... 65
6.2.2 Fluid migration along wells to biosphere ... 66
6.3 Ground motion ... 69
6.3.1 Subsidence and uplift ... 69
6.3.2 Induced seismicity ... 70
6.4 Interference with subsurface activities ... 71

6.4.1 Geothermal energy production and seismic hazard ... 72
6.4.2 Geothermal energy and hazard of fluid leakage ... 72
6.5 Monitoring strategies ... 73
6.5.1 Monitoring strategies for lateral fluid migration ... 73
6.5.2 Monitoring strategies of ground motion and seismicity ... 74
6.5.3 Monitoring strategies for methane migration along geological pathways and well bores 74
7 References ... 77
Appendices ... 83
A Clarification of flow diagram symbols ... 83
B Conceptual modelling of geological fluid migration pathways ... 85
B.1 Define elements of geological pathways ... 85
B.2 Fault tree analysis ... 90
B.3 References ... 96
C Regional pressure equilibration modelling ... 97
C.1 Geological model ... 97
C.1.1 Model area ... 97
C.1.2 Structural input data and grid ... 98
C.1.3 Properties ... 103
C.2 Overview input to dynamic reservoir model ... 103
C.2.1 Free Water Level ... 104
C.2.2 Relative Permeability and Capillary Pressure ... 104
C.2.3 Gas properties ... 105
C.2.4 Gas Production ... 106
C.3 History match ... 108
C.3.1 Data ... 108
C.3.2 Gas initially in place ... 110
C.3.3 Pressure ... 110
C.4 Prediction results ... 113
C.4.1 Base case ... 113
C.4.2 Sensitivities ... 117
C.5 References ... 125
D Fluid migration along wells ... 126

D.1 Numerical approach 126
D.2 Input parameters 127
D.3 Results and discussion 132
D.3.1 Reservoir leakage 132
D.3.2 Organic-rich clays (OC) 143
D.3.3 Breda Formation (BRD) 147
D.4 References 150
E Ground movement 153
E.1 Subsidence calculation sensitivities 153
E.2 Reactivation in uniaxially deforming parts of a reservoir 159
E.3 References 161

Executive summary

The work presented here has been carried out in the KEM-19 project, which is part of the national research programme "Knowledge Programme on Effects of Mining" (KEM), initiated by the Dutch Minister of Economic Affairs and Climate Policy. The full title of the project is "Evaluation of post-abandonment fluid migration and ground motion risks in subsurface exploitation operations in the Netherlands".

Background

Oil and gas production in the Netherlands is in steady decline, which is accelerated by the energy transition and public concerns on safety. More and more oil and gas fields and accompanying infrastructure will be abandoned. On the other hand, there is an expected increase of new activities in the subsurface of the Netherlands, such as energy production using geothermal sources and re-use of oil- and gas reservoirs for storage of hydrocarbons, carbon dioxide or hydrogen. The possible risks as a result of active production or storage activities can still develop long after the activity has been ceased. To date no risk assessment (and management) framework is available for assessing, monitoring and treating the undesired long-term effects of mining after abandonment of the facilities.

Post-abandonment risks can occur over long time scales (10's to 100's of years) and large spatial scales (100's to 1000's of metres). For instance, fluid migration processes are believed to continue well beyond the operational time spans and the field boundaries of gas production. Possible vertical migration of fluids out of the reservoir along geological pathways (e.g. natural faults) or along well trajectories may lead to leakage of fluids and deteriorate the quality of potable water resources. Potential effects also include changes in pore pressure and associated ground motion by rock compaction and re-activation of faults, which may lead to damage of buildings and other infrastructure. These long-term changes may interfere with future production or storage activities in the subsurface and increase their risk profile.

Objective

The KEM-19 project aimed to identify and characterize the hazards and risks associated with the long-term effects of mining operations in the Netherlands after abandonment (e.g. gas production). These relate to lateral pressure redistribution at the production level, vertical fluid migration via wells and geological pathways, and ground motion. Also the possible interference of (effects of) past gas production with future subsurface activities has been evaluated. The case selected for this study was the Groningen gas field and its direct surroundings. This aim has been achieved through the following objectives:

- Literature review regarding post-abandonment risk assessment. Results have been reported in a separate deliverable.
- Quantitative analysis of 1) pressure redistribution and their effects on ground motion and 2) of fluid migration along wells and development of conceptual models for migration along geological pathways.

- Recommendations for a quantitative risk assessment framework and monitoring strategies for effects of subsurface mining activities in the Netherlands after their abandonment.

Approach

The activities in the KEM-19 project have been embedded in a risk management framework, which is based on the ISO 31.000 standard for risk management (2nd edition 2018). The main components of the modified framework are:

- Establishment of the context;
- Risk identification and screening;
- Quantitative hazard and risk assessment;
- Monitoring and risk treatment;
- Stakeholder communication and risk review.

The process of risk management is of cyclic nature with several feedback loops, which results in regular updates during all stages of mining activities including the phase of stewardship after abandonment. Continuous monitoring will notify that indicators of assessed hazard or risk are kept below predefined threshold levels and thus comply with safety acceptance criteria. In case a critical threshold value would be exceeded, mitigation measures need to be deployed to reduce the hazard or risk level to an acceptable level. Additional contingency monitoring may be installed to monitor the effectiveness of the mitigation measures. Also, the assessment models may need an update to accommodate the learnings from the monitoring. These feedback loops may involve one or more components of the risk management framework.

Main outcomes of the hazard analysis

Long-term evolution of pressure redistribution

Numerical modelling of the pressures in the Groningen gas reservoir and adjacent aquifers revealed that over a long period of time (simulation time was up to 560 years after the start or production) the pressure may drop significantly in the adjacent aquifers whereas only little pressure build-up of a few bars is seen in the gas reservoir itself. In some areas, the region to the north of the gas field and the southern Lauwerszee Trough, the pressure in the aquifer may decrease with up to 30 to 50% of the pre-production pressure in 500 years, with the largest change occurring in the first 100 years.

The sensitivity of the pressure evolution has been studied for several parameters related to permeability, the characteristics of hydraulic barriers and the size of aquifers. The resulting range in pressure drop in the aquifers shows a considerable regional variation from more than 25 bar up to 90 bar at the end of the simulation period (560 years after the start of gas production).

In the area around the Groningen field, many small gas fields occur. The influence of these small nearby gas fields and their possible (additional) impact on fluid migration has not been accounted for in the present study. The study of the effect of small gas fields on the pressure drop in the southern Lauwerszee Trough (south-west of the Groningen gas field) is one of the recommendations.

Subsidence and uplift

Based on the pressure modelling the amount of subsidence and uplift has been quantified for a period of 100 years after abandonment of the Groningen gas field. The maximum additional subsidence expected is between 9 and 13 cm for the area to the NW of the Groningen gas reservoir and between 4 to 7 cm to the West of the reservoir. The maximum uplift has been calculated to about 1 cm above the southern part of the gas reservoir. Some uncertainties remain though, in the magnitude of the pressure depletion and in the aquifer compaction coefficients. Deviations from the modelled values will linearly propagate to the estimated surface movements. Pore pressure measurement in the aquifers would be of great help in constraining the size of the subsidence. Constraining by InSAR measurements will also be very helpful, in particular because they will give an areal distribution of the subsidence rather than single-point measurements of the pressure in the reservoir if wells would be present.

Induced seismicity

A full probabilistic quantitative assessment of the seismic hazard induced by gas production is a very complicated matter, which is far beyond the scope of the current project. The propensity for seismicity has been approached by analysing the potential of fault re-activation. For that purpose, a subdivision has been made between faults with no offset and faults with offset.

Subsurface compartments with no-offset faults could be approached as zones with uni-axial deformation. Mechanical analysis of the re-activation potential of this type of faults has shown that it is very unlikely to happen as it would require a pressure drop of about more than 200 bar. This is larger than the expected pressure drops in the aquifers.

Re-activation of bounding faults and faults with offsets in aquifers adjacent to the gas reservoir can be re-activated as a result of pressure depletion. This is confirmed by the occurrence of some seismic events in aquifer zones with significant pressure depletion.

Fluid migration along wells

Numerical radial symmetric modelling of fluid transport along wells revealed that there must be a source at sufficient pressure and a well migration path to allow leakage. What pressure is sufficient depends on the local subsurface conditions such as the thickness of the cap rock. In the present case study, the highly depleted gas reservoir is not a likely source for gas leakage. However, smaller depleted reservoirs with an active water-drive that can re-pressurize the gas after abandonment could still become a leak source. If a source of gas is present in the system at hydrostatic pressure, and the cement sheath is extremely damaged, a methane plume could extend hundreds of meters away from the well with free gas accumulating in the Peelo aquifer. The worst case could result in a leakage rate of a few tons per year into aquifers and the atmosphere. Shallow sources of gas are more likely to cause leakage. If wells intersect gas bearing formations above the target reservoir, they should be assigned a higher risk level.

Fluid migration along geological pathways

Conceptual modelling with support of fault tree analysis aided in identifying plausible geological migration pathways. For migration pathways to form, fault reactivation is the most likely process, in which case the fault needs to be transmissive. In addition, the source needs to be at sufficient pressure for gas to migrate upward. Alternatively, gas could migrate laterally (spill) and then migrate upwards in areas with poor sealing properties. Although the presence of a geological migration path seems to be unlikely in the studied subsurface because of the depleted conditions in the reservoir, the excellent seal and because of

the lack of shallow gas accumulations, it would need further scrutinizing potential local conditions before drawing a more definite conclusion. The fault tree is a helpful tool to develop a simulation plan to test the conditions that could lead to migration, or where in the migration pathway potential hazards could arise. Similarly, the results of the analysis can be used to inform future ground investigations and which subsurface properties to focus on to quantify or potentially falsify the occurrence potential events.

Interference with subsurface activities

In or near areas with past gas production activities, new subsurface activities may be deployed like geothermal energy production, storage of gases in porous / permeable (sedimentary) rocks or storage of gases or compressed air in salt caverns. For interference with subsurface activities, we distinguish future activities in the same, abandoned, reservoir, adjacent to the abandoned reservoir and in the rock sequence above the reservoir. Future activities below the reservoir have not been considered.

As geothermal energy production witnesses an enormous interest and growth in the Netherlands, the focus will be on the interference with geothermal energy. For salt caverns, which can cause subsidence, it is recommended to include subsidence from any nearby (abandoned) gas fields in the evaluation of potential subsidence.

Recommendations for quantitative assessment and monitoring

Based on the outcomes of the hazard screening and quantitative analyses, integrated workflows for regional hazard (and risk) assessment have been proposed. Integration refers to linking the various modelling routines to one another, incorporating other gas field in the region, nesting of more detailed models in the regional model and representing the outcomes in common assessment metric and maps.

A main aspect of the proposed assessment workflows is the identification and propagation of uncertainties in the modelling and agreement on the representation of the outcome with suitable metrics. Monitoring is key in calibrating the models and signalling of undesired levels of hazard (or risk) that call for preventative or mitigative measures. Also, the time window of decades or centuries needs to be decided upon as well as on the necessity to extend the hazard assessment to risk assessment.

In the hazard assessment of pressure redistribution and ground motion, particular attention is to be directed to the inclusion of more detailed models in areas with large pressure drops in aquifers and with neighbouring smaller depleted gas fields. Aquifer pressure monitoring at locations with higher uncertainty in these models is proposed for the calibration of the numerical models. InSAR data are key for constraining compaction in the subsidence modelling. The further quantitative assessment of fault re-activation and induced seismicity requires characterisation of the fault geometries and their mechanical properties. Seismic monitoring data from pressure depleting aquifer zones in combination with aquifer pressure monitoring are necessary to constrain the models for fault re-activation and induced seismicity.

Plausible scenarios of geological migration along geological pathways need to be defined in a systematic manner. Subsequent sensitivity analysis of leakage via geological pathways is recommended before any detailed quantitative hazard assessment of fluid migration along geological migration will be decided upon. For the quantitative hazard and risk assessment of fluid migration along well pathways, a systematic

screening of the integrity of all wells in the region, the presence of pressurized gas pockets and of the geometry of shallow aquifers is required to feed the modelling work.

For the evaluation of interference with future geothermal energy production or storage projects it is proposed to define Areas of Influence for pressure and stress changes in the subsurface, the resulting ground motion and gas leakage footprints as a result of former gas production. These should be fit-for-purpose for the development of future projects and associated well infrastructure and may include the size of areas of influence for temperature, pressure and stress changes, time dependence of these changes and volumes instead of areas.

Monitoring is key in calibrating and testing the models for assessing ground motion and gas leakage, and to initiate preventative or mitigative measures. For many decades to centuries to come regular measurements are considered to be necessary. Deep pressure monitoring, regular measurement of the quality of shallow ground water and ground motion monitoring including InSAR and seismometers are key components, which can be integrated in already existing monitoring networks. After the first period of equilibration of about 20 years the seismic monitoring resolution can probably be reduced.

Outcomes of the recommended regional quantitative assessment and monitoring are meant to inform the public, government organisations and companies who are active in performing subsurface production or storage activities or intend to do so in the future. It is of particular interest to entities who are involved in subsurface activities within the Area of Influence of past mining activities, e.g. gas production. When assessing the HSE footprint they will need to take the long-term effects of past mining activities into account. These companies may be active in production of geothermal energy, storage of heat, natural gas, CO_2 or hydrogen, production of oil or gas or salt extraction.

The recommended assessment work is relevant for the Ministry of Economic Affairs and Climate Policy and the State Supervision of the Mines to develop policies and regulation for the management of past subsurface production and storage activities and the development of guidance for new subsurface activities in the Area of Influence of past subsurface production or storage. The recommended assessment of past mining activities is of specific interest for the development of an approach for seismic hazard and risk assessment of geothermal operations. One option to approach this is to avoid the development of geothermal activities in the Area of Influence of former gas production. The geomechanical modelling in the present study indicates that in the absence of faults with larger offset seismicity is unlikely and such areas would thus not be included in the Area of influence for incremental seismic risk of former gas production.

Other stakeholders are representatives at the provincial and municipal levels as well as citizen interest groups and individuals.

1 Introduction

As the energy transition continues, oil and gas production will steadily decline, and more and more oil and gas wells will be abandoned. On the other hand, there is an expected increase of new activities in the subsurface of the Netherlands, such as energy production using geothermal sources and re-use of oil and gas reservoirs for storage of hydrocarbons and carbon dioxide (Verweij et al. 2012). The risks after the period of active development (e.g., production, storage) can still develop long after the activity has ceased (van Gessel, 2019; Lemay et al., 2019). To date no risk assessment (and management) framework is available for the undesired long-term effects of mining after abandonment of the facilities.

Post-abandonment risks can occur over long time scales and large spatial scales. For instance, fluid migration processes continue well beyond the operational time spans and the field boundaries of gas production. Possible vertical migration of gas and/or brine out of the reservoir along geological pathways or well trajectories may lead to leakage of fluids and deteriorate the quality of potable water resources. Potential effects also include changes in pore pressure and associated ground motion by compaction and re-activation of faults, which may lead to damage of built-up areas and other infrastructure. These long-term changes may interfere with future production or storage activities in the subsurface and increase their risk profile (see also Figure 1-1).

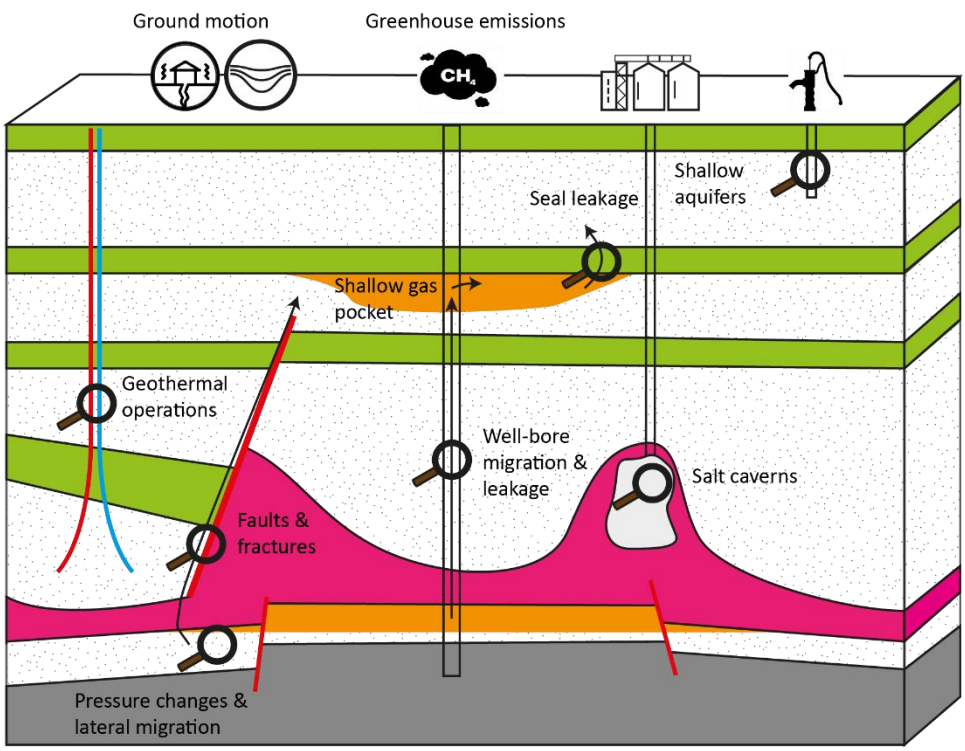

Figure 1-1. *Schematic representation of impacts and pathways of post abandonment fluid migration and ground motion. Gas occurrences are indicated in orange, aquifers are indicated in white, aquitards are indicated in green, and the rock-salt cap rock is indicated in pink. The deeper aquitard below the gas field is indicated in grey*

This project aims to identify and characterize the hazards and risks associated with the long-term effects of mining operations in the Netherlands after abandonment (e.g. gas production). These hazards and risks relate to pressure redistribution, vertical fluid migration via wells and geological pathways, and ground motion. Also, the possible interference of past gas production with future mining activities will be evaluated. This aim will be achieved through:

- Conducting a thorough literature review to understand the work that has been done in other jurisdictions regarding post-abandonment risk assessment.
- Creating quantitative models for the analysis of pressure redistribution
- Creating numerical models to quantitatively assess the long-term effects of well leakage on aquifers and conceptual models for fluid migration along geological pathways.
- An assessment of the effect of pressure redistribution in terms of subsidence and probability of fault reactivation (as a first step toward assessing risk of induced seismicity).
- Provide recommendations on developing a quantitative risk assessment framework and monitoring strategies for long-term effects of subsurface mining activities in the Netherlands after their abandonment.

The KEM-19 project included four project deliverables, which are:

- D1 – Literature survey on post abandonment risks related to fluid migration and ground motion - suggestions for modelling approaches, case studies and tools
- D2 – Simulations and case studies of fluid migration, leakage, and ground motion threats in selected hydrocarbon areas in the Netherlands
- D3 – Recommendations for the development of a quantitative post abandonment leakage hazard and risk assessment method
- D4 – Public summary of project key messages

The first step with a comprehensive literature review on relevant processes and impacts associated with long-term effects of gas fields after their abandonment has already been finished and reported in the first deliverable of the KEM-19 project (D1):

- TNO & Deltares (2021). KEM-19 Evaluation of post-abandonment fluid migration and ground motion risks in subsurface exploitation operations in the Netherlands - Literature Review and Proposed Activities for Phase-2. Phase-1, 81p.

The conceptual and quantitative modelling (D2) and the recommendations for quantitative hazard and risk assessment (D3) are reported in the present deliverable of the KEM-19 project in Chapters 5 and 6, which also includes a summary of the outcomes from the first deliverable D1 in Chapters 2, 3 and 4.

The expected users of the outcomes of the KEM-19 project are the Ministry of Economic Affairs and Climate Policy and the State Supervision of Mines in the Netherlands. The results will help in improving abandonment procedures for operators and monitoring strategies for delayed fluid leakage and ground motion effects. It may also inform the definition of requirements for regulating subsurface management and accompanying inspection.

The Province of Groningen may use this report as a refence for the evaluation of geothermal plans or other uses of the subsurface in the vicinity of the Groningen gas field, even whilst the study was not initiated and carried out for that purpose. More broadly the project results are of use for communication on the subject with stakeholders.

The chapter subdivision of this report follows the basic elements of the proposed risk management framework. After the introduction of the framework in Chapter 2, the scope of the risk management of gas fields after their abandonment is presented in Chapter 3. This includes a shortened description of the setting of the Groningen gas field from the first deliverable (TNO & Deltares, 2021). Chapter 4 identifies hazards and risk of past gas production, which includes a summary of the main findings in the 1st deliverable (TNO & Deltares, 2021) and the conceptual model for fluid migration along geological pathways. The quantitative analysis and assessment of pressure redistribution, fluid migration and ground motion are part of Chapter 5. Chapter 6 concludes the main report with recommendations for quantitative hazard and risk assessment. Several appendices with more detailed technical background are added to this deliverable.

2 Risk management framework for gas fields after abandonment

The ISO 31.000 (2nd edition 2018) Standard on Risk Management which has been adopted by the Nederlands Normalisatie Instituut (NNI, 2018), provides a suitable basis for the development of a framework for the management of regional post-abandonment risks. This framework, which includes risk assessment, monitoring and risk treatment as main elements, will enable the systematic assessment of past mining activities, e.g. gas production, and their effect on the quality of shallow groundwater and surface water and on ground motion. Gas production activities in the past may also constrain future mining activities, e.g. geothermal energy production.

The ISO framework consists of the following basic steps: define scope and criteria, perform risk assessment, define risk treatment, and develop monitoring plan. Execution and outcome of these exercises must be communicated with stakeholders and results of risk management activities be recorded (see Figure *2-1*). Risk management is a continuous cyclic process through all stages of subsurface activities from the preparation stage up to and including the post-abandonment stage (represented by the arrows in Figure *2-1*).

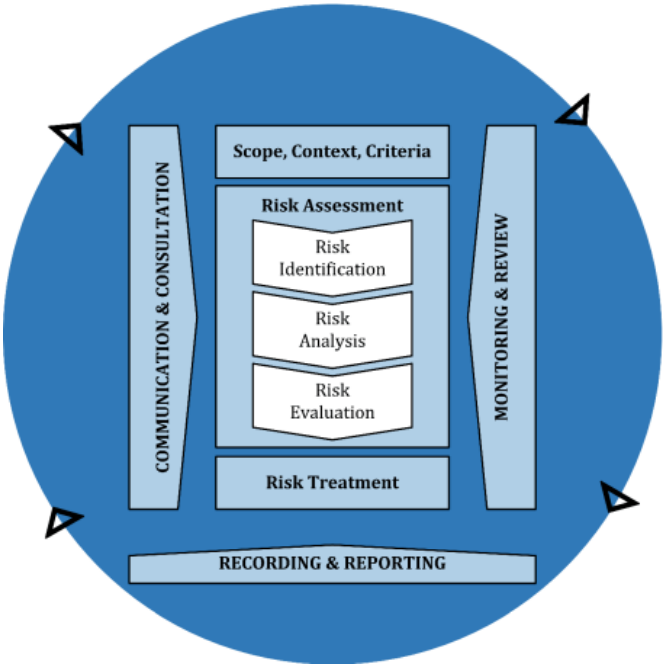

Figure 2-1.Risk management process in ISO Standard 30.100 (NNI, 2018)

Risk management frameworks have been developed for various subsurface technologies including geothermal energy production (Ikenwilo, 2016; Lohne et al., 2018), gas production (van Elk et al., 2017) and CO_2 storage (OSPAR, 2007; EC, 2011). These examples (see TNO & Deltares, 2021) provide useful building blocks for a framework on the *regional* management of risks resulting from gas production after abandonment, which includes but is not necessarily restricted to the risk of unintended migration of natural gas to the shallow subsurface or surface water, and emission towards the atmosphere, the risk of undesired ground motion and the interference with future activities in the deep subsurface.

Building on the ISO 31.000 standard for risk management and work done on designing a risk assessment approach in the GeoWell project (Lohne et al., 2018) a more detailed version of a framework for the regional assessment of mining activities after their abandonment has been developed (Figure *2-2*). The more detailed framework is a starting point for the development of methods and workflows for the hazard and risk assessment of mining activities after their abandonment with special reference to leakage of fluids (gas or brine) and ground motion. It consists of the following five main steps, which will be discussed in the next sections:

0. Establishment of the context
1. Risk identification and screening
2. Quantitative hazard and risk assessment
3. Monitoring and risk treatment
4. Stakeholder communication and risk review.

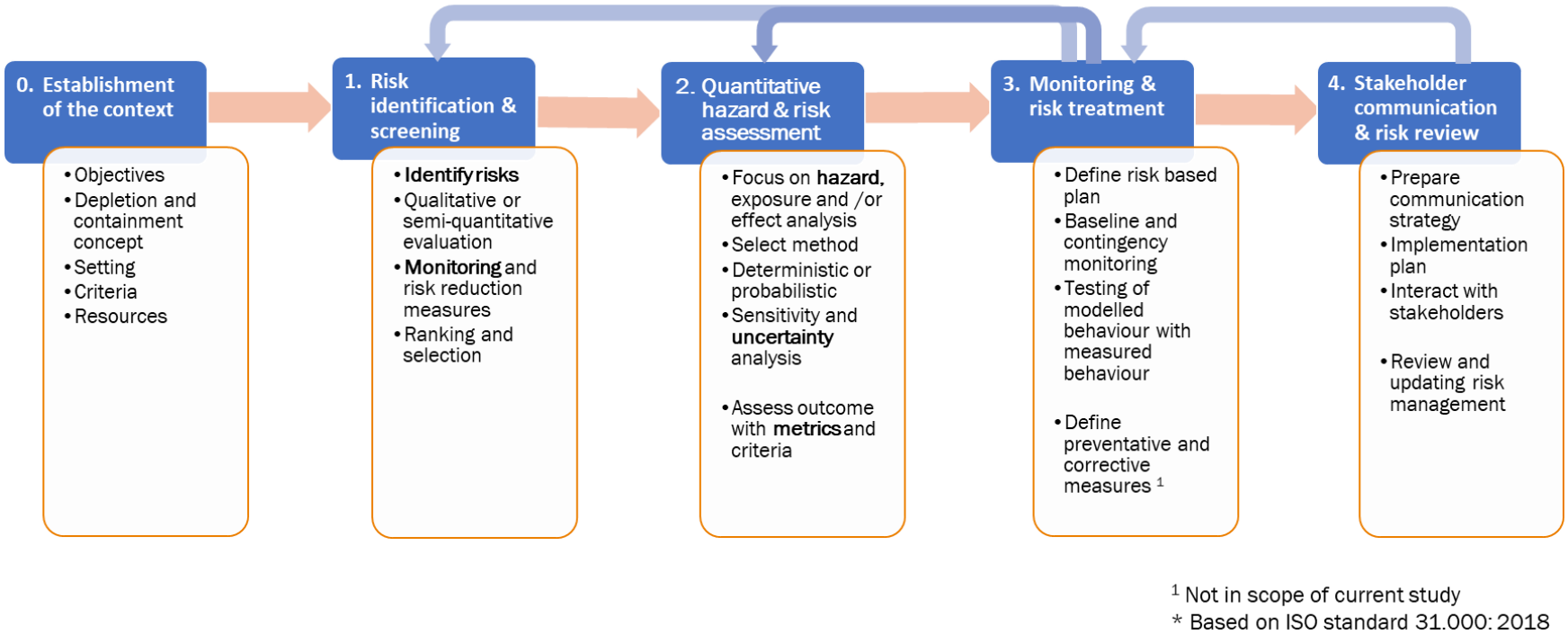

Figure 2-2. The proposed framework for risk management of fluid leakage and ground motion from abandoned depleted gas reservoirs sites

2.1 Establishment of the context

The first step in the process is to define the context of the risk management of fluid migration and leakage and ground motion resulting from past gas production. The context includes the specific objectives of risk management, the evaluation criteria, the reservoir depletion and containment concept with geological and engineered barriers and system boundaries, the time horizon, the site-specific geological and geographical setting and the resources needed.

Objectives describe what the risk management is aiming at in identifying and evaluating the risks of fluid migration to potable groundwater or surface water and ground motion resulting from abandoned mining sites, e.g., gas production, defining monitoring requirements and minimizing damage. It should consider any regulations or other requirements as to how the management is to be performed.

A good understanding of the reservoir depletion and fluid containment behaviour is essential for the execution of risk management activities, in particular for the identification of possible causes of unintended fluid migration and ground motion. The system boundaries will define the horizontal and vertical extent of the regional assessment area so that relevant flow and mechanical processes can be quantified properly.

The geological and geographical setting of the gas reservoir and related well infrastructure is especially important for characterizing the quality of the geological and well barriers and barrier deficiencies. Understanding of the geographical setting includes information on population density, protected water resources, land use, natural reserves and built-up areas.

Criteria or indicators are to be defined; these are measures for hazard or risk related to fluid migration and leakage, and ground motion after abandonment of depleted gas reservoirs. They can either be quantitative or qualitative. Criteria express the potential damage from fluid migration and leakage, or ground motion; indicators are proxies of increasing risk (e.g. pressure, temperature, corrosion etc.).

The definition of the time horizon of managing the effects of mining activities after their abandonment needs to be practical. One angle to define the time window is to judge the duration of the root cause of a risk, e.g. pressure depletion as result of gas production; risks need to be managed until a new quasi-stable situation arises. Another option is to judge the level of resulting incremental risk; if the incremental risk has become insignificant, the active risk management may come to an end. One needs to be cautious here, in particular when there is a delay between cause and effect. Also risk acceptance criteria may become more stringent in time, which would extend the time horizon of risk management. Defining the duration of risk management is a societal question, as it should limit the burden for future generations.

Successful risk management requires the availability of sufficient resources. This includes budget, personnel with required competences and skills, data and information concerning the abandoned depleted gas reservoir site, as well as tools for risk assessment and monitoring.

Chapter 3 provides more details on the context of risk management of gas reservoirs in north-eastern Netherlands after abandonment.

2.2 Risk identification and screening

A comprehensive overview of risk factors is to be assembled once the context of the risk assessment has been defined. Such an exercise may start with the identification of possible well barrier failure modes and their causes, which is also referred to with hazard identification. Depending on the assessment objectives, the identification could be limited to this part or extended to the identification of detrimental consequences of unintended loss of fluids from the gas reservoir, reservoir compaction or release of seismic energy for the environment, human beings, built-up areas and subsurface or surface resources. This complete set of activities is referred to as risk identification. Special attention is to be directed to the occurrence of cascading events which could result in adverse consequences.

The identified hazards and risks are qualitatively or semi-quantitatively characterized in terms of probability and severity of the impact. This offers the possibility for ranking and screening the various hazards and risks. A first evaluation of possible risk treatment and its expected reducing effect on the risk level is to be included. Risk treatment includes monitoring, preventative or corrective measures.

A preventative measure helps to reduce or avoid an irregularity (threat or consequence) before it is detected, and a corrective measure reduces or completely neutralizes an irregularity after it has been detected.

An appropriate method for risk identification and screening is to be selected or is prescribed by existing regulation. Various methods based on expert judgment and supporting databases are available; a broadly applied method is the bow-tie risk management in combination with risk registers and risk matrices (see also Van Gessel et al., 2019). Bow-tie risk management is a practical concept for risk management of undesired events linking their potential causes and consequences in a logical manner and subsequently help define barriers including monitoring to reduce the risks to acceptable levels (Figure *2-2*).

Bow-tie risk management has a lot of terminology which varies strongly among users of this concept. The following basic terms and definitions are proposed:

- Hazard: condition which may lead to damage (of men, environment or infrastructure). In the present study this is the presence of abandoned gas fields through loss of control and/or the natural re-equilibration with regional geological, hydrogeological, and geomechanical conditions;
- Undesired event: loss of control or natural consequence of production leading to damage, e.g. migration of fluids (gas, brines, formation water or a mixture) out of the reservoir, ground motion or interference with future subsurface activities after ceasing production and abandonment of the site;
- Cause (or threat): possible origin of undesired event;
- Consequence (or impact): possible effect of undesired event leading to exposure and damage;
- Barrier: measure to reduce the likelihood and magnitude of damage, which can be classified as preventative, detective or corrective action.

This method enables efficient communication of risks as it brings together all relevant aspects for risk management in a visual intuitive way.

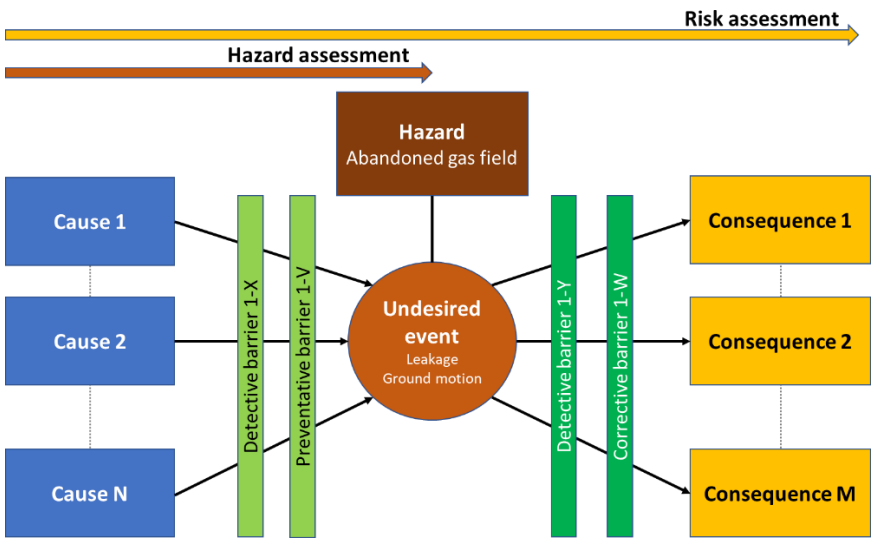

Figure 2-3. Bow-tie risk management concept with its principal elements and scope of hazard assessment versus risk assessment

The overview of risks and their assessment is to be updated and recorded during all stages of the project lifetime including the stage after abandonment of subsurface mining activities, which can come to an end once the incremental risk is proven to remain at a sufficiently low level. The acceptance level could relate to the Local Personal Risk or to the natural background level of methane concentration. Acceptance levels need to be defined upfront. Note that the updating and recording step is not part of the scope in the present study.

2.3 Quantitative hazard and risk assessment

A bowtie assessment typically relies on expert elicitation and is most often of qualitative nature and at best semi-quantitative. This type of evaluation is very helpful to screen and rank hazard and risk factors although some subjectivity and bias cannot be avoided. That's why a quantitative assessment based on sound physics and analysis of the main uncertainties is necessary which captures the main critical hazard and risk factors of the preceding qualitative assessment. Hazard or risk metrics can then be quantified in a deterministic or probabilistic manner and compared to tolerance thresholds. This provides a good basis for comparing the modelled behaviour in the assessment with the observed behaviour through monitoring and to decide on the order, timing and magnitude of intervention. As the workload for a quantitative risk assessment is orders of magnitude larger than for a qualitative approach, it requires an appropriate justification of its benefits.

Quantitative analysis is to be performed in a staged manner with methods varying from simple analytical models to complex coupled multi-physics numerical models. The required level of complexity of the analysis very much depends on the nature of the risks to be quantified. In some instances, a 'back-of-the-envelope' quantitative analysis is sufficient; in other situations, one may need to use sophisticated coupled Thermo-Hydro-Mechanical-Chemical models. Choices are to be made whether deterministic approaches are sufficient or fully probabilistic assessment lines are necessary.

There is a large number of methods for quantitative risk assessment (QRA) available, a selection of which is listed in Table *2-1*. An even larger number of QRA tools is available, see for example Van Gessel et al. (2019: Annex A). Fault and event tree analysis (FTA and ETA) which are integrated in the combined cause and consequence analysis, are logical extensions of the bowtie approach, discussed in the previous section. Fault tree analysis is further explained in Section 4.2.1.

Table 2-1 Overview of a selection of quantitative risk assessment methods and their suitability for different phases of risk assessment (modified after Lohne et al., 2017) Risk id = risk identification, risk an = risk analysis, risk ev = risk evaluation

QRA method	**Risk id**	**Risk an**	**Risk ev**	**Brief description**
FTA	X	X	X	Fault Tree Analysis: Graphical representation of failures and consequences, and risk reduction measures
ETA	X	X		Event Tree Analysis: Graphical representation of events leading to top event
DTA		X	X	Decision Tree Analysis: Graphical representation of the risk for different options and decision nodes
Cause & consequence analysis		X	X	Combination of FTA and ETA: Graphical representation of system failure with both causes and consequences
Markov chain analysis	X	X		Define system component states and transitions
ERA	X	X	X	Environmental risk assessment: Quantifying risk level for combinations of hazard and environmental damage
MCDA	X	X	X	Multi-Criteria Decision Analysis: Ranking of the options ranging from best to least preferred with weighted criteria
Monte Carlo simulation			X	Systems model with uncertainty represented by frequentistic statistical sampling from probability density distributions; can be integrated in previous methods
Bayesian statistics and networks		X	X	Systems model with causal links between variables with mathematically based prior and conditional probabilities (degrees of belief); can be integrated in previous methods

Depending on the assessment objective, the hazards are to be quantified in terms of resulting fluid migration and leakage or ground movement (hazard analysis), expressed in terms of concentrations or rates, or in vertical movement and seismic magnitude. Preferential flow paths need to be identified and characterized. Ultimately, fluid migration may lead to the exposure in the shallow subsurface or at the earth's surface (exposure analysis). Finally, the effects of exposure to various receptors (e.g. environment, drinking water resources, human beings, build-up areas and other infrastructure) can be quantified (effects analysis). The temporal and spatial scales of the hazards and risk need to be characterized.

Site-specific information including the characterization of uncertainties is required to execute a quantitative analysis. Uncertainties that remain in the subsurface characterization, need to be addressed. To understand the influence of the uncertainties on the risk level, one may perform sensitivity analysis to identify the most relevant parameters in the quantitative risk analysis. The outcome of the analyses will be assessed by verification with criteria or indicators for risk acceptance and a conclusion on compliance will be drawn. Any remaining critical uncertainties for the outcome of the evaluation will be identified and follow-up work may be defined to further reduce these uncertainties.

2.4 Monitoring and risk treatment

The outcome of the risk assessment in the previous step provides input for the development of risk-based monitoring strategies, which includes the required duration and intensity of specific monitoring activities. It will also serve as a basis for defining measures to reduce the risk level, e.g. preventative measures during the abandonment of mining sites. Monitoring provides information for the undesired migration of fluids originating from the abandoned subsurface mining activities or ground movement. A monitoring plan is to be established with the definition of monitoring parameters which are adjusted to the identified risk criteria, and any associated indicators. Suitable monitoring technologies with monitoring locations, durations and sampling frequencies are part of the plan. Any in-situ monitoring preferably needs to be implemented before the subsurface development is abandoned.

The output from the monitoring surveys is compared with the expected modelled fluid migration or ground movement. In case the observed behaviour is deviating from the expected behaviour, follow-up mitigation or remediation actions may be necessary. The initial monitoring system (like measurement of ground movement or groundwater quality) may need to be extended with additional monitoring activities to understand the nature of the fluid leakage and its consequences. If the deviating behaviour has been resolved, the additional monitoring can be stopped.

Risk reduction measures may be emplaced to reduce and keep the risks as low as reasonably achievable (ALARA). Developing these measures already starts in the phase of risk identification (see section 2.2). Once risks have been identified, potential risk reduction measures can be assigned to individual risks.

2.5 Stakeholders communication and risk review

Regular communication with and engagement of stakeholders is an integral part of risk management. Different groups of stakeholders can be identified with different interests, i.e., industrial mining companies (business case), regulator and inspector (compliance with safety and environment rules), local public (safety and environmental concerns) and local authorities (socio-economic wellbeing). Proper communication with and engagement of the various stakeholders require a communication strategy and implementation plan. For the interest of the local population one may consider to execute a benefit assessment of any future subsurface activity to balance any incremental hazard of the activities.

The presented framework for risk management of subsurface mining sites after their abandonment requires regular review and updating of risk management actions so that the risk is kept at a low, acceptable level (see Figure *2-2*). New data, rules or criteria, or monitoring results may require updating all or part of the risk management activities. This makes risk management to be of cyclic nature.

Plans for updating must be made, whether initiated at periodic intervals or triggered by events. Significant deviations should be documented, approved and distributed to the stakeholders.

The present KEM-19 project focuses in particular on the steps of risk identification and screening and quantitative hazard assessment.

3 Establishment of the context

The sections in this chapter are limited to the context of the current KEM-19 project and thus does not provide a complete risk management framework as has been described in the previous chapter.

3.1 Objectives, assessment parameters and resources

The *objective* of the present study is to assess:

- regional effects of (lateral) fluid migration at gas fields after their abandonment and the resulting pressure redistribution
- the extent to which fluids (gas or brine) may migrate via wells or geological pathways to shallow aquifers or to surface water where it may adversely impact the fresh water quality after the abandonment of gas reservoirs
- the possible influence of pressure redistribution on ground motion (subsidence, uplift or seismicity).
- Interference of past gas production activities with future mining activities, e.g. geothermal energy production.

The focus is on hazard assessment, the degree to which gas production may lead to undesired fluid leakage or ground motion after abandonment of the gas field. The evaluation does not elaborate on the exposure to and effect on protected goods and safety, and the resulting risks. Quantitative modelling work, with a focus on sensitivity analysis, is directed to pressure redistribution, fluid migration along wells and aseismic and seismic ground movement after abandonment of producing gas reservoirs. Considered time frames and assessment parameters are listed in Table 3-1.

Table 3-1.Chosen time frames and assessment parameters for quantitative fluid flow and transport modelling and mechanical modelling

Top event	**Time frame after abandonment (yr)**	**Criterion/indicator**	**Dimension**
Pressure redistribution	100-500	Pressure (t)	kPa (~10^{-2}*bar)
Fluid migration along wells	100	CH_4 leakage rate (t) Saturation (T) Plume extent	Kg/yr % x, z (in m)
Uplift and subsidence	100	Vertical movement earth's surface	m
Seismicity	100	Slip tendency or shear capacity utilization	[-]

Before the quantitative modelling work an inventory of potential causes and consequences of lateral and vertical migration of fluids, ground motion and interference with mining activities is executed. These results will feed into the quantitative modelling work. Potential geological fluid migration paths are to be described. Proposals for monitoring strategies will be given.

Conclusions on most important sensitivities are to be drawn and recommendations for Quantitative Risk Assessment to be given.

Execution of the study required expertise in numerical fluid flow and transport modelling, mechanical modelling and geological expertise for site characterisation. Furthermore, expertise in project and risk management are required. Access to suitable flow and transport modelling software is necessary.

3.2 Groningen setting

The area of the Groningen Gas Field was selected as the case study area for this project. During the lifetime of the field itself more than 350 wells were drilled that are now in different stages of well lifetime and abandonment. Several other hydrocarbon fields are located in a similar geological setting in the North-East of the Netherlands onshore region.

The main reservoir of the Groningen Gas Field is the Upper Permian Rotliegend Slochteren Sandstones. These sands were deposited under a dry arid climate in aeolian, fluvial or mixed conditions along the southern fringe of the Southern Permian Basin. The Slochteren Formation is the most important reservoir in the Netherlands (onshore and offshore) with about 2/3rd of the total gas production (Ministry of Economic Affairs and Climate Policy, 2019).

Permian-age halites and anhydrites of the Zechstein Formation form the main seal for the Groningen Gas Field as well as most of the other Rotliegend gas fields in the Dutch subsurface. The thickness of Zechstein salt deposits control the presence of gas in reservoir strata above or below the Zechstein. Its thickness is the dominant control on the structural style and history as well as the fault pattern of the overlying strata. The Groningen area shows Zechstein thicknesses between 50 m to more than 1500 m in varying structural configurations: layer cake, salt diapirs, and thin Zechstein due to salt withdrawal. The Groningen area is therefore considered a good example for Paleozoic gas fields with Zechstein salt present and a model for developing an approach to post-closure hazard assessments.

The overburden of the Groningen Gas Field is typical for platform structural settings in the Dutch subsurface, with Upper Triassic and Jurassic sediments mostly absent (Kombrink et al. 2012), though some remnants are still found along the southern and eastern margin of the field, close to the edge of the Lower Saxony Basin as well as in rim-synclines along salt structures. These sediments are overlain by shales of Lower Cretaceous age and thick Upper Cretaceous chalk. The deposits of the Cenozoic are dominated by deeper marine clays and marls from the Palaeocene to Miocene and during the Pliocene to Pleistocene by fluvial sediments of the Eridanos and the Rhine deltas. During the Quaternary the area was influenced by glaciations.

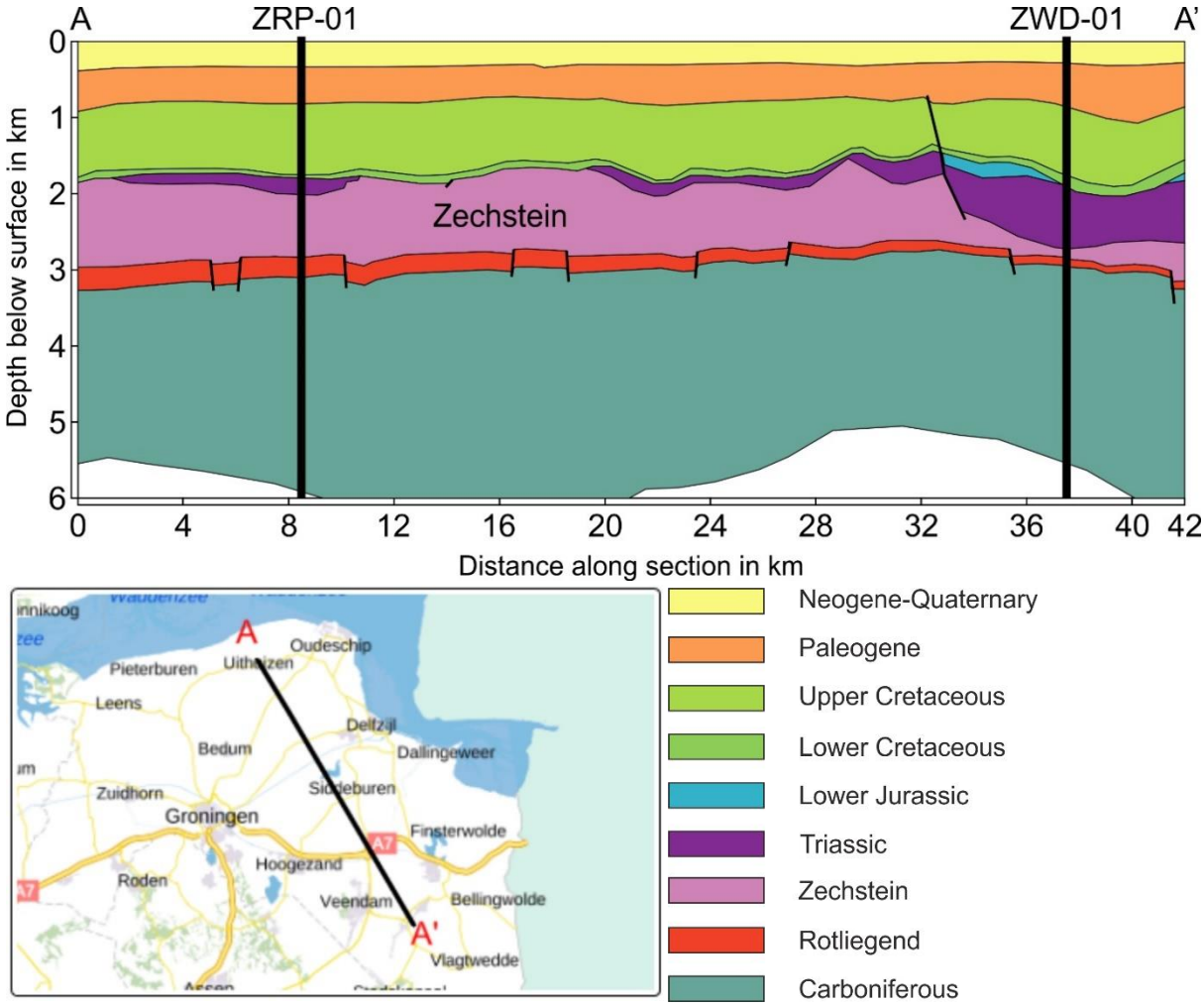

Figure 3-1. 2D Cross section through the Groningen Gas Field from NNW to SSE, crossing wells ZRP-01 and ZWD-01 showing the main structures and formations in the area (redrawn from www.dinoloket.nl)

The fault pattern in the Carboniferous and Rotliegend sediments shows normal faults trending mainly NNW-SSE with some minor faults trending E-W and N-S. Dating of the faults in the Rotliegend is difficult, due to the thick salt overburden. However, the area was affected by several phases of tectonic activity throughout the Paleozoic and Mesozoic. Most of these tectonic phases reactivated pre-existing structures, causing oblique movements along faults or inversion. The strongest tectonic phase in the area is related to the opening of the North Atlantic during the Late Jurassic to Early Cretaceous. Extensional movements during this time formed the main rift basins in the Dutch subsurface and triggered halokinesis. Most of the fault pattern observed in the Groningen area at present-day is believed to be related to this phase. In addition, small pop-up structures in the Rotliegend are seen as evidence for the influence of compressional movements during the Late Cretaceous to Paleogene (de Jager and Visser, 2017). The different stress directions during these later tectonic phases suggest oblique movement along these faults as well. The thick salt layer acts as detachment layer between the Paleozoic and the Mesozoic (Figure *3-1*) and hard linked faults are only expected where the total Zechstein thickness is less than 50 m. The

Mesozoic fault pattern can be mostly linked to salt tectonic activity as either crestal faults on top of large salt walls or diapirs or as collapse structures mostly linked to salt withdrawal (Logeman, 2017). More details can be found in TNO& Deltares (2021).

4 Hazard and risk identification, screening and measures

Chapter 4 describes part I of the ISO risk management framework with the qualitative risk identification and screening (Section 2.2). It builds on the main findings of the literature review in the first deliverable of the KEM-19 project. In addition, the results of the conceptual modelling of fluid migration along geological pathways have been described in Section 4.2.1.

4.1 Pressure redistribution and lateral migration

In its natural state, the pressure in the subsurface is in equilibrium: pressure increases with depth due to the overlying fluid column which is called a hydrostatic pressure distribution. Deviations from the hydrostatic pressure distribution (normally overpressure) can occur naturally due to the burial history and charging of gas fields. Due to the removal of gas (or oil) from the subsurface, a pressure sink is created. After gas production ceases pore pressures can redistribute towards a new equilibrium, which is associated with fluid flow. Pressure redistribution already starts during production and evidence of fluid flow can be identified during production or from the production history, such as: strong aquifer drive, reservoirs found below virgin pressure or experiencing pressure depletion without being produced, observations of pressure increase in shut-in and abandoned reservoirs, observed depletion in adjoining formations, and subsidence above aquifers connected to a gas reservoir. Such evidence suggests connectivity between gas reservoirs and adjacent reservoirs and/or aquifers. Many instances of such evidence of connectivity have been observed in the north of The Netherlands. The equilibration of pressures around abandoned gas reservoirs can take long and occurs over large distances. Usually, the equilibration results in a rise in pressure in the abandoned reservoir and a decrease in the surrounding area. The final equilibration pressure depends on the amount of gas produced and the volume and compressibility of aquifers attached. The higher the net production of gas (and water), the larger the resulting pressure sink and the more potential for depletion in the surrounding area. When the aquifers are very large compared to the depleted reservoir, considerable repressurization of the abandoned gas reservoir can occur. The permeability of the connected aquifers and surrounding formations are the most important factor to determine how fast the pressure can redistribute, including the permeability of faults.

The pressure redistribution can impact future subsurface operations, such as drilling operations (e.g. lost circulation), geothermal energy production and storage. The impact can be direct as a result of the low pressure, such as increased requirement for pumping in geothermal production or indirect. The change in pressure causes changes in in-situ stresses, which could potentially cause ground motion (compaction, subsidence, induced seismicity) at some (vertical or lateral) distance of the originally produced field. Subsidence and induced seismicity are discussed in Sections 4.3 and 4.4 respectively.

For the quantitative analysis on understanding how much and how fast the surroundings of an abandoned gas field decrease in pressure, including the uncertainty in the permeability distribution is of primary importance. Secondaries are the volume and compressibility of the connected formations.

4.2 Fluid migration to shallow freshwater aquifers and the atmosphere and biosphere

One of the concerns related to the abandonment of gas fields is that fluids can escape from the reservoirs and migrate upward as a consequence of the former production and subsequent abandonment. This could potentially lead to the contamination of shallow freshwater aquifers, the biosphere and atmosphere, and change conditions in the deeper subsurface which could impact future subsurface use.

In this study, two processes of vertical fluid migration as a result of field abandonment were considered. The first is fluid migration along natural geological pathways and the second along well bores. In the subsurface, these pathways may be linked for example when a fault crosses a well, but they are discussed separately.

4.2.1 Fluid migration along geological pathways

For upward fluid migration from the reservoir to occur as a result of reservoir abandonment along geological pathways, there needs to be a newly formed migration pathway out of the reservoir and a source of gas. The presence of the gas field is evidence that no current pathways out of the reservoir across the seal are present. For migration pathways to form across the seal, fault reactivation is the most likely process, in which case the fault needs to become transmissive. Fault reactivation can lead to permeable faults in particular for brittle rocks and less for faults in shale, clay or salt. Above the seal, pathways may already be present and are also most likely to be faults. In addition, the source needs to be at a sufficient pressure for gas to migrate upward (for an explanation of necessary conditions for upward gas migration see Appendix D.3.1). As a result, the highly depleted field itself will likely not be a source of upward migrating gas, and mostly little depleted or undepleted gas pockets adjacent to the reservoir can be a potential source. Another option would be the migration of gas across a spill point as a result of pressure lowering and fluid migration to an area with poor seal quality.

To make sure that all processes that could lead to upward fluid migration along geological pathways are considered, a conceptual model was developed with a team of experts. Subsequently a fault tree analysis was introduced in support of qualitative risk identification. This method is also recommended for later quantitative risk assessment, and in that phase can aid in identifying potential mitigative and preventive measures, as well as a monitoring strategy. These are provided in Appendix B.

Figure *4-1* shows a schematic drawing of the conceptual model of vertical fluid migration along geological pathways. The numbers refer to different stages that the upward migrating methane needs to pass before it would reach the shallow aquifer and/or the biosphere/atmosphere. For convenience, the vertical geological sequence is subdivided into eight levels. It should be realized that reality is far more complex, with a number of deep and intermediate heterogeneous aquitards and aquifers consisting of alternating layers with variable permeability, intercalations, fault zones etc. However, for the construction of a conceptual model working with eight levels is suitable as it allows the description of all processes associated with vertical gas migration.

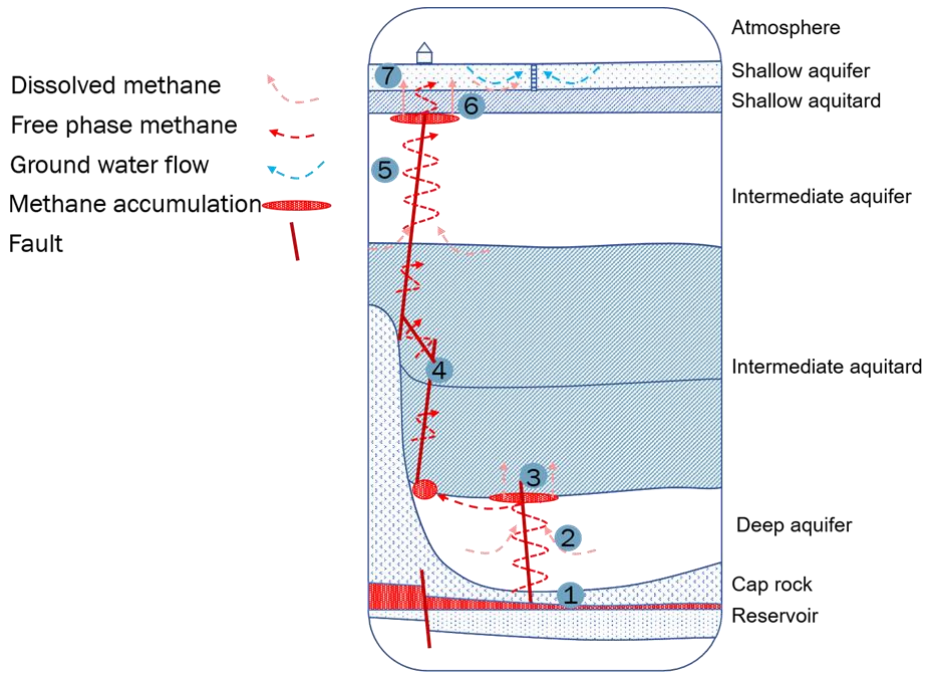

Figure 4-1. Drawing of the conceptual model of vertical fluid migration from a gas reservoir. Each described stage is indicated with a number.

The bow-tie diagram in Figure 4-2 summarized the threats that were identified, and the different impacts that could follow from upward migration as a result of abandonment.

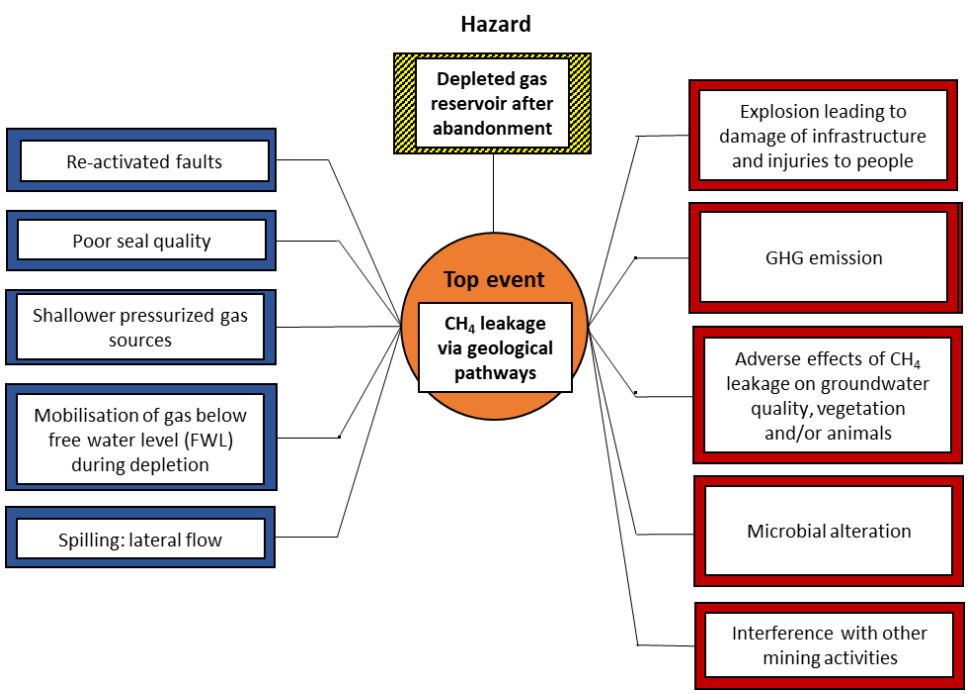

Figure 4-2. Simplified bow-tie for fluid migration along geological pathways; risk reduction and monitoring measures have not been included

A narrative of the conceptual model is provided in Appendix B which refers to these numbers. For each stage in the migration pathway, the conditions that are favorable for fluid migration are listed, and potential hazards that could occur related to these steps. These stages are 1) fluid escape from the reservoir; 2) Upward migration; 3) Accumulation below low conductive layer; 4) Upward migration through low conductive layer; 5) Further upward migration through intermediate unconsolidated aquifer; 6) Gas accumulation below shallow unconsolidated aquitard and 7) Gas enters the shallow aquifer.

Subsequently a fault tree was set up to determine what possible geological pathways there are for methane to vertically migrate to shallow aquifers. Fault tree analysis is an intuitive method to represent and quantify the probabilities of the conditions, combinations and sequence of events that could lead to undesired consequences. The method originates from safety engineering such as aerospace and nuclear power industries. It was introduced to groundwater quality related decision making by Tartakovski (Tartakovski, 2007, 2013). Figure 4-3 shows an example of such a fault tree. In practice they can become quite complex, but more revealing than a qualitative bowtie in terms of identifying risk treatments, monitoring, and other interventions.

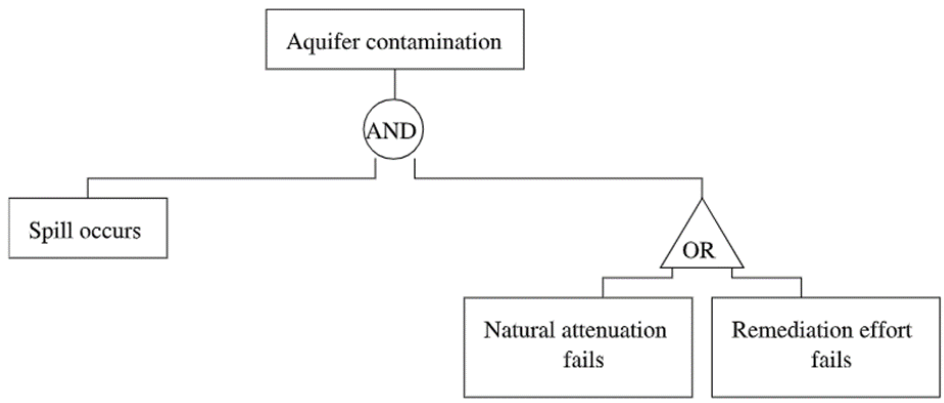

Figure 4-3. Simplified fault tree for possible aquifer contamination (Source: Tartakovski, 2007)

4.2.2 Fluid migration along well pathways

There are several types of cement failure that could occur in a wellbore, jeopardizing the cement integrity. The stress state in the wellbore changes throughout the life of the well, from the drilling stage, to completion, well testing, stimulation, production, and injection phases. The well leaks can manifest in the form of sustained casing pressure (SCP) measured at the wellhead, surface casing vent flow (SCVF), casing failure (CF), and gas migration (GM) observed as gas bubbling in the ponded area near the wellhead. The leaked gas can enter the atmosphere and contribute to the increase in greenhouse gases in the atmosphere. In addition, gas can enter freshwater aquifers and, in some cases, impact the water quality.

The following pathways in wellbores have been identified as possible routes for fluid leakage. It should be noted that the mere presence of a flow pathway is not sufficient for a well to leak. A *source of gas* and *sufficient pressure gradient* across the leakage pathway are also necessary conditions for well leakage to occur (for an explanation of necessary conditions for upward gas migration see Appendix D.3.1). A more comprehensive summary of the risk factors for zonal isolation in wells is provided in the KEM-18 report (van Oort, 2022). Van Oort (2022) provides a qualitative method to categorize wells according to the leakage risk.

1. Fluids can leak through the cement sheath due to cement mechanical failure and chemical interactions. This could occur due to high stresses induced by well operations such as pressure testing, or hydraulic fracturing; poor cement quality leading to high shrinkage and weak cement structure; changes in wellbore temperature due to injection of hot or cold fluids; chemical interactions between cement and in-situ fluids (Gill et al., 2012; King and King, 2013; Bois et al., 2011, Wasch and Koenen, 2019).

2. Poor cement placement practices can create leakage pathways. Cement channels could form due to poor mud removal or casing centralization. Gas migration through cement during curing could form permanent high permeability pathways (Dusseault et al., 2000; Davies et al., 2014).

3. Fluids can leak through the uncemented portion of the annulus. This depends on the local abandonment regulations as in some regions operators can leave a portion of the casing uncemented. This is particularly important for older wells that were abandoned before more rigorous abandonment practices were in place (Bachu, 2017).

4. Fluid leakage can occur at the interfaces between the casing, cement and the formation. This could be caused by cement shrinkage, or a drop in casing pressure and temperature during well operations (Moghadam et al., 2022).

5. Fluids can leak through the damaged casing wall or connections. This could be exacerbated in a corrosive environment (King and King, 2013).

6. Leakage can occur through cement plugs (Davies et al., 2014).

In terms of the source of gas, the following can influence the leakage risk that were not considered in the KEM-18 report:

1. The presence of thermogenic or biogenic gas anywhere along the path of the well increases the risk of leakage. This includes the target reservoir (for an oil and gas well), or shallower formations containing gas (organic-rich layers, coal seams, etc.)

2. The pressure of the gas source can determine the risk of leakage. Slightly depleted, hydrostatic, and over-pressured sources can leak while highly depleted formations are not likely sources of leakage.

3. Gas saturation at the source indicates the type of flow that can occur. If gas saturation is above 10-20%, advective flow could occur which leads to higher leak rates. Saturations below the critical value indicates diffusive flow which is typically small (Karra et al., 2015).

The various causes and consequences of fluid leakage via wells have been depicted in a simplified bowtie (Figure 4-4). If a source of gas, a leakage pathway, and sufficient pressure gradient across the pathway exist, leakage will occur. The magnitude of leakage and the fraction that reaches the atmosphere versus the aquifers depend on the properties of the system. The wells that meet all the criteria for leakage should be monitored, and remediation may need to take place depending on the magnitude of leakage and its impact. The following points should be considered for the monitoring strategies:

1. Permeable intermediate formations can act as a buffer and accumulate the leaked gas through the well. If no permeable formations are present between the source and the aquifers, the magnitude and impact of leakage will be more significant.
2. Unconfined aquifers will not store a significant amount of gas, therefore are not good candidates for monitoring.
3. The best locations for monitoring, would be under the confining layer of the deepest freshwater aquifer.
4. Groundwater movement can distort the shape of the gas plume in aquifers. Monitoring should be done as close as possible to the well, downstream from the well location in terms of groundwater flow.
5. Monitoring and water sampling should be done as close as possible to the well as the plume may not travel more than 500 m away from the well. The 500 m estimate does not take into account the impact of groundwater flow.

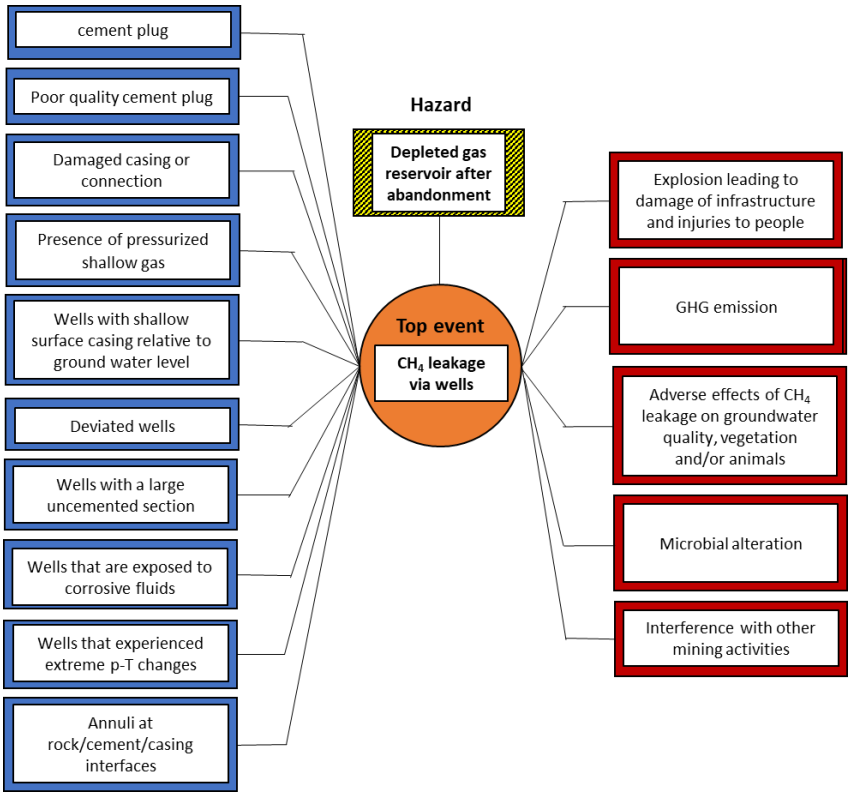

Figure 4-4. Simplified bow-tie for fluid migration along wells; risk reduction and monitoring measures have not been included

4.3 Subsidence and uplift

After shut-in of the Groningen production, pressure redistribution will continue to take place until an equilibrium has been reached. The pressure changes also induce geomechanical effects. Areas which experience pressure reduction will show compaction and stress changes. The largest changes take place in the connected aquifers: redistribution of the pressure between the aquifer and the gas reservoir results in much larger pressure changes in the aquifer than in the gas reservoir, due to the compressibility contrast between the gas in the gas-bearing strata and the water in the aquifers. The main causes and consequences of uplift and subsidence are graphically represented in a simplified bowtie (Figure *4-5*).

Based on the above analysis and discussion we have identified two issues that influence the risks associated with expected ground movement. The first is a larger-than-expected pressure depletion, the second the possibility of very different compaction coefficients in the aquifers versus in the gas-bearing parts. Regular subsidence estimates through interpretation of satellite data will help quantifying the surface movement. In addition, they can help to estimate the reservoir aquifer compaction and the associated stresses. Aquifer pore pressure measurements would also help greatly to better determine the pressure distribution and the associated compaction field and induced stresses.

The main effects of subsidence and uplift are in groundwater management. Substantial subsidence means that the groundwater level must be changed to be able to maintain the current functions of land use. The change in relative groundwater level (with respect to the surface) and the occurrence of inhomogeneities in the shallow subsurface lithology will jointly control if substantial differential subsidence takes place. A quantification additionally requires adequate understanding of the shallow soil mechanics response and damage models for infrastructure and buildings.

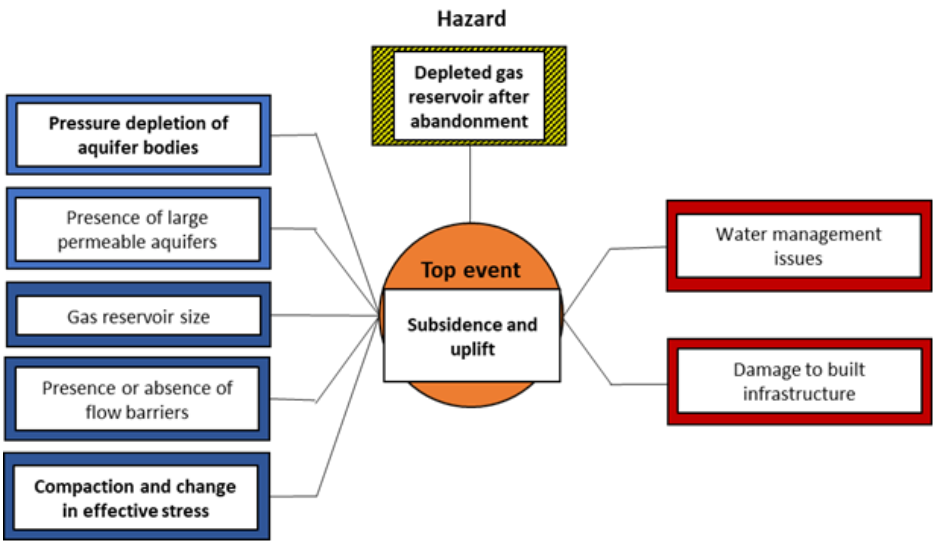

Figure 4-5. Simplified bow-tie for subsidence and uplift; risk reduction and monitoring measures have not been included

4.4 Induced seismicity

In the context of this study, we include ground motion in the form of earthquakes. Much work has been performed on this subject, and valuable reviews are available (Gaucher et al, 2015; Buijze et al, 2019b; Candela et al, 2018; Van Wees et al, 2014, 2018). A change in pore pressure or in in-situ temperature affects the stresses, both locally and at distances away from the distortion. Depletion of aquifers connected to a gas field, even after abandonment of the gas field, will thus cause changes in the criticality of faults present in the subsurface. Too large criticality can result in exceedance of the slip resistance and induce slip behavior. When the fault is slip-weakening, seismicity may take place. A first estimate of such behavior is therefore a slip tendency assessment. Approaches range from 1D analytical to 2D and 3D finite element studies on fault reactivation, with little or much detail on the geological context and the dynamic reservoir development (ter Heege et al, 2018).

The main volume of the depleted reservoir is in reservoir sections which are thin in comparison with their horizontal extent and of which the vertical variation is limited. For such blocks, a uniaxial approximation can be employed when computing deformation as a result of pore pressure changes.

Uniaxial deformation implies that there is no lateral displacement. In addition, the total vertical stress, controlled by the weight of the overlying subsurface strata, is constant. This means zero vertical stress change and zero horizontal strains. Within linear poroelasticity the compaction and the change in

horizontal stresses can then be calculated as a linear function of the pressure change. The compaction per unit of reservoir thickness is the vertical strain, and the properties on which it depends are the pressure change itself, the Poisson ratio and the Biot coefficient. In addition, for reactivation to take place, the failure criterion must be exceeded. This happens when the stress becomes critical, which, on its turn, is described by the friction coefficient and the cohesion. The original stress field in the Groningen area is arguably not critical. Therefore, a minimum depletion is required before fault reactivation can take place. This minimum needs to be determined as a function of the input parameters. Then the regions in which the minimum is exceeded can be identified as risk regions.

Faults that are bounding reservoir blocks or that divide parts of the reservoir into blocks at different heights (faults with offset) need to be treated differently. In fact, many seismic events in Groningen have been located on faults that exhibit considerable offset. A proper field-specific analysis should map the faults, consider their offsets, quantify the pressure drops around it, incorporate the stress field, and include all uncertainties connected to these parameters. Then the effect of the pressure drop on the stress could be quantified and related to a reactivation model like a Mohr-Coulomb failure analysis or a Dieterich rate-and-state friction approach. It would also integrate observations of seismicity, as well as hypocentre and focal mechanism determination. It would include on- and off-fault plasticity, dynamic behaviour of faults, stress transfer, creep in the reservoir and surrounding formations, properties of fault gouge, elasticity contrasts, slip-weakening, response of pore pressures to slip, etc. A comprehensive study in this sense is beyond the scope of what is described in the current report. What can be done, though, is to follow the guidelines that States Supervision of the Mines have formulated or follow a statistical interpretation on similar fields in the Netherlands. In all cases, the main parameters to be assessed and monitored are the pressure depletion, the in-situ stresses, and the fault locations and orientations.

The effects of induced seismicity can be damage to infrastructure and buildings, injuries if the seismicity involves large events, and interferences with other mining activities. A bowtie representation of causes and consequences of induced seismicity is shown in Figure 4-6.

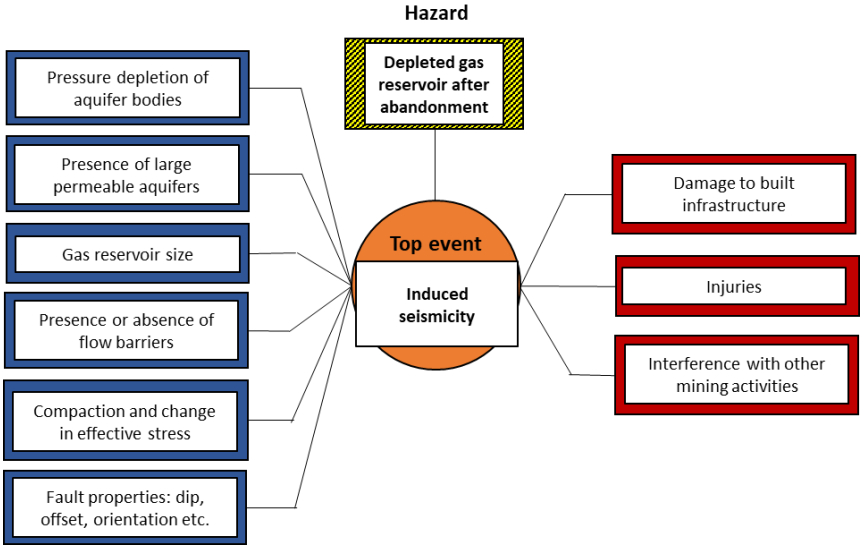

Figure 4-6. Simplified bow-tie for induced seismicity; risk reduction and monitoring measures have not been included

4.5 Interference with subsurface activities

For the interference with subsurface activities, we distinguish between future activities in the abandoned reservoir, adjacent to the abandoned reservoir, and in the rock sequence above the reservoir.

In the abandoned reservoir, the pressures are depleted and pressures will gradually increase due to inflow from adjacent aquifers. The rate and amount of increase in the pressure depends on the local conditions, such as the amount of produced gas, the size of aquifers and permeability. These changes should be taken into account when planning geothermal activities in the abandoned reservoir or re-using it as a storage medium. In addition, future wells should be planned in areas where fault re-activation and induced seismicity are unlikely to take place. A major concern is to what degree a geothermal project could influence the hazard of induced seismicity as a result of gas production in the past both from pressure and thermal effects.

In aquifers adjacent to the depleted reservoir, fluid migration towards the depleted area may take place, in combination with pressure lowering in the aquifers. Near existing faults this may lead to re-activation and induced seismicity. Also here, these factors should be taken into account when planning new wells for gas storage or geothermal activities.

The rock sequence above the reservoir is not expected to be in pressure communication with the depleted reservoir. However, in the rare case leakage has occurred, it may result in the formation of gas pockets which may pose a drilling hazard. Such leakage will only take place where a thin Zechstein (<50m) seal is present, faults with large offsets could be reactivated and undepleted or little depleted gas is present at the source. In addition, it should be realised that if low permeability strata are penetrated by abandoned wells, the strata may be short-circuited due to well-bore integrity loss.

In the process of geothermal drilling, operators are aware that gas pockets in the subsurface can occur and take measures to manage the risk of leakage. This means that there is no significant risk from gas pockets that originate from well leakage.

The ground motion effects of the reservoir abandonment should be included as an additional effect on top of any other ground motion calculation from subsurface activities, for instance in subsidence calculations for salt caverns. Apart from that, for the storage of energy carriers in salt caverns, no negative impacts from the abandonment of gas reservoirs could be reasoned, as long as the base of the caverns is 300 m or higher above the abandoned reservoir. This is based on observations that no faults seem to cross the Zechstein salts if the thickness is more than 300 m.

5 Quantitative hazard and risk analysis and evaluation

Based on the identified hazards and risk in the previous chapter, quantitative modelling work has been executed to understand the sensitivities of:

Subdivided for individual undesired events (aligned with context and screening stages in previous chapters):

- Pressure redistribution at the reservoir level (Section 5.1)
- Subsidence and uplift (Section 5.2)
- Induced seismicity (Section 5.3)
- Fluid migration along wells to biosphere (Section 5.4)

Fluid migration along geological pathways to biosphere and interference with subsurface activities have been analysed in qualitative terms only in Sections 4.2.1 and 4.5, respectively.

5.1 Pressure redistribution and lateral migration

In this section, numerical simulations are used to quantify the temporal and spatial scales of the pressure redistribution in the aquifers surrounding the depleted Groningen field and to evaluate the impact of subsurface uncertainty using sensitivity analysis. A workflow has been setup for a numerical modelling exercise (Figure 5-1). Results of the various steps are briefly described in the following subsections.

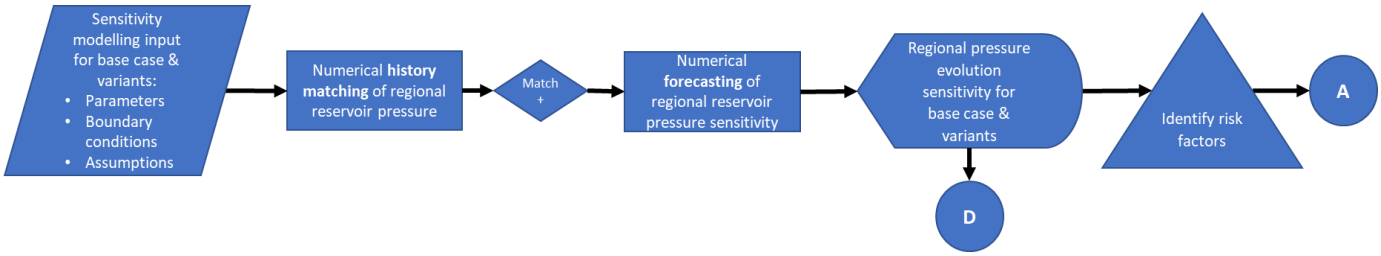

Figure 5-1. Workflow applied for sensitivity analysis of pressure equilibration in current KEM-19 project: D = input to sensitivity analysis of uplift and subsidence and induced seismicity; A = input to recommended workflow for quantitative assessment of pressure redistribution (see Chapter 6); flow diagram symbols are explained in Appendix A.

5.1.1 Modelling approach

The spatial and temporal scales of interest in this project are large: > 50 kilometers and > 200 years. Therefore, a simplified, regional, numerical fluid flow model has been developed to perform the required simulations.

Creating a fluid flow model consists of two components: a generic model code and the input values to make the model code applicable to a specific subsurface location (such as depth, thickness, porosity and permeability of the aquifers). These input values are normally adjusted to recreate observed behaviour. This process is called history matching or model calibration and is required to gain confidence in the forecasts made by the fluid flow model. Creating a detailed geological and fluid flow model of the region and history matching it to all available observations while at the same time honoring the uncertainty, is a massive effort. Here, a much simpler representation of the subsurface is created in order to capture the main trends and uncertainties. The goal here is an understanding of the general behaviour rather than the detailed representation of conditions at individual locations. The key parameters that should be represented with reasonable accuracy are the gas initially in place (before production start), the amount of gas produced, the initial and abandonment pressure distribution and the average permeability distribution in the field: the amount of gas produced determines the size of the pressure sink that has been created and the permeability determines how the pressure is redistributed.

To limit the vertical size of the model, the pressure redistribution is assumed to occur predominantly below the Zechstein seal and only that part of the subsurface is included in the model. The lateral extent of the model includes those areas which are possibly hydraulically connected to the depleted Groningen field. The simulations are done accounting for two phases: gas and water. The gas is simulated in a simplified way as a dry gas, i.e. not including condensate and water vapour, and with a constant composition in the entire area. Differences in temperature in the field and possible thermal effects are not included. A number of main faults is included in the model, but many faults are not simulated explicitly. The same is true for the small gas fields around the Groningen field: some of the larger ones are included in the model, but most are not. Production from these small fields is not included.

The goal is to understand the pressure behaviour after abandonment and thus it might seem logical to simulate only this time period. However, the historical production needs to be included in the simulations to capture the uncertainty in the aquifer pressure at abandonment. Aquifers already deplete during production of the gas field and although the pressure in the gas field at abandonment is quite well known and observed, this does not hold for the pressure in the aquifers. Therefore, the production history is simulated with different values for the aquifers to represent this uncertainty.

The industry-reference reservoir simulator ECLIPSE Black Oil v2019.3 is used for the simulations. Petrel 2019 is used for the generation of the geological model.

5.1.2 Input data

The input data and history match are described in detail in Appendix C. Suffice to mention, most of the input is based on the Petrel model made available by the NAM (NAM V6 model), various NAM status reports and data from ThermoGIS.nl (a website showing geothermal potential at the national level). A history matching was carried out: the amount of gas initially in place, the pressure history at the wells and the abandonment pressure distribution from the detailed model by NAM were matched in the history matching procedure. The model input parameters used to achieve the history match are the free water level for the gas initially in place and the permeability of aquifers, faults and flow barriers for the pressure related parameters.

In

Table 5-1 the Gas Initially In Place (GIIP) is compared to the best estimate by NAM (Zeeuw and Geurtsen, 2019). The estimate of GIIP is split up in different parts, but the bulk is contained in the Slochteren Sandstone (Sst) (first line of the table) and differs by 2.4%. The item "Gas below Free Water Level" is gas that is thought to be present in the aquifer below the gas field, which is not included in the model used in this report. The Limburg group of the Late Carboniferous (referred to in short as the Carboniferous) underlies the Slochteren Sst and also contains some gas. The smaller gas fields Norg and Annerveen are only part of regional model used in this report and not in the NAM model. The distribution of the gas in the model (in yellow) and as estimated by NAM (green outlines) is shown in Figure *5-2*. Overall, the distribution is quite similar, with a discrepancy on the north-east side. Also clearly visible are the many small gas fields not included in the model.

Table 5-1. Overview of Gas Initially In Place (GIIP) of NAM models and the model in this report (in normal BCM (1 atm, 0°C)).

Gas fields/main compartments	**NAM best match (Zeeuw and Geurtsen, 2019)**	**This report**
Groningen (above FWL) (incl. land assets included in NAM reservoir model)	2894 BCM	2964 BCM
Gas below Free Water Level	103 BCM	Not included
Carboniferous	42 BCM	34 BCM
Norg	Not included	69 BCM
Annerveen	Not included	36 BCM

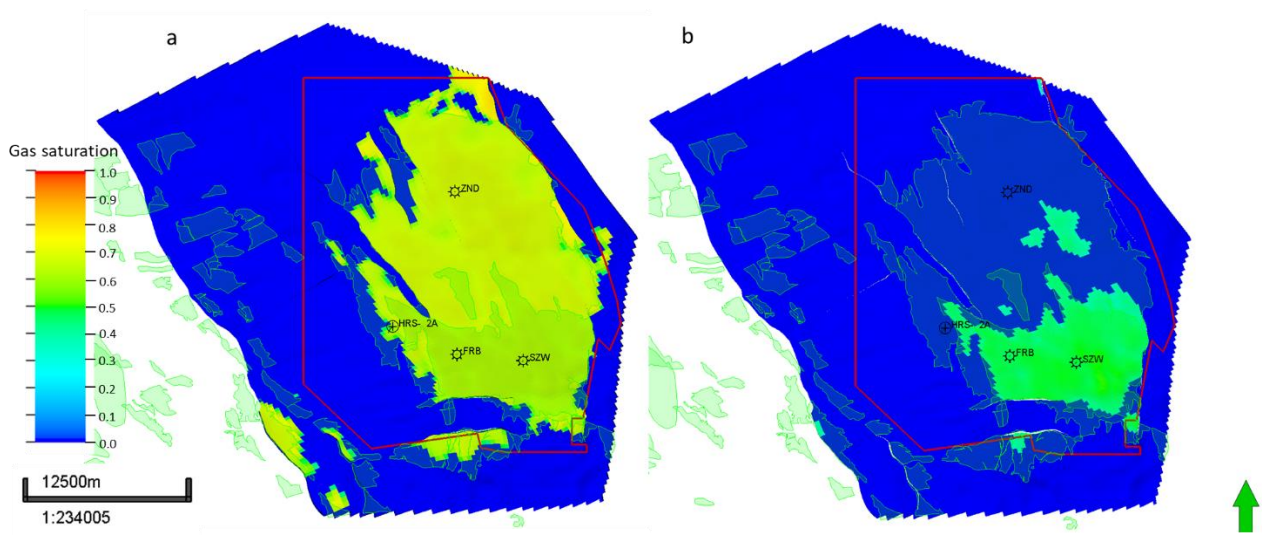

Figure 5-2. Gas distribution in the Upper Slochteren Sst (a, left) and Limburg Group of the Carboniferous (b, right) (blue is aquifer; yellow is gas, red outline is the outline of the NAM model; green outlines are gas fields).

To demonstrate the pressure match, in Figure *5-3* for four wells the observed and simulated pressures over time are presented, which show an adequate match for the pressure in the gas field.

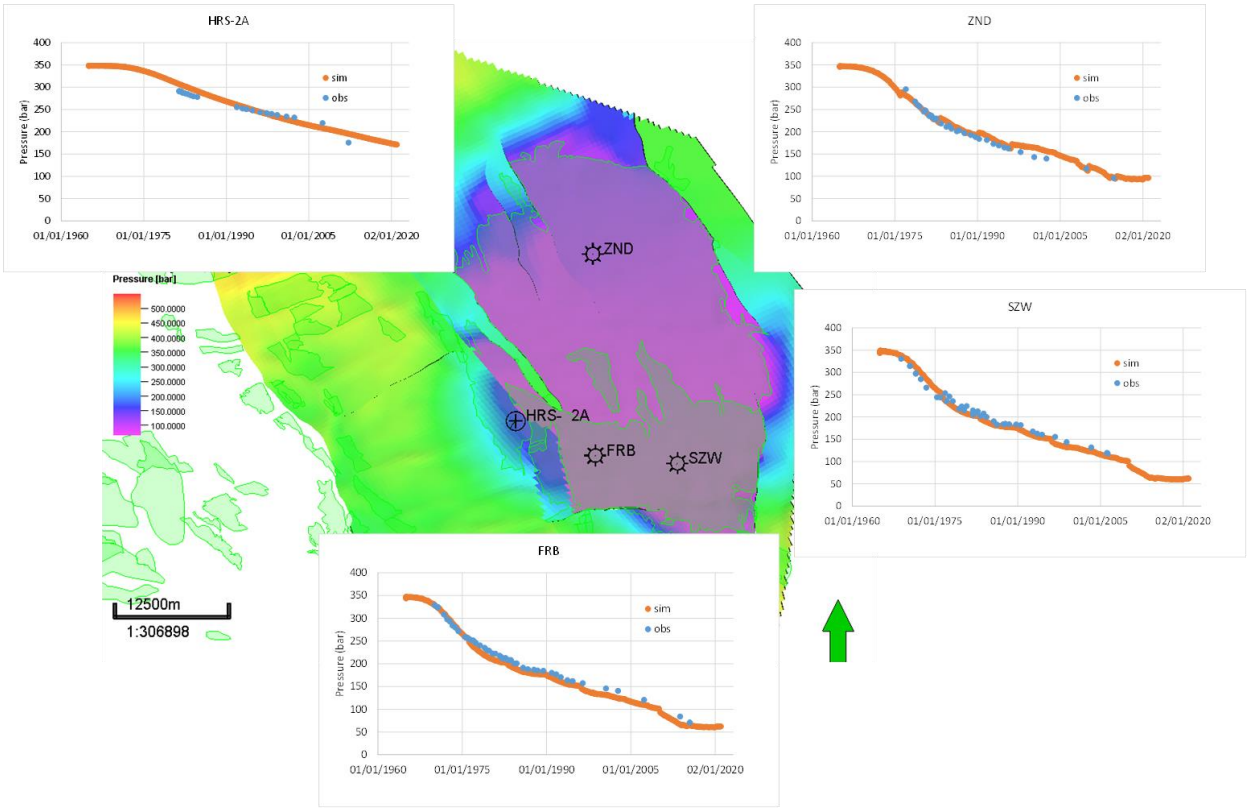

Figure 5-3. Comparison between observed static pressure ('obs' in blue) and simulated pressure ('sim' in orange) for four wells in the gas field. In the background is the pressure in 2026, the well locations and the gas field outlines (in green).

5.1.3 Sensitivity analysis results

The base case model described in the previous section was used to simulate the pressure redistribution for 500 years after abandonment. The results were compared to the predictions made by the NAM model. Both models predict only a small increase in pressure in the gas field: in the order of a few bar for the field average pressure for the next 50 years. This is consistent with mass balance analysis, which shows that the volume of the connected aquifers is insufficient to repressurize the depleted gas field (see Appendix C). Locally a larger pressure increase can occur due to pressure equilibration with the gas field. Over time, the depletion in the aquifers increases. In Figure *5-4* the depletion at the prognosed end of production (year 2026) and 100 years after the production has stopped (year 2126) is shown for the base case both at the top of the Upper Slochteren Sst and the top of the Limburg Group (Carboniferous). The depletion is shown as a percentage of the pre-production pressure. This shows that both in the Slochteren and the Carboniferous pressure decreases in the aquifers. It should be noted that the depletion of the small gas fields is not included in these simulations and these pictures show the depletion due to the Groningen field only.

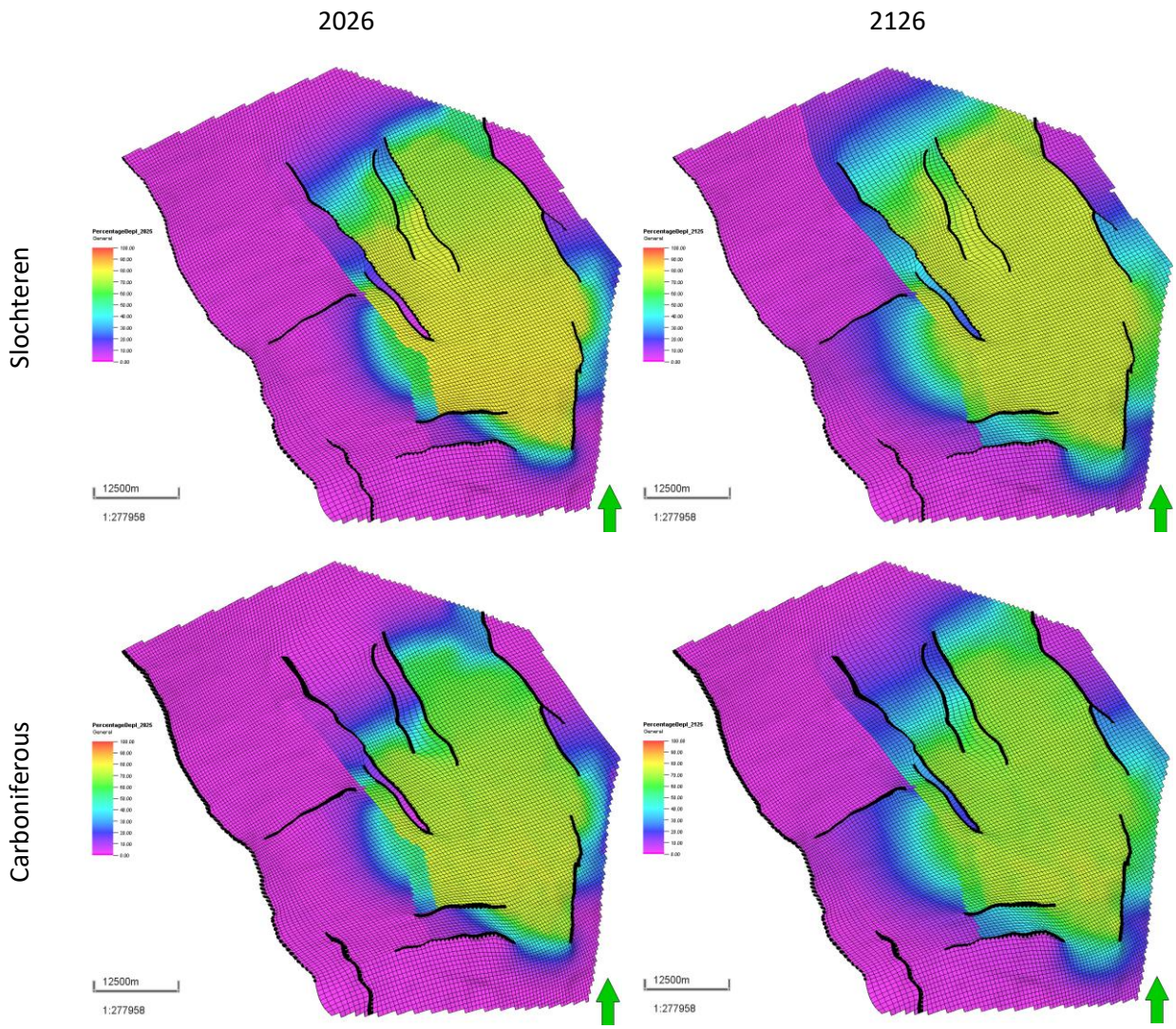

Figure 5-4. Percentage depletion in year 2026 (stop of production; left) and year 2126 (right) at the top of the model (top row; Slochteren) and the bottom part of the model (top of Limburg group (Carboniferous); bottom row). Color scale ranges from 0 (pink) to 100% (red).

The interest in this study is on the depletion of the aquifers surrounding the gas field. Therefore, the focus of the sensitivity analysis is on the aspects that impact the depletion in the surrounding aquifers. Since the permeability influence the pressure redistribution most, the sensitivity analysis was done on the following aspects:

- The permeability of the Limburg Group (Carboniferous, DC)
- The permeability of the aquifers in Upper and Lower Slochteren Sst
- Vertical permeability (general)
- The position of the Ameland clay which forms a barrier between the Upper and Lower Slochteren in the north of the field.

- The transmissivity of the barrier between Lower Slochteren and Carboniferous
- Fault permeability (all faults)
- Size of the analytical aquifers Rysum and Moewensteert (pore volume multiplier, see Appendix C)
- Transmissivity between segments (representing faults not explicitly included in the model, see Appendix C, Figure C-10)

In all sensitivities, the historical production and the prediction period were run as a single run. This workflow enables including the uncertainty in the conditions at abandonment, a history match check for all runs and physically consistent runs. For details the reader is referred to Appendix C. The averaged pressure depletion resulting from the sensitivity runs does not deviate much from the base case (in Figure *5-4*). More interesting is the range in the pressure depletion resulting from the sensitivity analysis, which is illustrated in Figure *5-5*. The background map represents the range in pressure depletion in year 2126 (maximum depletion 2126 – minimum depletion 2126). The graphs in Figure *5-5* A-F are time series of the pressure development over 500 years at various locations of interest. The regions in pink indicate the areas where very little variability is observed between the sensitivity runs, either because the runs differ very little (a few bar) like in the gas field or because the depletion is small overall (e.g. in the Northern Lauwerszee Trough (Figure *5-5* A) and near the gas storage site Norg in the south-west (Figure *5-5* C)). The largest variability occurs on the boundaries of the gas field (maximum range of ~130 bar) and the aquifers connected to the Harkstede area in the southern Lauwerszee Trough. Moreover, the simulations results indicate that at the gas storage sites Norg and Grijpskerk (near Figure *5-5* C), the depletion due to the Groningen field is not expected to arrive within the next 100 years.

Please note that in this report only the depletion due to the production of the Groningen field is shown. The impact of small fields was not accounted for in the pressure depletion shown in this report. However, the Groningen field is surrounded by smaller fields, in particular in the west and south. Therefore, for any local analysis, the impact of the nearby small fields should be included. The impact that the small fields can have on their surroundings is very similar to that of the Groningen field: for connected aquifers pressure is expected to decrease significantly as the case of the southern Lauwerszee Trough (see Figure *5-5* B and D) There is one large difference though: the smaller fields will recover in pressure due to the depletion of the aquifer (example: Roden field), thus limiting the potential depletion. The Groningen field is so large that that is not the case and the low pressure will remain in place for a very long time, thus allowing the pressure decline to move much further from the field than is possible for the smaller fields.

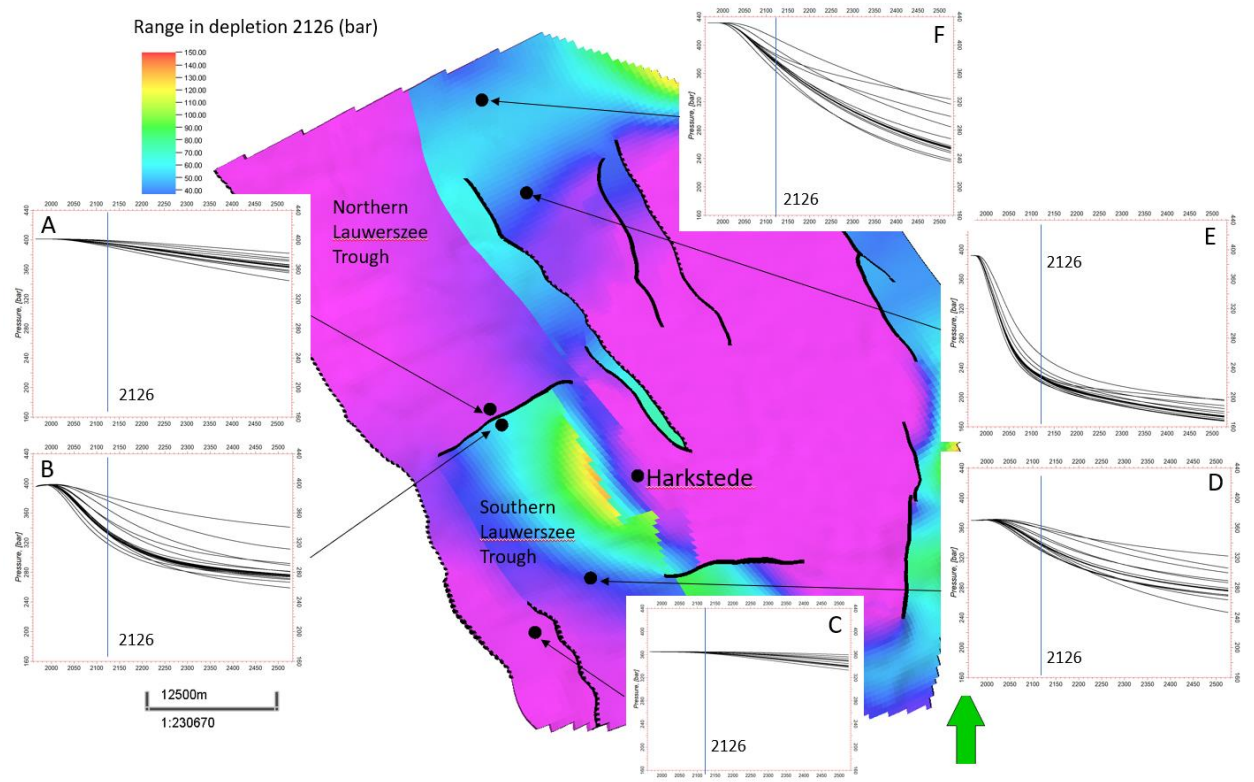

Figure 5-5. Time series of the pressure depletion for all sensitivity scenarios for six locations around the Groningen field. Time-axis: 1965 to 2526. Pressure y-axis: 160 to 440 bar. Background figure shows the range in depletion in 2126 (scale from 0 bar (pink) to 150 bar (red). This moment in time is also indicated on the time series plots.

5.1.4 Conclusions

In this section, a high-level, simplified model was used to investigate the ranges in pressure depletion due to the depletion of the Groningen gas field. The results show a continuing decline in pressure in the aquifers connected to the Groningen field. Some areas were identified in which the pressure decline is expected to be significant (up to 30-50% of pre-production pressure) in the next 500 years and in which the uncertainty is relatively large. These are the areas which should be prime areas for more detailed studies and monitoring. These areas are in particular to the north of the gas field and in the Southern Lauwerszee Trough. The uncertainty range in the gas reservoir itself and in the outlying, low-permeability areas such as the Northern Lauwerszee Trough is much smaller. In the gas reservoir itself, only little pressure increase is expected (up to ~10 bar averaged over the reservoir). In addition, areas with interference with other depleted gas fields should be further investigated since this was not included in the current analysis.

5.2 Subsidence and uplift

To analyse sensitivities of long-term subsidence and uplift after ceasing gas production a workflow has been set up for a quantitative modelling exercise (Figure 5-6). Results of the various steps are briefly described in the following subsections.

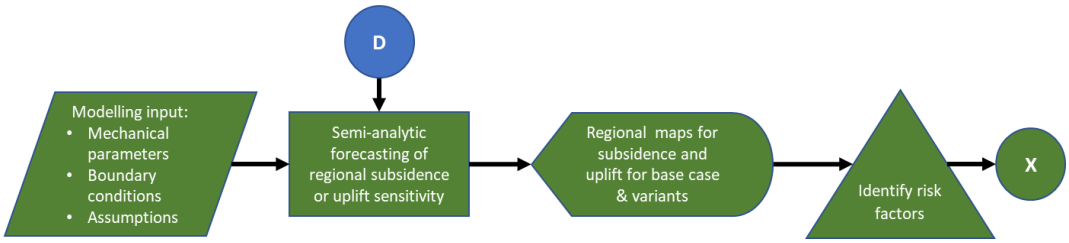

Figure 5-6. Workflow applied for sensitivity analysis of subsidence or uplift in current KEM-19 project: D = input from pressure redistribution modelling; X = input to recommended workflow for quantitative assessment of subsidence and uplift (see Chapter 6)

5.2.1 Modelling approach

After shut-in of production from the Groningen field the reservoir dynamics will not have ceased. Pressure redistribution will take place until an equilibrium has been reached. The pressure changes also induce geomechanical effects. Areas which experience pressure reduction will show compaction and stress changes. The largest changes take place in the connected aquifers. This is related to the compressibility contrast between the gas in the gas-bearing strata and the water in the aquifers. Redistribution of the pressure between the aquifer and the gas reservoir results in much larger pressure changes in the aquifer than in the gas reservoir.

For the subsidence we are interested in an estimate that is consistent with the surface movement history as observed above the Groningen gas reservoir and with the modelling by NAM [NAM, 2020]. Therefore, we have employed the Rigid Basement model that NAM also employed [van Eijs & van der Wal, 2017, Van Opstal, 1974]. The difference with the most simple possible geomechanical model, the Geertsma model [Geertsma, 1973], is very small due to the relatively deeply seated rigid basement.

5.2.2 Input data

Compaction is driven by the pressure depletion. Pressure fields for the years 1965, 2025, 2080 and 2126 have been used. The period between the years 2025 and 2126 is primarily controlled by the pressure redistribution. The various sensitivities have been discussed in Section 5.1.3.

For the geomechanical model we tuned the compaction coefficient to mimic the observed behaviour. For the Rotliegend sandstone we typically have a Poisson ratio $\nu = 0.25$. We use an average depth D = 3400 m. Then, with a compaction coefficient $C_m = 0.21*10^{-5}$ bar^{-1} we arrive at subsidence values in year 2026 of 0.4 m in the centre of the subsiding area, in accordance with the NAM-reported values [NAM, 2020]. We like to note here that the pressure calculations are not of the detail that is used for precise assessment of the Groningen behaviour, as the focus of the present study required coarser discretization. More advanced models than that of Geertsma and Van Opstal (e.g.; Fokker and Orlic [2006]) were considered to provide only little additional insights in the present context.

5.2.3 Sensitivity analysis results

We have calculated subsidence in the years 2025, 2080, and 2126 (Figure *5-7*). The difference between the 2025 and 2126 maps represents the additional subsidence realized through the pressure equilibration in that period. During this period we see subsidence continuing mostly above the NW part of the aquifer,

with a largest value of around 12 cm additional subsidence at RD coordinates (x,y) ~ (232000, 610000). A second maximum develops West of the field at RD coordinates (x,y) ~ (233000, 582000) with a value of around 6 cm additional subsidence. An uplift of about 1 cm above the southern part of the reservoir is also observed in this period. This is due to limited repressurization of that part of the field, due to pressure equilibration.

The incremental subsidence after shut-in was calculated for all scenarios defined above. The results are represented in the Appendix E. The scenarios show very little variation for the production period. For the post-shut-in period the sensitivities show the same qualitative behaviour with a limited variation in the maximum additional subsidence expected: 9 – 13 cm for the NW position and 4 – 7 cm for the West position.

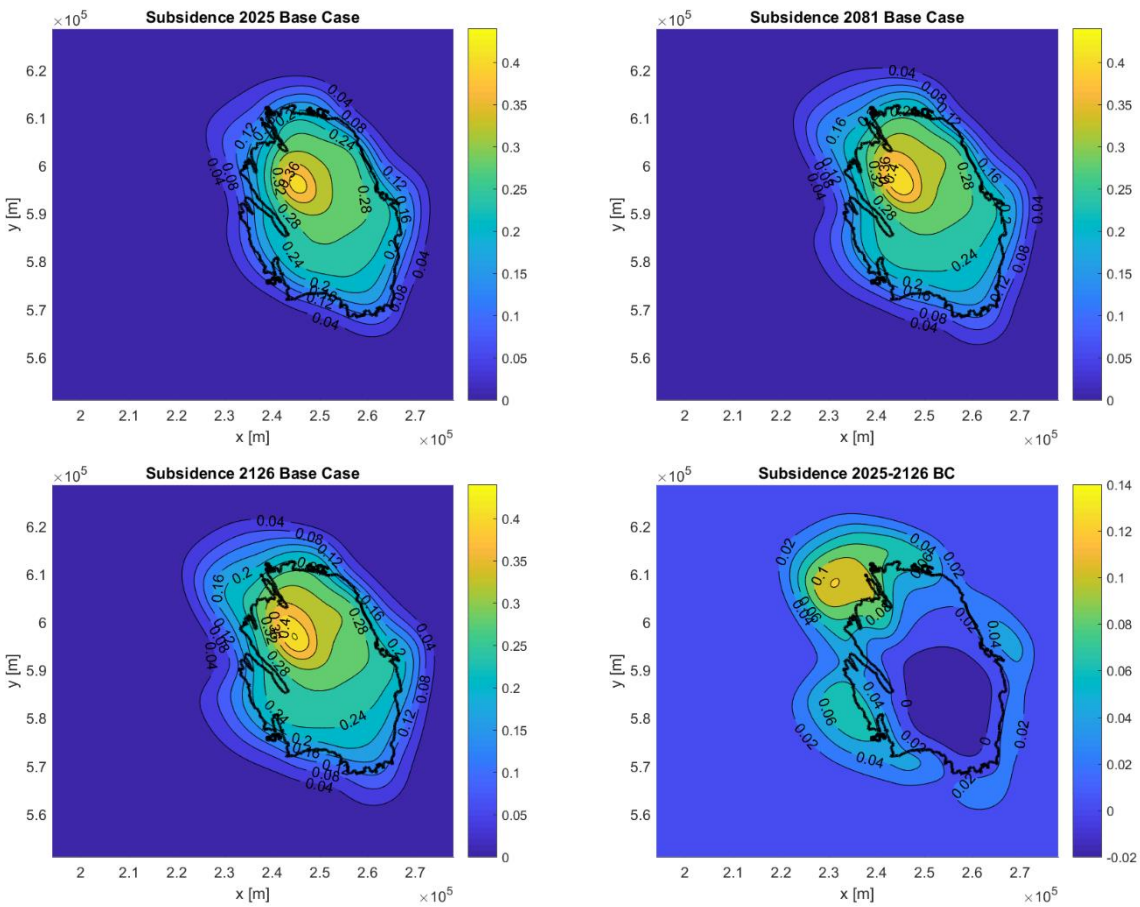

Figure 5-7. Subsidence fields in 2025 (left top), in 2080 (right top) and in 2126 (left bottom). Right bottom gives incremental subsidence between 2025 and 2126. The black line Is the outline of the Groningen reservoir. Scale is in m.

5.2.4 Conclusion

The scenarios show very little variation for the production period. The sensitivities show the same qualitative behaviour with a limited variation in the maximum additional subsidence expected. The absolute value of these numbers is rather limited, subsidence is not expected to pose an important threat after shut-in for the Groningen gas field.

However, there is some remaining uncertainty. The pressure depletion can be larger than expected – although this is unlikely because the pressure in the reservoir has been history-matched. Also, the compaction coefficient in the aquifer can be different from the values in the gas-bearing parts. Monitoring and interpretation in terms of the driving force can be deployed to better constrain the subsurface mechanical behaviour. Regular subsidence estimates through interpretation of satellite data will help quantifying the surface movement. In addition, they can help constrain the reservoir aquifer compaction and the associated stresses. Aquifer pore pressure measurements would also help greatly to constrain the pressure distribution and the associated compaction field and induced stresses. The optimal amount and the placement of additional wells requires more investigation and sensitivity analysis.

5.3 Induced seismicity

5.3.1 Modelling approach

The Groningen gas field has shown considerable seismicity. Therefore, the risk on seismicity in connected aquifers upon their depletion is an issue deserving attention. We will provide here a brief assessment of the possibility of fault reactivation that underlies seismicity. We base ourselves on the pressure development as given in the previous section. A similar treatment was given by Buijze et al [2019].

The main volume of the depleted reservoir is in reservoir sections which are thin in comparison with their horizontal extent and of which the vertical variation is limited. For such blocks, a uniaxial approximation can be employed when computing deformation as a result of pore pressure changes. Faults that are bounding such blocks or that divide parts of the reservoir into blocks at different heights (faults with offset) need to be treated differently because the approximation of uniaxial behavior cannot be used. Larger changes in stress will develop locally because of stress concentrations developing at the fault.

5.3.1.1 Reactivation in uniaxially deforming parts of the reservoir

To analyse sensitivities of long-term reactivation of faults with no offset after ceasing gas production a workflow has been set up for a quantitative modelling exercise (Figure 5-8). Results of the various steps are briefly described in the following subsections.

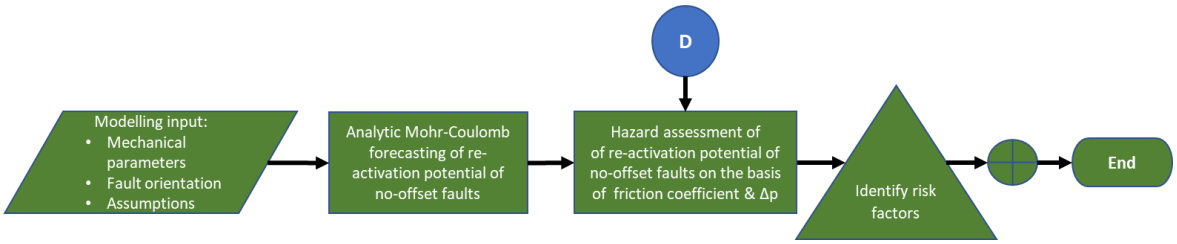

Figure 5-8. Workflow applied for analysis of reactivation potential of faults with no offset in current KEM-19 project; D = input from pressure redistribution modelling; process ends as it is believed that the risk of reactivating faults with no-offset is low.

Uniaxial deformation implies that there is no lateral displacement and the total vertical stress is constant. With Hooke's law including poro-elasticity (Fjaer et al [2008]) the compaction and the change in horizontal stresses can be calculated as a linear function of the pressure change. The proportionality constant is a complex expression containing the Biot coefficient and the Poisson ratio (see the Appendix E).

Both the horizontal and the vertical effective stresses increase upon depletion – i.e. negative pressure change. Whether destabilization takes place is determined by examining the movement of shear stress and the effective normal stress with respect to the Mohr-Coulomb failure envelope. Movement of the stress in the direction of destabilization happens when the slope of the increase in the Mohr diagram is larger than the friction coefficient μ (Figure 5-9). The slope is given by $\frac{\Delta\tau}{\Delta\sigma'}$. Depletion causes a stress development in the direction of destabilization when this number is larger than μ.

Whether destabilization happens depends on the Biot coefficient α, the Poisson ratio ν and the friction coefficient μ itself. For every pair of Biot coefficient α and Poisson ratio ν we can calculate the friction coefficient at which the slope is neutral, i.e. equal to μ.

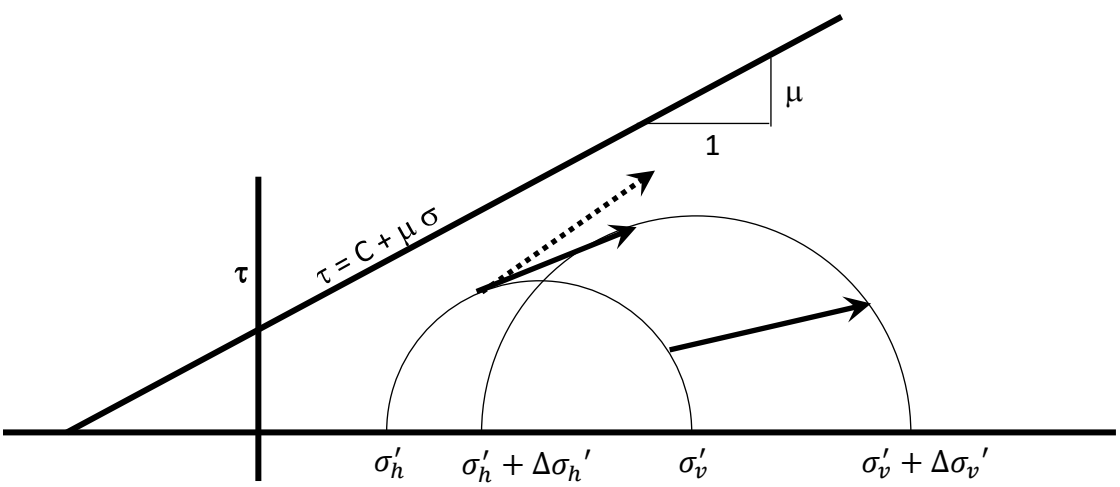

Figure 5-9 Mohr-Coulomb diagram with moving Mohr circle. Depending on the relative movement of the horizontal and vertical effective stresses, the stress for the most critical orientation can move toward or away from criticality

An alternative way to approach the sensitivity to reactivation is by determining the percentage of fault orientations for which the stress develops towards more critical values. In such analysis all possible orientations are considered, not only the most error-prone ones.

Finally, when the stress path is critical, an important question is how much pressure change is required to reach the Mohr-Coulomb failure line. This pressure change can be assessed if both the original distance to the failure line and the rate of movement toward it are known. For the stress at a fault that is most critically oriented we can calculate the stress distance to failure in the Mohr diagram as the distance between the start of the dotted arrow to the failure line in Figure *5-9*. We can also calculate how much this distance changes with a change in pressure when we know how far the arrow will reach upon a change in pressure. Combining these values we can calculate the minimum pressure at which activation can be expected.

5.3.1.2 Reactivation in bounding faults and in offset faults

We also briefly consider faults which show an offset or faults that exhibit a pressure drop between the two sides, i.e. where the behaviour across the two sides of the fault exhibits a discontinuity. The analysis of the long-term reactivation of faults with offset after ceasing gas production has been based on guidelines for pressure depletion at the location of seismic events in aquifers adjacent to the gas reservoir (Figure 5-10). Results of the various steps are briefly described in the following subsections.

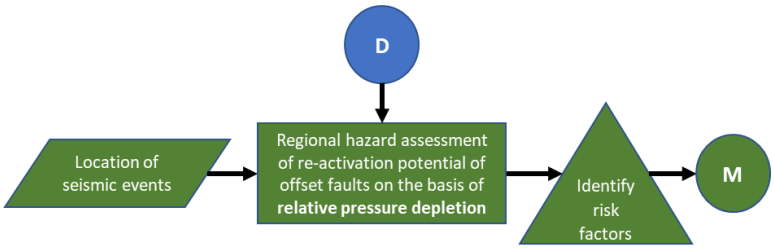

Figure 5-10. Simplified workflow applied for the analysis of reactivation potential of faults with offset in current KEM-19 project; D = input from pressure redistribution modelling; M = input to recommended workflow for quantitative assessment of induced seismicity in Chapter 6

A proper field-specific analysis should map the faults, consider their offsets, quantify the pressure drops around it, incorporate the stress field, and include all uncertainties connected to these parameters. Then the effect of the pressure drop on the stress could be quantified and related to a reactivation model like a Mohr-Coulomb failure analysis or a Dieterich rate-and-state friction approach. It would also integrate observations of seismicity, as well as hypocentre and focal mechanism determination. It would include on- and off-fault plasticity, dynamic behaviour of faults, stress transfer, creep in the reservoir and surrounding formations. Properties of fault gauge, elasticity contrasts, slip-weakening, response of pore pressures to slip, etc. A comprehensive study in this sense is beyond the scope of the current study.

Muntendam-Bos [2021] performed an analysis with some elements of the above description for all the gas fields in the Netherlands. She analysed the stress development on bounding faults and on reservoir-

internal faults with small and large offsets, upon the actual depletion, with the 2D analytical stress solutions by Jansen et al [2019]. Again, the magnitude of the stress change will be proportional to the pressure depletion. Now, in Muntendam-Bos's analysis, the shear capacity utilization reaches criticality in the Groningen gas field at around 43% of the pressure depletion in 2016.

A study like the one by Muntendam-Bos can only give a general idea about the issue of induced seismicity to be expected. Many complexities are not addressed, and a number of caveats must be considered. One issue in this paper is the change of stress ratio as inspired by the larger-than-expected number of fields under a considerable evaporite seal where seismicity occurred. This change appears to be rather ad-hoc. Another is the possibly different slip behaviour of faults in gas-bearing and water-bearing strata. The physical and chemical behaviour of faults which are saturated with water may be different. Further, the vertical extent of the faults and the distribution of pressure along it will be different from typical faults in the gas-bearing part. This can affect both the onset of reactivation and the slip behaviour itself. Yet another issue is the effect of stress changes due to the depleted gas field. Close to the gas field and its large numbers of depletion, Coulomb stresses have already distorted the stresses in the aquifer. Finally, the approach we have followed is completely based on linear poroelastic, behaviour. The mechanical response of Groningen has also shown inelastic creep [Pijnenburg et al, 2018]. This complicates matters, especially when pressure changes are large and long times are considered.

The guidelines of States Supervision of the Mines prescribe the use of a deterministic hazard analysis for induced seismicity as a first screening to determine whether a more elaborate assessment is warranted [SodM, 2016; Van Thienen-Visser et al, 2012]. Although a deterministic approach has limited validity when the uncertainties are large, we discuss it here for completeness. The very first criterion considered is the pressure drop related to the initial pressure. When this ratio is less than 28%, the probability of seismicity is considered negligible. It must be mentioned, however, that the method has been formulated specifically for gas fields, not for aquifers. It is questionable whether pressure depletion in an aquifer will lead to the same activity as a similar pressure depletion in a gas field.

5.3.2 Input data

For the reactivation in uniaxially deforming parts of the reservoir only a sensitivity to the geomechanical analysis is presented. For the reactivation on bounding faults and faults with an offset, we have compared the pressure change that was indicated as a threshold with the actual fields calculated in the previous chapters, and we have incorporated seismic events outside the gas-bearing part of the reservoir, as observed during the production period of Groningen.

5.3.3 Sensitivity analysis results

5.3.3.1 Reactivation in uniaxially deforming parts of the reservoir

Whether pressure depletion in the aquifer results in destabilization is represented in Figure 5-11. For every point in the (ν, α) plane, the friction coefficient must be larger than the indicated value to ensure stabilization upon depletion. Critical movement is reached earlier (neutral coefficients are larger) if the Poisson ratio is smaller or the Biot coefficient is larger.

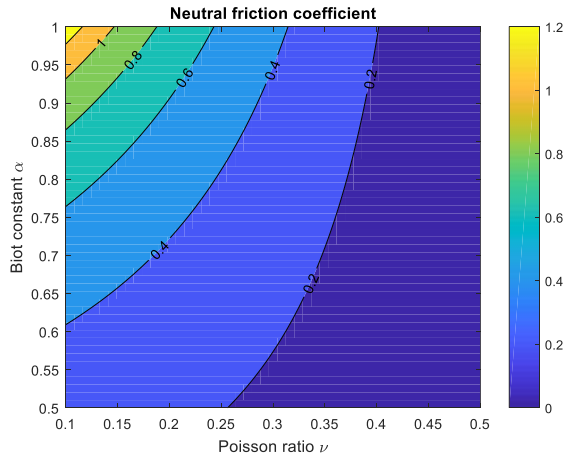

Figure 5-11 Friction coefficient for which stress development upon depletion is neutral. This is the minimum coefficient for which the stress depletion is not towards critical numbers

The next step to approach the sensitivity to reactivation is by determining the percentage of fault orientations for which the stress develops towards more critical values. As an example, consider a friction coefficient of 0.4. The combination of Biot constant and Poisson ratio for which the most error-prone fault orientation moves towards criticality is to the left-upper part of Figure 5-11, left and above the line indicated with 0.4. Only in that region, there are fault orientations possibly moving towards criticality. We have quantified the percentage of possible orientations, inspired by the work of Levandowski [2018]. We calculated the stress path for a number of evenly distributed fault orientations in a horizontally isotropic normal stress field. Then, we determined the fraction of paths that are critical when the friction coefficient is 0.4 or 0.6, respectively. The results are represented in Figure 5-12.

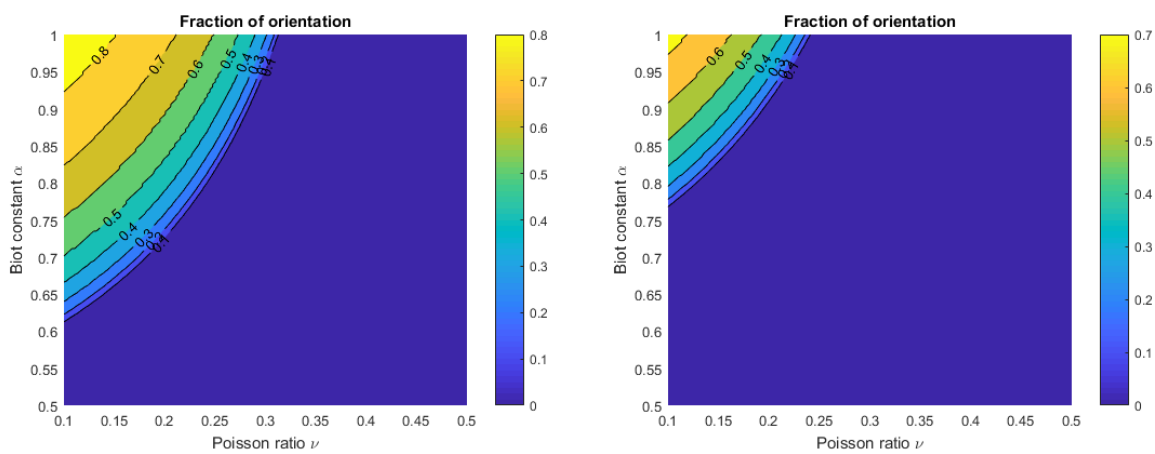

Figure 5-12 Fraction of fault orientations that are critical for different combinations of Biot constant and Poisson ratio, for friction coefficient 0.4 (left) and 0.6 (right).

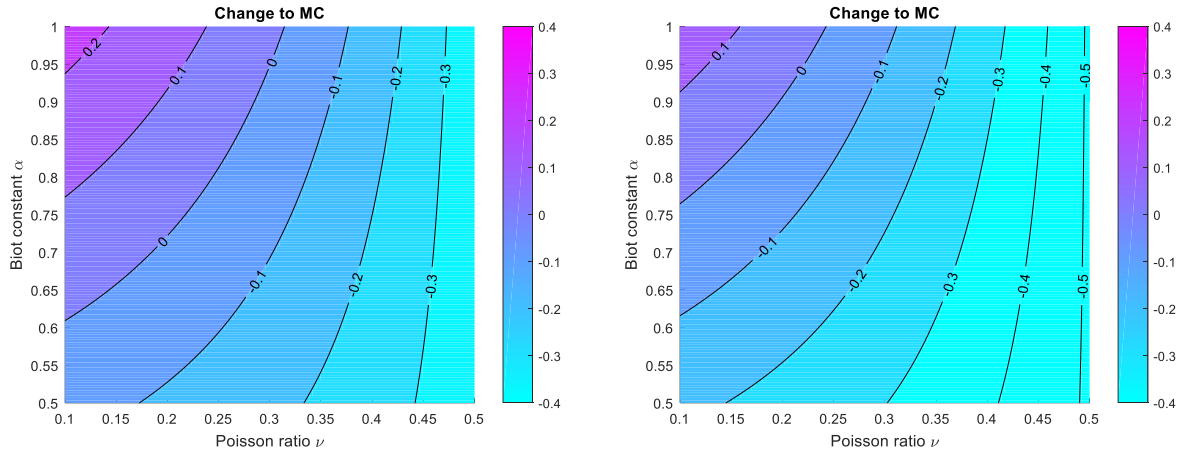

Figure 5-13 Change of distance to failure line as fraction of pressure change. Left: friction $\mu = 0.4$. Right: friction $\mu = 0.6$. As an example, a value of 0.1 indicates that 10 MPa change in pressure will change the stress at a fault at the most critical orientation towards the failure line with 1 MPa. The Change = 0 lines coincide with the lines of neutral friction coefficient for $\mu = 0.4$ and $\mu = 0.6$ in Figure 5-11.

Finally, we wish to assess the pressure change that is required for activation. In the scheme of Figure *5-9* we want to know how much pressure change we need to bring the end of the dotted arrow to the failure line. We need for that the original stress field. In the Groningen area this field is arguably not critical [Van Wees et al, 2014, Van Eijs, 2015, Muntendam-Bos, 2021]. The estimate leading to the most critical initial stress state in Groningen has been given by Muntendam-Bos [2021] on the basis of earlier leakoff tests but with a correction for the effect of overlying evaporites. She used a stress ratio σ_h/σ_v of ~0.7 for the Rotliegend reservoirs. With zero cohesion and a friction coefficient of 0.6 this corresponds to a distance to the failure envelope of approximately 4.5 MPa at 3.4 km depth. The Poisson ratio of the formations in Groningen are of the order 0.2 – 0.3 [Muntendam-Bos, 2021]. Reactivation of no-offset faults is then only possible for MC friction parameters of 0.6 or smaller, and for pressure drops that exceed 10 times the distance to the MC line, i.e. ~45 MPa. Even incorporating a factor 2 for safety, the pressure depletion would have to be more than 20 MPa. This is much larger than the pressure drops envisaged in the aquifers studied.

All these results suggest that reactivation of an internal fault in the depleting aquifer without offset and without pressure drop across it is unlikely to show reactivation. This is an important observation, since the largest events in Groningen have been observed on faults with small or zero offset, consistent with numerical evaluations [Buijze et al, 2019]. The levels of depletion required for activation of no-offset faults have been reached in the later stages of the depletion of the Groningen gas field but will not be reached in the connected aquifers.

5.3.3.2 Reactivation in bounding faults and in offset faults

Seismic events in Groningen typically start earlier on bounding faults and faults that exhibit considerable offset than on faults without offset and without pressure drop across it. This was already indicated by the value of depletion of 43% of the total pressure drop. Still, 43% is considerably more than the values reached in the aquifer as reported in the previous Chapter and reactivation based on this criterion is

unlikely, except very close to the gas reservoir outline. However, the margins are considerably smaller than when considering non-offset faults.

Following the guidelines of States Supervision of the Mines, we need to calculate whether the relative pressure drop is larger than 28% of the virgin value. Based on the relative pressure fields presented in Figure 5-14, the pressure drops are smaller in virtually the complete aquifer. For the parts of the aquifer where a larger pressure drop is envisaged, the fault density and the elastic modulus contrast between overburden and aquifer must be studied in more detail. We recommend a more elaborate geological and reservoir characterization than possible in the present study to be able to do such analysis. Starting with an identification of the regions where the largest pressure drops after shut-in occur, the most important faults in those regions should be mapped. In particular their offset and dip are important for the stress analysis. Ranges of input parameters should then be defined and the Janssen et al model [2019] could be used to calculate stress drop and activation risk.

A preliminary insight can be provided by mapping the seismicity in the aquifer that has already been detected. These events are also given in the 2025 map in Figure 5-14. The white dots indicate the events which have been attributed to the Groningen gas field and are located outside the boundary of the gas reservoir. Seismic events associated with nearby fields have been excluded since our study has not accounted for the pressure drops in those fields.

A number of issues must be mentioned here. In the first place, the uncertainty of the localization of the events is such that events within a distance of 3 km of a gas field are usually attributed to that gas field. These events can therefore not be unequivocally associated with the aquifer. The 7 events in the mid-west can be associated with the Bedum field. Still, we see more events northwest and southwest of the field than in other locations. Those are exactly the locations where the aquifer is in pressure contact with the gas reservoir and some aquifer depletion is seen. Therefore, the conclusion that pressure drop is the first main driver of seismicity is underlined. This is in line with the conclusion of Muntendam-Bos et al (2022).

Four seismic events fall outside the 3-km distance contour from the gas field. Three of them are located in the southwest. The locations of these events, however, reveals that they could also be connected to nearby gas fields not studied in the present context, Pasop, Roden and Vries. These fields are known to have active aquifers which extend in the direction of the Groningen field. NAM (Zeeuw en Geurtsen, 2018) has assumed that these fields cause pressure drop at the locations of the 3 events identified. The lack of north-south orientated faults in this area could explain the good connectivity, however, no direct pressure observations are available to support this. The remaining event in the northwest is located far into the Waddensea. The mechanism there is not yet completely clear.

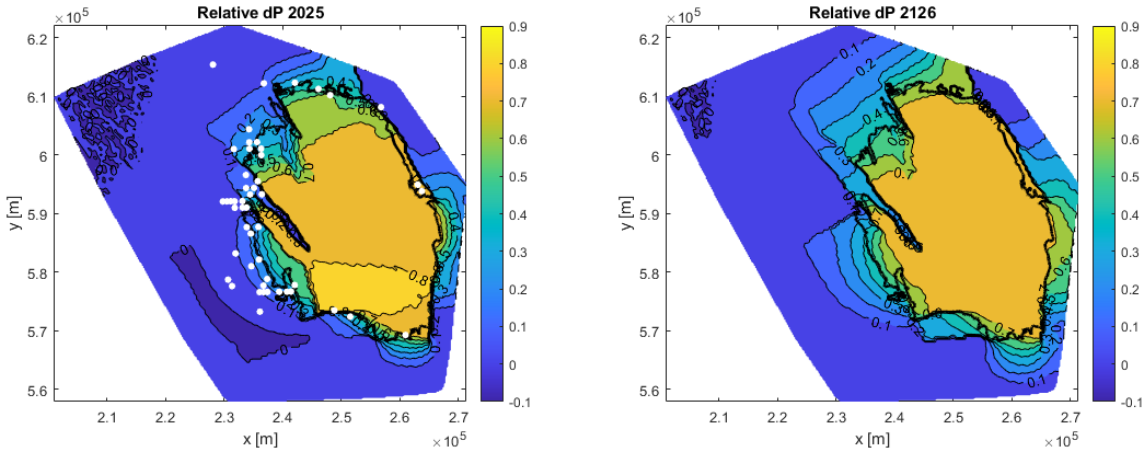

Figure 5-14 Base case pressure drop relative to initial pressure, in 2025 (left) and 2126 (right). The seismic events which happened during production, and which are located outside the boundary of the gas-bearing layers, are indicated with white dots

5.3.4 Conclusion

Induced seismicity is related to depletion. This in in line with conclusions in the context of the study of Muntendam-Bos et al (2022) assessing all events of induced seismicity in the Netherlands.

We have limited ourselves here to identifying critical factors for fault reactivation. Induced seismicity is always caused by reactivation of faults, therefore fault reactivation is a first proxy for induced seismicity. Too large criticality on a fault can result in exceedance of the slip resistance and induce slip behaviour. When the fault is slip-weakening, seismicity may take place. A first estimate of such behaviour is therefore a slip tendency assessment. A full analysis, however, involves also the identification whether slip is seismic or aseismic, rupture modelling, magnitude determination, and risk analysis based on such aspects. Such a study involves a scope much larger than was possible within the present setup.

Reactivation of faults without offset and without pressure drop across it is unlikely in the aquifers connected to the Groningen gas field, because they require large pore pressure drops. This is an important outcome since these fault types in the Groningen field are usually responsible for the larger events. The pressure drops in the gas-bearing parts of the Groningen field are much larger than in the aquifer, thus making possible the activation of non-offset faults in the gas-bearing parts at the later stages of the field life.

Offset faults and bounding faults which are present in the southwest and northwest aquifers can show reactivation upon the ongoing depletion of the aquifers in those regions. Figure 5-14 (right) clearly shows the expected extension of depletion after 100 years of shut-in. The variability in these areas is, according to the results presented earlier, limited. It is therefore important to follow the present study up with a more in-depth geomechanical study of the behaviour of the aquifers in the southwest and the northwest. In such a study, the incorporation of nearby gas fields is critical. In addition, more information is required with regard to the parameters involved: fault locations, orientations, and frictional properties, but also general mechanical properties like the virgin stress field, stress anisotropy and subsurface heterogeneity.

A monitoring system needs to be kept in place to map all possible future seismicity. Building that database and incorporating the acquired knowledge in the models will help constrain the uncertainties and sharpen forecasts.

5.4 Fluid migration along wells to biosphere

The goal of the proposed numerical model in this project is to calculate the extent of the methane plume in a shallow aquifer over long time frames (100 years or more). This includes the saturation of free methane near the leakage site and the level of dissolved methane in the water. This enables the regulators and operators to understand the extent of methane contamination of the aquifer over time and judge the necessity of a mitigation strategy. In addition, understanding the expected radius and intensity of the methane plume can assist with the design of monitoring campaigns. Particularly, the rate and location of water sampling needed to monitor the methane levels in aquifers.

The geological setting and formation properties will control the methane contamination levels of shallow aquifers. The focus of the numerical model will be on the wells in the Groningen field, in the Netherlands. However, the qualitative impact of various risk factors on well leakage should be applicable to different regions. After analyzing the logs and lithostratigraphy of the wells in the area, we selected the ZWD-01 well to be the focus of the case study. The Zechstein salt formation (the caprock) is thin at this well's location and a thick section of an organic-rich claystone at a depth of nearly 2 km is present, which could be a source of gas. The ZWD-01 well also intersects shallow coal seams that could also act as sources of methane. Considering the higher potential leakage risks in the ZWD-01 well (thinner Zechstein and thicker organic-rich claystone), the numerical model will be based on the geology at the ZWD-01 well location. The formation properties will be collected from different sources, such as ThermoGIS for the aquifers, well logs and reports from NLOG, and NAM reports. Where relevant data is lacking, we will use estimates based on the values reported in the literature.

To analyse sensitivities of fluid migration along wells a workflow has been setup for a numerical modelling exercise (Figure 5-15). Results of the various steps are briefly described in the following subsections.

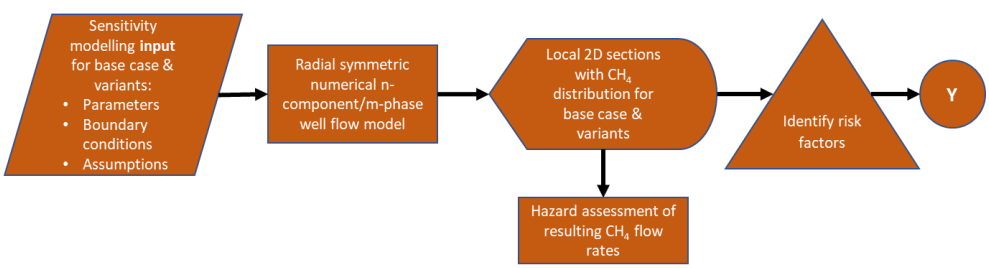

Figure 5-15. Workflow applied for sensitivity analysis of CH_4 migration along wells to the biosphere in current KEM-19 project: Y = input to recommended workflow for quantitative regional assessment of fluid leakage via wells (see Chapter 6)

5.4.1 Modelling approach

In this section, a brief summary of the modelling approach and the results is presented. A more detailed description of the modelling approach, input data, and results, is provided in Appendix D.

The numerical simulations in this work were conducted using the commercial compositional simulator, CMG GEM. A two-phase (gas and liquid), two-component (methane and water) model was developed with a 2D axisymmetric geometry around the wellbore. The modelled domain is a cylindrical wedge around the wellbore. Only one grid is considered in the tangential direction, effectively making the model two dimensional. This geometry is valid assuming that the formations are homogeneous in the horizontal direction. The model extends from the base of the Slochteren Formation (the main reservoir) up to the surface for a total depth of approximately 3000 m. The outer radius of the model is 1 km, while the inner radius is the radius of the cement sheath in the well.

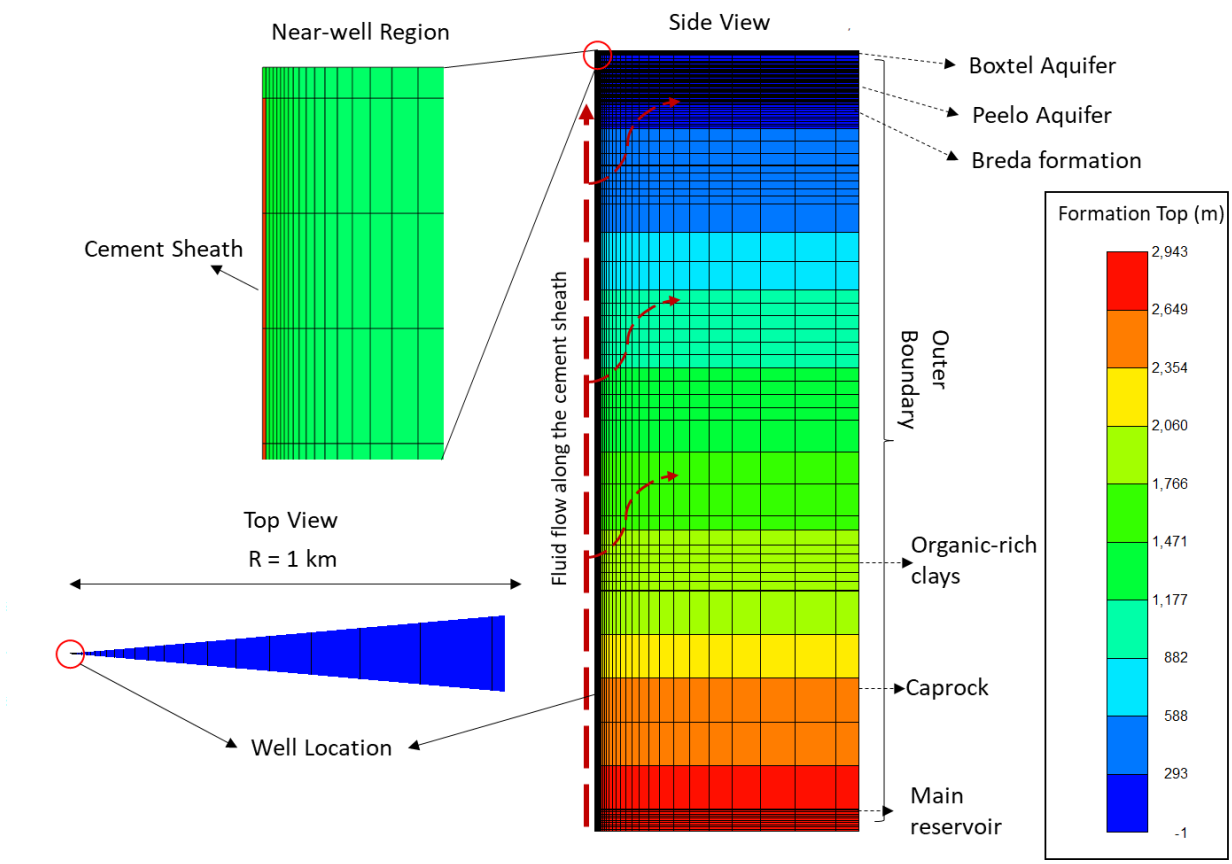

Figure 5-16: A schematic of the domain of the numerical study. The near-well region is magnified on the top left (color scheme correlates with permeability). The bottom left section shows the top view of the cylindrical wedge with a radius of 1 km. The well (cement sheath) is located at the left corner of the wedge and connects all the formations. The image in the center illustrates the side view of the domain. The stratigraphy in the region is summarized and represented in the model from the base of the reservoir at the depth of 2950 m, to the surface at sea level.

Figure 5-16 illustrates the schematic of the domain of the numerical model. The grid blocks at the left corner of the cylindrical wedge represent the cement sheath. The cement sheath connects all the formations from the reservoir all the way to the atmosphere. The fluid leakage along the well is assumed to occur through the cement sheath. The casing on the left of the cement sheath is assumed to be a no-flow boundary. A no-flow boundary is also assumed at the base of the reservoir. The outer boundary on the right side of the wedge is assumed to be at a constant pressure. The radius of the wedge is large enough that the impact of gas leakage over 100 years does not reach the boundary in any of the simulations in this work. The top of the model is assumed to be at a constant pressure representing the atmosphere.

5.4.2 Input data

There is uncertainty associated with the input parameters for the numerical model. We attempted to collect all the available data to constrain the parameters and use best assumptions from the literature. The goal of this simulation exercise is to conceptualize a risk assessment framework for well leakage in the study area. Therefore, the focus of the simulation study was placed on the impact of the presence of various gas sources in the system and the cement sheath damage, indicating the permeability of the leakage pathway. A more comprehensive sensitivity analysis of the impact of the multiphase flow parameters on well leakage can be found in the literature (Nowamooz et al., 2015; Rice et al., 2018; Reagan et al., 2015).

Based on the stratigraphy and the gas shows during drilling (www.dinoloket.nl, EBN Gas Shows database, retrieved Jan. 2021), three potential sources of free gas were identified: the Slochteren Formation (main reservoir), Organic-rich clays (OC), and the Breda Formation (BRD). The gas saturation in the reservoir is approximately 80% (SGS Horizon BV, 2016). However, the saturation is uncertain in the remaining two potential gas sources (The organic-rich clay and the Breda Formation). We used 10% and 60% gas saturations for both sources to investigate the impact of the uncertainty in saturation. The permeability of the shallow sources (OC and BRD) was also changed by an order of magnitude to quantify the impact of the uncertainty. The cement sheath was considered to be mildly or extremely damaged. Based on the recent analyses in the literature, average cement sheath permeability of 100 md is at the top of the range of the measured or inferred values in wells (Gasda et al., 2013; Kang et al., 2015; Tao and Bryant, 2014; Moghadam et al., 2020; Moghadam et al., 2021). Therefore, an extremely damaged cement sheath is assumed to have a permeability of 100 mD. A mildly damaged cement sheath is assigned an average permeability of 1 mD.

The simulation domain is initialized assuming all the formations are fully saturated with water, except 1 to 3 formations that potentially contain free gas (depending on the simulation case). The water gas contact in the reservoir is below the base of the model (only gas cap is modelled in the reservoir). The initial pressure in the entire model was hydrostatic, except the caprock and the reservoir. The caprock in this field is over pressured by approximately 11 MPa and is modelled as an ultra-low permeability porous medium. The reservoir was initialized at its expected abandonment pressure of 6 MPa, likely in 2023. Methane is assumed to be dissolved in water in all the formations, except the freshwater aquifers (Boxtel and Peelo). In total 25 cases were considered. All simulations were run for 100 years after the start of gas leakage.

5.4.3 Sensitivity analysis results

Cases 1 to 9 assume the reservoir to be the only source of gas. The results indicate that methane does not escape the reservoir through the cement sheath, as long as the reservoir pressure is sufficiently below hydrostatic. Due to the depleted pressure state of the reservoir, water from the caprock and permeable overlying formations flows into the reservoir through the cement sheath (some water will also flow from the caprock to the reservoir directly but is ignored in this study). The water leakage into the reservoir increases the pressure and water saturation around the well. Figure 5-17 illustrates the pore pressure and water saturation at the top of the reservoir after 100 years. For the extremely damaged cement sheath, the pressure near the wellbore increases by 500, to 6500 kPa and the water saturation increases to 0.45, from 0.2. This pressure increase is relatively small and should not lead to adverse effects near the wellbore. The results overall indicate that even for a highly damaged cement sheath, a highly depleted reservoir is not a major risk for gas leakage. Buoyancy, diffusion, and localized pressurization are not strong enough to counteract the large downward pressure gradient, rendering upward gas flow unlikely. However, for this to be the case, the reservoir needs to be sufficiently depleted. We have included a more detailed discussion on gas flow out of a depleted gas zone in the Appendix D.3.1.

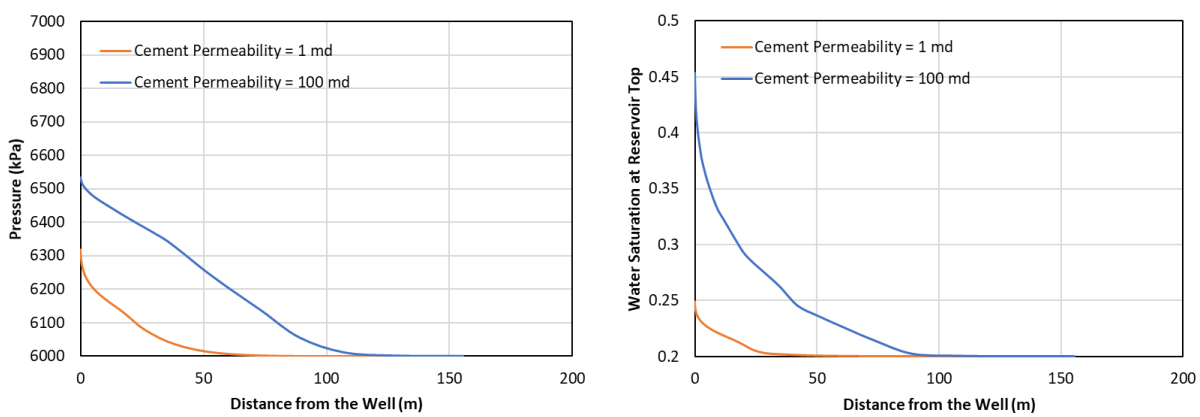

Figure 5-17: Pressure and water saturation at the top of the reservoir after 100 years.

Cases 10 to 19 consider both the reservoir and the Organic-rich clays (OC) to be sources of free gas. The reservoir is set to its abandonment pressure of 6 MPa for all the OC related cases. A point of uncertainty for the OC layer is the gas saturation. We considered gas saturations of 10 and 60% to investigate its impact on the leakage rate, while critical gas saturation for the OC layer was assumed to be 10%. At 10% gas saturation the leakage is entirely due to diffusive flow. Only when gas saturation in the OC layer goes above the critical saturation, bulk gas flow can occur.

For the bulk phase flow, the cement permeability becomes the dominant parameter controlling the leakage rate. Figure 5-18 illustrates the leakage rate into the atmosphere and the Peelo aquifer for the mildly and extremely damaged cement sheaths. The results show a higher leakage rate into the Peelo aquifer compared to the atmosphere. Mild cement damage leads to small steady-state leakage rates, 24 and 8 kg/year for the Peelo aquifer and atmosphere, respectively. The extremely damaged cement sheath

shows significantly higher leakage rates, 3400 and 800 kg/year for the Peelo and atmosphere, respectively. In total, 4200 kg/year of methane leaks into the aquifer/atmosphere system.

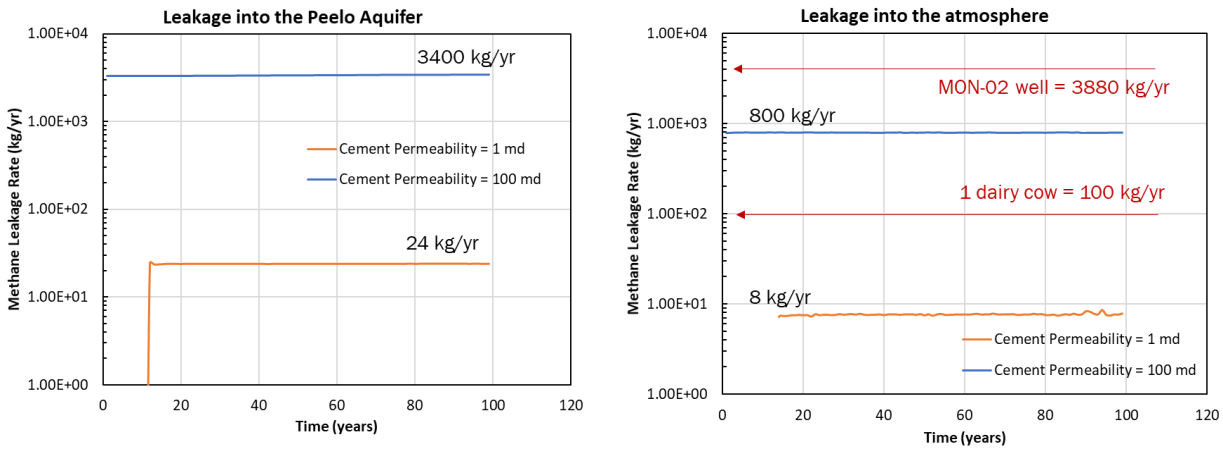

Figure 5-18: Methane leakage rate into the atmosphere and Peelo aquifer for mildly and extremely damaged cement sheaths (cases 12 and 16).

For context, the MON-02 well in the Netherlands had an estimated leakage rate of 3880 kg/year into the atmosphere (Schout et al., 2019). Boxtel aquifer does not show significant accumulation of methane in any of our simulations. Most of the methane that enters the unconfined Boxtel aquifer escapes to the atmosphere. Therefore, there is minimal methane accumulation in the formation.

A similar analysis is conduced assuming Breda Formation is the source of free gas. Cases 20 to 25 cover various scenarios pertaining to the Breda Formation. Figure 5-19 shows the methane leakage rate in the Peelo aquifer for several cases that assume a mildly damaged cement. The leakage rate into the atmosphere is not shown as the values are too small (less than 10 kg/year). Case 20 assumes a gas saturation of 10%, which is below the critical saturation. No leakage is observed due to a lack of bulk phase flow in gas. Gas saturation in case 21 is 60% which leads to a leak rate of 115 kg/yr. Case 22 considers a permeability of 10 md for the Breda Formation, up from 1 mD. The increase in permeability only increases the leak rate from 115 to 124 kg/yr. This is consistent with the results from the OC analysis, that source rock permeability does not appear to increase the leak rate significantly. This is likely due to the fact that the limited cement permeability is choking the gas leakage. Case 23 assumes both an increase in permeability and a 10% over-pressure in Breda Formation. The leakage rate in this case increases to 330 kg/yr.

Overall, the mildly damaged cement shows a higher leakage rate from Breda Formation compared to the OC formation with an approximately five-fold increase (ranged from 20's to 100 kg/yr). The shorter leak distance between the source and the surface is expected to increase the leakage rate. Another factor is the lack of intermediate formations between the Breda and the shallow aquifers. Presence of shallow gas is more detrimental if no permeable formations exist between the source and the aquifers to act as a buffer.

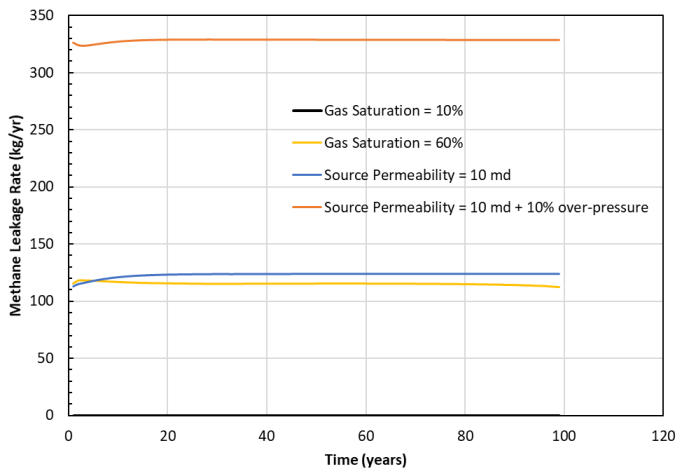

Figure 5-19: Methane leakage rate in the Peelo aquifer for the mild cement damage assuming Breda is a gas source (cases 20 to 23).

5.4.4 Conclusions

The following conclusions can be drawn from the numerical modelling of gas leakage along an abandoned wellbore:

The leakage is fundamentally balanced between the capacity of the source to leak, the capacity of the cement sheath to transport, and the capacity of the aquifer/atmosphere system to receive the leaking gas. Depending on the parameters of the system, one of these links in the flow chain can be the controlling one. In the OC case, the cement sheath permeability plays the dominant role in controlling leakage. At a high cement permeability in the Breda case, the source permeability plays the dominant role.

Gas source

A highly depleted reservoir is not a likely source of gas leakage, as long as the gas flow potential (defined as: $\Phi = P - \rho g z$) at the top of the reservoir pressure is below the gas potential of the closest aquifer overlying the caprock (please refer to Appendix D.3.1.1.2). Based on our results for the Groningen reservoir in the region of study gas pressure must be above 20 MPa for leakage to begin (Appendix D.3.1.1.2). Considering the abandonment pressure of 6 MPa, the reservoir in the Groningen field will not be a likely source of leakage. Buoyancy and diffusion are not sufficient forces against the pressure gradient (across the cement sheath, between the reservoir and the shallow aquifers), if the reservoir is sufficiently depleted. It is more likely that water moves into the reservoir through a damaged cement sheath. However, this should not lead to reservoir pressurization due to high compressibility of gas. Smaller depleted reservoirs with an active water-drive that can re-pressurize the gas after abandonment could still become a leak source.

Cement damage and the gas source

For a mildly damaged cement sheath with an average permeability of 1 mD, all scenarios show relatively low levels of gas leakage. The highest value in cases 1 to 9 was 31 kg/year, well below average emissions

of a dairy cow (100 kg/year). When the cement sheath is extremely damaged (100 mD average permeability), methane flow (biogenic or thermogenic in origin) into the freshwater aquifers is likely. If the gas source is sufficiently depleted, the magnitude of the leakage is expected to be small (under 20 kg/year) with a plume extending up to 20 m away from the well after 100 years. The source of gas will likely be dissolved methane in the underlying formations, not the gas from the target reservoir.
If the reservoir and the caprock are at hydrostatic pressure (a case for new/active leaky wells), extreme cement damage can lead to significant methane leakage into the atmosphere and aquifers. In this case methane plume can extend hundreds of meters away from the well after 100 years. Free gas can accumulate at the top of the Peelo aquifer. The worst-case scenario indicates a leak rate of a few tons of methane per year into the atmosphere and aquifers.

Shallower formations
Presence of gas at hydrostatic pressure in formations shallower than the target reservoir can lead to methane leakage along the damaged cement sheath. Shallower gas sources at or above hydrostatic pressure can lead to higher leakage rates due to the shorter travel distance. Gas saturation in the shallow formation has to be above the critical saturation to lead to significant leakage (due to advective flow).
The majority of the leaked gas will be stored at the base of aquitards making them suitable locations for sampling. Unconfined aquifers such as the Boxtel Formation will not store significant amounts of the leaked gas. Permeable intermediate formations between the source and aquifers can act as gas storage. Natural groundwater flow in aquifers can change the extent of the methane plume in their direction, while reducing the size of the plume in the opposite direction. The quantitative impact of groundwater flow is not studied in this work. Lack of permeable formations to store the leaking gas can also increase the ultimate leakage into the atmosphere and aquifers.

Monitoring
Water sampling should be done at the top of the deepest aquifer, as close as possible to the wellbore (ideally less than 100 m, and no more than 500 m). The sampling should be done in the direction of the groundwater flow at the well location for more concrete results.

6 Recommendations for quantitative hazard & risk assessment and monitoring

Building on the work carried out in KEM-19 which has been described in the previous chapters 4 and 5, an approach will be proposed for the quantitative hazard and risk assessment of pressure and stress re-equilibration after the production of gas has stopped and the related facilities have been abandoned. Also preliminary monitoring strategies will be recommended, in particular for the pressure evolution in the deep subsurface, leakage of methane in the shallow subsurface, and seismic or aseismic ground movement.

The risk assessment focuses on the following undesired aspects in regions with abandoned gas fields:

- Pressure redistribution as a consequence of depletion of gas reservoirs
- Vertical migration of fluids to shallow aquifers and surface water
    - Via wells
    - Via geological pathways
- Ground movement
    - Subsidence and uplift
    - Induced seismicity

These physical processes could lead to damage to built-up areas or infrastructure, to quality of potable water resources or to interference with other production or storage activities in the subsurface.

Quantitative modelling work including sensitivity analysis has been done for pressure redistribution, fluid migration along wells, subsidence, and, to some extent, for seismic ground movement. Conceptual models have been defined for migration along geological pathways but no quantitative modelling. Interference with other subsurface activities was described in qualitative terms. This implies that the recommendations for further development of approaches for quantitative hazard and risk assessment work starts at different levels of maturity for the individual items listed above.

The quantitative modelling work in the KEM-19 project dealt primarily with characterisation of the hazards and much less on the resulting damage to buildings and other infrastructure, to the quality of potable water and to undesired interference with other activities in the deep subsurface. This will require particular attention in the recommendations. Also the (re-)definition of suitable assessment time frames and assessment metrics will be touched upon.

Outcomes of the recommended regional quantitative assessment and monitoring are meant to inform companies and other organisations who are active in performing subsurface production or storage activities or intend to do so in the future. It is of particular interest to entities who are involved in subsurface activities within the Area of Influence of past mining activities, e.g. gas production. When assessing the HSE footprint they will need to take the long-term mechanical or hydraulic effects of past gas production activities into account. These companies may be active in production of geothermal

energy, energy storage, storage of natural gas, CO_2 or hydrogen, production of oil or gas or salt extraction. Results from the regional assessment and monitoring are also relevant for people living in the neighbourhood.

The recommended assessment work is relevant for the Ministry of Economic Affairs and Climate Policy and the State Supervision of Mines in the Netherlands to develop policies and regulation for the management of past subsurface production and storage activities and the development of guidance for new subsurface activities in the Area of Influence of past subsurface production or storage. The recommended assessment of past mining activities is of specific interest for the development of an approach for seismic hazard and risk assessment of geothermal operations.

Other stakeholders are representatives at the provincial and municipal levels as well as citizen interest groups and individuals.

6.1 Pressure redistribution and lateral migration

The quantification of the pressure redistribution due to lateral migration of fluids in the deep subsurface as a consequence of past gas production plays a central role in the hazard and risk assessment as it feeds into several other parts of the quantitative evaluation, including ground movement and interference with other subsurface activities.

Figure 6-1 shows the workflow proposed for the assessment of the regional pressure redistribution after the abandonment of producing gas reservoirs. This work builds on the outcome of the sensitivity analysis (depicted with A), the results of which have been described in Section 5.1. The outcome of this analysis is used in other parts of the hazard and risk assessment (indicated with B).

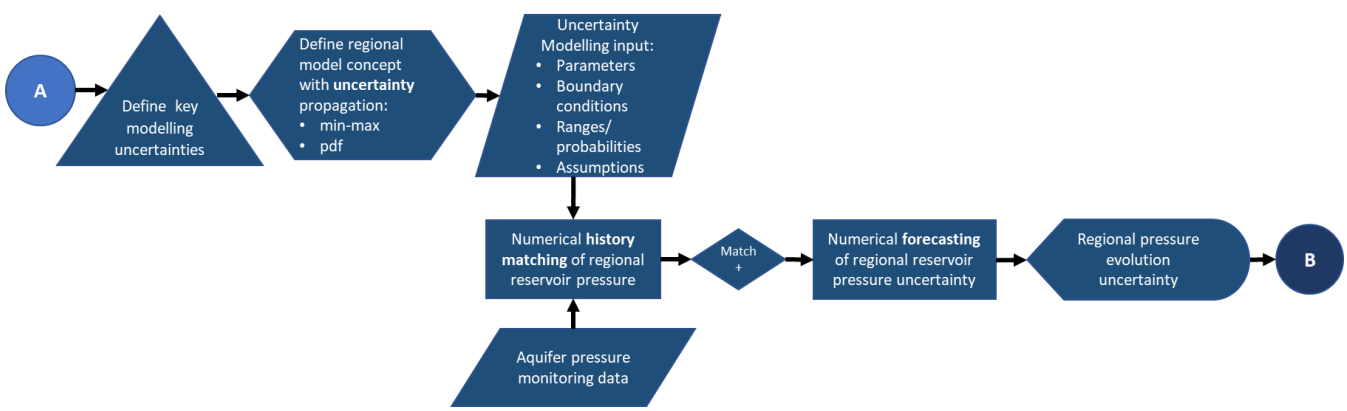

Figure 6-1 Proposed workflow for the quantitative assessment of regional pressure redistribution in the deep subsurface with input from the sensitivity analysis in the KEM-19 project (A) and output to the assessment of vertical fluid flow, ground motion and interference (B); flow diagram symbols are explained in Appendix A.

A first preparatory decision is to be taken on the *key uncertainties* to be included in the quantitative modelling. These will at least include the permeability of the aquifers, the faults properties (position,

orientation, permeability), the position and type of the model boundaries and the presence of gas. The modelling concept will build on the approach developed for the sensitivity analysis. A challenge is to define a pragmatic approach for the propagation of the uncertainties in the quantitative modelling. The history matching should preferably incorporate pressure monitoring data in wells transecting the aquifers adjacent to the gas reservoirs. The outcome of the pressure evolution modelling with propagated uncertainties is used as input for the hazard and risk assessment of fluid migration and ground movement (see Section 6.2 and 6.3).

The metrics to be produced include pressure related parameters like pressure (P), pressure depletion (ΔP) and relative pressure depletion (ΔP_{rel}) for different time steps on decadal to centennial time scales. Time scales could extend to several centuries. Only very little repressurization of the Groningen gas field is expected on a time scale of up to 500 years (up to about 10 bar averaged over the gas reservoir), thus a steady state condition with pre-production pressure distribution in the gas field is only expected to occur on geological timescales. The rate of pressure change will decrease with time and thus monitoring frequency can decrease. To express the uncertainty, one could represent pressure values for p_{10}, p_{50} and/or p_{90} or more simply p_{min}, p_{av}, p_{max} depending on the approach to express uncertainty.

The proposed workflow and metrics for regional analysis provides insight in the regional hazard distribution and uncertainties, however for local analysis these results are likely to be too coarse. At the local scale, more detailed analysis is required including the information from small gas fields in the vicinity and a more detailed representation of faults. The results from the regional workflow can be used as input for the local scale, in particular for the boundary conditions. An example of a smaller region requiring a local model is the Southern Lauwerszee Trough. The aquifer in this area has few barriers in north-south direction and appears to deplete both due to the Groningen field and the small gas fields in the west (Roden, Vries and Pasop). Although seismicity has been observed in the aquifer in this area, it is not unequivocally clear that they can all be attributed to the pressure drop in the aquifer; (see Section 5.3). The model area could be bounded on the east by the Groningen field, which can serve as a time-varying pressure boundary condition. To the north, the very low permeable fault between the northern and southern Lauwerszee Trough can be used as boundary condition (NAM 2020). To the west, the small gas fields and the gas storage site Norg should be included and history matched. Although the coarse model used here did not show depletion from the Groningen field near Norg in the near future, a more detailed study including the depletion from the small gas fields, could lead to more certainty on this topic. The south boundary can probably be the bounding fault of the Annerveen field, but this requires some further investigation. For other locations, different choices for the boundary conditions will be appropriate and additional data collection may be required, for example to the east of the Groningen field.

6.2 Fluid migration to biosphere

Past gas production activities may trigger the vertical migration of fluids, e.g. natural gas, along geological pathways or wells and influence the quality of potable water in the shallow subsurface or at the surface. The current assessment is restricted to the incremental effects of gas production. Quantitative modelling work has been done for migration of fluids along well, the results of which are presented in Chapter 5. For the migration along geological pathways conceptual models have been developed but which have not been quantitatively assessed. So the starting points for defining recommendations for quantitative assessment of migration along wells and geological pathways differ strongly.

6.2.1 Fluid migration along geological pathways to biosphere

A quantitative risk analysis for fluid migration to shallow freshwater aquifers is challenging since the assessment of the magnitude of the consequences is associated with large assumptions about migration pathways and associated with many unknowns. It is easy to discard the probability of fluid migration to be insignificant based on not well-founded ideas about the processes at play and properties of the seal and rock sequence. Therefore, there is a danger that biases, beliefs or ruling theories are adopted if the hazard not elaborated further. To identify the actual threats and the potential impacts it is advised to first further develop a conceptual model of potential pathways with a team of experts from different fields. This reduces the chance that potential threats or impacts are overlooked, all potential pathways are taken into account and a validated hypothesis is formulated.

Conceptual models of fluid migration along geological pathways for the general Groningen setting have been described and illustrated with graphs and fault tree diagrams in Chapter 4 and Appendix B. Subsequently, a fault tree analysis can be progressed and consolidated out which describes the sequence of events and conditions that need to be fulfilled before undesired consequences take place. This intuitive way of representing the different steps to failure aid in the identification of preventive and mitigation measures and the design of a monitoring strategy (see Section 6.5). In addition, by associating probabilities to the different events a semi-quantitative estimate can be made of failure. Further details of the fault tree analysis method are in Appendix B.

This represents the starting point (C in Figure 6-2) for the recommendations for quantitative hazard (and risk) assessment of fluid flow to shallow freshwater aquifers or surface water.

After consolidation of the different potential geological migration routes for fluids which have been identified in this project, it is suggested to select the plausible and most critical pathways for an in-depth sensitivity analysis of the migration and leakage hazard. An example workflow is presented in the upper part of Figure *6-2*. In case scenarios with significant leakage hazard have been identified, this could be followed up by a systematic regional quantitative assessment of the leakage hazard and its consequences for groundwater quality (see lower part of Figure *6-2*). This might for example be the case in areas with a very thin (<50 m) or absent rock-salt seal. The outcome of the assessment may indicate areas with a significant geological leakage hazard where monitoring of methane concentration could be beneficial. Suitable assessment metrics in line with existing rules for compliance need to be defined; these could

include methane leakage rate, saturation or another concentration term and plume extent for different time steps. Agreement should be reached on the time frame to be considered.

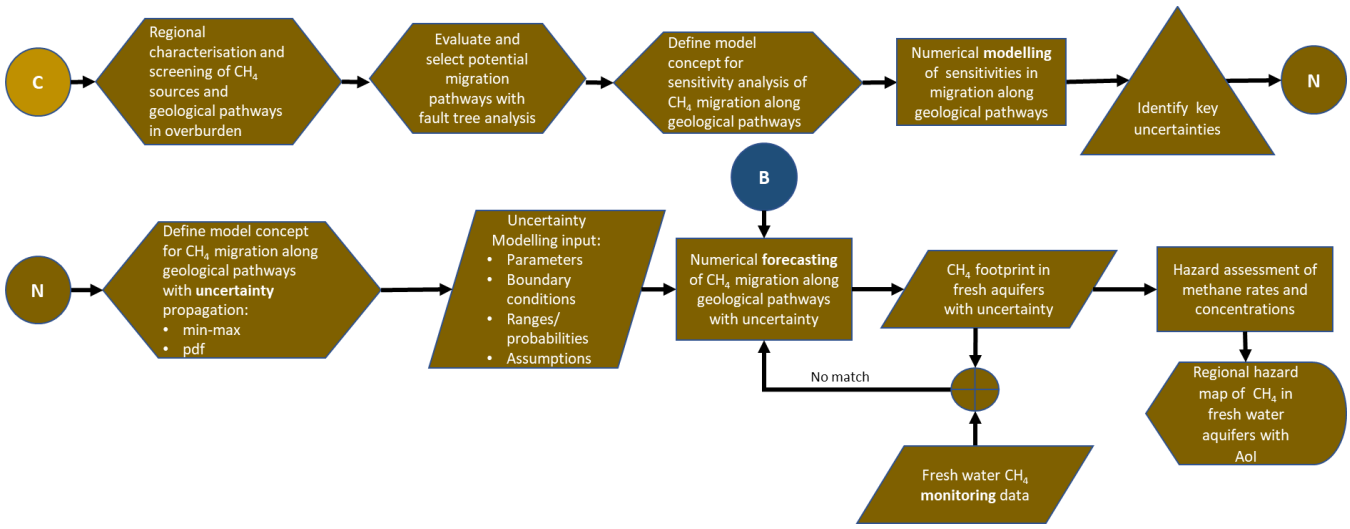

Figure 6-2 Flow diagram for the hazard (and risk) assessment of fluid migration along geological pathways to shallow fresh water resources or to surface water. The upper part depicts a flow diagram to identify main uncertainties in the hazard of fluid migration and leakage along geological pathways. The lower part shows the optional workflow for quantitative assessment of the leakage hazard as a result of migration along geological pathways. AoI = Area of Influence

6.2.2 Fluid migration along wells to biosphere

In Chapter 5 the main outcomes of the quantitative modelling of fluid migration along wells and leakage to potable water resources have been presented. The results show there are scenarios in which methane leakage is possible and contamination of upper groundwater bodies could occur that are used for drinking water and spray irrigation. In these cases, groundwater monitoring should be carried out. Building on this work a workflow for the quantitative hazard and risk assessment of methane leakage is recommended here.

It is proposed to do a screening of all wells which were drilled for gas production purposes. The approach with fault tree analysis for migration along geological pathways could be applied to the screening of the well barrier elements as well. Potential sources of methane and fresh water aquifers and surface water near wells need to be characterized. The study presented in this report, has revealed that shallower sources of gas pose the main risk, particularly if they are normally pressured or over pressured and above the critical gas saturation for advective flow (see upper part of Figure 6-3). Furthermore, the number and properties of the permeable intermediate formations between the fresh water aquifer and the source, and the confinement of the fresh water aquifer are to be specified. Identifying the locations with shallow sources of gas can narrow down the number of wells and locations in need of further analysis.

Once the potential gas sources are identified, the seal integrity of the wells can be evaluated on the basis of the description of the well barriers (cement and casing quality) and indications of fluid migration like sustained annular pressures, fluid losses etc. Fault tree analysis for well related pathways may support this exercise. This can provide a list of high-risk wells that demand a closer attention (due to the presence of shallow gas and potential well integrity issues), possibly requiring monitoring and/or remediation. A pragmatic approach for qualitative or semi-quantitative assessment of leakage hazards from wells is provided by Van Oort (2022). Based on an example from literature, they suggest to score the overall risk level of individual wells on the basis of a number of risk factors and map these geographically. A more quantitative probabilistic risk assessment approach has been recommended for wells with high risk levels and scarce data.

The quantitative assessment could start from the modelling approach which has been described in Chapter 5. After specification of the uncertainty ranges and distributions, the modelling could be performed for specific cases of loss of well integrity, methane sources and aquifer geometries. The outcome could then be presented in maps with well leakage hazards (see lower part of Figure *6-3*). A large part of the work, i.e. characterisation of methane sources and aquifer geometries and properties, could be lined up with similar work for migration along geological pathways described in the previous section. The proposed metrics for leakage to potable ground water are similar to those proposed for leakage resulting from migration along geological pathways. Well-abandonment solutions have a finite life and probabilities of future failure that need to be considered if wellbore migration modeling shows there can be consequential impacts to receptors.

Monitoring of shallow groundwater could aid in calibrating and testing of the numerical models. Best place for water sampling is the top of deepest confined aquifer as close as possible to the well up to 100 to 300 m away in the direction of groundwater velocity. A similar approach could be deployed for monitoring of leakage via geological pathways.

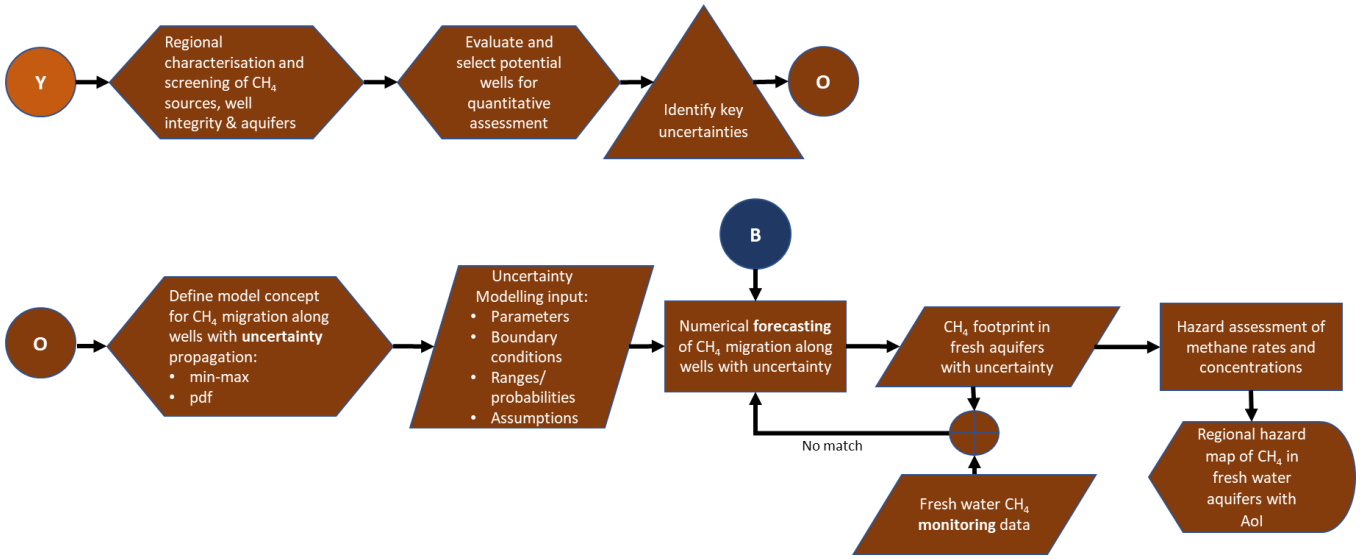

Figure 6-3 A workflow for quantitative assessment of leakage hazard from fluid migration along wells; Aoi = Area of Influence

6.3 Ground motion

Past gas production has left pressure and stress footprints in the deep subsurface which may trigger effects at the earth's surface, in this case aseismic or seismic movements. Approaches for the quantitative assessment of both processes will be elucidated below.

6.3.1 Subsidence and uplift

The general conclusion from the quantitative modelling work presented in Chapter 5 is that the expected additional subsidence after abandonment of the gas reservoirs is limited and hardly any uplift is anticipated above the gas reservoirs themselves. The small amount of anticipated uplift is related to the small amount of expected pressure increase during the pressure equilibration process.

Building on the findings from the preceding sensitivity analysis (X in Figure 6-4) the main uncertainties for the probabilistic modelling, e.g. aquifer compaction coefficients, need to be characterized. Uncertainties in the pressure depletion are transferred from the pressure redistribution modelling (B in Figure *6-4*), which is described in a previous section of Chapter 6. Compaction and the resulting stress field are input for the assessment of fault re-activation (Y in Figure 6-4; see next section). Monitoring data, e.g. InSAR satellite data, are key to constrain aquifer compaction and resulting stress changes.

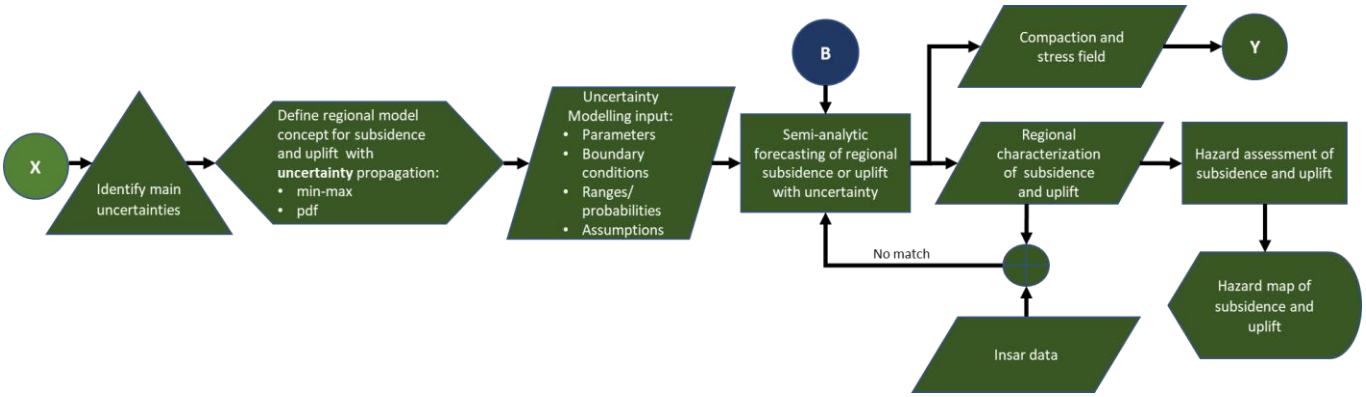

Figure 6-4 A proposed workflow for the quantitative assessment of vertical aseismic ground movement above gas reservoirs after their abandonment

The assessment metrics include the rate of vertical movement and cumulative movement of the earth's surface for different time steps. A decision has to be made on the time window of interest. The pressure redistribution has not yet equilibrated after 100 years. One may consider a longer time window, which would be closer to a new pressure equilibrium and higher values for vertical ground movement. In addition to the rates in movement one may also express the outcome as horizontal gradients expressing differential movements.

6.3.2 Induced seismicity

Quantitative modelling of the seismic hazard and risk as a consequence of gas production is a complicated matter, even in cases with ample passive seismic monitoring data like for the Groningen gas field. Little data are available to constrain the hazard of induced seismicity in or near depleting aquifers adjacent to gas reservoirs. For that reason the modelling of induced seismicity in Chapter 5 has been reduced to the hazard of fault re-activation, which is an indicator of the seismic hazard. In the assessment of fault re-activation in the adjacent aquifers and accompanying seismicity the following risk factors are to be considered:

- Initial criticality of the stress field
- Friction parameters of faults in the water-bearing aquifer
- Larger than expected pressure depletion
- Unmapped faults
- Model step from reactivation to seismicity

In the recommended quantitative hazard (and risk) assessment of induced seismicity after abandonment of producing gas reservoirs the following parameters with their associated uncertainties are to be included (upper part of Figure 6-5):

- Virgin stress,
- Elastic moduli,
- Fault properties:
    - Distribution,
    - Density,
    - Orientation,
    - Offset
    - Frictional properties,
    - Permeability,
    - Rupture behaviour.

An analytical modelling similar to the sensitivity analysis of fault re-activation (Chapter 5) will propagate the uncertainties to the regional hazard of fault re-activation. Seismic monitoring data from the aquifers will be used to constrain the model output (see lower part of Figure 6-5). The modelling of re-activation further requires input from the modelling of pressure depletion, compaction and stress distribution (B and Y in Figure 6-5). Suitable metrics for the quantitative assessment of fault re-activation are the slip tendency (ratio of shear and normal effective stresses on a fault) and the shear capacity utilization (ratio

of shear stress and critical shear stress on a fault) for selected time steps. A decision has to be made on the time window of interest after ceasing gas production.

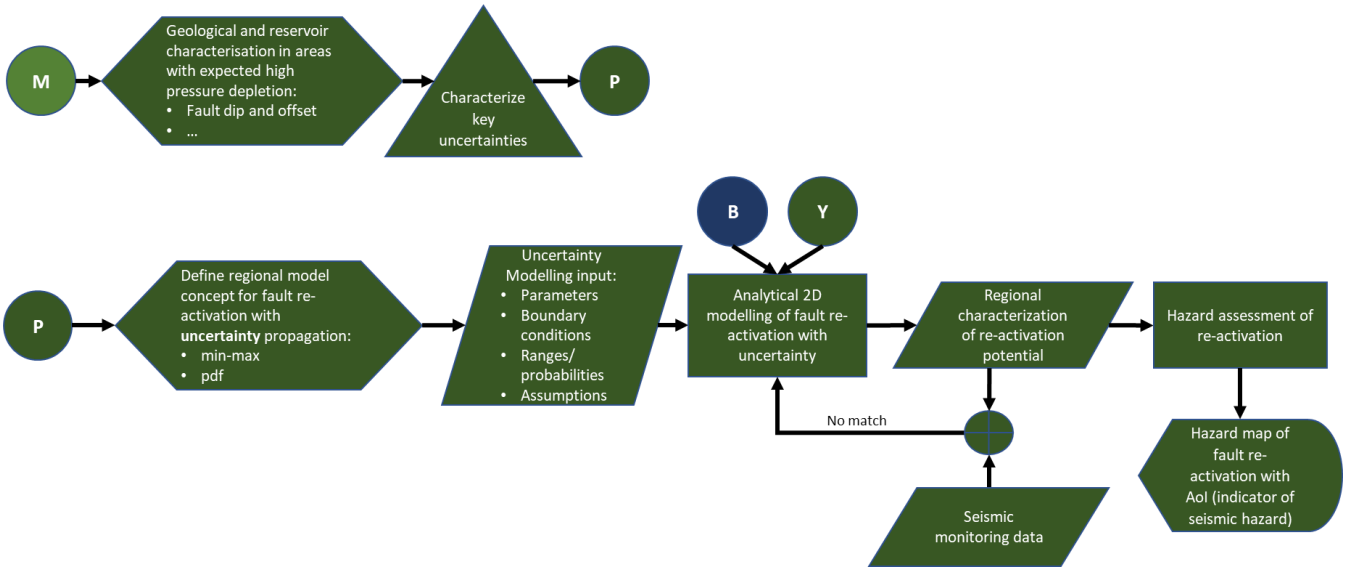

Figure 6-5 A proposed workflow for the quantitative hazard assessment of fault re-activation as an indicator of induced seismicity; AoI = Area of Influence

Expansion of the hazard assessment of fault-re-activation to a full probabilistic assessment of seismic risk (damage resulting from induced seismicity) would require a lot more work, which requires the inclusion of the following aspects (e.g. TNO, 2020):

- Nucleation of seismicity at a fault;
- Propagation of rupture along a fault;
- Ground motion in deep subsurface propagating to the earth's surface;
- Damage to buildings (collapse);
- Human safety (probability of lethal accident).

The procedure that is currently used for the risk assessment for seismicity in Groningen can be used for this purpose but it needs to be filled with specific information for the aquifer that is the subject of the present study.

6.4 Interference with subsurface activities

In or near areas with past gas production activities, new subsurface activities may be deployed like geothermal energy production or gas or hydrogen storage in porous / permeable (sedimentary) rocks or gas, compressed air or hydrogen storage in salt caverns. These may interfere with the pressure and stress

footprint and abandoned well infrastructure left by earlier gas production and the resulting hazards of fluid leakage, subsidence or induced seismicity. As geothermal energy production witnesses an enormous interest and growth in the Netherlands, the focus will be on the interference with geothermal energy. For salt caverns, which can cause subsidence, it is recommended to include subsidence from any nearby (abandoned) gas fields in the evaluation of potential subsidence. For storage activities, interference is possible with respect to induced seismicity.

In the possible interaction between geothermal energy production and past gas production two possible effects are considered here, which are the mutual effects of geothermal energy production and past gas production on the level of seismic hazard and on the hazard level of fluid leakage.

6.4.1 Geothermal energy production and seismic hazard

Geothermal energy production in closed loop systems leads to changes in temperature, and in open systems to a local change in pressure and temperature near the production and injection well. In particular the cooling effect of the injected brine on the stress state of nearby faults must be evaluated. The final effect requires the incorporation of the stress changes induced earlier. We suggest to define an *Area of Influence* (AoI) both for the altered stress state near faults and for the expected alterations of stress due to the geothermal activities. The AoIs can be made time dependent and either can be deterministic or probabilistic. Construction of the hazard map of fault re-activation in Figure 6-5 can then be focused to where these areas overlap. If the Area of Influence of a geothermal project overlaps with the (2D or 3D) AoI resulting from former gas production, the geothermal project developer needs to take the pressure and stress effects of former gas production into account. A criterion for defining the Area of Influence could be a threshold value for the stress change. The threshold values for defining the Areas of Influence need to be defined. The identification of fault reactivation hazard in the overlap of the Areas of Influence can be done by assessing the slip tendency or the shear capacity utilization in those regions.

6.4.2 Geothermal energy and hazard of fluid leakage

Geothermal energy production may also interfere with fluid migration and leakage as a result of former gas production. When existing gas production wells would be re-used for geothermal energy production this may directly interfere with fluid migration along wells and leakage to potable water resources. The recommended regional assessment of the hazard of leakage via wells described in a previous section of Chapter 6, identifies wells with a significant hazard of fluid leakage. A geothermal project developer should address this hazard and re-instate the sealing integrity of the well if necessary. Existing or new wells that transect faults which could act as a fluid migration path (see previous section in Chapter 6) should undergo precautions to prevent unintended fluid migration along the well.

Plumes of methane may develop in shallower aquifers above the rock salt as a result of fluid migration along wells or geological pathways, which may also be target reservoirs for geothermal energy production. These plumes may be represented as Areas of Influence. The production and injection activities associated with geothermal energy production may mobilize (part of) these plumes. Geothermal projects in areas

with possible presence of methane plumes need to evaluate the increased hazard of fluid leakage to potable water resources.

When geothermal wells are planned near an abandoned well, there may be some risk of gas leakage interference between the abandoned and new geothermal wells. If there is a hydrostatic source of gas below the geothermal target, there is a possibility of gas leakage into the aquifer. The extent and the severity of the plume largely depend on the level of cement damage and aquifer permeability. The simulations in section 5.2 indicate that the extent of the plume will likely be limited to 500 away from the well (a conservative estimate particularly for a deeper aquifer). Operating a geothermal producer within 500 m of an abandoned well may lead to a small amount of methane being produced with the hot water. Adding an injection well near the abandoned well may interfere with the plume shape and reduce the leakage rate due to an increase in aquifer pressure near the abandoned well. A geothermal doublet design should not include an abandoned well between the injector and the producer.

6.5 Monitoring strategies

A good monitoring strategy follows relevant processes in time which makes it possible to act timely so that the occurrence of undesired events can be mitigated or prevented. This chapter discusses a monitoring strategy for each of the main issues related to reservoir abandonment discussed in this report. It should be realized that this monitoring strategy is based on the current practices and will probably be suitable for the coming decades. The risks associated with abandonment are expected to be present for at least several hundreds of years. In the meantime, global and climate changes will occur that are not known yet: is it under the conditions that will be present at that time still necessary to monitor and mitigate risks concerning seismic hazards, subsidence and leakage to the shallow aquifers? It is recommended to update the monitoring strategy every decade to keep updated on the current use of the subsurface or more frequently if monitoring results so indicate.

The proposed strategies presented here are preliminary as robust monitoring strategies would follow the quantitative risk assessments including acceptance criteria, cost-benefit tradeoffs of monitoring and the intervention designs. At the same time some *in-situ* monitoring in wells need to be considered now before the abandonment is realized.

The outcome of the risk assessment informs the design of monitoring systems, which together help defining interventions to prevent loss of control or to mitigate the consequences in line with Part 3 of the ISO risk management process. In this manner the main elements of bowtie risk management will have been addressed.

6.5.1 Monitoring strategies for lateral fluid migration

Lateral fluid migration results in pore pressure changes in the reservoir. These changes at depth can only be monitored directly through dedicated pressure sensors at the bottom of the abandoned gas wells or in dedicated observation wells. Such a network of pressure sensors would deliver valuable information on the actual response of the reservoir to abandonment and would also alert to anomalous values that

indicate processes in action that may lead to undesired consequences. Monitoring locations should be focused on wells that are in or near the surrounding aquifers of the gas field. Monitoring in abandoned gas wells will mostly show the response in the gas reservoir, which is relatively insensitive to changes in pressure in the surrounding aquifers. Locations for monitoring could be based on the locations where the largest uncertainty in the future pressure has been identified. The simulated range in pressure in Figure 5-5 shows this to be in south-west and on the north side of the Groningen field. More detailed simulations are required to refine the pressure predictions and optimize the monitoring strategy.

Apart from measuring the pressures at the base of the abandoned wells, an indirect signal of fluid migration is expected to show up in vertical movements at surface level. These can be accurately monitored with InSAR satellite measurements. These measurements can be used to increase the understanding of the reservoir and its interconnections and can be used for model calibration so that future effects of re-use of the reservoir can be better predicted.

6.5.2 Monitoring strategies of ground motion and seismicity

At present, the KNMI monitoring network in Groningen consists of 23 acceleration stations, 70 bore-hole stations with acceleration and geophones, and 8 bore-hole stations with only geophones. This present monitoring network can register seismic events with a magnitude as low as 0.5 (KNMI.nl) and is designed for the gas field in production. Since the largest pressure equilibration in the gas zone takes place in the first 20 years after closure, it is recommended to keep this monitoring resolution during this period and to compare to predictions.

The monitoring strategy after this first period should depend on the results until that time and on the aim of the monitoring. If the purpose of the future monitoring is to accurately follow the evolution of the abandoned field and to calibrate seismicity predictions, high resolution of monitoring of magnitude 0.5 could be continued since the effects are expected to be low event rate and low magnitude. To combine effort, pressure monitoring wells in the aquifers surrounding the gas field could be equipped with geophones.

If future monitoring is aimed at registering events that could lead to damage or impact safety and the measurements are in line with expectations, the sensitivity of the monitoring could be lowered to magnitude 1.5. This is standard in areas in which seismicity can be expected; a magnitude 1.5 event is near what can be felt at ground level (knmi.nl). It should be considered to extend the monitoring network outside of the outer contours of the field to register seismicity related to equilibration in the aquifers surrounding the field.

Apart from seismicity monitoring, InSAR satellite measurements and analyses should be continued to monitor ongoing slow ground motion after the abandonment of gas reservoirs. It is recommended to embed the requirement of such monitoring in regulation.

6.5.3 Monitoring strategies for methane migration along geological pathways and well bores

Methane is naturally present in groundwater bodies (Stuyfzand et al., 1994). To be able to detect an abnormal increase in methane concentrations due to leakage from abandoned gas fields or abandoned gas wells, the baseline methane concentrations should be well known. Additionally, the natural variability

(spatial, in depth, and over time) of methane concentrations needs to be known and understood as well as the geochemical processes that take place in the groundwater that influence the methane concentrations. Also, other sources of methane leakage may exist in the area like industrial installations, storage tanks at the surface, and petrol stations. Therefore, an overview of potential sources other than the abandoned gas fields should be made to be able to distinguish an increase in methane leakage from an abandoned gas field or abandoned gas well.

In Groningen, but also other areas with gas fields present, many groundwater-monitoring locations have already been installed by the drinking water companies, municipalities, and waterboards. Additionally, a provincial groundwater quality monitoring network and a national groundwater quality monitoring network exist, which consist of groundwater wells and sampling and analyses techniques of high accuracy (Meinardi et al., 2003). The depths of the filters of these monitoring networks is however limited (up to 25 m below the surface). Data from all of the above-mentioned monitoring networks form the baseline groundwater quality dataset available. However, an inventory should be made of information applicable to the monitoring location. Are measurements of water quality parameters available or are only pressure heads measured? And if quality data are available, are these relevant for the detection of methane? For the specifications of all the monitoring wells as well as information about the owner of the wells the Dino database can be consulted through the Dinoloket (www.dinoloket.nl).

In the case of well bores, fluid migration is mostly expected to pose a threat when gas pockets migrate upward from under a seal along a damaged well bore. This could lead to undesired consequence in shallow freshwater aquifers such as greenhouse gas emissions, water quality changes or explosion or asphyxiation hazards. Upward migrating gas can be monitored with groundwater monitoring wells in which water samples are periodically sampled at multiple depths. If increased methane concentrations are measured, an isotope analysis should be used to determine the source of the methane (biogenic or thermogenic).

The results of the numerical modeling indicated that water sampling at the top of (the deepest) confined aquifers is the best place to detect leakage. The monitoring well should be placed as close as possible to the wellbore (ideally less than 100 m, and no more than 500 m). The sampling should be done downstream of the groundwater flow direction with respect to the well so that an eventual methane plume can be detected.

The location where fluid migration along geological pathways could lead to near-surface methane leakage is less easy to pinpoint. For some of the levels in the fault tree that was developed for this kind of fluid migration a dedicated monitoring strategy for detecting methane leakage could be designed. Such a strategy could be focused on the events at the bottom of the fault tree that would happen first (migration from the reservoir). However, it could also be aimed at the detection of a process to take place just before they could lead to undesired consequences, in order to take timely preventive or mitigative measures. The first case is suitable if the initiation of a process may likely lead to undesired consequences. The latter case may be sufficient if the probability of occurrence of an undesired event is low or the consequences manageable. For fluid migration along geological pathways, monitoring migrating gas near the surface just before a hazard can take place is considered adequate.

If vertical fluid migration along geological pathways would occur, it is only expected to take place in areas above a thin (<50 m) Zechstein seal in combination with high offset faults that could be re-activated and

the presence of an undepleted or little depleted gas source. In addition, large faults that cross many strata in the overburden are favorable for migration. In areas that fulfil these conditions, the existing monitoring network should be extended at strategic locations, such as below aquitards underlying the capture zone of drinking water well fields, or in groundwater flow paths towards vulnerable groundwater dependent nature.

Recent developments in remote sensing have made it possible to detect methane emissions into the atmosphere, such as the TROPOMI satellite (Hu et al., 2018). For large sources of leakage this has proven to be a valuable tool. However, at present the ground resolution of minimal 25 km^2 and expected relatively low flux of a potential gas migration compared to the background flux are not expected to be picked up by this sensor. However, future technologies may be better suited.

7 References

Békési, E., Struijk, M., Bonté, D., Veldkamp, H., Limberger, J., Fokker, P. A., Vrijlandt, M., van Wees, J.D., 2020. An updated geothermal model of the Dutch subsurface based on inversion of temperature data. Geothermics, 88, 101880.

Bonté, D., van Wees, J.-D., Verweij, H., 2012. Subsurface temperature of the onshore Netherlands: new temperature dataset and modellin. Netherlands Journal of Geoscience, 91 (4), 491-515.

Brooks, R. H., and A. T. Corey (1964), Hydraulic properties of porous media, in Hydrology Papers, vol. 3, 37 pp., Colo. State Univ., Fort Collins.

Buijze, L., Van den Bogert, P. A. J., Wassing, B. B. T., & Orlic, B. (2019). Nucleation and arrest of dynamic rupture induced by reservoir depletion. *Journal of Geophysical Research: Solid Earth*, *124*(4), 3620-3645.

Buijze, L., van Bijsterveldt, L., Cremer, H., Paap, B., Veldkamp, H., Wassing, B., Van wees, J.D. and ter Heege, J., 2019b. *Review of worldwide geothermal projects: mechanisms and occurrence of induced seismicity.* TNO 2019 R100043

Candela, T., Wassing, B., Ter Heege, J., & Buijze, L. (2018). How earthquakes are induced. *Science*, *360*(6389), 598-600.

Collins, D.A., Grabenstetter, J.E. and Sammon, P.H., "A Shared-Memory Parallel Black-Oil Simulator with a Parallel ILU Linear Solver", SPE 79713, SPE Reservoir Simulation Symposium, Houston, TX, February 3-5, 2003.

EC / European Commission. (2011). Implementation of Directive 2009/31/EC on the Geological Storage of Carbon Dioxide - Guidance Document 1 - CO_2 Storage Life Cycle Risk Management Framework.

Fanchi, John R. Principles of Applied Reservoir Simulation (Fourth Edition), 2018.

Fjaer, E., Holt, R. M., Raaen, A. M., & Horsrud, P. (2008). *Petroleum related rock mechanics*. Elsevier.

Fokker, P. A., & Orlic, B. (2006). Semi-analytic modelling of subsidence. *Mathematical Geology*, *38*(5), 565-589.

Fokker, P. A., Muntendam-Bos, A. G., & Kroon, I. C. (2007). Inverse modelling of surface subsidence to better understand the Earth's subsurface. *First Break*, *25*(8).

Gasda, S.E., Celia, M.A., Wang, J.Z., and Duguid, A., 2013. Wellbore permeability estimates from vertical interference testing of existing wells. Energy Procedia 37, 5673–5680.

Gaucher, E., Schoenball, M., Heidbach, O., Zang, A., Fokker, P.A., Van Wees, J. and Kohl, T., 2015. Induced seismicity in geothermal reservoirs: A review of forecasting approaches. *Renewable and Sustainable Energy Reviews,* **52**, pp. 1473-1490.

Geertsma, J. (1973). A basic theory of subsidence due to reservoir compaction; the homogeneous case. Trans. R. Dutch Soc. Geol. Min. Eng. 28, pp 43–62.

Hu, H., Landgraf, J., Detmers, R., Borsdorff, T., Aan de Brugh, J., Aben, I., et al. (2018). Toward global mapping of methane with TROPOMI: First results and intersatellite comparison to GOSAT. Geophysical Research Letters, 45, 3682–3689. https://doi.org/10.1002/2018GL077259

Huet, C. C., J. A. Rushing, K. E. Newsham, and T. A. Blasingame (2005), A modified Purcell/Burdine model for estimating absolute permeability from mercury injection capillary pressure data, paper IPTC 10994 presented at the 2005 International Petroleum Technology Conference, Doha, The Am. Assoc. of Pet. Geol., 21–23 Nov.

Ikenwilo, Ogo (WG Intetech, WEP, Baker Risk) (2016). *Geothermal well integrity study - Report for LTO Glaskracht Nederland, Kas als Energiebron & Ministerie van Economische zaken*.

Jager, J. de and Visser, C., 2017. Geology of the Groningen field – an overview. Netherland Journal of Geosciences. 96 (5), 3-15.

Jansen, J. D., Singhal, P., & Vossepoel, F. C. (2019). Insights from closed-form expressions for injection- and production-induced stresses in displaced faults. *Journal of Geophysical Research: Solid Earth*, *124*(7), 7193-7212.

Jossi, J.A., Stiel, L.I. and Thodos, G., "The Viscosity of Pure Substances in the Dense Gaseous and Liquid Phases", AIChE Journal, Vol. 8, (1962), pp. 59-63.

Kang, M., Baik, E., Miller, A.R., Bandilla, K.W., and Celia, M.A., 2015. Effective permeabilities of abandoned oil and gas wells: analysis of data from Pennsylvania. Environ. Sci. Technol. 49 (7), 4757-4764.

Karra, S., N. Makedonska,H. S. Viswanathan, S. L. Painter,and J. D. Hyman, 2015. Effect ofadvective flow in fractures and matrixdiffusion on natural gas production. Water Resour. Res 51, 8646–8657.

Kestin, J., Khalifa, H.E. and Correia, R.J., "Tables of the Dynamic and Kinematic Viscosity of Aqueous NaCl Solutions in the Temperature Range 20-150 °C and Pressure Range 0.1-35 MPa", J. Phys. Chem. Ref. Data, Vol. 10, (1981) pp. 71-87.

Kombrink, H., Doornenbal, J.C., Duin, E.J.T., Dulk, M. den, Gessel, S.F. van, Veen, J.H. ten, and Witmans, N., 2012. New insights into the geological structure of the Netherlands; results of a detailed mapping project. Netherlands Journal of Geosciences, 91 (4), 419-446.

LeMay T.G., Singh A. Parks, K., Wiersma A., Palombi D., Babakhani M., Berhane H., Hathway B., Vermeulen P., Marsman A., (2019). A Risk-Based Methodology for Commingled Well Abandonment – Southeastern Alberta Gas Field Case Study A Risk-Based Methodology for Commingled Well Abandonment – Southeastern Alberta Gas Field Case Study report AER/AGS.

Levandowski, W., Weingarten, M., & Walsh III, R. (2018). Geomechanical sensitivities of injection-induced earthquakes. *Geophysical Research Letters*, *45*(17), 8958-8965.

Li, K., and Horne, R. N. (2006), Comparison of methods to calculate relative permeability from capillary pressure in consolidated water-wet porous media, Water Resour. Res., 42, W06405,

Logeman, T. (2017). Fault Interpretation of the Groningen area supra-Zechstein Overburden. NAM report. March.

Lohne, Hans Petter and Eric P. Ford, Mohammad Mansouri Majoumerd, Erlend Randeberg, Santiago Aldaz, Thomas Reinsch, Ton Wildenborg, Logan G. Brunner (2017). Barrier definitions and risk assessment tools for geothermal wells. GeoWell Deliverable D6.3, 101p.

Lohne, H. P., Eric P. Ford, Mohammad Majoumerd Mansouri, Erlend Randeberg, Arnaud Barré, Ton Wildenborg, Logan Brunner (2018). Foundations for well integrity and risk assessment - GeoWell D6.4. https://www.researchgate.net/publication/327744820_Foundations_for_well_integrity_and_risk_assessment

Lopez, O., Berg, C.F., Bakke, S., Boassen, T., Rustad, A.B., 2013. “Thin section image analysis for estimation of initial water saturation in siliciclastic reservoir rocks”. Paper presented at the International Symposium of the Society of Core Analysts held in Napa Valley, California, USA, 16-19 September.

Meinardi, C.R., Groot, M.S.M., Prins, H.F. (2003). Basiswaarden voor spoorelementen in het zoete grondwater van Nederland; gegevens uit de landelijke en provinciale meetnetten (LMG, PMG, LMB, sprengen Veluwe). RIVM rapport 714801028/2003

Ministry of Economic Affairs and Climate Policy (2019). Natural resources and geothermal energy in the Netherlands. 2019 Annual review - An overview of exploration, production and subsurface, 181p.

Moghadam, A., Castelein, K., ter Heege, J., van der Valk, K., Orlic, B., and Wollenweber, J., 2020. Large-scale laboratory investigation of the microannulus behavior in the casing-cement interface. In Proceedings of the 54th US Rock Mechanics / Geomechanics Symposium (ARMA), ARMA 20-1325.

Moghadam, A., Castelein, K., ter Heege, J., Orlic, B., 2022. A Study on the Hydraulic Aperture of Microannuli at the Casing-Cement Interface Using a Large-Scale Laboratory Setup. Geomechanics for Energy and Environment 29, 100269.

Muntendam-Bos, A. G. (2021). Geomechanical characteristics of gas depletion induced seismicity in The Netherlands. ARMA 2021.

Muntendam-Bos, A. G., Hoedeman, G., Polychronopoulou, K., Draganov, D., Weemstra, C., van der Zee, W. & Roest, H. (2022). An overview of induced seismicity in the Netherlands. *Netherlands Journal of Geosciences*, *101*.

NAM, 2020. Bodemdaling door Aardgaswinning. NAM-gasvelden in Groningen, Friesland en het noorden van Drenthe. Statusrapport 2020 en Prognose tot het jaar 2080. www.nam.nl/feiten-en-cijfers/onderzoeksrapporten.html.

Nedmag, B. V. (2018). Winningsplan 2018. November. NLOG.nl

Nghiem, L.X. and Li, Y.-K., "Phase-Equilibrium Calculations for Reservoir Engineering and Compositional Simulation", Second International Forum on Reservoir Simulation, Alpbach, Austria, September 4-8, 1989.

Nederlands Normalisatie-instituut – NNI (2018). Risk management – Guidelines, NEN-ISO 31.000, 2nd edition

Nowamooz, A., Lemieux, J.M., Molson, J., and Therrien, R., 2015. Numerical investigation of methane and formation fluid leakage along the casing of a decommissioned shale gas well. Water Resour. Res. 51 (6), 4592–4622.

OSPAR Commission, 2007. Guidelines for Risk Assessment and Management of Storage of CO_2 Streams in Geological Formations.

Peng, D.Y. and Robinson, D.B., "A New Two-Constant Equation of State", Ind. Eng. Chem. Fundamen., Vol. 15, (1976), pp. 59-64.

Pijnenburg, R. P. J., Verberne, B. A., Hangx, S. J. T., & Spiers, C. J. (2018). Deformation behavior of sandstones from the seismogenic Groningen gas field: Role of inelastic versus elastic mechanisms. *Journal of Geophysical Research: Solid Earth*, *123*(7), 5532-5558.

Reagan, M.T., Moridis, G.J., Keen, N.D., and Johnson, J.N., 2015. Numerical simulation of the environmental impact of hydraulic fracturing of tight/shale gas reservoirs on near surface groundwater: background, base cases, shallow reservoirs, short-term gas, and water transport. Water Resour. Res. 51 (4), 2543–2573.

Rice, A.K., McCray, J.E., and Singha, K., 2018. Methane leakage from hydrocarbon wellbores into overlying groundwater: numerical investigation of the multiphase flow processes governing migration. Water Resour. Res. 54, 2959–2975.

Rowe, A.M. and Chou, J.C.S., "Pressure-Volume-Temperature-Concentration Relation of Aqueous NaCl Solutions", J. Chem. Eng. Data, Vol. 15, (1970), pp. 61-66. Bachu, S., 2017. Analysis of gas leakage occurrence along wells in Alberta, Canada, from a GHG perspective – Gas migration outside well casing. Int. J. Greenh. Gas Control 61, 146-154.

Schout, G., Griffioen, J., Hassanizadeh, S.M., Cardon de Lichtbuer, G., and Hartog, N., 2019. Occurrence and fate of methane leakage from cut and buried abandoned gas wells in the Netherlands. Sci. Total Environ. 659, 773–782.

SGS Horizon BV, 2016. Independent Review of Groningen Subsurface Modelling, Update for Winningsplan 2016 with Opinion Letter. https://www.nam.nl/over-nam/onderzoeksrapporten.html

Shi, S., Belhaj, H. & Bera, A. Capillary pressure and relative permeability correlations for transition zones of carbonate reservoirs. J Petrol Explor Prod Technol 8, 767–784 (2018).

Staatstoezicht op de Mijnen (2016) Methodiek voor risicoanalyse omtrent geïnduceerde bevingen door gaswinning. Tijdelijke leidraad voor adressering MBB.24.1.P, versie 1.2

Stuyfzand, P.J., F. Lüers & G.K. Reijnen (1994). Geohydrochemische aspecten van methaan in grondwater in Nederland. H2O, 27: 500-510.

Tao, Q., Bryant, S.L., 2014. Well permeability estimation and CO2 leakage rates. Int. J. Greenhouse Gas Control 22, 77–87.

Tartakovsky, 2007. Probabilistic risk analysis in subsurface hydrology. Geophysical Research Letters 34, 5. doi.org/10.1029/2007GL029245

Tartakovsky, 2013. Assessment and management of risk in subsurface hydrology: A review and perspective. Advances in Water Resources 51, 247-260.

Ter Heege, J., Osinga, S., Wassing, B., Candela, T., Orlic, B., Buijze, L. and Chitu, A., 2018. Mitigating induced seismicity around depleted gas fields based on geomechanical modeling. *The Leading Egde,* **37**(5), pp. 334-342.

Thomas, G.W. and Thurnau, D.H., "Reservoir Simulation Using an Adaptive-Implicit Method", SPEJ, Vol. 23, (October 1983), pp. 759-768.

TNO (2020). Probabilistic Seismic Hazard and Risk Analysis in the TNO Model Chain Groningen. TNO report TNO2020 R11052 | 2, 72p.

TNO & Deltares (2021). KEM-19 Evaluation of post-abandonment fluid migration and ground motion risks in subsurface exploitation operations in the Netherlands - Literature Review and Proposed Activities for Phase-2. Phase-1 Revised Draft Report, 81p.

TNO-GDN, 2022. Breda Formation. In: Stratigraphic Nomenclature of the Netherlands, TNO – Geological Survey of the Netherlands. Accessed on 03-02-2022 from http://www.dinoloket.nl/en/stratigraphic-nomenclature/breda-formation.

Van Eijs, R.M.H.E. 2015. *Neotectonic Stresses in the Permian Slochteren Formation of the Groningen Field*. Assen: NAM.

Van Elk, J., Doornhof, D., Bommer, J. J., Bourne, S. J., Oates, S. J., Pinho, R., & Crowley, H. (2017). Hazard and risk assessments for induced seismicity in Groningen. *Netherlands Journal of Geosciences — Geologie en Mijnbouw*, *96*(5), 259–269. doi: 10.1017/njg.2017.37

Van Elk, J., Landmann,, A.J., van Eijs, R., 2021. Reservoir Pressure and Subsidence Groningen Field update for Production Profile GTS – raming 2021. https://www.nam.nl/over-nam/onderzoeksrapporten.html

Van Gessel, S., Thienen-Visser, K. van, Maarten-Pluymaekers, Huijgen, M., Hoogendoorn, B., Marsman, A., & Dost, B. (2019). Towards a national research agenda and risk toolbox for mining effects in The Netherlands. (July). Retrieved from https://www.kemprogramma.nl/blog/view/57979344/kem-03a-mining-effect-hazard-and-risk-assessment-models-toolbox-ownership-development-public-access-and-quality-assurance-finished

Van Oort, Eric (2022). Qualitative Risk Assessment of Long-Term Sealing Behavior of Materials and Interfaces Boreholes KEM-18 – Final Report, EVO Energy Consulting, 175p.

Van Opstal, G. H. (1974). The effect of base-rock rigidity on subsidence due to reservoir compaction, in: Proc. Third Congr. Int. Soc. Rock Mech., vol. 2, pp. 1102–1111.

Van Thienen-Visser, K., Nepveu, M. & Hettelaar, J. (2012) Deterministische hazard analyse voor geïnduceerde seismiciteit in Nederland. TNO rapport 2012 R10198.

Van Wees, J. D., Buijze, L., Van Thienen-Visser, K., Nepveu, M., Wassing, B. B. T., Orlic, B., & Fokker, P. A. (2014). Geomechanics response and induced seismicity during gas field depletion in the Netherlands. *Geothermics*, *52*, 206-219.

Van Wees, J.; Osinga, S.; Van Thienen-Visser, K.; Fokker, P A. "Reservoir creep and induced seismicity: inferences from geomechanical modeling of gas depletion in the Groningen field." *Geophysical Journal International* 212.3 (2018): 1487-1497.

Verweij, J.M., H.J. Simmelink, J. Underschultz & N. Witmans, 2012. Pressure and fluid dynamic characterisation of the Dutch subsurface. Netherlands Journal of Geosciences — Geologie en Mijnbouw, 91(4) 465 – 490.

Wilke, C.R. and Chang, P., "Correlation of Diffusion Coefficients in Dilute Solution", AIChE Journal, Vol. 1, (June 1955), pp. 264-270.

Zeeuw, Q. de, L. Geurtsen, 2019. Groningen Dynamic Model Update 2018. https://www.nam.nl/feiten-en-cijfers.html.

Appendices

A Clarification of flow diagram symbols

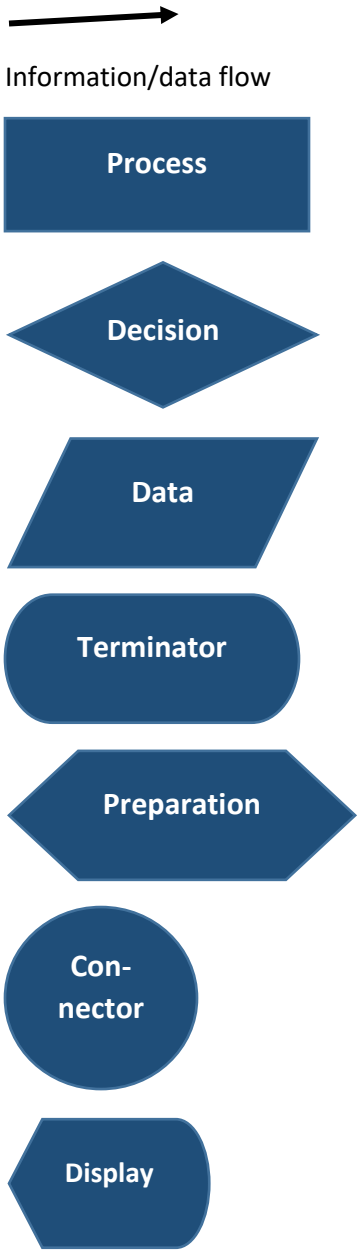

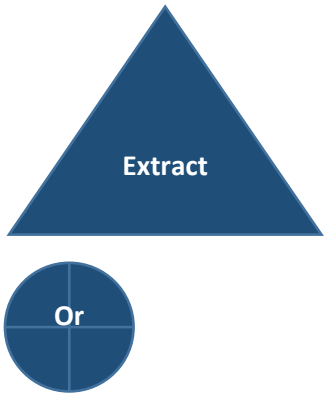
Extract
Or

B Conceptual modelling of geological fluid migration pathways

B.1 Define elements of geological pathways

One of the concerns related to the abandonment of gas fields is that fluids can escape the reservoirs and migrate upward as a consequence of the former production and subsequent abandonment. This could potentially lead to the contamination of shallow freshwater aquifers, the biosphere and atmosphere, and affect future subsurface use. To assess vertical fluid migration, first a conceptual model of potential pathways was developed with a team of experts. Subsequently, the migration pathway in the conceptual model was translated in a fault tree analysis, which describes the sequence of events and conditions that need to be fulfilled before undesired consequences would take place.

Figure B-1shows a schematic drawing of the conceptual model. The numbers refer to various stages that the upward migrating methane needs to pass before it would reach the shallow aquifer and/or the biosphere/atmosphere. For convenience, the vertical geological sequence is subdivided into eight levels: 1) the reservoir (in this case the Rotliegend sandstone formation), 2) the cap rock (in this case the Zechstein salt formation), 3) a hypothetical deep aquifer, 4) a hypothetical intermediate aquitard, 5) a hypothetical intermediate (unconsolidated) aquifer, 6) a hypothetical shallow unconsolidated aquitard, 7) a shallow (freshwater) aquifer and 8) the atmosphere. It should be realized that reality is more complex, with a number of deep and intermediate heterogeneous aquitards and aquifers consisting of alternating layers with variable permeability, intercalations, fault zones etc. However, for the construction of a conceptual model working with eight levels is suitable as it allows the description of all processes associated with vertical gas migration.

Below is a narrative of the conceptual model which refers to these numbers. For each stage in the migration pathway, the conditions that are favorable for fluid migration will be listed, and potential hazards that could occur related to these steps.

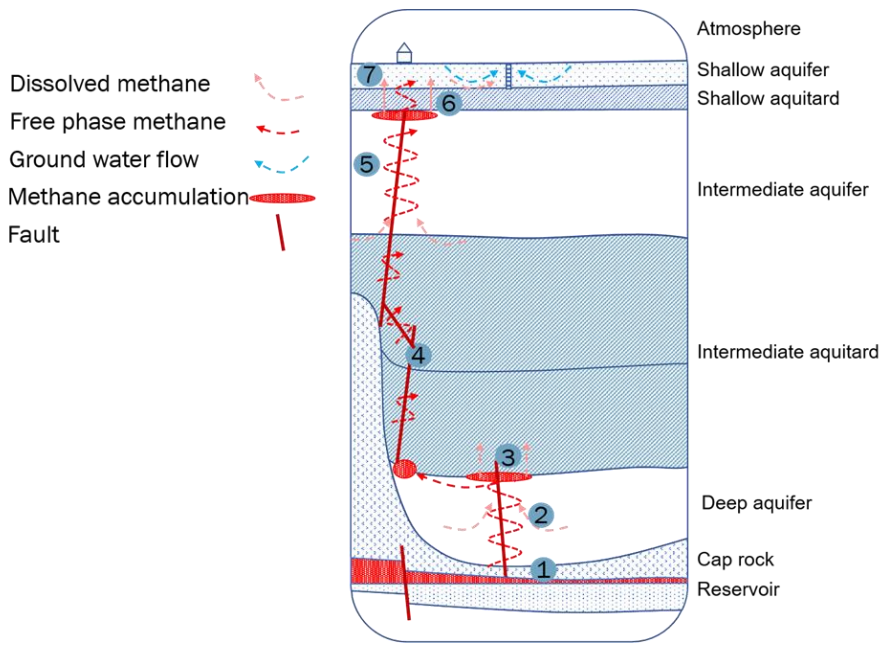

Figure B-1.Drawing of the conceptual model of vertical fluid migration from a gas reservoir. Each described stage is indicated with a number.

Stage 1: Fluid escape from the reservoir

For fluids to migrate upward, there needs to be a ***source*** and there needs to be a ***migration pathway***. The source is the methane in reservoirs that has been stored there over geological time-scales. Therefore, for fluid to escape from the reservoir along natural pathways as a consequence of reservoir abandonment, first new pathways need to be created related to the changed conditions due to abandonment.

Source

Pressures in the depleted reservoir are much lower than virgin conditions. This inhibits upward fluid migration since pressure gradients will be directed towards the depleted reservoir. The resulting downward counterflow enhances the capillary force of the original trap which counteracts the buoyant force generated by the height of the gas column of the depleted reservoir. This means that the depleted reservoir itself is unlikely to be the source and will more likely act as a sink for fluids. Upward fluid migration resulting from changed conditions due to reservoir abandonment is considered more likely from little depleted or undepleted fields adjacent to the depleted reservoirs, or in the overlying rock sequence.

Another potential option is that the equilibration of pressures after abandonment results in the growth of gas pockets resulting from volumetric expansion due to depressurization and migration of gas. Similarly, gas-water contacts may tilt in response to head changes. As a result, gas pockets may cross spill points. This could result in gas migration to spots with a weak or absent cap rock that could subsequently migrate upward.

The following conditions favoring migration of gas from a source can be identified:

Undepleted fields adjacent to the depleted reservoir;
Fields at relatively high abandonment pressure;
(Unidentified) Pockets of gas in the rock sequence above the main reservoir;
Presence of spill points near weak seals.

Migration pathway through caprock

The only likely newly formed natural migration pathway through the caprock related to the production and abandonment of a reservoir is fault reactivation due to the pressure depletion and compaction in the reservoir. For these faults to form a migration pathway they need to be transmissive and cross the entire cap rock. Earlier studies have shown that faults are only hard linked (i.e. they can be traced above and below the Zechstein) if the thickness of the Zechstein is less than 50 m (Ten Veen et al., 2012). The conditions favoring the formation of migration pathways are summarized below:

Conditions making faults most susceptible to reactivation
High offset faults
Differential depletion between both sides of the faults
High compaction (high porosity / high rock compressibility)
Critically stressed faults: in this case orientation NNW-SSE
Conditions making faults more susceptible to permeability creation
Zechstein < 50m (Ten Veen et al., 2012)
Juxtaposition of Basal Zechstein caprock to Slochteren sandstone (Hunfeld, 2020)
Faults with high offset: the larger the fault the wider the damage zone around the fault
Hanging wall side of the fault (normal faults)
Strike-slip faults with undisturbed rock in the fault core (Bonson et al., 2007)
No or little salt along the fault
No or little clay/shale along the fault
Faults extending into the shallow subsurface.
Along and over salt domes transmissive faults extending over large depth may exist (Schroot & R.T.E Schüttenhelm, 2003).

It should be noted that the stress conditions in Groningen with a normal faulting regime and near-isotropic horizontal stress, no full fault failure is expected, and usually reactivation is limited to reservoir level (below the Zechstein).

Stage 2: Upward migration through high conductive layer

If a source and a migration pathway are both available, it will lead to the upward migration of free gas into the overlying rock sequence. In this rock sequence the gas will migrate upward through the deep aquifer until it meets a layer of low permeability, here indicated as the intermediate aquitard under which gas will accumulate. This upward migration can take place in the porous rock sequence, but also through a preferential pathway such as transmissive faults that cross the rock sequence. While migrating upward, methane may come out of solution from the formation water increasing the amount of free methane. This is a self sourcing mechanism which may accelerate the migration process and increases the volume and mass of free methane.

Conditions increasing the susceptibility for upward migration
High permeability strata
Presence of long transmissive faults
High concentration of dissolved methane in pore water

Stage 3: Accumulation below low conductive layer

The gas will migrate upward until it is intercepted by low permeability layers. If this happens, free gas will accumulate and form gas pockets under these layers. These may pose a drilling hazard. In addition, awareness of potential newly formed gas accumulations is important for the planning of future subsurface use activities, such as geothermal operations.

Conditions favourable for formation of gas pockets
Presence of continuous low permeability layers

Stage 4: Upward migration through low conductive layer

Upward migration of the methane can proceed if horizontal expansion of the gas accumulation finds an area of high permeability, such as a transmissive fault or a spill point due to discontinuity or lateral heterogeneity of the low permeability layer. Also, when the buoyancy pressure of the gas column eventually exceeds the capillary forces in the layer of low permeability gas will migrate upward. As the gas migrates to more shallow strata, the entrapment efficiency of the low permeability layers decreases as porosities are higher and stress and capillary gradients are lower.

Conditions favourable for further upward migration through overburden
Transmissive faults
Heterogeneous or discontinuous aquitards
Build up of gas columns

Stage 5: Further upward migration through intermediate unconsolidated aquifer

The upward migration through intermediate aquifers is identical to the upward migration through deep aquifers. The gas will migrate upward through the intermediate aquifer until it meets a layer of low

permeability. This upward migration can take place in the porous rock sequence, but also through a preferential pathway such as transmissive faults that cross the porous rock sequence. While free gas migrates upward, dissolved gas may come out of solution from the formation water increasing the amount of free methane and accelerate the migration process. Groundwater flow systems will start playing an increasingly important role as the gas migrates into shallower reaches. Hence, dissolved gas will be advected along with the groundwater flow.

Stage 6: Gas accumulation below shallow unconsolidated aquitard

When the rising free gas encounters a barrier again it will accumulate and form a gas pocket. Eventually, a gas pocket could form below the uppermost layer of low conductivity, right below or in the shallow freshwater aquifer. From here, the expanding gas pocket could seep through to the shallow aquifer through heterogeneities or discontinuities in the low permeability layer. Moreover, if the gas pocket grows higher, it may overcome the capillary forces and break through the low permeability layer. Faults are not present in the young and plastic clays at such shallow depths.

Apart from the potential of free gas seeping through this layer, diffusion of methane through the low permeability layer may take place if there is a concentration gradient between the top and bottom of the low permeability layer. This may result in a flux of dissolved methane into the freshwater aquifer.

Conditions increasing the susceptibility for gas to migrate upward through a shallow low permeability layer
Discontinuity / heterogeneity of low permeability zone
Vertical buildup of gas columns
Thickness (for diffusion)
Diffusion coefficient (for diffusion)
Concentration gradient (for diffusion)

Stage 7: Gas in the shallow aquifer

Eventually, if all previous barriers have been passed, gas will enter the shallow freshwater aquifer. Here, it can escape into the atmosphere where it will add to the greenhouse gas load. In addition, it could accumulate in confined spaces, such as basements, where it could pose an explosion or asphyxiation risk. Dissolved methane could lead to groundwater quality changes which could form a threat to environmental protection zones. Finally, it could form a hazard when it is pumped up in drinking water wells.

B.2 Fault tree analysis

As part of the risk assessment methodology, we propose the use of fault tree analysis. Fault tree analysis is an intuitive method to represent and analyse the conditions and sequence of events that could lead to undesired consequences. The method originates from safety engineering such as aerospace and nuclear power industries. It was introduced to groundwater quality related decision making by Tartakovsky (Tartakovsky, 2007; 2013). Figure *B-2* shows an example of such a fault tree. In practice they can become quite complex.

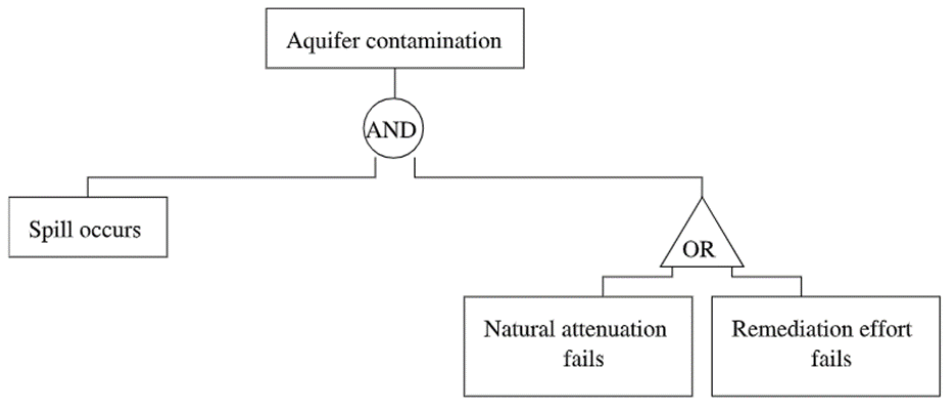

Figure B-2. Simplified fault tree for possible aquifer contamination (Source: Tartakovski, 2007)

In a fault tree, the basic events that could occur or conditions that could be present in the subsurface that contribute to undesired consequences are isolated and put in a logical order, and subsequently linked with Boolean AND or OR operators. The top of the fault tree represents the undesired consequence (also “top event” or “failed state”).

The fault trees map the potential pathways to failure (undesired consequence) very intuitively. Advantage of this is that it supports the design of a dedicated simulation plan that tests the different levels in the fault tree for consequentiality. In other words, the simulations test what conditions (physically or geologically) need to be fulfilled to pass to the next level in the fault tree. This way, through simulations a fault tree can be falsified (if one level is impossible to take place) or be deemed consequential (potentially passing the entire sequence of levels leading to an undesired consequence is physically possible). In the latter case, the conditions under which a fault tree is consequential can then be compared with data from literature or site investigations to determine the likelihood and severity. For instance, if the simulation shows that to pass a level the hydraulic permeability value of a layer needs to be higher than 0.1 m/day, and data shows that these conditions cannot realistically be present in this setting, the consequential model can be falsified. Similarly, the results of the analysis can also be used to inform future ground investigations and which subsurface properties to focus on to quantify or potentially falsify the occurrence potential events.

In addition, the fault tree analysis can be used to design preventive and mitigative measures. Moreover, it can be used to design monitoring networks, as it intuitively shows at which levels monitoring is useful and where mitigative measures are optimal.

Application of Fault Tree analysis in the case of fluid escape along geological pathways to shallow freshwater aquifers in Groningen.

For this project, a fault tree was set up to determine what possible geological pathways there are for methane to vertically migrate to shallow aquifers. This fault tree is based on the conceptual model discussed previously. It assumes that due to gas production pressure depletion has taken place, and the resulting compaction leads to fault reactivation. The following section describes the fault tree narrative for the causal nodes and gives a short description of the processes at play at each of these nodes. The actual fault tree is shown in Figure *B-3*.

Table B-1. Fault tree narrative for the upward migration of methane. The fault tree is provided in Figure B-3.

Level	Sequence of events	Favorable conditions	Monitoring
A	An accumulation of undepleted or little depleted methane is present adjacent or above the depleted reservoir (1),	Remaining methane accumulations at (near) virgin pressures	Seismic survey
	OR Gas expansion crosses a spill due to expansion by nearby pressure lowering (2),	Presence of spill points	InSAR surface deformation measurements
	THEN a source of free gas is present (3),		
	AND if the pore pressure of the gas is higher than hydrostatic pressure groundwater (4)		
	THEN a potential source of upward migrating gas is present (5).		
B	Fault reactivation due to compaction takes place (6),		Seismic monitoring network
	AND fault links rocks above and below the cap rock (7),	Zechstein < 50m Large offset faults	
	AND the fault becomes transmissive (8),	No or little salt or shale	
	THEN a migration pathway is available (9)		
C	IF a potential source is present (5),		
	AND a migration pathway is available (9),		

	THEN free methane enters overlying rock sequence (10).		Pore pressure changes at well base
D	IF the overlying rock sequence is permeable (11),	Presence of sand stone	
	OR if it is crossed by transmissive faults (12)	Presence of long faults, little salt / shale gouge	
	THEN gas migrates further upward (13),	High concentration of dissolved methane present coming out of solution	
E1	IF methane encounters a barrier of a low permeability layer (14),		
	AND		
	OR a transmissive fault is present (15),		
	OR discontinuity or permeable heterogeneity present (16),		
	OR a gas column builds up with a buoyance force higher than the capillary pressure in the low permeability layer (17),		
	THEN free gas enters the overlying rock sequence (18).		
E2	IF methane encounters a barrier of a low permeability layer (14),		
	THEN this could create a drilling hazard or interfere with future subsurface use (19)	Low permeability strata with geometric traps	Seismic survey
F	IF the rock sequence is permeable (20),		
	OR if it is crossed by transmissive faults (21)		
	THEN free gas migrates further upward (22),		
G1	IF methane encounters the uppermost low permeability layer (23),		
	AND		
	OR the layer is heterogeneous or laterally discontinuous (24),		
	OR a gas column builds up with a buoyance force higher than the capillary pressure in the low permeability layer (25),		
	THEN free gas enters the shallow freshwater aquifer (26),		Groundwater quality monitoring network

G2	IF methane encounters the uppermost low permeability layer (23),		
	THEN this may give rise to a shallow gas pocket drilling hazard of have implications for future subsurface use, such as ATES (27).		Seismic survey
	AND if a concentration gradient of dissolved methane exists across the layer of low permeability (28)		
	THEN dissolved gas enters the shallow freshwater aquifer through diffusion (29).		Groundwater quality monitoring network
H1	IF free gas enters the shallow freshwater aquifer (26),		
	AND it can accumulate in a confined space (30),		
	THEN an asphyxiation hazard or explosion hazard can occur (31)	Built environment Infrastructure	
H2	IF free gas enters the shallow freshwater aquifer (28),		Groundwater quality monitoring network
	AND it escapes to atmosphere (32)		Tropomi satellite mission
	THEN it will add to the greenhouse gas load (33)		
I1	IF dissolved gas will enter the shallow freshwater aquifer flow system through diffusion (29),		
	AND provided that the capture zone of a drinking water well intersects the flow system carrying the dissolved methane (34),	Drinking water protection zone	
	AND provided that the dissolved methane concentration reaching the well is around the saturation concentration (35)	High methane flux No natural attenuation	
	AND provided there is no methane separator at the site of the well (36)		
	THEN explosive methane can develop by exsolution in enclosed spaces (37)		
I2	IF dissolved gas will enter the shallow freshwater aquifer flow system through diffusion 29),		
	AND if the dissolved methane impacts the groundwater quality exceeding standards (38),	High methane flux	Groundwater quality monitoring network

		Vulnerable groundwater quality	
	AND the groundwater discharges in a vulnerable groundwater dependent ecosystem in an environmental protection zone (39),	groundwater dependent ecosystems	
	THEN an environmental hazard can occur (40)		

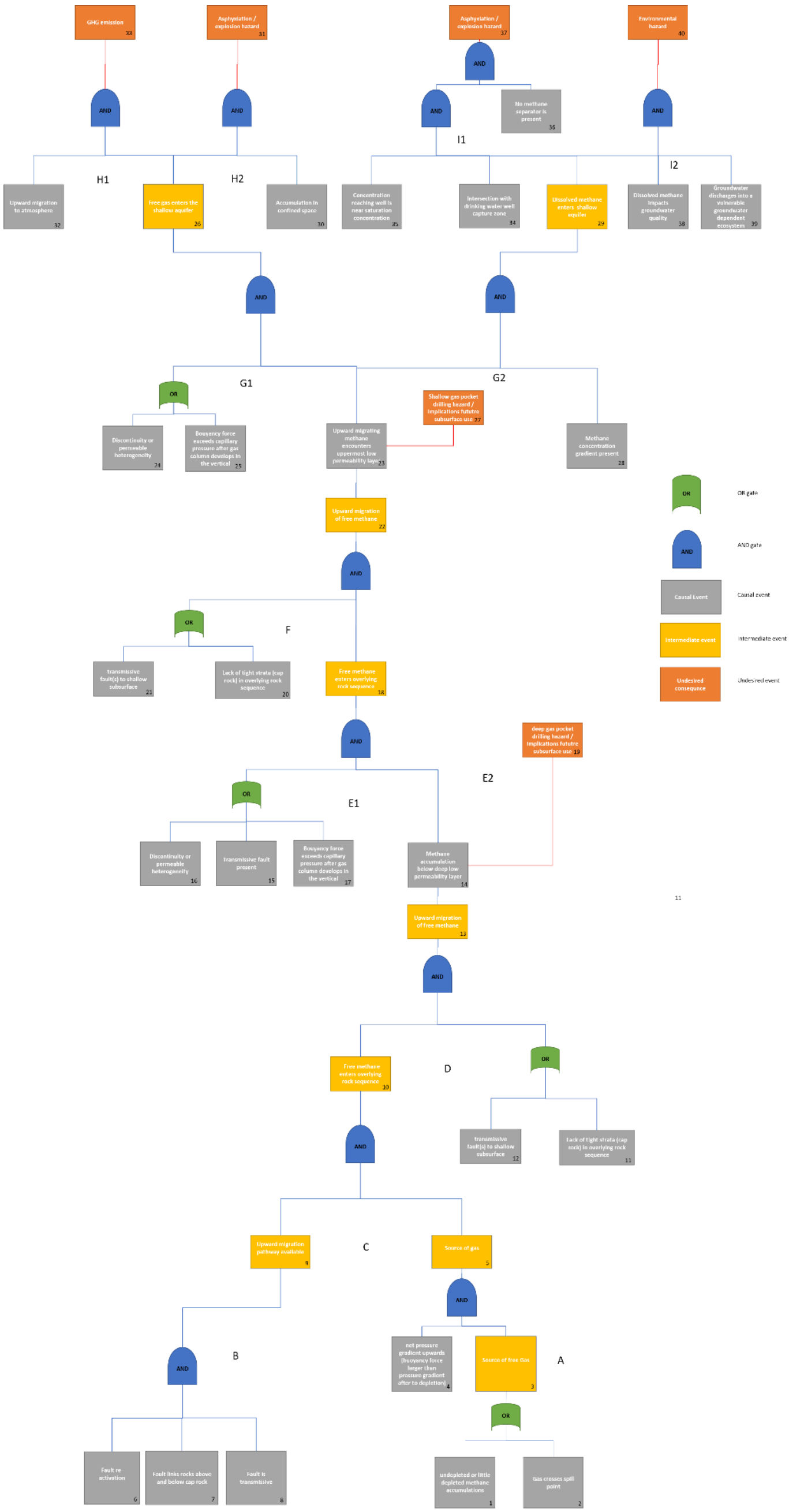

Figure B-3. Fault tree for the vertical migration of gas to shallow aquifers.

B.3 References

Tartakovsky, 2007. Probabilistic risk analysis in subsurface hydrology. Geophysical Research Letters 34, 5. doi.org/10.1029/2007GL029245

Tartakovsky, 2013. Assessment and management of risk in subsurface hydrology: A review and perspective. Advances in Water Resources 51, 247-260.

C Regional pressure equilibration modelling

In this section, the regional model used for the pressure redistribution calculation and the results are described in detail. Sensitivities will be used to evaluate the impact of some of the uncertain parameters, in particular those that influence the pressure in the aquifers.

C.1 Geological model

C.1.1 Model area

The regional flow model in this study should include all areas around the Groningen gas reservoir that could potentially be depleted over the time period of interest (i.e. 500 yrs). These areas are all active aquifers as identified by NAM (NAM, 2020) (see Figure C-1). The geological model made available by NAM (NAM V6 model, available via public.yoda.uu.nl), however, it does not cover the required area and needs to be extended. There are some practical limitations on the extension of the model in the areas in Germany to the east of the Groningen field, for which very little information is available. The same is true for the far north part of the field which lies beneath the Waddenzee. Taking these limitations into account the following boundaries were selected compared to the NAM model:

- North: extend the NAM model to include the northern aquifers: include the Ruby and N07-B fields, north of the island of Schiermonnikoog
- South: extend the NAM model to include the Annerveen field
- West: the Lauwerszee Trough is included in the geological model, because from history matching the Groningen model (Zeeuw and Geurtsen, 2019), it is known that the depletion in the southwestern fringe of the Groningen field is influenced by the depletion from the gas fields in the Lauwerszee Trough. The Hantum fault from DGM v5.1 (Digital Geological Model v5.1 made available by the Geological Survey of The Netherlands) is selected as the boundary of the model. Although currently no interference with the northern Lauwerszee Trough is observed, it is included for sensitivity analysis purposes.
- East: In the north-east part of the model in the Eems area, the model surfaces were extended and matched to well tops (see below for a more detailed specification of the surfaces used).

Most aquifers have been included explicitly by extending the model size. However, for the aquifers Rysum and Moewensteert it is possible that the aquifer extend is underestimated (see Figure C-1). To account for the potential underestimation of the aquifer size, the block pore volume was increased on the edges, instead of increasing the model size to keep the model size manageable. The impact of the size of these aquifers is investigated in the sensitivity analysis.

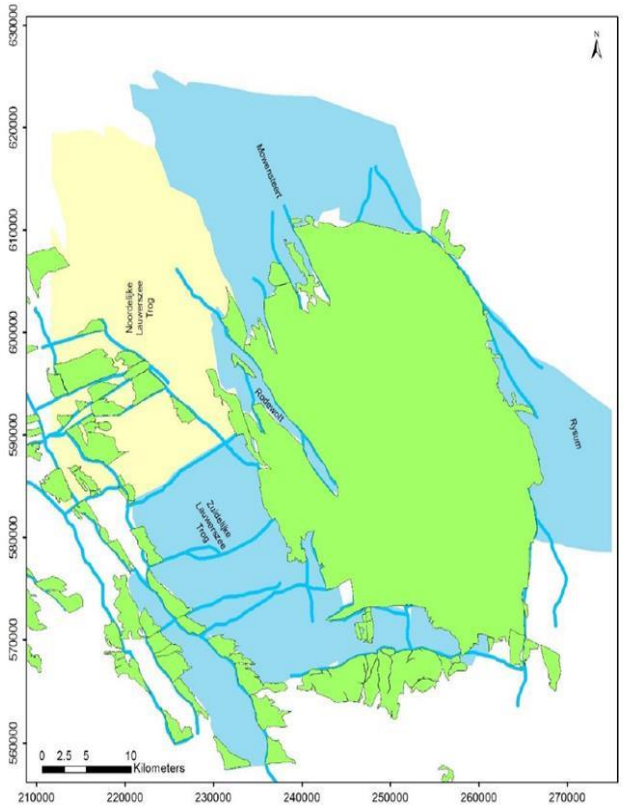

Figure C-1. schematic representation of the aquifers (in blue) surrounding the Groningen gas field (figure 20 from NAM, 2020).

C.1.2 Structural input data and grid

There is a wealth of technical information and data available on the Groningen gas field, including a full-field Petrel reservoir model (Zeeuw & Geurtsen, 2019). For the main reservoirs of the Groningen field, the Upper and Lower Slochteren Sandstone, a nation-wide property grid is available from ThermoGis (Vrijlandt et al, 2019).

The geological model was built using the following surfaces:

- ThermoGIS Top ROSLU (Upper Slochteren Sst) grid (Sept 2018), 250 x 250 m resolution
- NAM V6 model: thickness grids of Ten Boer Claystone (ROCLT), Upper Slochteren Sst (ROSLU), and Lower Slochteren Sst (ROSLL) (https://public.yoda.uu.nl/geo/UU01/1QH0MW.html)
- ROSLL is not present everywhere in the Groningen field, so the Top ROSLL grid was extended to the south by merging with the base ROSLU grid
- ThermoGIS Top ROSLU grid is really the top of the Ten Boer Claystone (ROCLT), that overlies ROSLU. A ROCLT isopach map was extracted from NAM's Groningen model, extrapolated to cover the areal extent of our model, and used to construct the real Top ROSLU grid. In a similar way, the top and base ROSLL were constructed.

- Carboniferous is included in the model by creating a zone of 300m thick (analogues to NAM V6 model)
- The Ameland Clay is not included in the model explicitly, but as a transmissivity multiplier.
- In the Eems area the surfaces needed to be conditioned to well tops, because the maps did not extend into this area. Wells used are: GHS-Z1, GHS-Z8, MNSL-Z1, EMH-Z 1A

The following faults were used in the model:

- Faults from NAM Groningen model (NAM Fault Nomenclature) that are used are shown in Figure C-2).
- Simplifications NAM faults:
    - B83-B24 merged
    - Simplified faults B46 and B51
- Hantum fault from DGM v5.1, 3 parts (not shown in Figure C-2):
    - II_Hantum_noord_1_RO_ZE
    - VI_29_RO_ZE
    - VI_26_RO_ZE

The resulting model size and faults can be seen in Figure C-3.

By using these input surfaces and faults, the geological model is discretized in space with a grid which has a resolution size of 500 x 500 m in the horizontal direction. In vertical direction the grid size is variable, in total 15 layers are identified. The resulting grid is presented in Figure C-4. In Figure C-5, a cross section showing the different geological formations is shown.

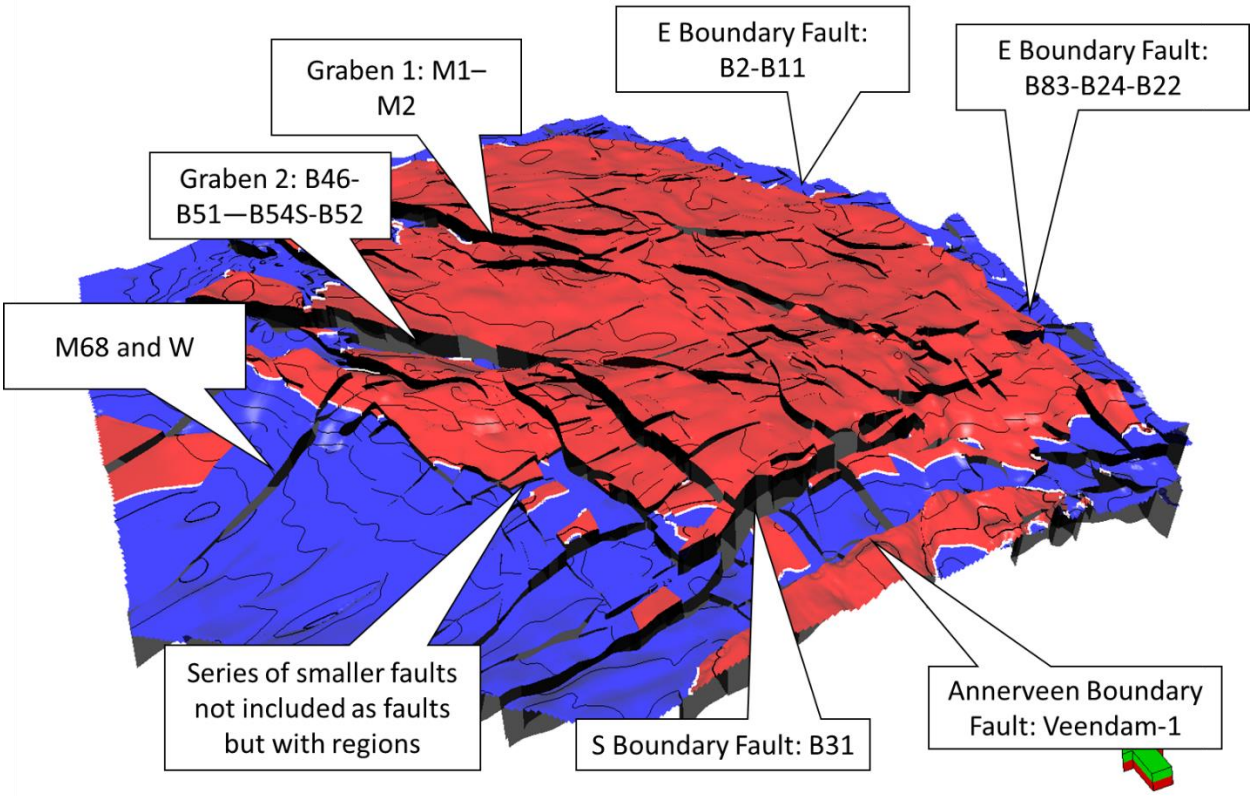

Figure C-2. Overview of the faults from the NAM model used in the regional model

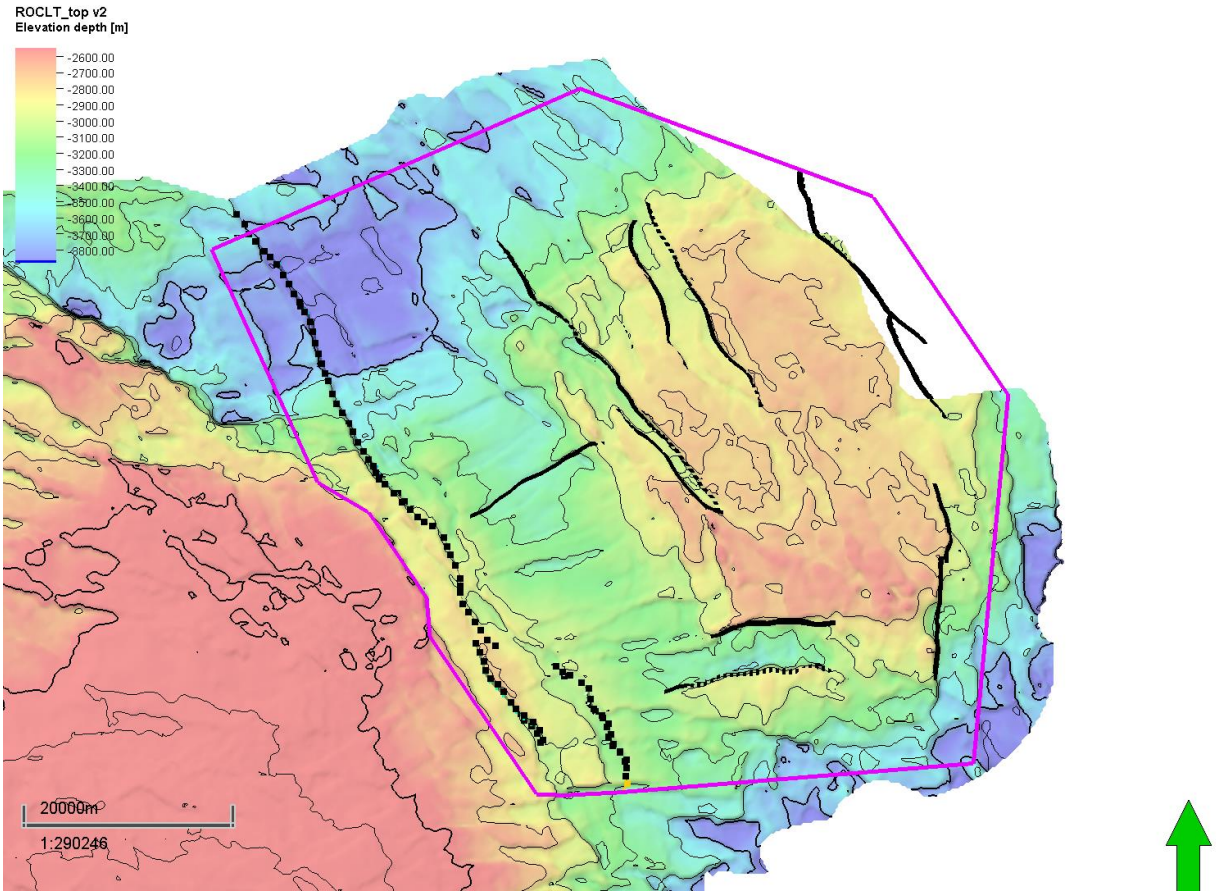

Figure C-3. Model area (pink outline) and faults included in the model and ThermoGIS surface of the top depth of the Ten Boer Claystone.

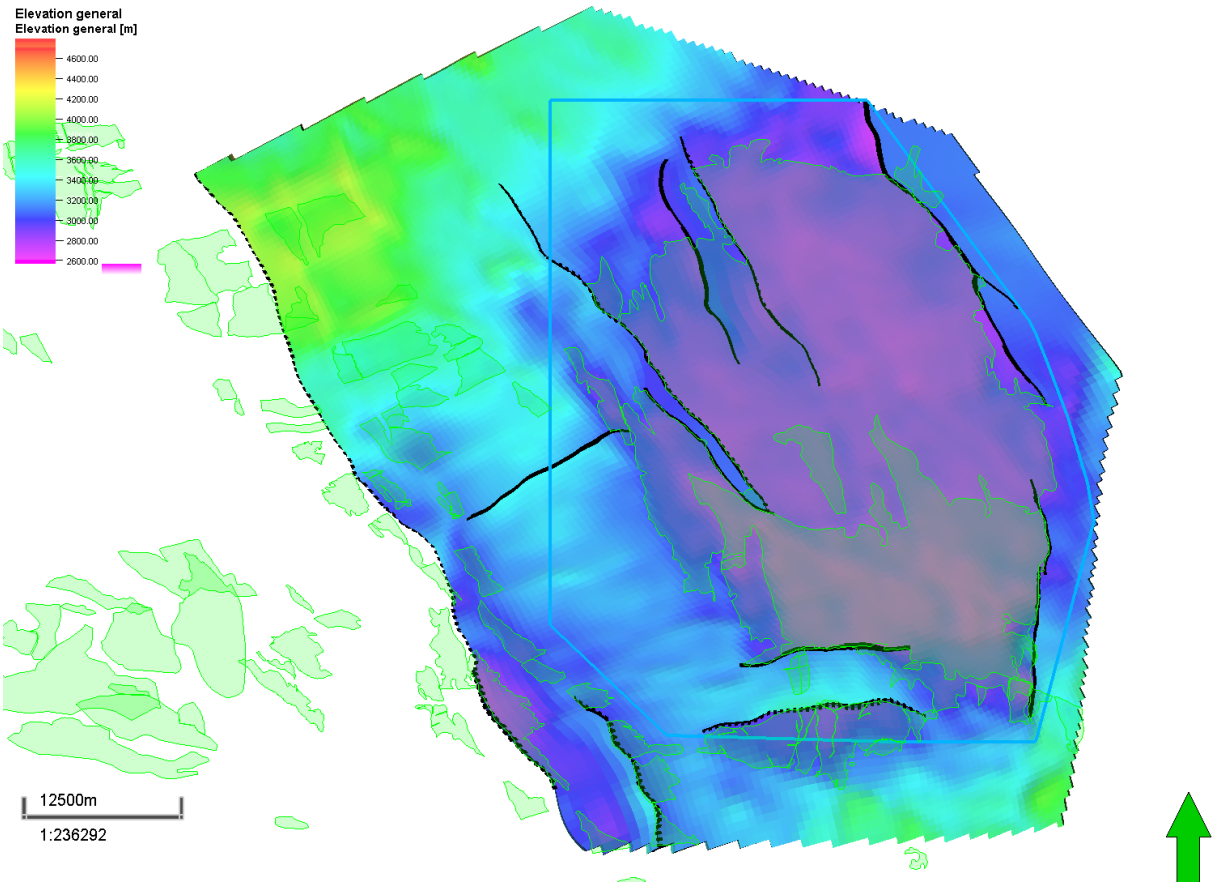

Figure C-4 Depth map of the top of the grid. Gas fields are shown in green, blue outline indicates the size of the NAM model, black dotted lines are faults.

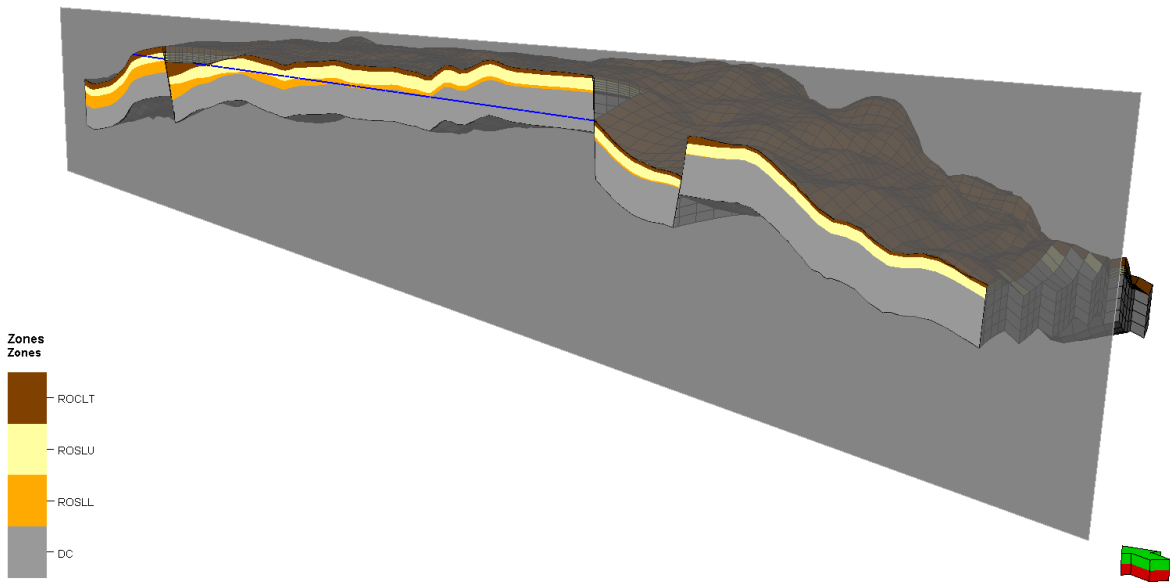

Figure C-5. Cross section of the model showing the geological layers and in blue the gas water contact (From top to bottom: ROCLT = Ten Boer Claystone; ROSLU = Upper Slochteren Member, ROSLL = Lower Slochteren Member and DC = Limburg Group of the late Carboniferous).

C.1.3 Properties

The properties porosity, net-gross ratio (NtG) and permeability for the Slochteren (ROSLU and ROSLL) are based on the ThermoGIS maps. The Ten Boer Claystone is assumed to have zero net reservoir and is thus not included in the flow simulations. The Limburg Group (referred to as Carboniferous) is based on the average properties of the NAM Petrel model. In overview:

- Ten Boer Claystone (ROCLT): 1 layer, por = 0.0, perm = 0.001 mD, NtG = 0.0
- Upper Slochteren Sst (ROSLU): 5 layers, por, perm and NtG from ThermoGIS 2.0
- Lower Slochteren Sst (ROSLL): 5 layers, por, perm and NtG from ThermoGIS 2.0
- Carboniferous (DC): 4 layers, por = 0.085 and perm=1.6 mD, NtG=0.1

C.2 Overview input to dynamic reservoir model

Based on the geological model a dynamic reservoir simulation model is created. Simulations are done using the black oil simulator ECLIPSE 100 by Schlumberger (v2019.3). In addition to the model with properties described in the previous section, the following additional information is used to construct the dynamic model (Burkitov et al., 2016; Zeeuw and Geurtsen, 2019; NAM, 2020):

- Gas water contact depth: Main field: -2985 m TVNAP; Lauwerszee Trough: 3065 m TVNAP; Annerveen: 3020 m TVNAP.

- Gas properties: 86% CH_4, 14% N_2, gravity: 0.644 sg air (modelled as dry gas using Petrel default correlations: (Dranchuk and Abou-Kassem, 1975) for the Z-factor and (Carr et al., 1954) for gas viscosity)
- Average reservoir temperature of 102.2°C
- Initial pressure: 347 bara @ 2875 m TVNAP
- Water properties are based on a water salinity of 280,000 ppm (Petrel default correlations used: (Spivey and McCain, 2003) for density and (Kestin et al., 1981) for viscosity)
- Pore compressibility: 3E-5 1/bar (representative for por=0.15)
- Relative permeability: Rotliegend representative for por=0.15; Carboniferous see Figure *C-6*
- Capillary pressure: Rotliegend representative for por=0.15; Carboniferous see Figure *C-6*

C.2.1 Free Water Level

Free water level (FWL) varies from 2972 m TVDSS on the East side of Groningen to 3016 m TVDSS in the Harkstede block. A value of -2985 m TVDSS for the main field provided a good match to NAM Gas Initially In Place (GIIP) values.

In the southern Lauwerszee Trough are a number of small fields (e.g. Roden, Vries). To allow studying the impact of pressure decline on such fields, FWL was lowered in this area to create small gas fields. The surfaces are too coarse to get an accurate representation of the GIIP of these field. The FWL selected was 3065 m TVDSS.

To the south of the Groningen field, is the Annerveen gas field. This field is not included in the NAM model. GIIP of this field was severely underestimated. Therefore, FWL was lowered to 3020 m TVDSS to come nearer to the observed GIIP.

C.2.2 Relative Permeability and Capillary Pressure

Two sets of relative permeability and capillary pressure were taken: one for the Rotliegend reservoir (ROSLU and ROSLL; saturation function 1 in Figure C-6) and one for Carboniferous (DC, saturation function 2 in Figure C-6). Both are imbibition curves, since drainage occurs only in very few places in the model. Capillary Pressure of the Rotliegend is based on the NAM curves for por=0.15 (Burkitov et al., 2016). For the relative permeability of the Rotliegend the base case values for the Brooks-Corey functions were used with Swc=0.16 and Sgr (at por=0.15) = 0.31.

Capillary Pressure for DC (Limburg Group of the Carboniferous) is based on the NAM curves for por = 0.08 for the curves in (Zeeuw and Geurtsen, 2019). The relative permeability curves for the Carboniferous are based on the curves from Zeeuw and Geurtsen, 2019 for por = 0.08.

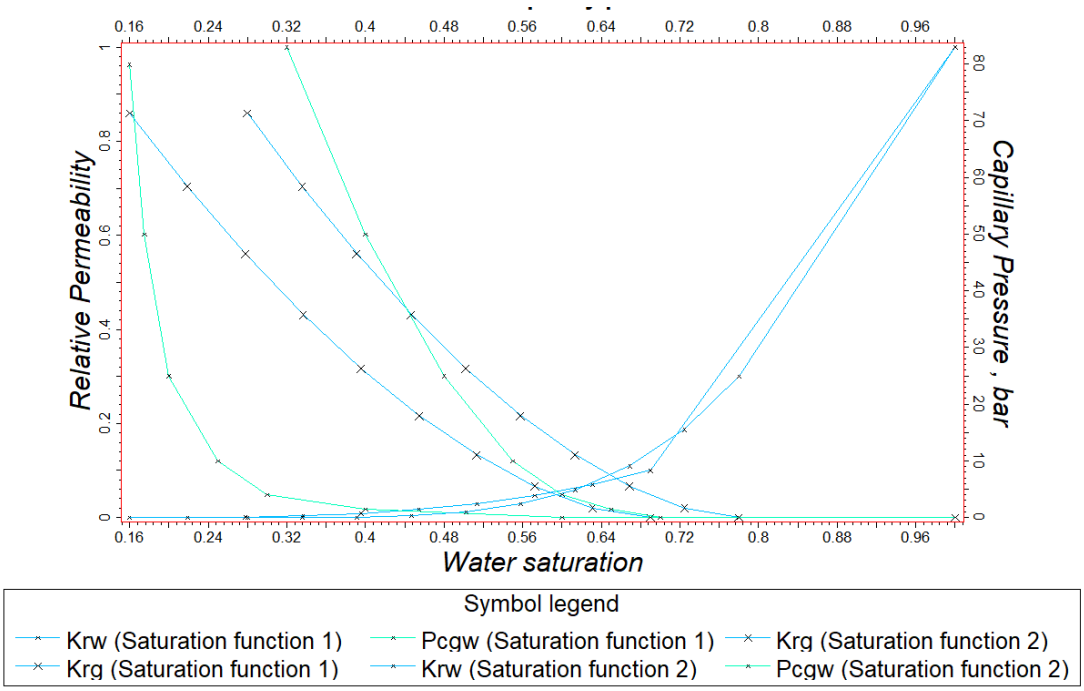

Figure C-6. Relative permeability and Capillary pressure used for the Rotliegend (Saturation function 1) and Carboniferous (Saturation function 2).

C.2.3 Gas properties

Gas properties are taken constant over the entire model area: 86% CH_4, 14% N_2, gravity: 0.644 sg air. The default correlations used in Petrel for Bg (gas formation volume factor) and gas viscosity are used (see Figure C-7). A dry gas simplified model is used which does not take into account water content (5 to 10 m^3/Nm^3) and condensate (~0.55 m^3/Nm^3) (from the Winningsplan Groningen, 2007 available on NLOG.nl). The dry gas simplification was also used by NAM up to 2012 (Burkitov et al. 2016).

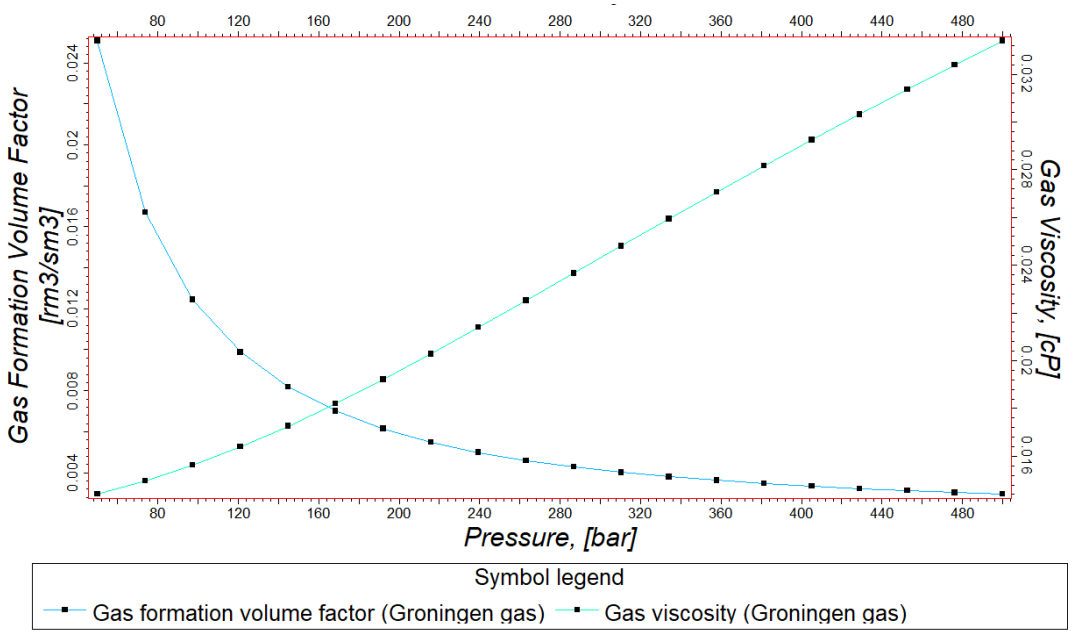

Figure C-7. Gas formation volume factor and viscosity used in the model.

C.2.4 Gas Production

The gas production of the Groningen field is implemented in a simplified manner. The annual historical gas production (Figure C-8) is divided over all clusters via a group constraint. This means the gas production per cluster is proportional to the wells potential. Each cluster is represented by a single well with large diameter (20 inch) and high negative skin (-5) that is perforated over the entire depth of the reservoir. Bottom hole pressure (BHP) calculated in this setup is not representative of the observed bottom hole pressure. Flow to tubing head is not accounted for.

Gas production from other fields is not included in the model. Thus, the depletion from the Groningen field only is simulated. Historical gas production is available up to 2020. But some production is expected up to 2025. The expected gas production for 2021 to 2025 is based on the published values in the advice on the security of supply from January 2021" (Gasunie Transport Services BV, 2021). In addition to the gas production a minimum BHP is implemented to avoid that some wells depleted much more than others. The minimum BHP decreases over time (Figure C-9). The water injection at Borgsweer is not included in the model since these small volumes influence the pressure only locally.

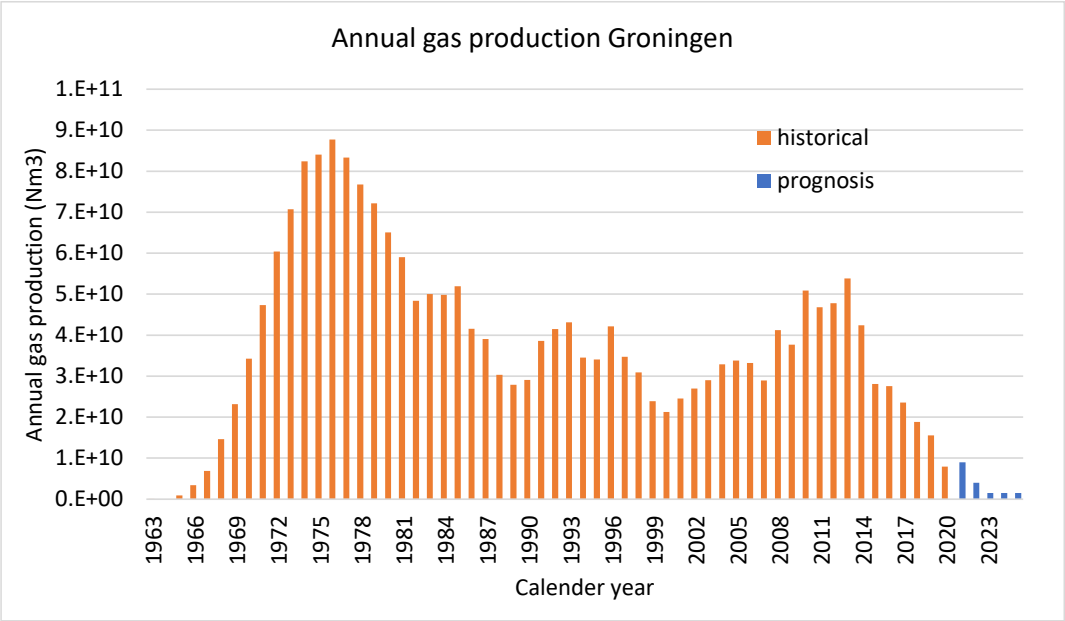

Figure C-8. Historical annual gas production of the Groningen gas field including prognosis for the last years of production.

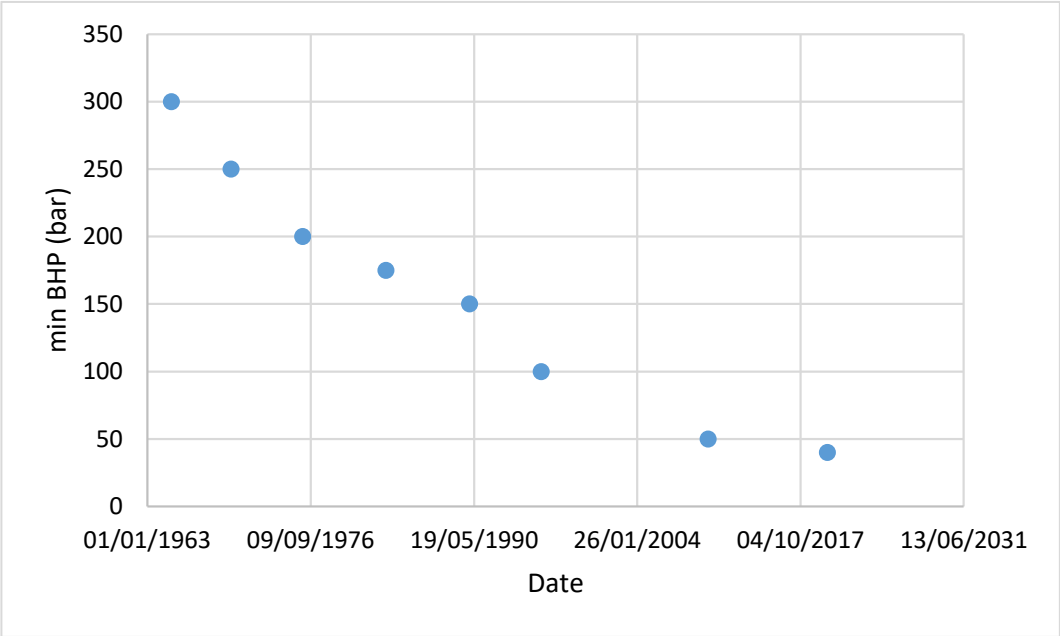

Figure C-9. Minimum Bottom Hole Pressure (BHP) over time used as additional constraint for the production wells.

C.3 History match

C.3.1 Data

The following data are used for matching the reservoir model to the historical behaviour:

- Amount of gas initially in place (GIIP)
- Historical gas production
- Historical water production
- Pressure in the gas reservoir: time series available from the NAM website “feiten en cijfers” (https://www.nam.nl/over-nam/feiten-en-cijfers.html).
- Average pressure estimated by NAM using their more detailed, but smaller simulation model.

Because this is a very coarse model, the match done here is qualitative. Only the historical gas production of the Groningen field is exactly reproduced. For the historical water production no accurate data was available, because no distinction is made between formation and vapour water in the reporting of the produced amounts of water (SGS Horizon B.V. 2016). However, due to the dry gas assumption, vapour water was not included in the model. The amount of vapour water produced is expected to be around 11 to 22 million m^3 (based on 5 to 10 m^3 water per million Nm^3 of gas). Formation water has been produced in very few wells historically. In this study the following guideline was used: the cumulative amount of formation water to be produced should not exceed 1 million m^3.

In the following first the model parameters that were adjusted in the history match are presented and then the match to the data.

Flow barriers (horizontal)
The main horizontal flow barriers are the Ameland Clay and a barrier between the Slochteren and Carboniferous (Limburg Grp). The Ameland clay divides the Slochteren in the Upper and Lower Slochteren and is only present in the north of the field. The layer is not included explicitly, but as a multiplier. The multipliers decrease from 0.01 in the middle of the field to 0.0001 in the north. The multiplier representing the barrier between the Slochteren and Carboniferous is 1 in the base case model.

Flow barriers (vertical)
Vertical flow barriers (mostly faults) form barriers to horizontal flow. All fault transmissibility multipliers have been set to 0.001 in the base case model. In addition to the faults, in some areas transmissibility multipliers were defined between segments to represent additional faults. In particular, the connection between Groningen, Harkstede and the southern Lauwerszee Trough is characterised by a range of small faults (Figure C-2). This is represented via regions with multipliers in between, because the grid is too coarse to represent these faults accurately. An overview of these regions and multipliers is presented in Figure C-10.

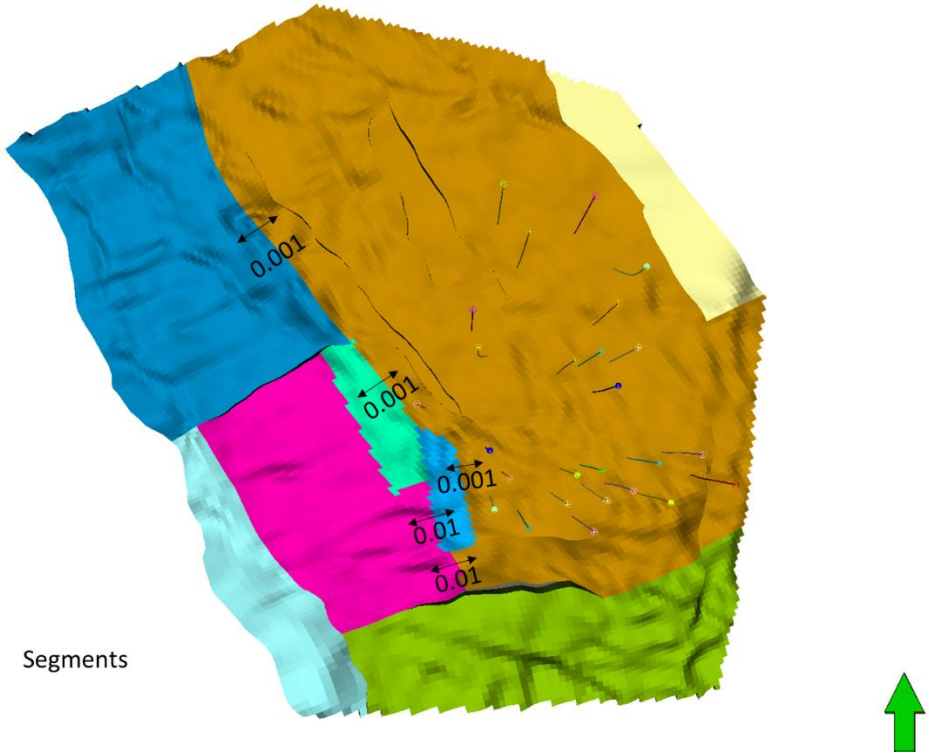

Figure C-10. Segments defined in the model and the transmissibility multipliers used between them.

Aquifer permeability

Permeability of the aquifers was reduced compared to the values from ThermoGIS. The permeability is model dependent: because this is a regional model in which few faults have been included, these flow barriers have to be accounted for implicitly in the permeability. Thus, the large scale permeability entered in this model is not representative for the local permeability.

Rotliegend:

- Permeability of the aquifer: aquifer permeability was reduced by a factor 50 compared to the ThermoGIS permeability.
- NtG was estimated at 0.7 (was: 0.9 for ROSLU and 0.8 for ROSLL).

Carboniferous:

- Initial permeability for the Carboniferous was 1.6 mD (average from NAM model). This was reduced by a factor 50.
- NtG was estimated at 0.1

Vertical permeability was 0.1*permeability throughout the model.

C.3.2 Gas initially in place

The match to the amount of gas initially in place is presented in Table C-1. The difference in GIIP for the Groningen field is 2.4%. Since the goal of the model is to investigate long term and large scale pressure development in the aquifer, the fit in GIIP is accepted as being fit-for-purpose. Also the surfaces are too coarsely represented to accurately model the smaller gas accumulations. In Figure C-11, the distribution of the gas is shown for the Upper Slochteren and the Carboniferous. The overall gas distribution matches with the contours of the Groningen gas field. In a small area in the north-east the gas distribution is not well reproduced. Most smaller gas fields are not included.

Table C-1. Overview of Gas Initially In Place (GIIP) of NAM models and the model in this report (in normal BCM (1 atm, 0°C)).

	NAM best match (Zeeuw and Geurtsen, 2019)	**This report**
Groningen (above FWL) (incl. land assets included in NAM reservoir model)	2894 BCM	2964 BCM
Gas below Free Water Level	103 BCM	Not included
Carboniferous	42 BCM	34 BCM
Norg	Not included	69 BCM
Annerveen	Not included	36 BCM

C.3.3 Pressure

Figure C-12 shows the match of the simulated pressure over time in four example locations in the Groningen gas reservoir. This shows that the pressure behaviour in the main gas field is represented well. Figure C-13 shows the difference between the depth-averaged pressure from the NAM reservoir model and the reservoir model from this report. These differences are explained as follows:

- To the west, depletion is underestimated in the Bedum field (13.5 BCM) in the model presented here compared to the NAM model, because production from this field was not included in this model. The Bedum field is isolated from the Groningen field by faults.
- To the North of Bedum is the Warffum field (12.3 BCM). Depletion from this field is also not included in our model causing overestimation of the pressure in this area. In contrast to Bedum, Warffum is connected to the Groningen field and thus the difference between the models is smaller.
- The same is true in the southern Lauwerszee Trough: here the depletion from the fields Roden and Vries is missing. In the south the depletion from Kielwindeweer and Annerveen are missing.
- On the east side of the model a few discrepancies are present which are artifacts caused by subtracting two models with a difference in the position of the boundary.

Pressure in the gas field itself are very close to the pressures in the NAM model. Overall, the model was judged fit-for-purpose.

For the southern Lauwerszee Trough, the history match requires a special note. For the southern Lauwerszee Trough no direct pressure measurements are available in the aquifer. To guide the history match despite the lack of measurements, NAM assumed that the depletion in this area should be larger than 90 bar based on the earthquakes in the aquifer at Paddepoel and Eelderwolde (Zeeuw and Geurtsen, 2019). This is based on the observation that earthquakes are only observed for reservoirs at more than 28% depletion (see the discussion in Section 5.2.1). This depletion was partially attributed to the depletion resulting from the fields Vries, Roden and Pasop which are located at the west boundary of the southern Lauwerszee Trough ((Zeeuw and Geurtsen, 2019). The depletion of these fields was implemented on the boundary of the NAM model and this resulted in a drawdown of more than 100 bar in the entire aquifer already by 2006. At Eelderwolde which is in the middle, the depletion would be caused in approximately equal amounts by the Groningen field and the small fields. The southern Lauwerszee Trough has few north-south oriented faults, which could explain the good east-west connectivity. In the model used in this report, the depletion of the small fields Vries, Roden and Pasop was not included resulting in different results as the NAM model. At this point, no consistent match has been done for the entire Lauwerszee Trough and the gas fields in it and thus it is not clear whether such an active aquifer and large depletion matches the observations in both the Groningen field and the small fields Faan, Pasop, Roden and Vries.

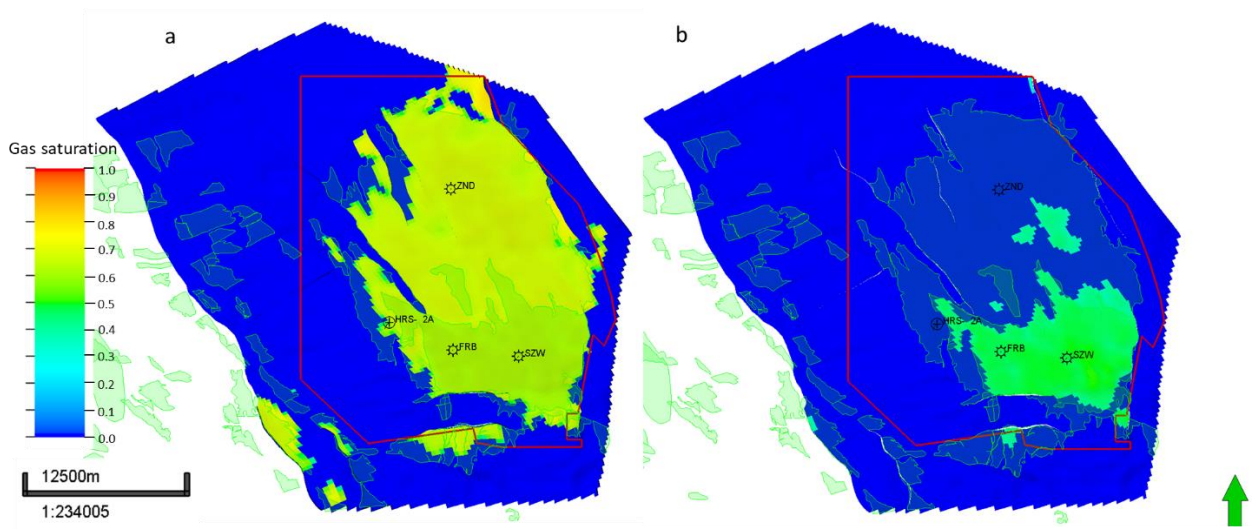

Figure C-11. Gas distribution in the Upper Slochteren Sst (a, left) and Limburg Group (Carboniferous) (b, right) (blue is aquifer; yellow is gas, red outline is the outline of the NAM model; green outlines are the gas fields).

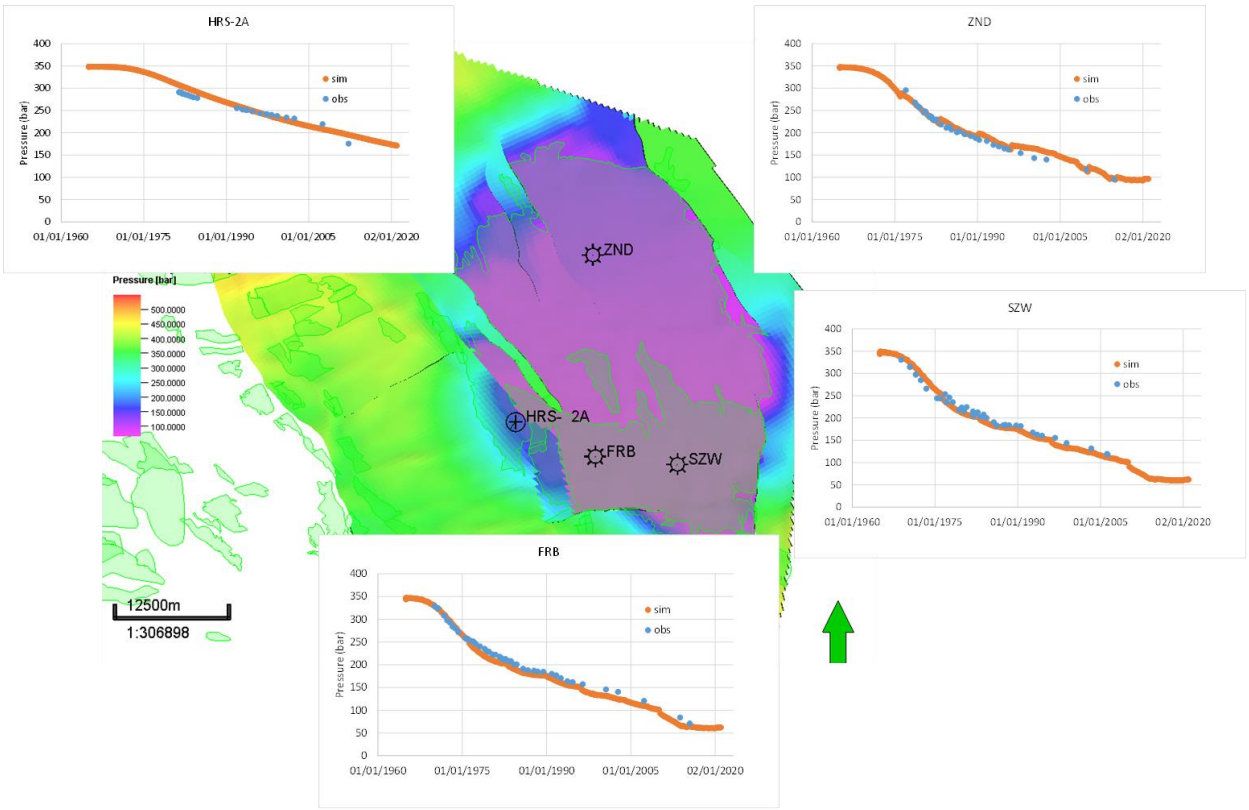

Figure C-12. Comparison between observed static pressure ('obs' in blue) and simulated pressure ('sim' in orange) for four wells in the gas field. In the background is the pressure in 2026, the well locations and the gas field outlines (in green).

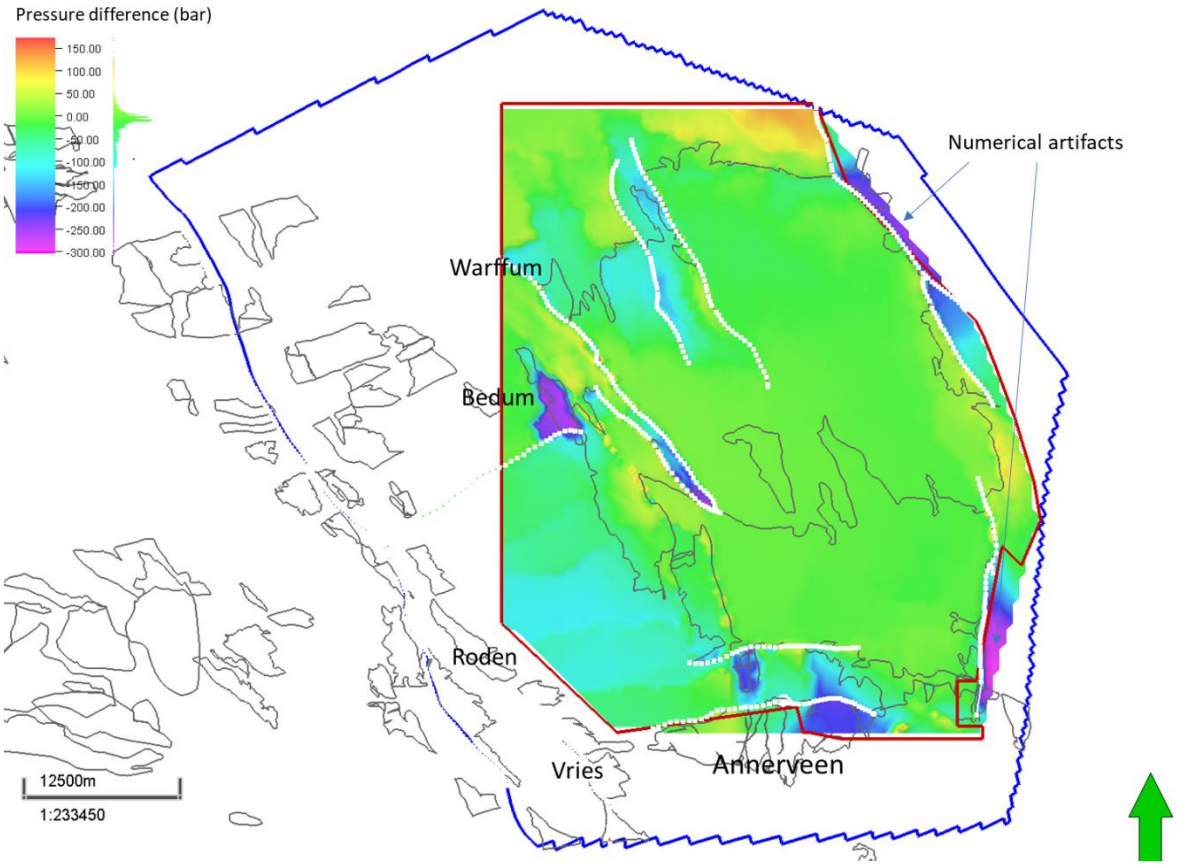

Figure C-13. Difference between the pressure in 2020 as simulated by NAM and the model in this report (Pressure NAM – pressure this report). For positive values, NAM pressures are higher. Negative values indicate pressure in this report are higher. Red and blue outline indicate the boundaries of the NAM model and model from this report respectively. Grey outlines are gas fields. White dotted lines are faults.

C.4 Prediction results

C.4.1 Base case

The base case model described in the previous section is used to simulate the pressure development for the next 500 years. NAM has published pressure predictions up to year 2080. These predictions are compared to those from our model. In Figure *C-14* and Figure C-15 the pressure development in the gas field is compared. At year 2080, the range in pressure predicted by NAM is slightly larger than in our model, but the predicted pressure is very similar. Figure C-16 shows the difference in pressure between the NAM model and our model in year 2053. It is clear that the pressures are much more in line in 2053 than they were in 2020. This is because the pressure has equilized over the field and depends less on the details of the production. From this it can be concluded that the predictions from this model are in line with the much more detailed NAM model in the immediate area of the gas field. Next, it will be investigated what happens in the aquifers.

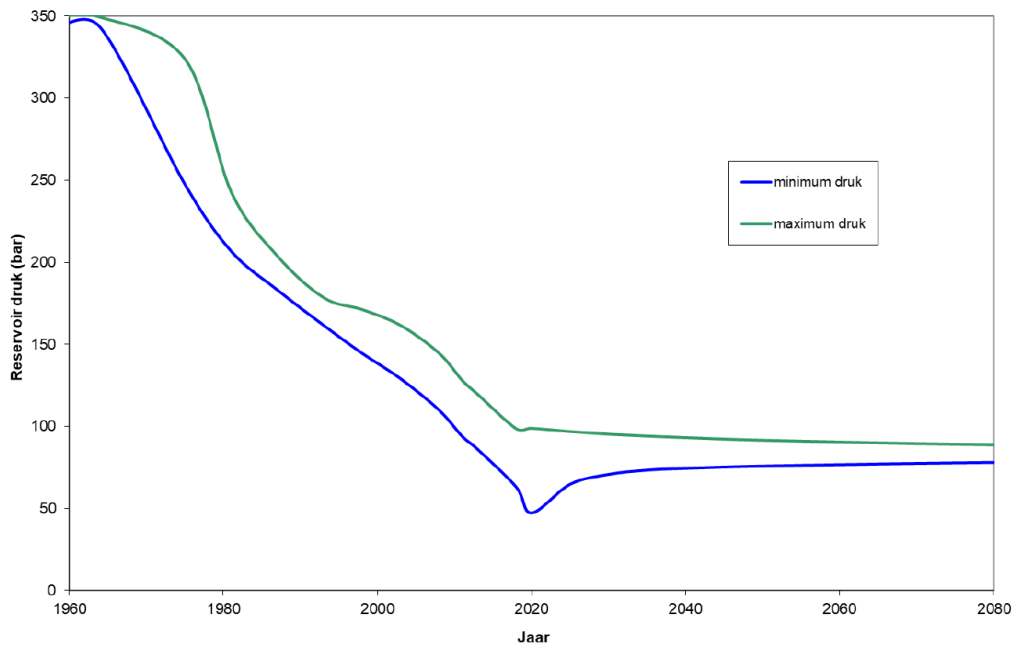

Figure C-14. Prediction of the reservoir pressures in the Groningen field from the Status rapport 2020 (NAM, 2020) indicating the range of expected pressures in the field up to 2080.

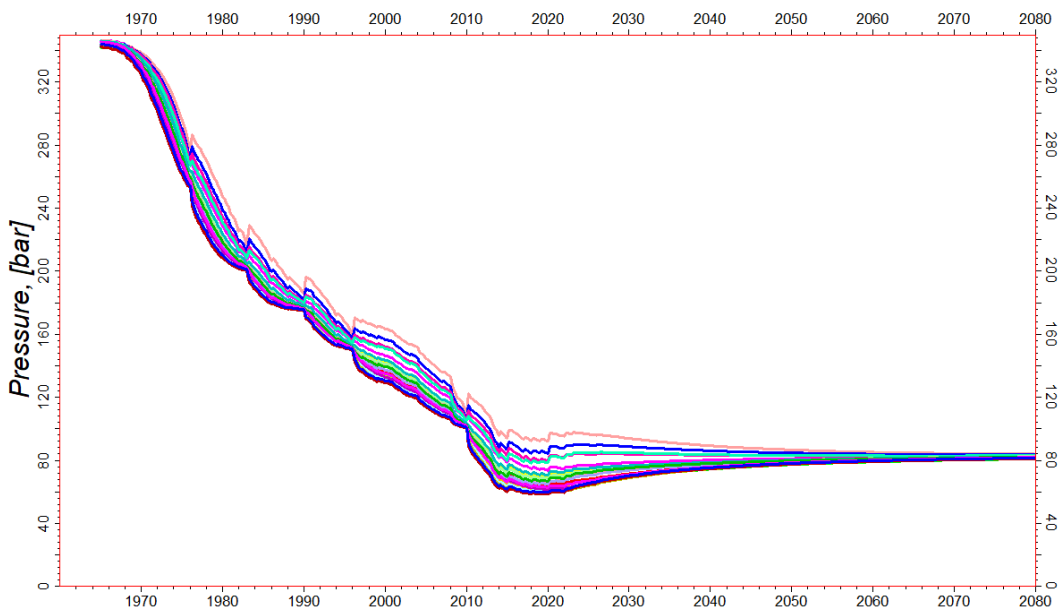

Figure C-15. prediction of the reservoir pressure over the same period of time from the base case model. Each colored line indicates the pressure development at a well location.

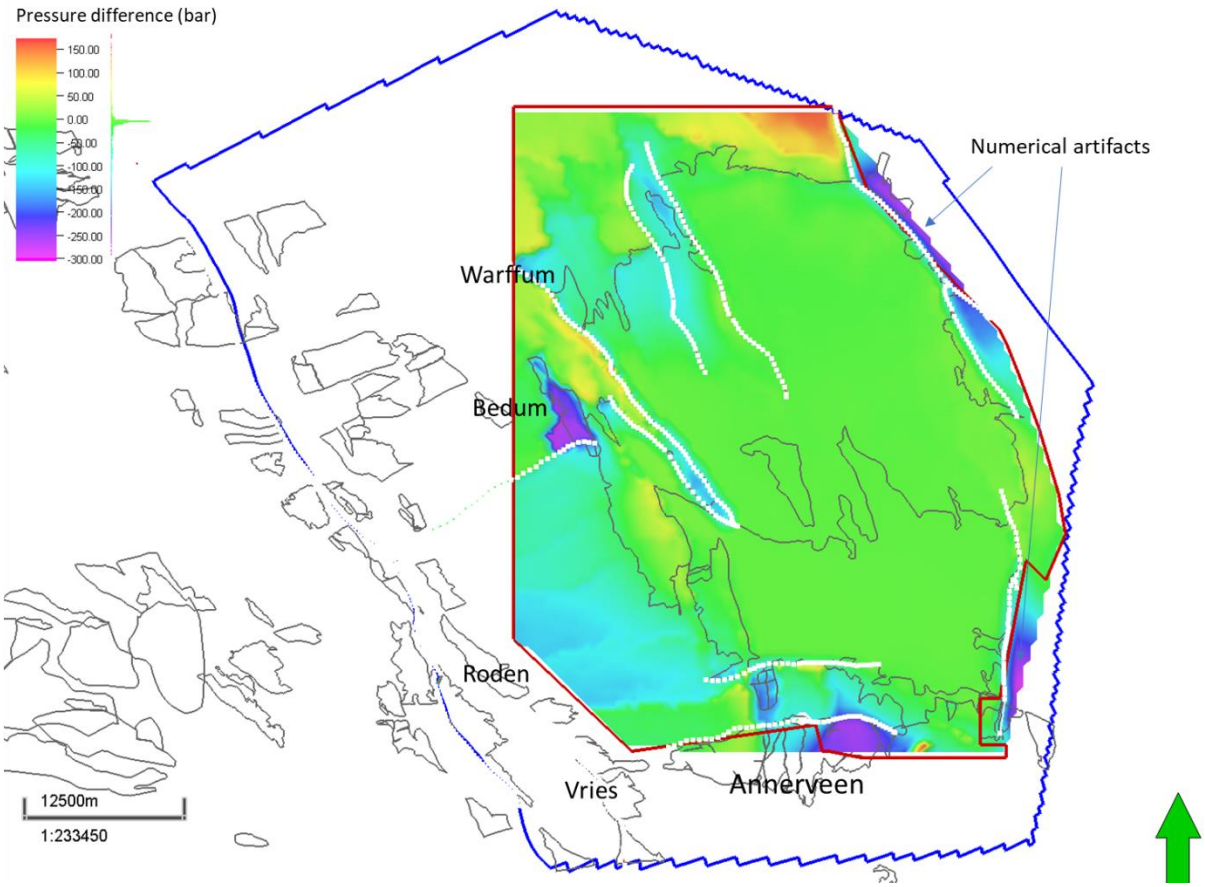

Figure C-16. Difference between the pressure in 2053 as simulated by NAM and the model in this report (Pressure NAM – pressure this report; in bar). For positive values, NAM pressures are higher. Negative values indicate, pressures in this report are higher. Red and blue outline indicate the boundaries of the NAM model and model from this report respectively. Grey outlines are gas fields. White dotted lines are faults.

Figure C-17 shows how the pressure depletion changes in the first 100 years after the stop of gas production. In the gas filled area the pressure rises only a few bar. In the Slochteren Fm the depletion in the aquifers clearly increases in particular in the north and in the south-west. The depletion in the north-east is probably overestimated, because the model lacks a fault in this area. This can also be seen in Figure C-16 (red area on the east side of the northern boundary of the model). On the west side the aquifer depletion is likely to be realistic. It is known that in this area, the gas field is connected to an active aquifer. Figure C-18 shows the depletion percentage 500 years after stop of production. Now large parts of connected aquifers have depleted more than 40%, in particular in the north. In the south-west in the southern Lauwerszee Trough, the pressure dissipates slowly due to the low transmissivity of the Slochteren in this area.

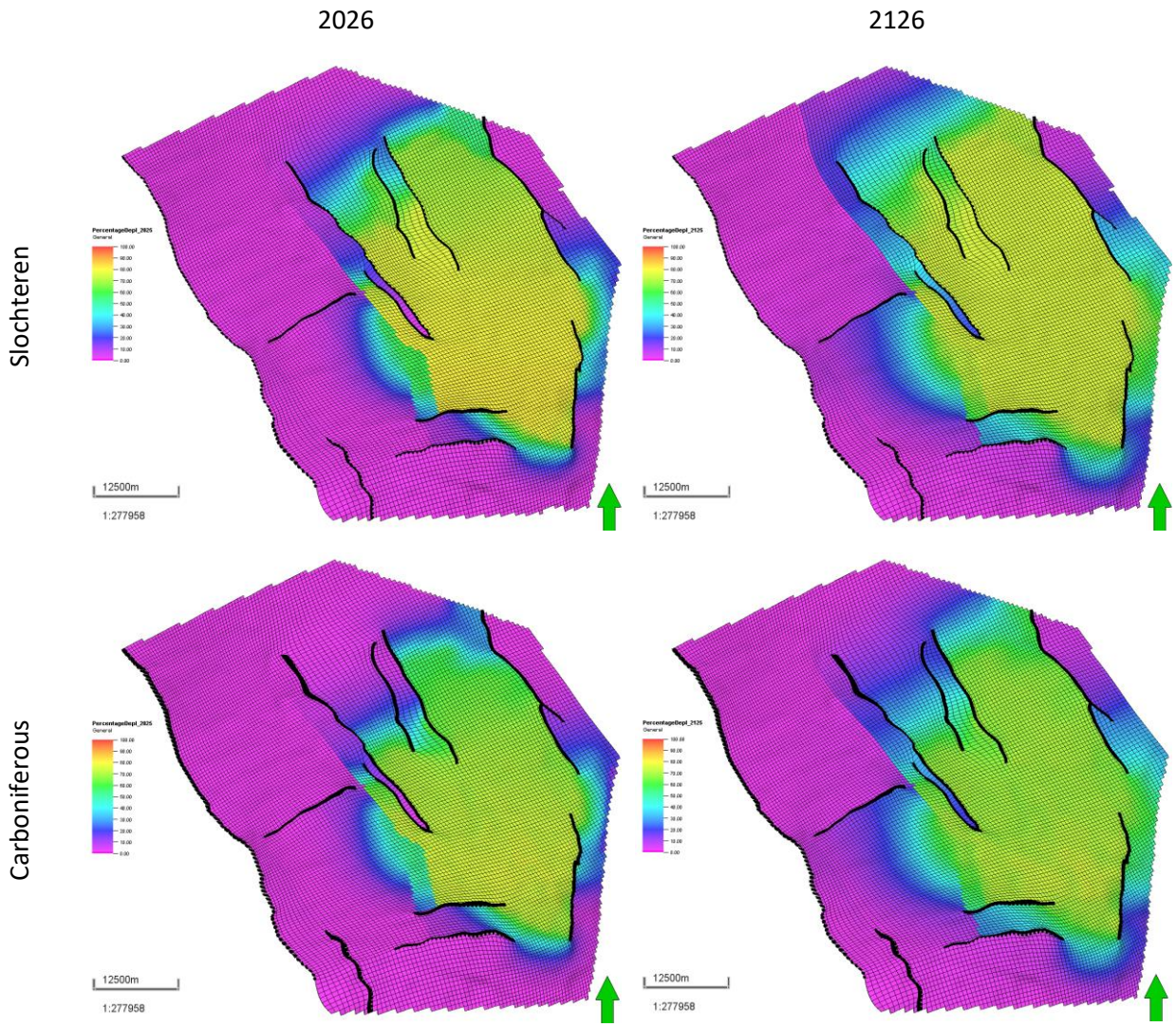

Figure C-17. Percentage depletion in 2026 (stop of production; left) and 2126 (right) at the top of the model (top row; Slochteren) and the bottom part of the model (top of Limburg group (Carboniferous); bottom row). Color scale ranges from 0 (pink) to 100% (red).

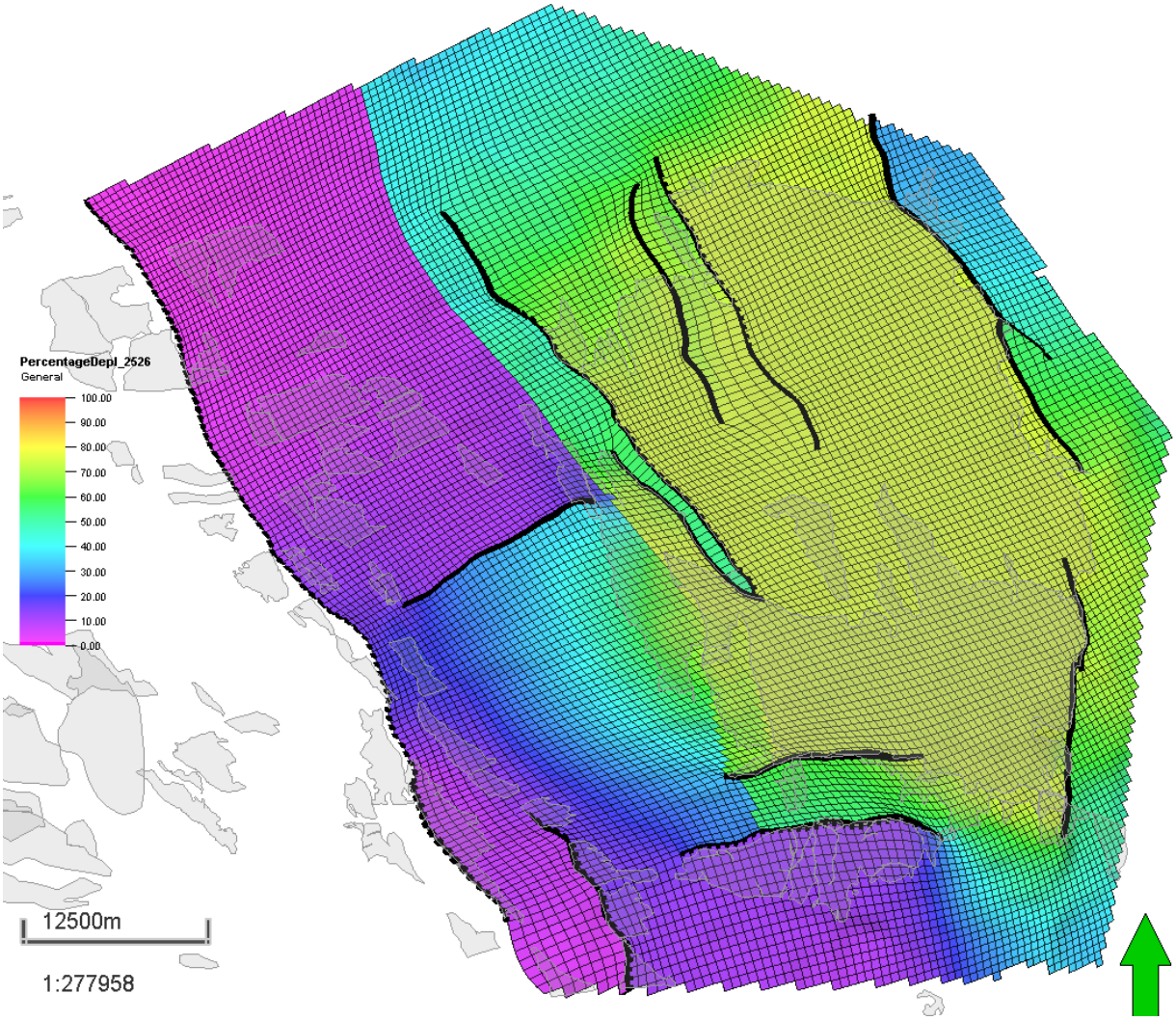

Figure C-18. Percentage depletion 500 years after the stop of production (year 2526) (depth averaged). In grey overlay the outline of the gas fields is shown. Black dotted lines are faults.

C.4.2 Sensitivities

C.4.2.1 Sensitivity analysis mass balance

Before the sensitivities with the numerical model are run, first some sensitivities are investigated with an analytical approach based on the mass balance. Given the volumes water and gas in the subsurface, it can be calculated what the pressure will become if the water and gas equilibrate completely.

The pressure after full equilibration (P_{end}) for an aquifer in contact with a depleted gas field, can be described from the compressibility equations and assuming that the pore volume doesn't change:

$$c_w = -\left(\frac{dV_w}{dP}\right)/V_w$$

$$c_g = -\left(\frac{dV_g}{dP}\right)/V_g$$

$$c_w V_w = -\left(\frac{V_{w,end} - V_{w,ini}}{P_{end} - P_{w,ini}}\right)$$

Assuming a constant pore volume ($V_{por} = V_{w,ini} + V_{g,ini} = V_{w,end} + V_{g,end}$), gives

$$P_{end} = \frac{c_w V_{w,ini} P_{w,ini} + c_g V_{g,ini} P_{g,ini}}{c_w V_{w,ini} + c_g V_{g,ini}}$$

Where:

c : compressibility (1/bar)

V : reservoir volume (m^3)

P : pressure (bar)

subscripts *w* and *g* refer to gas and water respectively; subscripts *ini* and *end* refer to the initial and final pressure. In this case the initial pressure would be the pressure at the end of production. The impact of the assumption that the pore volume is constant depends on the compressibility of the pore volume. Pore compressibility for the gas reservoir is ~3E-5 1/bar, which is very similar to the water compressibility (Table C-2). The compressibility of the aquifers is probably similar or lower. The effect of the pore compressibility can be evaluated by changing the water compressibility. The impact of changing the compressibility is investigated in the sensitivity cases below.

Four cases are considered in the analytical model:

- Base case which is based on the base case numerical model
- Gas in aquifer: by adjusting the compressibility of the water, the presence of gas in the aquifer below the gas water contact can be mimicked. If 5% of the water is replaced by gas, compressibility can be calculated from:

  $$c_{w,eff} = 0.05 * c_g(@\ P_w) + 0.95 * c_w$$

  If 5% water replaced by gas would amount to around 900 s.Bcm of gas (this depends a lot on the assumed pressure). In the NAM model around 100 N.Bcm (106 s.Bcm) was taken for gas below free water level.
- Case with lower gas compressibility which would represent a different initial pressure.
- Large aquifer: The volume of aquifer attached to the Groningen might be underestimated. In addition, only the net pore volume is assumed to deplete. Therefore, a case with a 5 times larger aquifer has been calculated.

In Table C-2, the resulting equilibration pressures (P_{end}) for these cases are presented. The average, initial pressure of the entire gas is assumed to be 90 bar ($P_{g,ini}$). In the main gas zone, the pressure is lower, but

this includes all the gas in the model area which includes less depleted areas. The initial average pressure in the aquifer connected to the reservoir is assumed to be 400 bar ($P_{w,ini}$),. The comparison between the initial aquifer pressure and the equilibration pressure indicates that the depletion caused by the gas production is so large that in the long run all connected aquifers can deplete. The main question is how long it takes. The time scale of the pressure redistribution, is controlled by the dissipation time, which is given by:

$$t \sim \frac{L^2 \mu \varphi c_t}{k}$$

Where:

L : characteristic length scale
μ : viscosity
φ : porosity
c_t : total compressibility
k : permeability

Of these parameters, the permeability has the largest uncertainty by far, in particular the fault and aquifer permeability. Therefore, the uncertainty analysis of the numerical model is focused on permeability.

Table C-2. Overview of the equilibration pressure for four cases.

Case	c_w 1/bar	c_g 1/bar	$V_{w,ini}$ rm^3	$V_{g,ini}$ rm^3	$P_{w,ini}$ bar	$P_{g,ini}$ bar	P_{end} bar
Base case	2.8E-05	0.02	7.4E+10	1.2E+10	400	90	92.7
Gas in aquifer	**1.3E-04**	0.02	7.4E+10	1.2E+10	400	90	102.3
Different gas compressibility	2.8E-05	**0.01**	7.4E+10	1.2E+10	400	90	95.3
Gross pore volume depleting	2.8E-05	0.02	**3.7E+11**	1.2E+10	400	90	103.0

C.4.2.2 Sensitivity analysis numerical model

The following model parameters are included in the sensitivity analysis with the numerical model:

- The permeability of the Limburg Group (Carboniferous, DC)
- The permeability of the aquifers (in Upper and Lower Slochteren Sst)
- Vertical permeability
- The position of the Ameland clay
- The transmissivity of the barrier between Lower Slochteren and Carboniferous

- Fault permeability (all faults)
- Size of the analytical aquifers Rysum and Moewensteert (pore volume multiplier, see section C.1.1)
- Transmissivity between segments (representing faults not explicitly included in the model, see Figure C-10)

The parameters used in the simulations are given in Table C-3. The sensitivities were done one-at-a-time, resulting in a total of 30 simulation runs (excluding the base case). Only low, mid, high cases were done as a first exploration of the uncertainty. When the mid case is identical to the base case, this run was not repeated.

Table C-3. Overview of the variables included in the sensitivity analysis and the values used.

Variable	**base**	**low**	**mid**	**high**
DC permeability multiplier	0.02	0.001	0.0019	0.025
Aquifer permeability multiplier	0.02	0.01	0.014	0.025
Vertical permeability multiplier	0.1	0.033	0.05	0.1
Ameland clay position	Row 60	As base	5 km to the north	10 km to the north
ROSL_DC barrier multiplier	1	0.01	0.505	1
Fault permeability multiplier	0.001	0.0001	0.001	0.01
Rysum and Moewensteert	10	5	27.5	50
Inter-segment transmissivities	1 to 0.001	0.01 to 0.0001	0.1 to 0.001	1 to 0.01

Figure C-19 shows the averaged depletion in year 2126 (100 years after the production stop). The results are very similar to the base case.

More interesting is to look at the pressure range resulting from the sensitivity runs. Figure C-20 shows the range in pressure from the 30 simulation runs in 2025 and in 2126. In pink are the areas where very little variability is observed between the sensitivity runs, either because the runs differ very little (in the gas field) or because the depletion is small overall (e.g. in the northern Lauwerszee Trough and near Norg in the south-west). The largest variability occurs on the boundaries and the aquifers connected to the Harkstede area. Clearly the range increases with time as the impact of the uncertain parameters increases.

Figure C-21 shows the range in the depletion in year 2126 in a cross section. The range in the depletion in the Carboniferous is much larger than in the Slochteren, which reflects the uncertainty about the properties of this formation. It should be noted that in this study the permeability of the Carboniferous

was homogeneous, which means that these results do not reflect the spatial heterogeneity of Carboniferous.

It should be noted that the sensitivity runs with the multiplier on the fault between Harkstede and Groningen have not been included in the calculation of the average and range because these runs had a poor history match to the observed pressures in well HRS-2A (see Figure C-23).

Please also note that the focus was on areas to the west of the field and less on the south and east. In the south the analysis has to be done on a more detailed scale, because this area is highly faulted and holds many other gas fields. In the east the information is very limited.

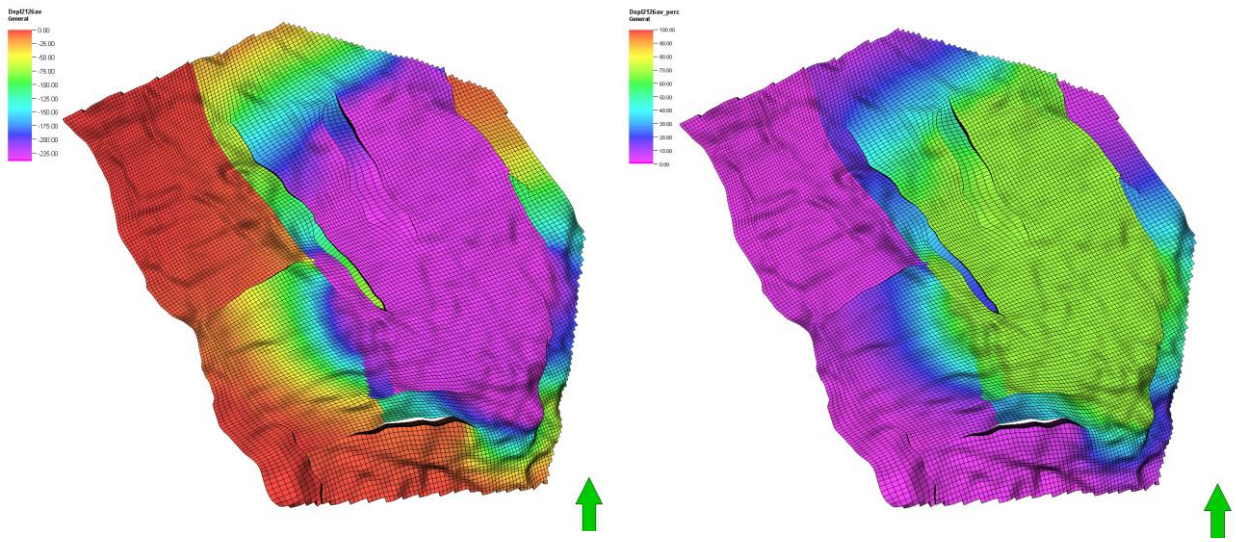

Figure C-19. Average depletion from the sensitivity runs in 2126 at the top of the reservoir (left: in bar; right: % of pre-production pressure). Depletion compared to pre-production pressure. Not depth averaged.

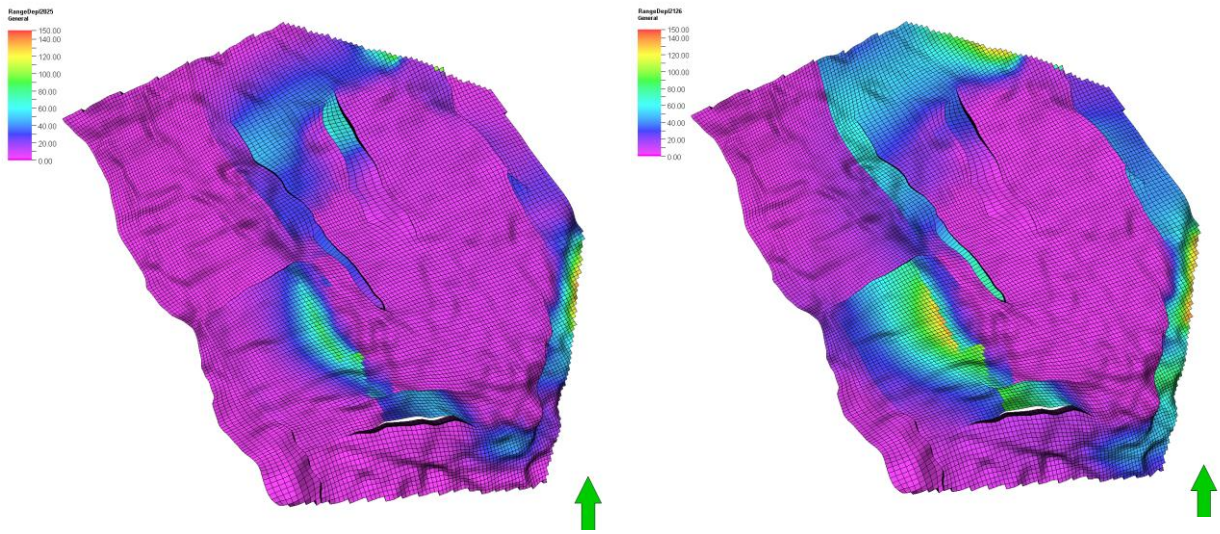

Figure C-20. Range (max – min depletion) of the depletion at production stop (2025, left) and 100 years later (2126, right) at the top of the reservoir (in bar).

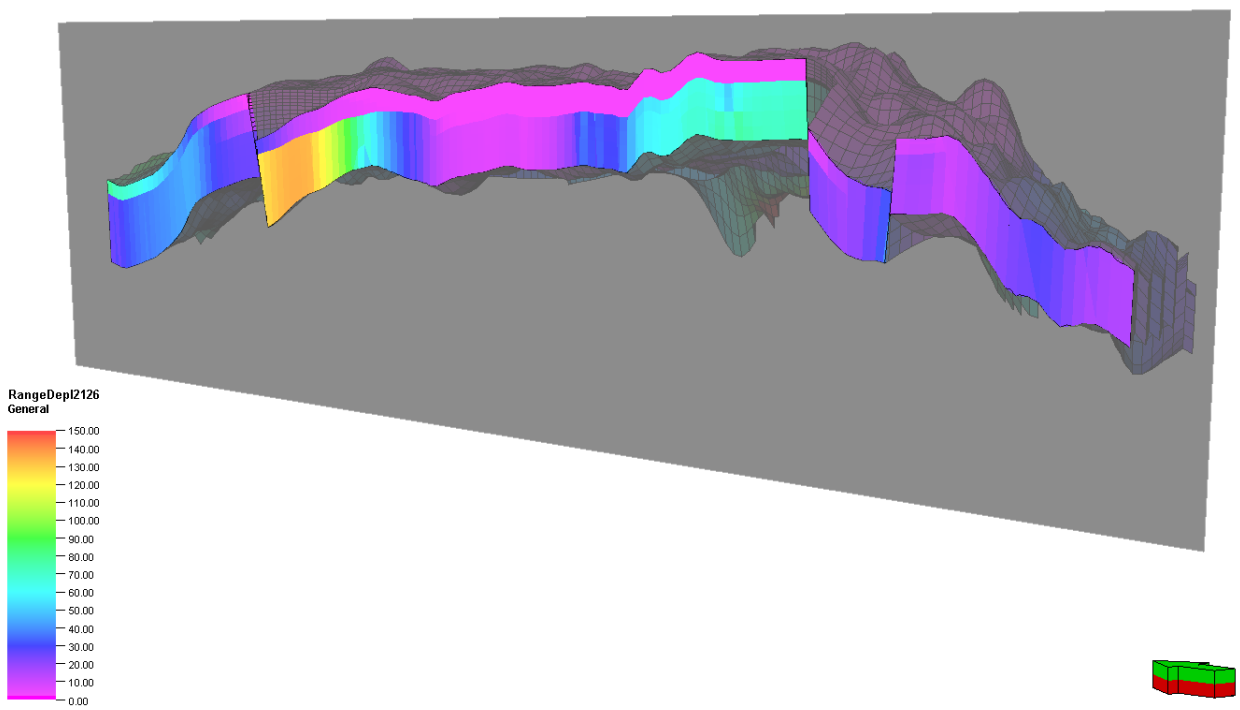

Figure C-21. Cross-section showing the pressure depletion range (bar) from the sensitivity runs in year 2126. Depletion compared to pre-production pressure.

In Figure C-22, in addition to the spatial distribution of the range in pressure from the sensitivity runs, also the development in time of the pressure is presented. For six locations the pressure development for 500 years is plotted. This shows that even locations that experience hardly any depletion in 2126, experience

depletion later. Absence of depletion observed today is no guarantee for the future, since the pressure response in some areas is strongly delayed.

The location near the gas fields Roden, Vries and Norg on the opposite site of the Southern Lauwerszee Trough experiences very little depletion from the Groningen field in these simulation runs. Since these fields have been produced, the area has experienced depletion in reality. Here only the depletion due to the production of the Groningen field is shown. Also, since it is known that the Roden field has a strong aquifer, it might be that the connectivity (permeability) is underestimated here. A more detailed study in this area would allow to define the total uncertainties better. See also the discussion at the end of Section C.3 on this topic.

Finally, in Figure C-23 the pressure development in the Harkstede area is shown for the Upper Slochteren and the Carboniferous. The pressure observations in the well HRS-2A are added (black dots). The figure shows the two scenarios with the very poor fit to observed data that were removed from further calculations. This also shows how the observations reduce the spread in the uncertainty. This is especially true in the gas field. In the aquifers, very few observations are available. Also, in order to take into account observations in detail, a more detailed model might be required to account for the local variability.

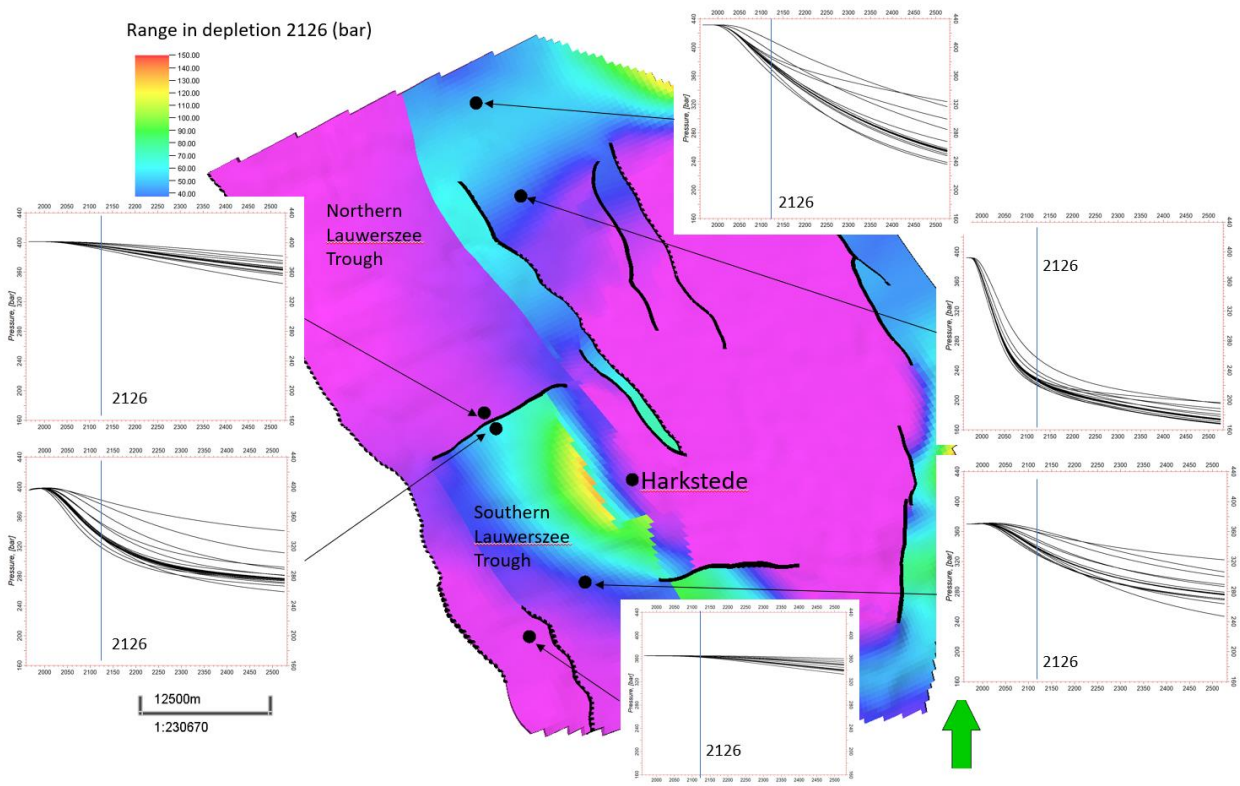

Figure C-22. Time series of the pressure depletion for all sensitivity scenarios for six locations around the Groningen field. Time-axis: 1965 to 2526. Pressure y-axis: 160 to 440 bar. Background figure shows the range in depletion in 2126 (scale from 0 bar (pink) to 150 bar (red). This moment in time is also indicated on the time series plots.

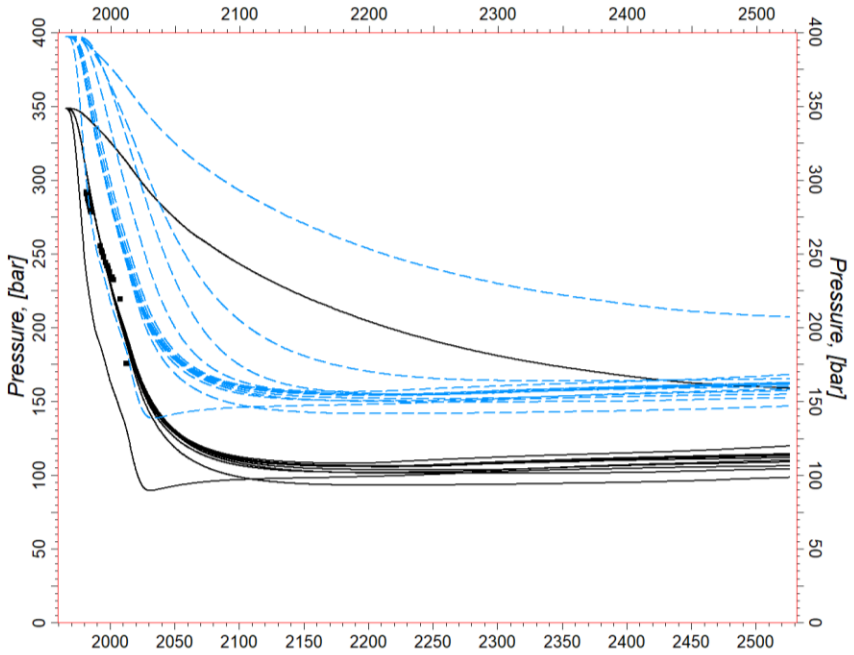

Figure C-23. Pressure development at Harkstede in the Slochteren Fm (black) and Limburg Group (blue dashed). Black dots indicate observations HRS-2A well . Location Harkstede is shown in Figure C-22.

C.5 References

Burkitov, U., H. van Oeveren and P. Valvatne, 2016. Groningen Field Review 2015. Subsurface Dynamic Modelling Report. https://www.nam.nl/feiten-en-cijfers.html.

Carr, N.L., Kobayashi, R., and Burrows, D.B.: 'Viscosity of Hydrocarbon Gases Under Pressure,' Trans. AIME (1954) 201, 264-272

Dranchuk and Abou-Kassem: 'Calculation of z-Factors for Natural Gases Using Equations of State,' JCPT (July-Sept. 1975) 34-36.

Gasunie Transport Services BV, 2021. Advies leveringszekerheid voor benodigde Groningen-volumes en -capaciteiten gasjaar 2021/2022 en verder. Kenmerk: L21.0042.

Kestin, Khalifa, & Correia, 'Effect of Pressure on the Viscosity of Aqueous NaCl Solutions in the Temperature Range 20-150degC,' J. Chem. Phys. Ref. Data, Vol 10, No. 1, 1981, p 71.

NAM, 2020. Bodemdaling door Aardgaswinning. NAM-gasvelden in Groningen, Friesland en het noorden van Drenthe. Statusrapport 2020 en Prognose tot het jaar 2080. EP202011201629. https://www.nam.nl.

SGS Horizon B.V. 2016. Independent Review of Groningen Subsurface Modelling Update for Winningsplan 2016. https://nam-onderzoeksrapporten.data-app.nl/reports/download/groningen/en/5820d1c5-d989-45f7-80b7-638156ee661e

Spivey, J.P. and McCain, W.D., Jr.: 'Recommended Correlations for Fluid Property Estimation,' unpublished September 2003

Van Eijs, R. “Correlation between hydrocarbon reservoir properties and induced seismicity in the Netherlands,” Elsevier, 2006.

Vrijlandt, M.A.W., E.L.M. Struijk, L.G. Brunner, J.G. Veldkamp, N. Witmans, D. Maljers, J.D. van Wees. 2019. ThermoGIS update: a renewed view on geothermal potential in the Netherlands. EGC, The Hague, June 2019.

Zeeuw, Q. de, L. Geurtsen, 2019. Groningen Dynamic Model Update 2018. https://www.nam.nl/feiten-en-cijfers.html.

D Fluid migration along wells

D.1 Numerical approach

The numerical simulations in this work were conducted using the commercial compositional simulator, CMG GEM. A two-phase (gas and liquid), two-component model was developed with a 2D axisymmetric geometry around the wellbore. Water and methane were the only components included in the entire system. Peng-Robinson equation of state was used to calculate gas density (Peng and Robinson, 1976), while gas viscosity was calculated using Jossi and Stiel correlation (Jossi et al., 1962). Henry's law was used to calculate gas solubility in the aqueous phase. Harvey's correlation was used to calculate Henry's constant for methane as a function of pressure and temperature (Harvey, 1996). Aqueous phase density was calculated using the Rowe and Chou (1970) correlation, while aqueous phase viscosity was estimated using the correlation by Kestin et al. (1981). Darcy's equation was used to calculate fluid flow for each phase. Diffusive flow was calculate using Fick's law in the aqueous phase. Wilke-Chang correlation was used to estimate molecular diffusion coefficients in the aqueous phase (Wilke and Chang, 1955). Diffusion in the gas phase and the presence of water vapor in the gas phase were ignored as their impact on the results was deemed to be negligible. The flow equations were discretized using an adaptive-implicit finite difference approach (Collins, et al, 2003, Thomas and Thurnau, 1983, Nghiem and Li, 1989).

The modelled domain is a cylindrical wedge around the wellbore. Only one grid is considered in the tangential direction, effectively making the model two dimensional. This geometry is valid assuming that the formations are homogeneous in the horizontal direction. The model extends from the base of the Slochteren Formation (the main reservoir) up to the surface for a total depth of approximately 3000 m. The outer radius of the model is 1 km, while the inner radius is the radius of the cement sheath in the well. The domain is discretized with 6,150 hexahedral elements (123 × 1 × 50 in the radial, tangential and vertical direction, respectively). The grid block sizes are more refined closer to the wellbore, down to a few centimeters in the radial direction, while significantly larger block sizes are used closer to the outer boundary of the domain. The grid sizes were more refined in permeable formations compared to the low-permeability clay formations. This strategy reduced the total number of grid blocks and the run-time with minimal impact on accuracy of the flow calculations, as most of the leakage is concentrated in high permeability pathways and formations. A version of the model with 60,000 grid blocks was also run to test the impact of grid block sizes, which largely showed the same results as our base model.

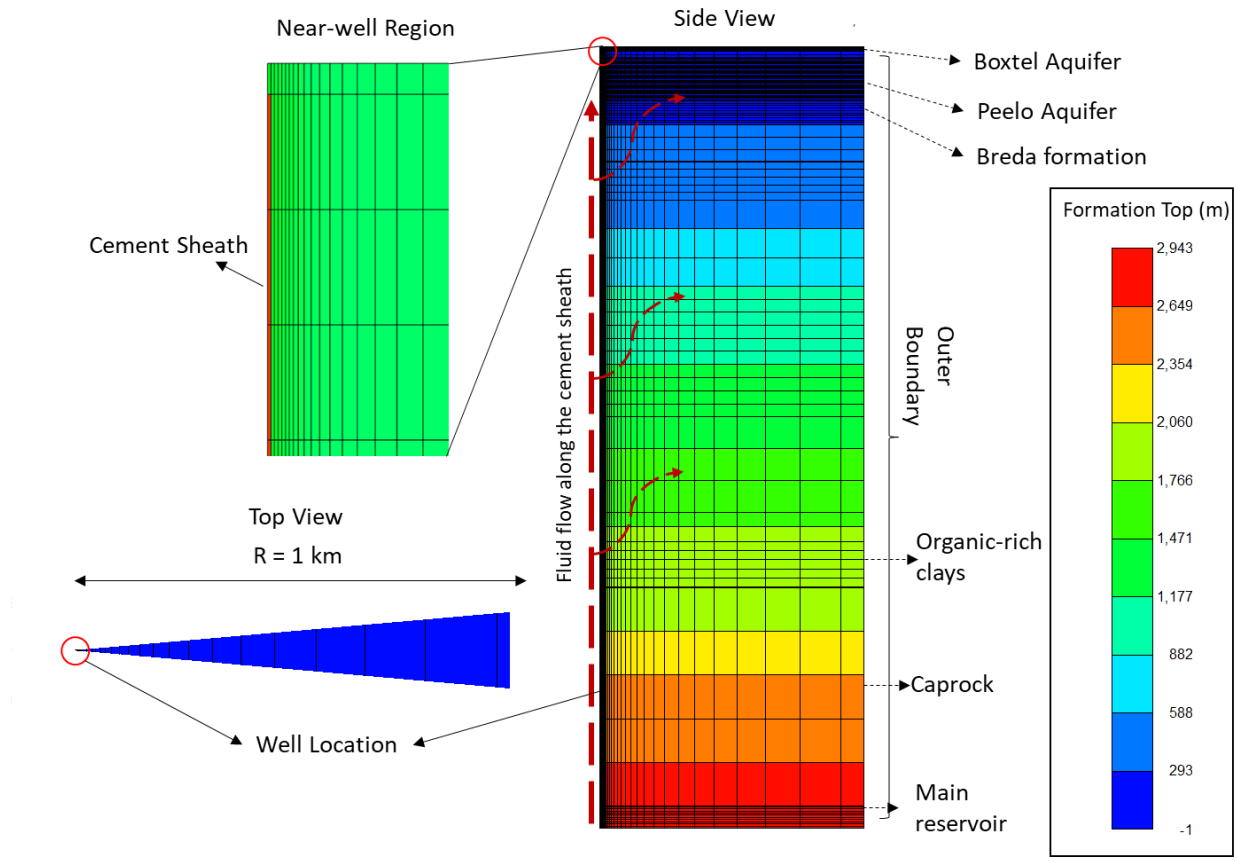

Figure D-1: A schematic of the domain of the numerical study. The near-well region is magnified on the top left (color scheme correlates with permeability). The bottom left section shows the top view of the cylindrical wedge with a radius of 1 km. The well (cement sheath) is located at the left corner of the wedge and connects all the formations. The image in the centre illustrates the side view of the domain. The stratigraphy in the region is summarized and represented in the model from the base of the reservoir at the depth of 2950 m, to the surface at sea level.

Figure D-1 illustrates the schematic of the domain of the numerical model. The grid blocks at the left corner of the cylindrical wedge represent the cement sheath. The cement sheath connects all the formations from the reservoir all the way to the atmosphere. The fluid leakage along the well is assumed to occur through the cement sheath. The casing on the left of the cement sheath is assumed to be a no-flow boundary. A no-flow boundary is also assumed at the base of the reservoir. The outer boundary on the right side of the wedge is assumed to be at a constant pressure. The radius of the wedge is large enough that the impact of gas leakage over 100 years does not reach the boundary in any of the simulations in this work. The top of the model is assumed to be at a constant pressure representing the atmosphere.

D.2 Input parameters

The simplified stratigraphy of the region is reflected in the model. The detailed stratigraphy was obtained from the NLOG database (e.g., wells ZRP-01 and ZWD-01, nlog.nl – retrieved Jan. 2021). We simplified the

stratigraphy by removing thin and insignificant (in the context of fluid flow) layers and lumping several formations that likely have similar flow properties. Table D.1 presents the simplified stratigraphy represented by the model in Figure D-1.

Table D.1: Summary of the stratigraphy and petrophysical properties at the ZWD-01 well location

Summarized Stratigraphy	Description	Formation Top (m)	Thickness (m)	Pressure Condition	Porosity	Permeability (mD)	Data Sources
Boxtel Aquifer	Sand	0	19	0	0.4	4500	Porosity and permeability: ThermoGIS Full stratigraphy: NLOG, well name ZWD-01 Pressure: PSNS database
Peelo Aquitard	Clay	19	22	Normally pressured	0.5	0.1	
Peelo Aquifer	Sand	41	163	Normally pressured	0.4	20000	
Breda Formation	Sandy clay (potential gas source)	204	91	Normally pressured	0.5	1	
Clay 1	Clay	295	142	Normally pressured	0.35	0.1	
Brussel Member	Sand	437	145	Normally pressured	0.34	500	
Clay 2	Clay	582	324	Normally pressured	0.32	0.1	
Ommelanden - top	Chalk	906	494	Normally pressured	0.33	100	
Ommelanden - bottom	Chalk	1400	361	Normally pressured	0.1	0.5	
Clay 3	Clay	1761	110	Normally pressured	0.21	0.01	
Organic-rich clays	Clay (potential gas source)	1871	173	Normally pressured	0.14	5	
Caprock	Marl, claystone, evaporites	2043	829	Over-pressured (11 MPa excess)	0.03	0.0001	
Slochteren Formation	Sand (target reservoir)	2872	81	Depleted (6 MPa)	0.15	32	

Boxtel Formation is a 20 m thick unconfined fresh water aquifer in the region of study. Peelo Formation is a confined fresh water aquifer, extending down to 204 m depth. Breda Formation underlies the Peelo formation and could be a source of free gas due to the presence of thin coal layers (TNO-GDN, 2022). Some of the sealing formations were lumped together as Clay 1, Clay2, and Clay 3. The Brussel Member is a sand formation saturated with brine. The Ommelanden formation is a thick chalk layer that is permeable in the upper zone and impermeable in the bottom portion. Organic-rich clays is a collection of

organic-rich marl and clay members dispersed with coal that could be a source of free gas. The caprock is 800 m thick, over-pressured and is comprised of marl, claystone, and evaporites. Slochteren Formation is the main reservoir that is depleted, currently at 7 MPa with a planned abandonment pressure of 6 MPa (SGS Horizon BV, 2016, van Elk et al. 2021). The virgin reservoir pressure was 34.5 MPa. A temperature gradient of 31.3 °C/km with a surface temperature of 10.1 °C was used to estimate the temperature profile (Bonté et al. 2012, Békési et al. 2020). The impact of water salinity was neglected.

The following modified Brooks-Corey relationships were used to calculate gas and water relative permeability terms (Fanchi, 2018):

$$k_{rg} = k_{rg}^{max}\left(\frac{s_g - s_{gc}}{1 - s_{wc} - s_{gc}}\right)^{n_g} \quad \text{Eq. 1}$$

$$k_{rw} = k_{rw}^{max}\left(\frac{s_w - s_{wc}}{1 - s_{wc}}\right)^{n_w} \quad \text{Eq. 2}$$

where, k_{rg} and k_{rw} are gas and water relative permeabilities. k_{rg}^{max} and k_{rw}^{max} are the maximum relative permeability values for gas and water, respectively. s_g and s_w refer to gas and water saturation. s_{gc} and s_{wc} are the critical gas and irreducible water saturations, respectively. n_g and n_w are empirical exponents.

Capillary pressure curves were estimated using the formulation proposed by Brooks and Corey (1964) , presented in Eq. 3:

$$P_c = P_e\left(\frac{s_w - s_{wr}}{1 - s_{wr} - s_{gr}}\right)^{\frac{-1}{\lambda}} \quad \text{Eq. 3}$$

where, P_c is the gas-water capillary pressure, P_e is the capillary entry pressure, and λ is the pore size distribution index. s_{wr} and s_{gr} refer to the residual (irreducible) water and gas saturations, respectively.

For the leakage conditions modelled in this work, gas is expected to escape the reservoir or other sources, travel upwards through the cement sheath to invade shallower brine saturated formations. This indicates that drainage to be the primary invasion process. Therefore, the relative permeability and capillary pressure terms used for the model were selected to be suitable for the drainage process. For the drainage process, k_{rw}^{max} can be set to 1 (Li and Horne, 2006; Shi et al., 2018). To reduce the number of parameters, we assumed that the critical and residual gas saturations were equal. The irreducible water saturation was estimated using the relationship proposed by Lopez et al. (2013) based on formation permeability. Capillary entry pressures were estimated using the correlation proposed by Huet et al. (2005), converted to a gas-water system. The Leverett J-function was used to scale the capillary entry pressure when formation permeability was changed for a simulation case. Critical gas saturation was assumed to be 1% for the high permeability aquifers increasing to 25% for the caprock. The relative permeability exponents were assumed to be 5 for the caprock, decreasing with an increase in formation permeability. λ was assumed to 0.75 for the caprock, increasing to 3 for the high permeability aquifers. The cement sheath was assumed to be debonded from the casing along the entire length of the well. Therefore, the flow properties of the cement sheath were assumed to be similar to a fracture, i.e., a low capillary entry pressure and higher relative permeability curves. The petrolphysical and multiphase flow properties of

the main reservoir were taken from NAM models (Burkitov et al., 2016). In total, six rock types were considered to cover the entire domain of study. Each modelled formation in Table D.1 is assigned to a rock type. Table D-1 provides a summary of the parameters and the assigned formations for each rock type.

Table D-1: Summary of the input parameters for 6 rock types considered in this study.

Rock type	Formations	k_{rg}^{max}	n_w, n_g	s_{gc}	s_{wc}	λ	$P_e\ (kPa)$
1	Slochteren Formation (reservoir)	0.86	4	0.15	0.16	1.0	100
2	Caprock, Clay 3	0.20	6	0.25	0.65	0.5	3043
3	Clay 1, Clay 2, Peelo aquitard, Ommelanden - bottom	0.60	5	0.20	0.40	0.75	593
4	Organic-rich clays, Brussel Member, Ommelanden - top , Breda Formation	0.75	3	0.10	0.20	1.5	22
5	Peelo aquifer, Boxtel aquifer	1.0	2	0.01	0.10	3.0	2
6	Microannulus (cement sheath)	1.0	1	0.05	0.10	3.0	1

There is some level of uncertainty associated with the input parameters for the numerical model. We attempted to collect all the available data to constrain the parameters and use best assumptions from the literature. The goal of this simulation exercise was to conceptualize a risk assessment framework for well leakage in the area of study. Therefore, the focus of the simulation study was placed on the impact of the presence of various gas sources in the system and the cement sheath damage, indicating the permeability of the leakage pathway. A more comprehensive sensitivity analysis of the impact of the multiphase flow parameters on well leakage can be found in the literature (Nowamooz et al., 2015; Rice et al., 2018; Reagan et al., 2015).

Based on the stratigraphy and the gas shows during drilling (www.dinoloket.nl, EBN Gas Shows database, retrieved Jan. 2021), three potential sources of free gas were identified: the Slochteren Formation (main reservoir), Organic-rich clays (OC), and the Breda Formation (BRD). The gas saturation in the reservoir is approximately 80% (SGS Horizon BV, 2016). However, the saturation is uncertain in the remaining two potential gas sources. We used 10% and 60% gas saturations for both sources to investigate the impact of the uncertainty in saturation. The permeability of the source was also changed by an order of magnitude to quantify the impact of the uncertainty. The cement sheath was considered to be mildly or extremely damaged. Based on the recent analyses in the literature, average cement sheath permeability of 100 md is at the top of the range of the measured or inferred values in wells (Gasda et al., 2013; Kang et al., 2015; Tao and Bryant, 2014; Moghadam et al., 2020; Moghadam et al., 2022). Therefore, an extremely damaged cement sheath is assumed to have a permeability of 100 mD. A mildly damaged cement sheath is assigned an average permeability of 1 mD.

Table D-2 provides a description of all the simulation cases in this study. Cases 1 to 9 consider the main reservoir to be the only source of free gas. Cases 10 to 19 assume that the main reservoir and Organic-rich clays contain free gas, while cases 20 to 25 consider the reservoir and Breda Formation to be the potential sources of gas.

Table D-2: Details of the simulation cases considered in this work. "OC" refers to Organic-rich clays, and "BRD" refers to the Breda Formation. For each case, the values of gas saturation, pressure, and permeability of each gas source are presented in the same order as the gas source. "NP" indicates "normally-pressured", and "OP" means Over-pressured".

Case number	Gas source	Gas saturation at each source	Pressure at each source (kPa)	Permeability of each source (mD)	Cement sheath permeability (mD)
1	Reservoir	0.8	6000	32	1
2	Reservoir	0.8	6000	32	100
3	No Gas source	0.8	6000	32	100
4	Reservoir	0.8	34500	32	1
5	Reservoir	0.8	34500	32	100
6	Reservoir	0.8	34500	32	100
7	Reservoir	0.8	34500	32	1
8	Reservoir	0.8	34500	32	100
9	Reservoir	0.8	34500	32	1
10	Reservoir, OC	0.8, 0.1	6000, NP	32, 5	1
11	Reservoir, OC	0.8, 0.1	6000, NP	32, 5	100
12	Reservoir, OC	0.8, 0.6	6000, NP	32, 5	1
13	Reservoir, OC	0.8, 0.6	6000, NP	32, 50	1
14	Reservoir, OC	0.8, 0.6	6000, 10% OP	32, 5	1
15	Reservoir, OC	0.8, 0.6	6000, 10% OP	32, 50	1
16	Reservoir, OC	0.8, 0.6	6000, NP	32, 5	100
17	Reservoir, OC	0.8, 0.6	6000, NP	32, 50	100
18	Reservoir, OC	0.8, 0.6	6000, 10% OP	32, 5	100
19	Reservoir, OC	0.8, 0.6	6000, 10% OP	32, 50	100
20	Reservoir, BRD	0.8, 0.1	6000, NP	32, 1	1
21	Reservoir, BRD	0.8, 0.6	6000, NP	32, 1	1
22	Reservoir, BRD	0.8, 0.6	6000, NP	32, 10	1
23	Reservoir, BRD	0.8, 0.6	6000, 10% OP	32, 10	1
24	Reservoir, BRD	0.8, 0.6	6000, NP	32, 1	100
25	Reservoir, BRD	0.8, 0.6	6000, NP	32, 10	100

The simulation domain is initialized assuming all the formations are fully saturated with water, except 1 to 3 formations that potentially contain free gas (depending on the simulation case). The thickness of the gas cap in Organic-rich clays and Breda Formation is assumed to be approximately 15 and 5 meters, respectively. The water gas contact in the reservoir is below the base of the model (only gas cap is modelled in the reservoir). The initial pressure in the entire model was hydrostatic, except the caprock and the reservoir. The caprock in this field is over pressured by approximately 11 MPa. The reservoir was initialized at its expected abandonment pressure of 6 MPa, likely in 2023. Methane is assumed to be dissolved in water in all the formations, except the freshwater aquifers (Boxtel and Peelo). All simulations were run for 100 years after the start of gas leakage.

D.3 Results and discussion

In this section, we present the results of the gas leakage modelling study. The results are organized according to the main source of gas considered. A brief discussion is also provided for each section.

D.3.1 Reservoir leakage

D.3.1.1 Depleted reservoir

The initial simulation cases assume the reservoir to be the only source of gas. The results indicate that methane does not escape the reservoir through the cement sheath, as long as the reservoir pressure is sufficiently below hydrostatic. Due to the depleted pressure state of the reservoir, water from the caprock flows into the reservoir through the cement sheath (some water will also flow from the caprock to the reservoir directly but is ignored in this study). Figure D-2 presents the cumulative methane and water entering the reservoir. After 100 years, 2 million m^3 of water enters the reservoir for the extremely damaged cement sheath (100 md permeability). In comparison, 7000 kg of methane flows into the reservoir in the form of dissolved methane in the water (water in the caprock is assumed to be fully saturated with dissolved methane). For the mildly damaged cement sheath, the fluid leakage into the reservoir is relatively negligible.

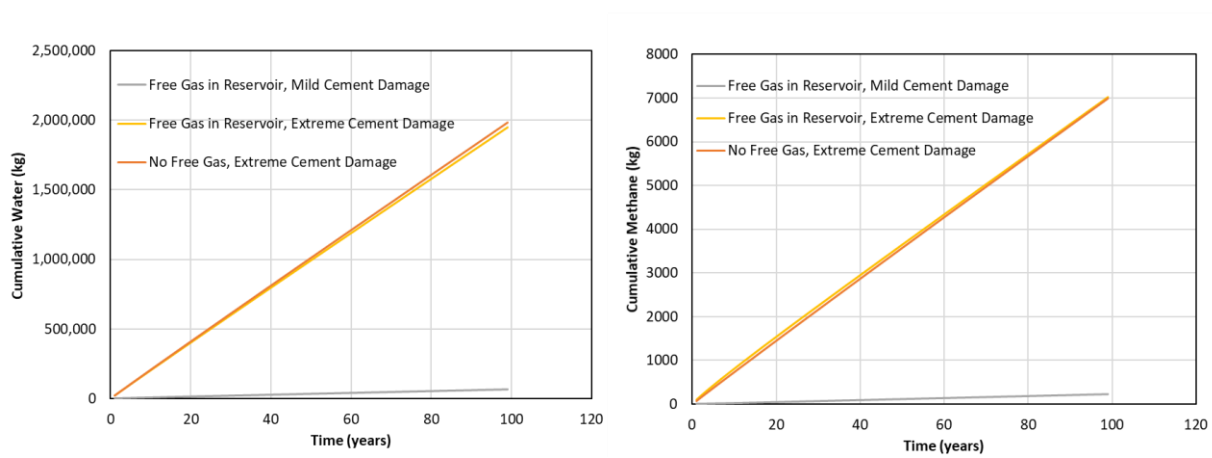

Figure D-2: Cumulative water and methane entering the reservoir over 100 years.

The water leakage into the reservoir increases the pressure and water saturation around the well. Figure D-3 illustrates the pore pressure and water saturation at the top of the reservoir after 100 years. For the extremely damaged cement sheath, the pressure near the wellbore increases by 500, to 6500 kPa and the water saturation increases to 0.45, from 0.2. This pressure increase is relatively small and should not lead to adverse effects near the wellbore. The results overall indicate that even for a highly damaged cement sheath, a highly depleted reservoir is not a major risk for gas leakage. Buoyancy, diffusion, and localized pressurization are not strong enough to counteract the large downward pressure gradient, rendering upward gas flow unlikely. A discussion is provided in the next section to elaborate on this point.

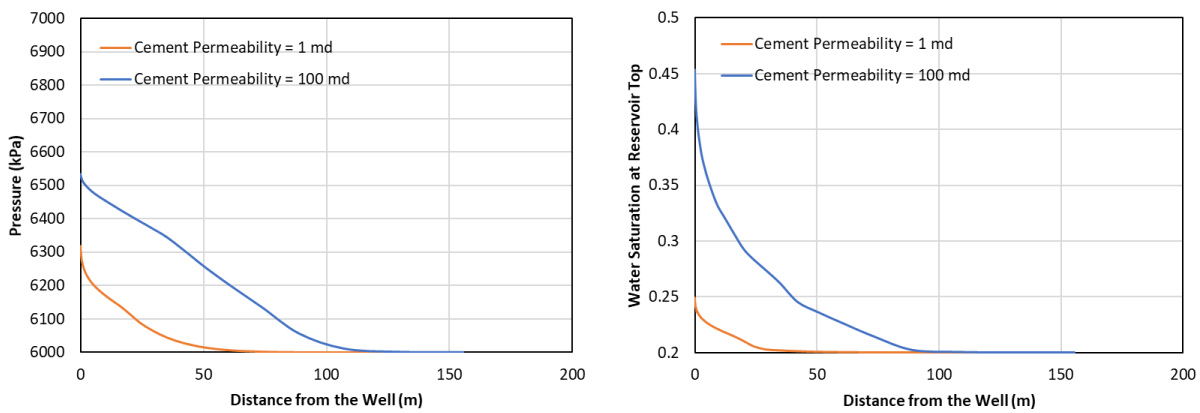

Figure D-3: Pressure and water saturation at the top of the reservoir after 100 years.

The rate of methane leakage into the aquifers was also investigated. While no gas escapes the reservoir, methane leakage into the aquifers is still observed. Figure D-4 shows the methane leakage rate into the freshwater aquifers (Peelo and Boxtel combined). The mildly damaged cement shows negligible leakage. However, the extremely damaged cement scenarios indicate a steady state leakage rate of 15 kg/year (for context, a dairy cow releases 100 kg/year of methane). This leakage, however, is only due to the diffusion of the dissolved methane through the damaged cement sheath. Diffusion is a slow process and therefore the leakage rates even for the worst case damage scenario are relatively small. In case 3, it is assumed that no free gas exists in the entire domain, including the main reservoir. The results show a similar magnitude of leakage, further indicating that the source of leakage is the dissolved methane, and not the free gas in the reservoir.

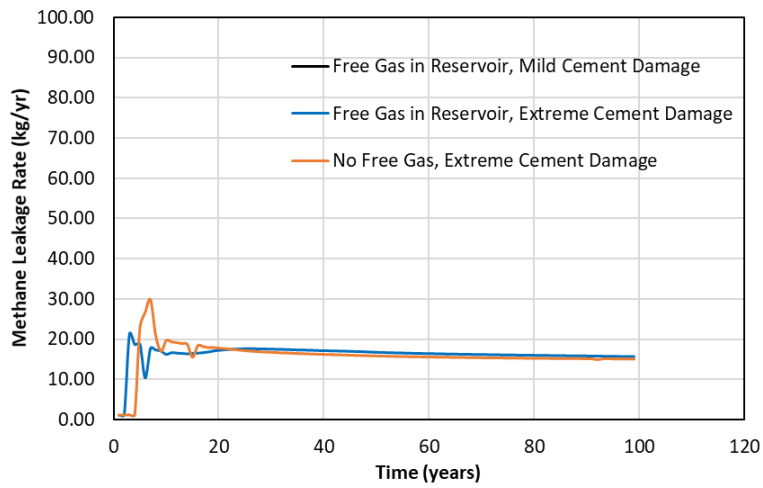

Figure D-4: Methane leakage rate into the freshwater aquifers for the depleted reservoir cases (cases 1-3).

The leakage rates are calculated assuming that all the formations below the freshwater aquifers are fully saturated with dissolved methane. Therefore, if less dissolved methane exists in the underlying formations, diffusive leakage rate is expected to be smaller. The results indicate that in case of an extremely damaged cement sheath, small leakage rates can be expected due to the diffusion of dissolved methane. Figure D-5 illustrates the dissolved methane plume in the freshwater aquifers. Dissolved methane over 1 mg/l is presented in red. According to Figure D-5, the methane plume can extend up to a maximum of 20 m away from the wellbore after 100 years of leakage (not considering the impact of groundwater flow). Free gas is not observed in the shallow aquifers for the depleted reservoir cases (cases 1-3).

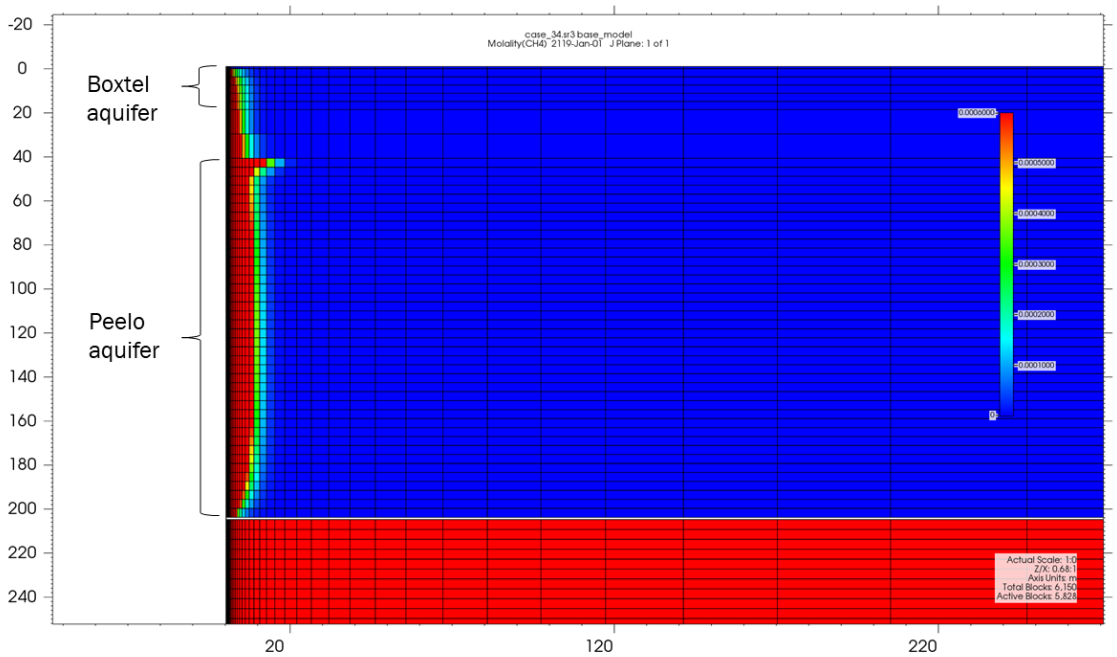

Figure D-5: Methane plume in freshwater aquifers after 100 years for the extremely damaged cement sheath scenario and a depleted reservoir (case 2).

D.3.1.2 Buoyancy and upward gas flow

The claim that under-pressured gas will not flow upwards through the microannulus may seem counter-intuitive. Due to its lower density, it is intuitive to think that gas when placed against water in a permeable path should flow upwards. However, this can only occur if the buoyancy is sufficient to overcome the pressure difference between the under-pressured gas in the reservoir and the water in the microannulus and overlying formations. We can support this claim conceptually as follows.

The equation below can be used to calculate fluid flow in the microannulus considering the density effects:

$$\dot{m} = \frac{\rho(P,T)}{\mu(P,T)} \times \frac{\pi R w^3}{6} \frac{\partial(P - \rho g z)}{\partial z} \qquad \text{Eq. 4}$$

This is a form of the Darcy equation suitable for fracture flow, where the permeability is approximated using the cubic law. The term $\Phi = (P - \rho g z)$ is the flow potential and is a representation of buoyancy flow (assuming z is positive in downward direction). In order for flow to occur, there must be a flow potential gradient present between two points along a microannulus, i.e. the gravity term $\rho g z$ must overcome the pressure P.

Let's consider the following conceptual model. A reservoir (permeable formation) underlies a caprock and is connected to a microannulus. The microannulus is a crack along the outside of the casing. The cement sheath is typically 2 cm thick and can contain disking cracks due to shrinkage. Therefore, it can be assumed that, barring any flow, at each depth the initial pressure of the microannulus is in equilibrium with the formation and is likely filled with brine above the gas-filled reservoir. The capillary pressure (Pc) for a crack is in the range of a few kPa which is orders of magnitude less than the pressures involved in this study. The capillary pressure inside the reservoir rock is higher than the microannulus. However, this value is still small as the reservoir is a permeable sandstone (expected Pc in the range of a few hundreds of kPa). Therefore, the impact of the capillary pressure gradient for gas invasion in the microannulus is small. Let us consider two depths of interest, one at the top of the reservoir and another in the caprock. In order for fluids to flow from the reservoir upwards, $\Phi_1$needs to be larger than Φ_2. Figure D-6 illustrates the conceptual model assuming only water present in the reservoir/caprock system. If pressures are hydrostatic, we have:

$$P_{w,1} = \rho_w g h_1,\ P_{w,2} = \rho_w g h_2 \qquad \text{Eq. 5}$$

This leads to a flow potential of zero at both points 1 and 2. Therefore, no flow will occur in a system where no density difference exists and pressures are hydrostatic.

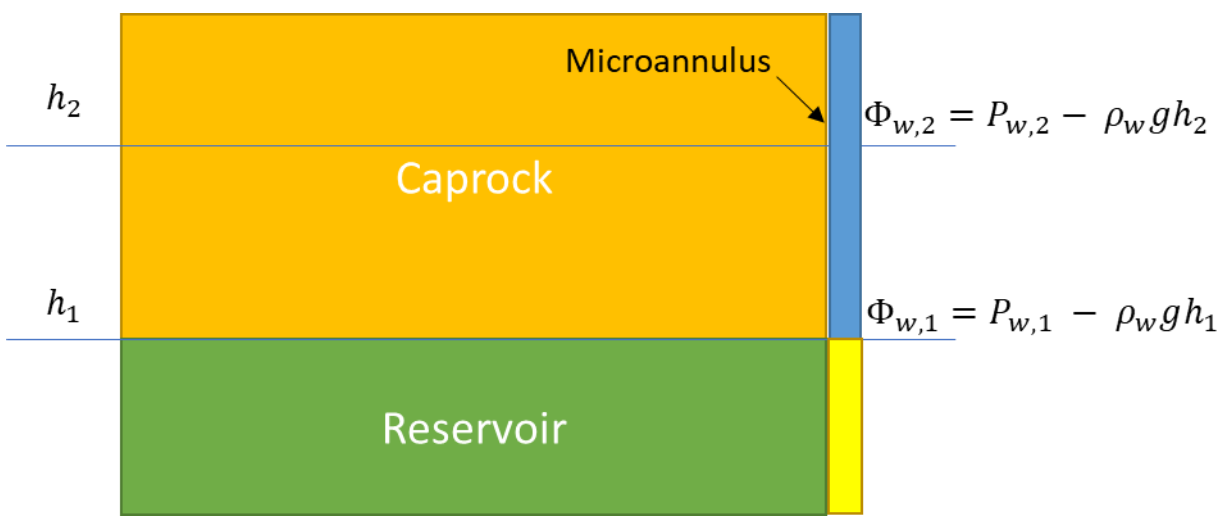

Figure D-6: Conceptual model for flow through a microannulus from a reservoir saturated with water.

Figure D-7 presents the same conceptual model but now with the reservoir saturated with gas in pre-production conditions. The water column is again assumed to be at hydrostatic pressure. The initial pressure of the gas in the reservoir depends on the height of the gas column above the gas-water contact (GWC) at which $P_g = P_w = \rho_w g h$. The flow potential is now calculated for the gas phase using the gas density ρ_g for the gravity term. The flow potential of the gas at h_1 is:

$$\Phi_{g,1} = P_g - \rho_g g h_1 = \rho_w g h_{GWC} - \rho_g g (h_{GWC} - h_1) - \rho_g g h_1 = \rho_w g h_{GWC} - \rho_g g h_{GWC} \qquad \text{Eq. 6}$$

The flow potential of gas according to Eq. 6 is non-zero. This shows that due to buoyancy, gas will flow upwards if no caprock exists. The presence of the caprock with a high capillary entry pressure prevents flow. However, if a microannulus exists along the length of the well, gas has a path with a negligible capillary entry pressure to flow upwards.

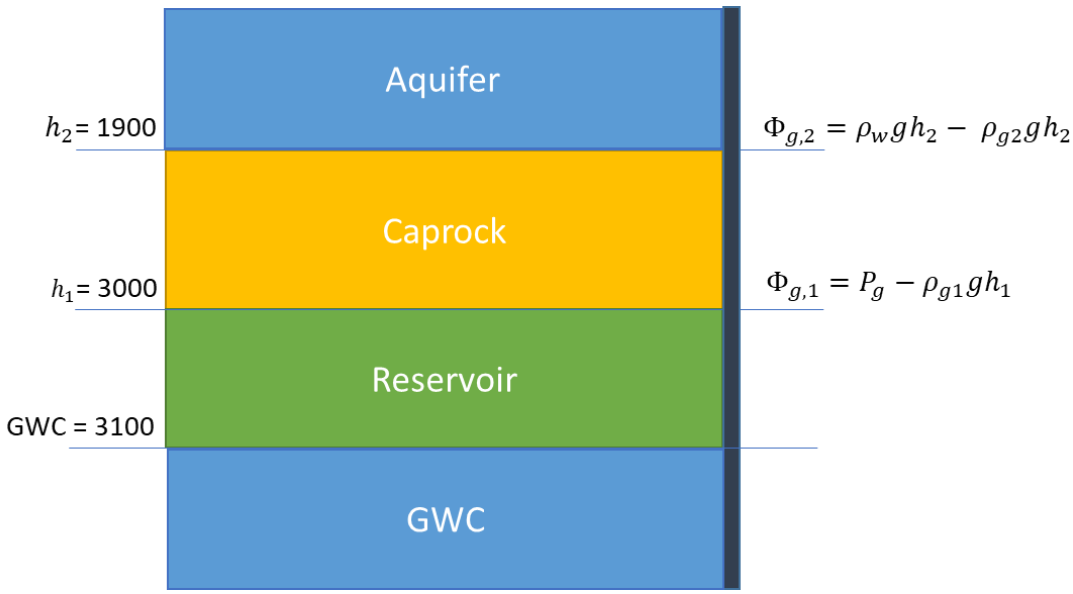

Figure D-7: Conceptual model for flow through a microannulus from a reservoir saturated with gas.

The key assumption is the pressure state in the microannulus. The microannulus is initially filled with water. The caprock may not provide enough pressure support to the microannulus to maintain water pressure (water will flow into the reservoir and gas will further depressurize water over time). However, it is plausible that at a certain depth an aquifer with sufficient permeability exists that can maintain a constant pressure at the microannulus (maintain a water column). The microannulus has an aperture between 20-200 microns and therefore small volumes of water can be sufficient to provide pressure support. As the reservoir is depleted, the flow potential of the water in the reservoir will become negative and water will flow down through the microannulus into the reservoir. For the flow potential of the gas, we need to make an assumption about the pressure in the microannulus. If the microannulus has no contact with permeable aquifers and is gas filled, the pressure would be based on the reservoir pressure and for example 6 MPa would still be higher than the gravity term, because of the very low density of gas at low pressure (~0.8 kg/m^3 for 0.1 MPa; ~35-40 kg/m^3 at 6 MPa). However, since the microannulus is filled with water at a much higher pressure, and there is pressure support in the aquifer, the gas pressure at the aquifer is likely to be raised as well. This would stop the upward flow of the gas, because the flow potential would increase at the aquifer level.

Assuming the top of the reservoir at 3000 m, and an aquifer at a depth of 1900 m (a conservative estimate), we can estimate the gas flow potential for the conceptual model in Figure D-7. Table D.2 summarizes the gas potential calculations. Initially, the water flow potential is zero at 3000 and 1900 m. As the reservoir depletes and water pressure declines, the water flow potential becomes negative. This

indicates flow will occur from permeable aquifers into the reservoir through the microannulus. For gas however, the flow potential is positive at both depths. Initially, there is a strong flow potential drop between the reservoir and the aquifer, indicating a higher leakage rate. As the reservoir pressure declines to 28.5 MPa, the $\Delta\Phi$ is still positive indicating gas leakage continues. As the reservoir depletes further, in this case to 20 MPa, the $\Delta\Phi$ becomes negative and the leak has to stop. Therefore, there is a certain level of pressure depletion that can stop leakage due to buoyancy. This assessment depends on the depth of the aquifer. If the aquifer is deeper, then the constant pressure boundary can prevent flow at a higher gas pressure (for example if aquifer is at 2800 m, leak stops as gas pressure drops below 28 MPa). If no such aquifer exists, then gas will continue leaking. Since the downward water rate is very small (according to our simulations 0.05 m^3/day), most formations with a permeability above 1 mD and 50 m thickness should be able to supply that water with little pressure drop over 100 years.

Table D.2: Gas flow potential calculation for the conceptual model.

$P_{g@3000}$	ρ_g	$\Phi_{w@3000}$	$\Phi_{w@1900}$	$\Phi_{g@3000}$	$\Phi_{g@1900}$	$\Delta\Phi$
MPa	kg/m3	MPa	MPa	MPa	MPa	MPa
30.8	196	0.0	0	25.03	16.61	8.43
28.5	184	-1.5	0	23.09	16.61	6.48
19.1	128	-10.9	0	15.32	16.61	-1.29
12.0	80	-18.0	0	9.68	16.61	-6.92
7.3	47	-22.7	0	5.94	16.61	-10.67

This behaviour can be similar to overbalanced drilling. During this operation, drilling fluid will invade the near wellbore region of a gas-bearing formation. The invading fluid will displace the gas (create a flushed zone) and prevent it from entering the wellbore. The high pressure water in an aquifer above the gas reservoir would act as the overbalanced fluid that flushes the gas away from the wellbore and prevents leakage.

Our simulations show water flowing into the reservoir through the microannulus at a rate of 20 m^3 per year (though the velocity is high as the microannulus is a small opening). This rate is too small to cause meaningful pressurization of gas around the well and lead to flow upwards along the microannulus. It is conceivable that as the water invades and pushes the gas away from the wellbore, it will isolate some gas bubbles in the pores and pressurize them. Therefore, in the near vicinity of the well, some bubbles may be able to get pressurized enough to flow upwards. However, this effect is very local and likely negligible as trapped gas bubbles also have a very low relative permeability in the porous media near the well.

It is conceivable that over time, the aquifers near the reservoir will pressurize it back to and above hydrostatic levels. At that point gas leakage through the cement sheath becomes significant. In WP2, we showed that the pressurization will not occur during the 500 years of simulation time in Groningen. However, smaller depleted reservoirs with an active water-drive that can re-pressurize the gas after abandonment could still become a leak source.

The claim that depleted reservoirs are likely not a source of leakage is also supported by field measurements. Over 90% of the leaking wells are likely sourced from shallow formations above the target reservoir (Bachu, 2017). This is likely due to the fact that target reservoirs are somewhat depleted,

particularly close to the wells, and therefore leaks are less likely. The normally-pressured formations above the target are the likely culprits for the leakage.

D.3.1.3 Reservoir at virgin pressure

Cases 4 to 9 assume that the reservoir was still at its virgin pressure of 34.5 MPa. This scenario can occur for new/active wells that have a damaged or debonded cement sheath. Cases 4 and 5 represent mild and extremely damaged cement sheaths, and the caprock is at a higher pressure than the reservoir, which is the case in the region of study. Figure D-8 shows the methane leakage rate for both cases. The mild damage case, similar to case 1, shows negligible leakage in the aquifers. The extremely damaged cement shows a similar leakage rate as case 2, approximately 15 kg/year. This indicates that the source of leakage is still the diffusive flow of the dissolved methane, and free gas does not escape the reservoir due to the overpressure in the caprock.

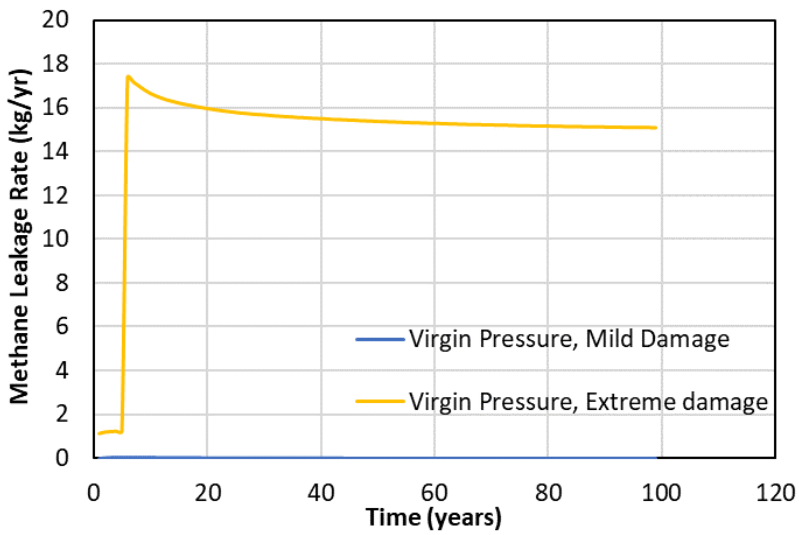

Figure D-8: Methane leakage rate in the freshwater aquifers for cases 3 and 4.

Cases 6 and 7 are similar to 4 and 5 but assume that the caprock has the same pressure gradient as the reservoir. In this scenario, gas can escape the reservoir due to its lower density and higher pressure compared to the caprock fluid. Figure D-9 shows the methane leakage rate in aquifers and the atmosphere for both cases. Mild cement damage can lead to a steady-state leak rate of 22 kg/year. Gas seepage into the aquifers begin 30 years after the leakage pathway is created. The extreme cement damage case shows gas breakthrough within the first year, reaching a steady state rate of 860 kg/year. Figure D-10 illustrates the methane plume developed for the extremely damaged cement case. The plume at the top of Peelo reaches up to 80 m away from the well, after 100 years. Free gas is accumulated in this case at the top of Peelo, up to a saturation of 8%. The extent of the free gas plume is less than the dissolved methane plume. The plume in Boxtel aquifer does not develop to the same extend, as methane can escape to the atmosphere due to a lack of confinement.

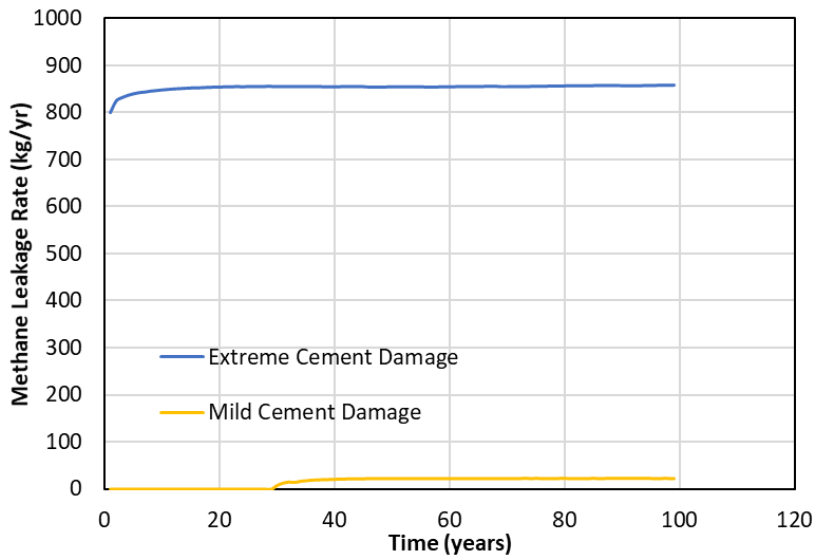

Figure D-9: Methane leakage rate in freshwater aquifers and atmosphere for cases 6 and 7.

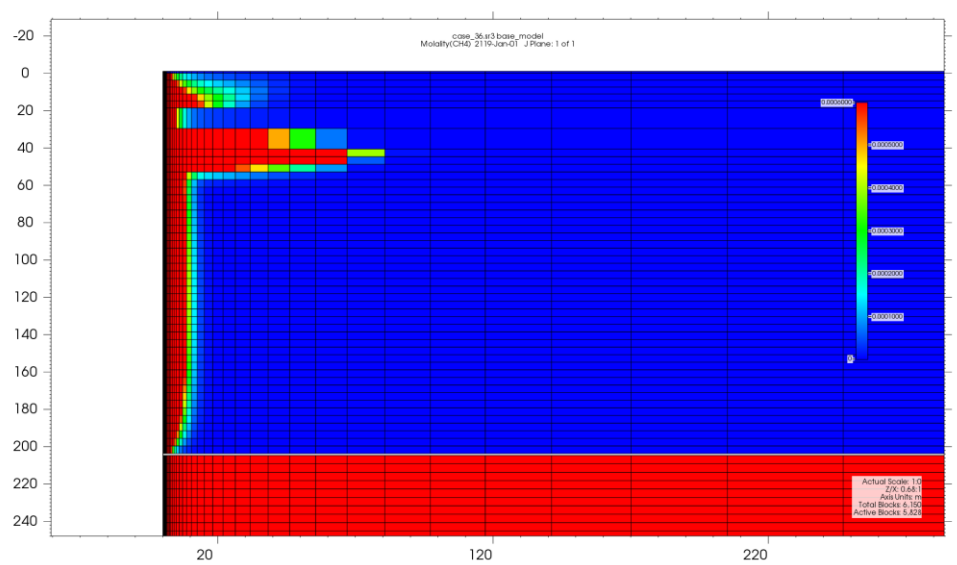

Figure D-10: Methane plume in freshwater aquifers after 100 years for the extremely damaged cement sheath scenario at virgin reservoir pressure and a hydrostatic caprock pressure (case 7).

Case 8 and 9 assume that the caprock does not contain any fluids, representing a thick salt section which is common in parts of the Groningen gas field. To simulate this, blocks representing the caprock are disabled. Therefore, there is no pore pressure in the caprock to act as a barrier to the reservoir fluid in the

damaged cement sheath. Figure D-11 illustrates the methane leakage rate into the aquifers and atmosphere for both the mild and extreme cement damage cases (cases 8 and 9). The mild cement damage shows a minor leakage rate at 31 kg/year. However, the extremely damaged cement sheath leads to a leakage rate of 4200 kg/year. The evolution of the methane plume in the aquifers is depicted in Figure D-12, for the extremely damaged cement scenario (case 8). According to Figure D-12, methane plume extends up to 450 m away from the well after 100 years. The plume reaches the farthest at the top of the Peelo aquifer. Free gas saturation near the wellbore can reach as high as 23%.

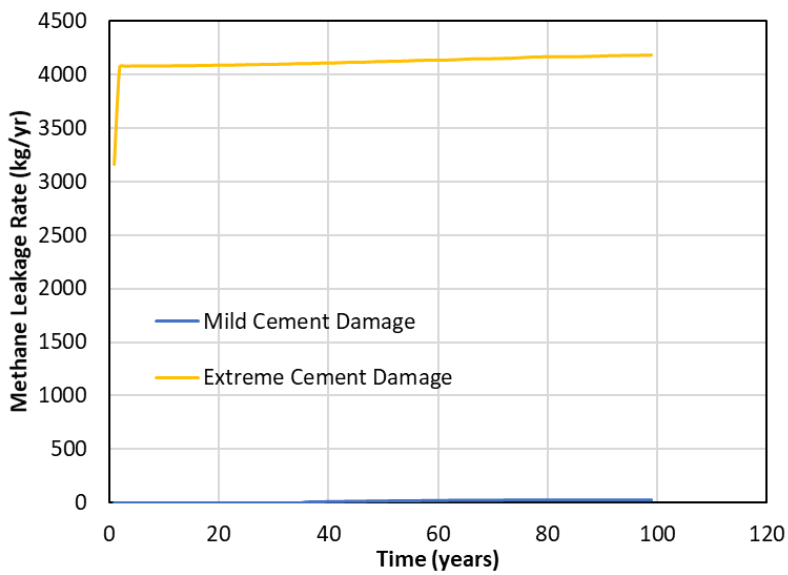

Figure D-11: Methane leakage rate in freshwater aquifers and atmosphere for cases 6 and 7.

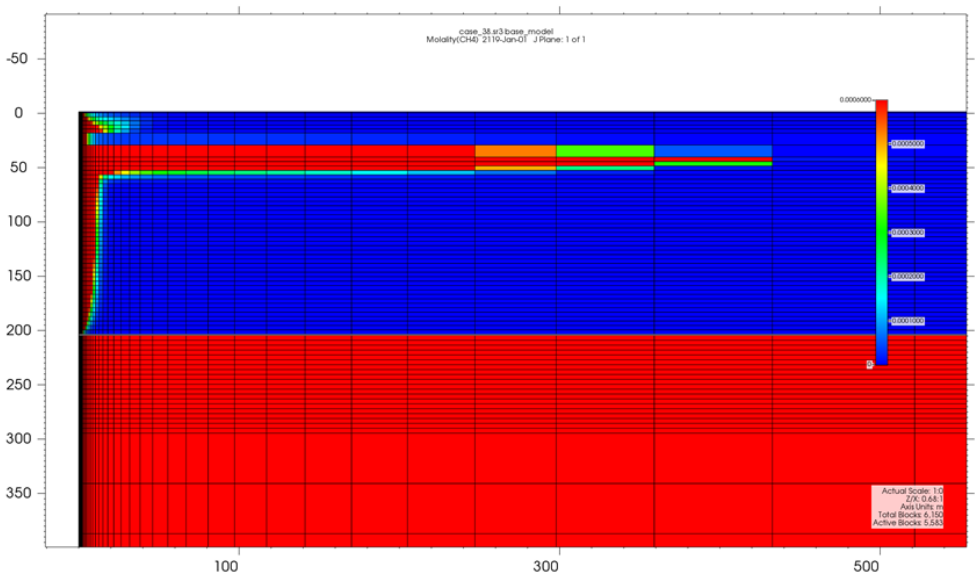

Figure D-12: Methane plume in freshwater aquifers after 100 years for the extremely damaged cement sheath scenario at virgin reservoir pressure and a caprock with no pore pressure (case 8).

While salt formations do not contain pore pressure, they are excellent seals due to their lack of permeability and high creep rates. Therefore, the likelihood of a highly damaged cement sheath occurring against a thick salt section is low, as the salt will creep and press the cement against the casing to close the leaky pathways such as microannuli.

The main findings related to cases where the reservoir is the main source of gas can be summarized as follows:

- A depleted reservoir is not a likely source of gas leakage, as long as its pressure is below that of the overlying formations. This indicates that buoyancy and diffusion are not sufficient forces against the pressure gradient.
- It is more likely that fluids move into the reservoir through a damaged cement sheath. However, this should not lead to reservoir pressurization due to high compressibility of gas.
- For a mildly damaged cement sheath with an average permeability of 1 md, all scenarios show relatively low levels of gas leakage. The highest value in cases 1 to 9 was 31 kg/year, well below average emissions of a dairy cow (100 kg/year).
- When the cement sheath is extremely damaged (100 md average permeability), diffusive methane flow (biogenic or thermogenic in origin) into the freshwater aquifers is likely. If the gas source is depleted, the magnitude of the leakage is expected to be small (under 20 kg/year) with a plume extending up to 20 m away from the well after 100 years. The source of gas will likely be dissolved methane in the underlying formations.

- If the reservoir and the caprock are at hydrostatic pressure (a case for new/active leaky wells), extreme cement damage can lead to significant methane leakage into the atmosphere and aquifers. In this case methane plume can extend hundreds of meters away from the well after 100 years. Free gas can accumulate at the top of the Peelo aquifer. The worst case scenario indicates a leak rate of a few tons of methane per year into the atmosphere and aquifers.

D.3.2 Organic-rich clays (OC)

Cases 10 to 19 consider both the reservoir and the Organic-rich clays (OC) to be sources of free gas. The reservoir is set to its abandonment pressure of 6 MPa for all the OC related cases. According to Figure D-2, the depleted reservoir is not a source of gas leakage. A point of uncertainty for the OC layer is the gas saturation. We considered gas saturations of 10 and 60% to investigate its impact on the leakage rate, while critical gas saturation for the OC layer was assumed to be 10%. Figure D-13 indicates the cumulative methane leakage into the Peelo aquifer for an extremely damaged cement sheath at gas saturations of 10% and 60%. At 10% gas saturation the leakage is entirely due to diffusive flow. Only when gas saturation in the OC layer goes above the critical saturation, bulk gas flow can occur.

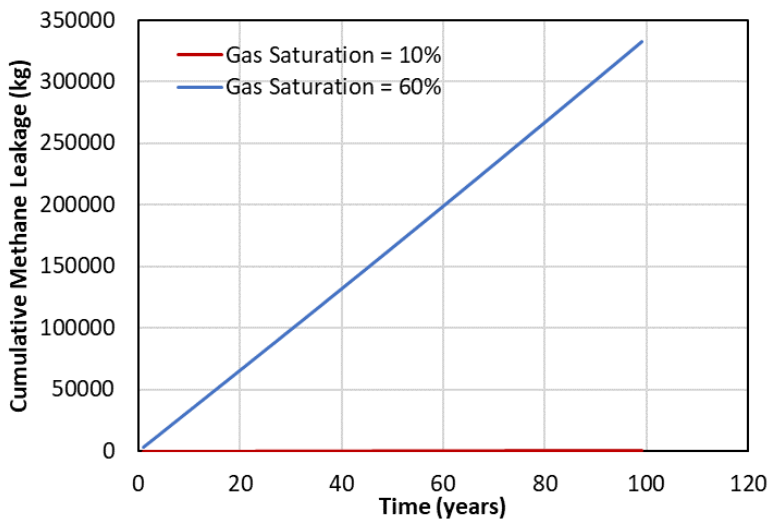

Figure D-13: Cumulative methane leakage into the Peelo aquifer for the extremely damaged cement at different gas saturations (cases 11 and 16).

For the bulk phase flow, the cement permeability becomes the dominant parameter controlling the leakage rate. Figure D-14 illustrates the leakage rate into the atmosphere and the Peelo aquifer for the mildly and extremely damaged cement sheaths. The results show a higher leakage rate into the Peelo aquifer compared to the atmosphere. Mild cement damage leads to small steady-state leakage rates, 24 and 8 kg/year for the Peelo aquifer and atmosphere, respectively. The extremely damaged cement sheath shows significantly higher leakage rates, 3400 and 800 kg/year for the Peelo and atmosphere, respectively. In total, 4200 kg/year of methane leaks into the aquifer/atmosphere system.

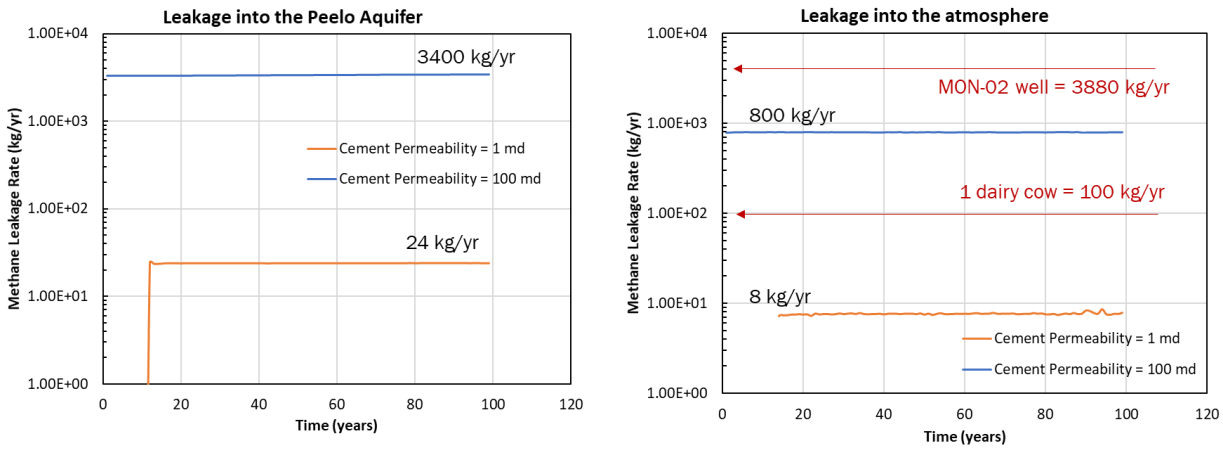

Figure D-14: Methane leakage rate into the atmosphere and Peelo aquifer for mildly and extremely damaged cement sheaths (cases 12 and 16).

For context, the MON-02 well in the Netherlands had an estimated leakage rate of 3880 kg/year into the atmosphere (Schout et al., 2019). Boxtel aquifer does not show significant accumulation of methane in any of our simulations. Most of the methane that enters the unconfined Boxtel aquifer escapes to the atmosphere. Therefore, there is minimal methane accumulation in the formation.

Presence of hydrostatic free gas in OC can lead to methane leakage, particularly at higher cement damage levels. The methane plume mainly develops in the Peelo aquifer due to its confinement. Free gas is observed for both the mild and extreme cement damage levels. Figure D-15 demonstrates the methane saturation development at the top of the Peelo aquifer. For the mildly damaged cement case, gas saturation is less than 5%, extending up to 20 m away from the well. For the extremely damaged cement, the near well gas saturation can increase to 20% with a saturation front extending to 400 m after 100 years.

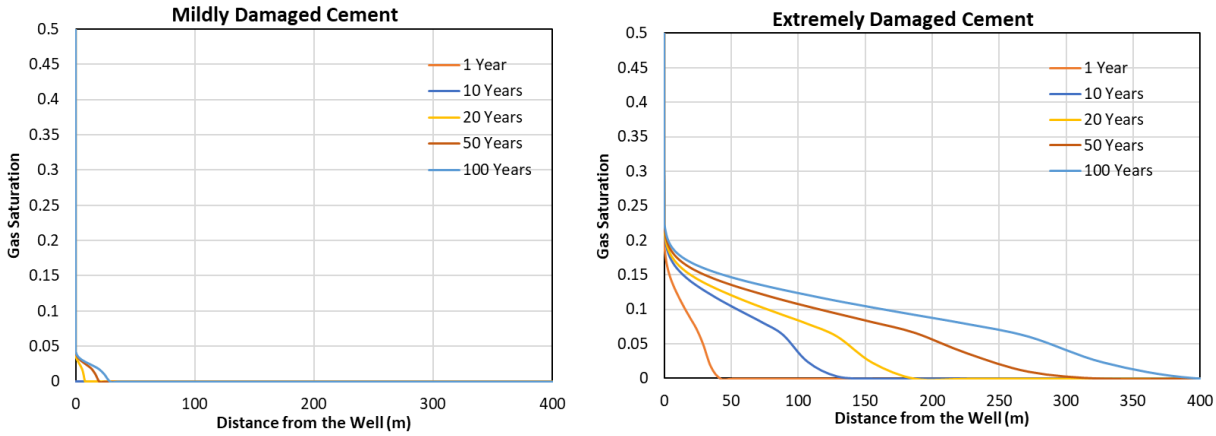

Figure D-15: Methane saturation development at the top of Peelo aquifer over time for the midl and extremely damaged cement (cases 12 and 16).

Cases 14 to 19 include the impact of the uncertainty in the gas source permeability and pressure. Figure D-16 indicates the cumulative methane leakage into the atmosphere and aquifers for mild cement damage. The plot compares leakage for case 12, 13, and 15. Case 12 assumes OC layer permeability of 5 md while case 13 assumes a permeability of 50 mD. Case 15 assumes the gas source is 10% over-pressured and has a permeability of 50 mD. The results show that an increase in OC layer permeability and pressure does not lead to a significant rise in methane leakage into the atmosphere/aquifer system. The results for the extremely damaged cement show a similar behavior (not shown here). To investigate this further, we can compare the amount of gas leaving the source and the gas entering the atmosphere/aquifer system for each case.

Figure D-17 illustrates the cumulative gas leakage into the atmosphere/aquifer systems for cases 12 and 15. Additionally, the amount of gas that leaves the OC layer over time is plotted for both cases. Both cases show a similar amount of leakage in the atmosphere/aquifer system. However, case 15 shows that a significantly higher volume of gas escapes the OC when it is over-pressured. The difference between the gas that leaves the source and the gas that leaks into the atmosphere/aquifers is taken up by the permeable intermediate formations above the source. For the present study, most of the leaked gas is stored in Ommelanden-top and the Brussel Member. This highlights the impact of shallow permeable formations as a buffer in terms of gas leakage.

The increase in gas outflow from the source is only observed in cases with an over-pressure. Case 13 for example where an increase in source permeability is modelled does not show a significant increase in gas flowing out of the OC layer.

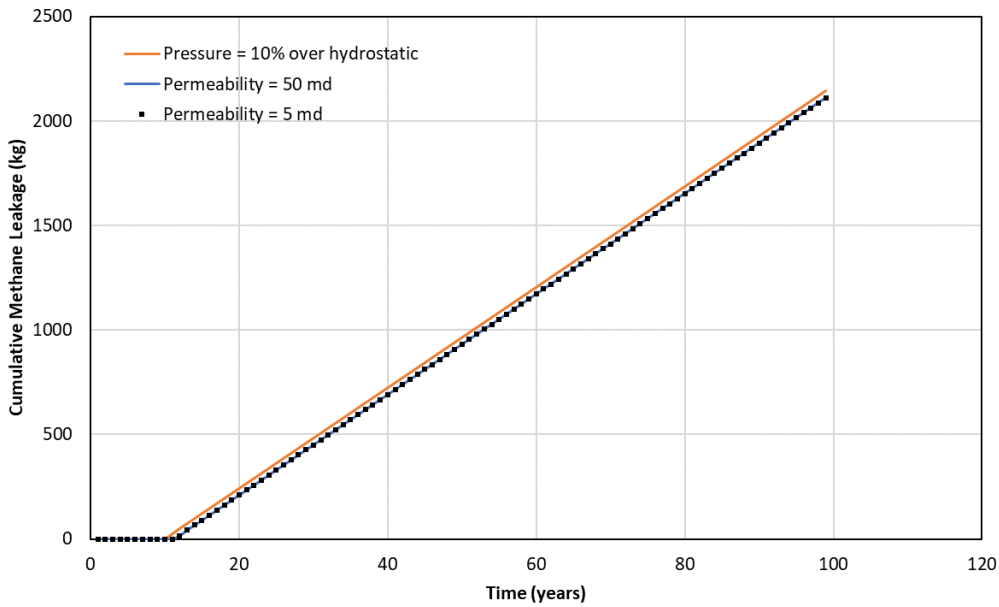

Figure D-16: Cumulative methane leakage into the atmosphere and aquifers for varying OC permeability and initial pressure for the mildly damaged cement (cases 12, 13, and 15)

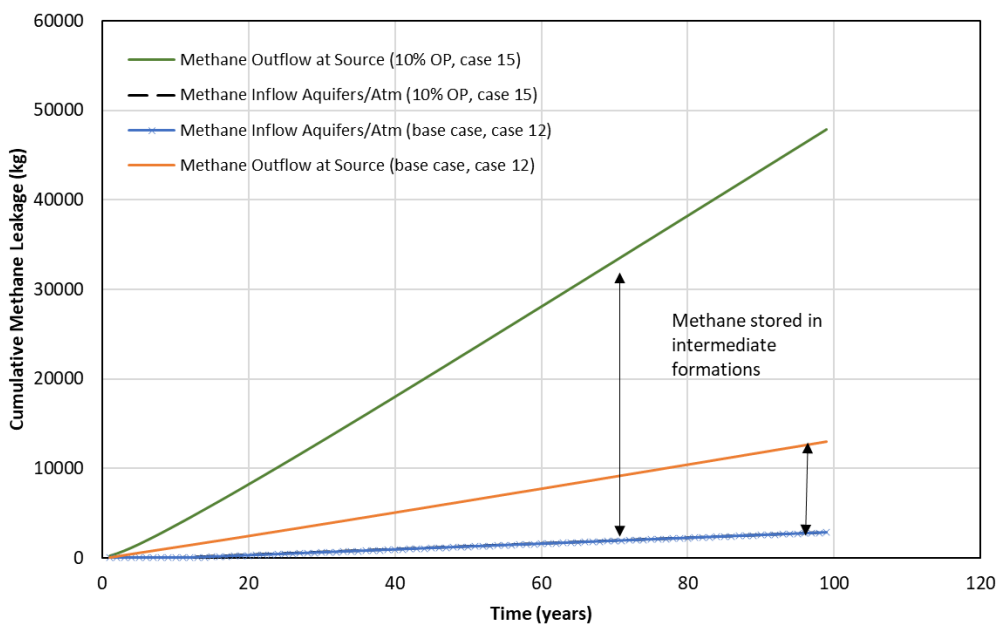

Figure D-17: Cumulative methane leakage compared to the methane that has escaped the OC formation (cases 12 and 15).

The main conclusions regarding the impact of presence of free gas in OC can be summarized as follows:

- Presence of gas at hydrostatic pressure in formations shallower than the target reservoir can lead to methane leakage along the damaged cement sheath.
- Gas saturation in the shallow formation has to be above the critical saturation to lead to significant leakage (due to advective flow).
- The mild damage in cement (1 md) leads to relatively small amount of leakage (5-30 kg/year).
- The extremely damaged cement sheath can lead to high leakage rates, with free gas accumulating in the Peelo formation as far as 500 m away from the well (after 100 years).
- Unconfined aquifers such as Boxtel will not store significant amounts of the leaked gas.
- The majority of the gas will be stored at the base of aquitards making them suitable locations for sampling.
- Permeable intermediate formations between the source and aquifers can act as gas storage.
- Natural groundwater flow in aquifers can change the extent of the methane plume in their direction, while reducing the size of the plume in the opposite direction. The quantitate impact of groundwater flow is not studied in this work.
- Water sampling should be done at the top of the deepest aquifer, as close as possible to the wellbore (ideally less than 100 m, and no more than 500 m). The sampling should be done in the direction of the groundwater flow at the well location for more concrete results.
-

D.3.3 Breda Formation (BRD)

A similar analysis is conduced assuming Breda Formation is the source of free gas. Cases 20 to 25 cover various scenarios pertaining to the Breda Formation. Figure D-18 shows the methane leakage rate in the Peelo aquifer for several cases that assume a mildly damaged cement. The leakage rate into the atmosphere is not shown as the values are too small (less than 10 kg/year). Case 20 assumes a gas saturation of 10%, which is below the critical saturation. No leakage is observed due to a lack of bulk phase flow in gas. Gas saturation in case 21 is 60% which leads to a leak rate of 115 kg/yr. Case 22 considers a permeability of 10 md for the Breda Formation, up from 1 mD. The increase in permeability only increases the leak rate from 115 to 124 kg/yr. This is consistent with the results from the OC analysis, that source rock permeability does not appear to increase the leak rate significantly. This is likely due to the fact that the limited cement permeability is choking the gas leakage. Case 23 assumes both an increase in permeability and a 10% over-pressure in Breda Formation. The leakage rate in this case increases to 330 kg/yr.

Overall, the mildly damaged cement shows a higher leakage rate from Breda Formation compared to the OC formation with an approximately five-fold increase (ranged from 20's to 100 kg/yr). The shorter leak distance between the source and the surface is expected to increase the leakage rate. Another factor is the lack of intermediate formations between the Breda and the shallow aquifers. Presence of shallow gas

is more detrimental if no permeable formations exist between the source and the aquifers to act as a buffer.

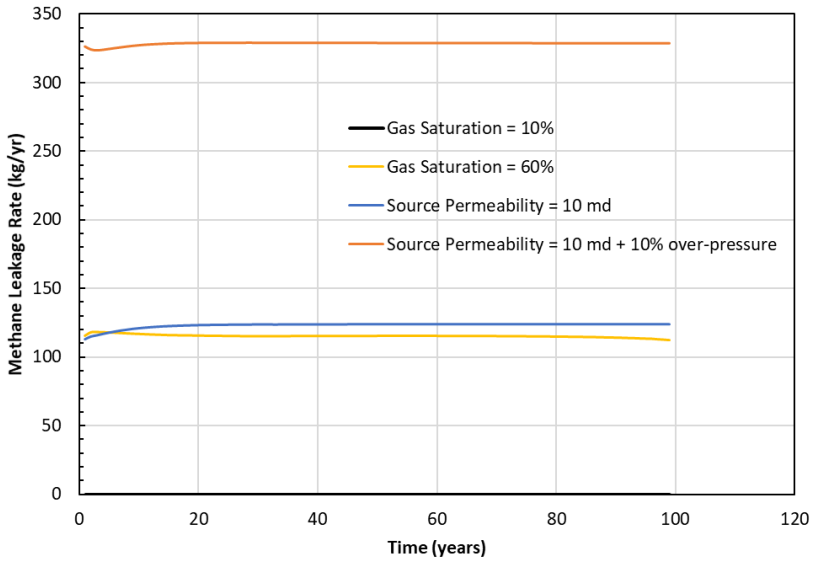

Figure D-18: Methane leakage rate in the Peelo aquifer for the mild cement damage assuming Breda is a gas source (cases 20 to 23).

Figure D-19 presents the leakage rates for cases 24 and 25 for both the Peelo aquifer and the atmosphere. These cases assume an extremely damaged cement sheath. In this scenario, cement permeability is not the limiting factor and an increase in source permeability (Breda) increases the leakage rate significantly. The high permeability of the cement sheath means that the formation permeability and pressure control the leakage rate. However, leakage rate drops over time in Peelo due to depletion.

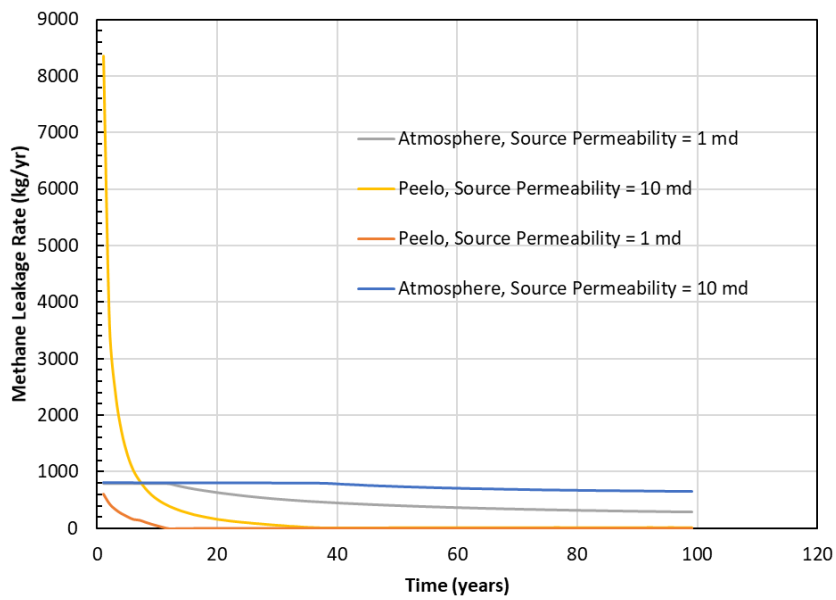

Figure D-19: Methane leakage rate in the Peelo aquifer and atmosphere for the extreme cement damage assuming Breda is a gas source (cases 24 to 25).

The following conclusions can be made related to Breda Formation as the source:

- Shallow gas sources at or above hydrostatic pressure can lead to higher leakage rates due to the shorter travel distance.
- Lack of permeable formations to store the leaking gas can also increase the ultimate leakage into the atmosphere and aquifers.
- The leakage is fundamentally balanced between the capacity of the source to leak, the capacity of the cement sheath to transport, and the capacity of the aquifer/atmosphere system to receive the leaking gas. Depending on the parameters of the system, one of these links in the flow chain can be the controlling one. In the OC case, the cement sheath permeability plays the dominant role in controlling leakage. At a high cement permeability in the Breda case, the source permeability plays the dominant role.

D.4 References

Békési, E., Struijk, M., Bonté, D., Veldkamp, H., Limberger, J., Fokker, P. A., Vrijlandt, M., van Wees, J.D., 2020. An updated geothermal model of the Dutch subsurface based on inversion of temperature data. Geothermics, 88, 101880.

Bonté, D., van Wees, J.-D., Verweij, H., 2012. Subsurface temperature of the onshore Netherlands: new temperature dataset and modelling. Netherlands Journal of Geoscience, 91 (4), 491-515.

Brooks, R. H., and A. T. Corey (1964), Hydraulic properties of porous media, in Hydrology Papers, vol. 3, 37 pp., Colo. State Univ., Fort Collins.

Burkitov, U., H. van Oeveren and P. Valvatne, 2016.Groningen Field Review 2015. Subsurface Dynamic Modelling Report. https://www.nam.nl/feiten-en-cijfers.html.

Collins, D.A., Grabenstetter, J.E. and Sammon, P.H., "A Shared-Memory Parallel Black-Oil Simulator with a Parallel ILU Linear Solver", SPE 79713, SPE Reservoir Simulation Symposium, Houston, TX, February 3-5, 2003.

Gasda, S.E., Celia, M.A., Wang, J.Z., and Duguid, A., 2013. Wellbore permeability estimates from vertical interference testing of existing wells. Energy Procedia 37, 5673–5680.

Huet, C. C., J. A. Rushing, K. E. Newsham, and T. A. Blasingame (2005), A modified Purcell/Burdine model for estimating absolute permeability from mercury injection capillary pressure data, paper IPTC 10994 presented at the 2005 International Petroleum Technology Conference, Doha, The Am. Assoc. of Pet. Geol., 21–23 Nov.

John R. Fanchi, in Principles of Applied Reservoir Simulation (Fourth Edition), 2018.

Jossi, J.A., Stiel, L.I. and Thodos, G., "The Viscosity of Pure Substances in the Dense Gaseous and Liquid Phases", AIChE Journal, Vol. 8, (1962), pp. 59-63.

Kang, M., Baik, E., Miller, A.R., Bandilla, K.W., and Celia, M.A., 2015. Effective permeabilities of abandoned oil and gas wells: analysis of data from Pennsylvania. Environ. Sci. Technol. 49 (7), 4757-4764.

Kestin, J., Khalifa, H.E. and Correia, R.J., "Tables of the Dynamic and Kinematic Viscosity of Aqueous NaCl Solutions in the Temperature Range 20-150 °C and Pressure Range 0.1-35 MPa", J. Phys. Chem. Ref. Data, Vol. 10, (1981) pp. 71-87.

Li, K., and Horne, R. N. (2006), Comparison of methods to calculate relative permeability from capillary pressure in consolidated water-wet porous media, Water Resour. Res., 42, W06405,

Lopez, O., Berg, C.F., Bakke, S., Boassen, T., Rustad, A.B., 2013. “Thin section image analysis for estimation of initial water saturation in siliciclastic reservoir rocks”. Paper presented at the International Symposium of the Society of Core Analysts held in Napa Valley, California, USA, 16-19 September.

Moghadam, A., Castelein, K., ter Heege, J., Orlic, B., 2022. A Study on the Hydraulic Aperture of Microannuli at the Casing-Cement Interface Using a Large-Scale Laboratory Setup. Geomechanics for Energy and Environment 29, 100269.

Moghadam, A., Castelein, K., ter Heege, J., van der Valk, K., Orlic, B., and Wollenweber, J., 2020. Large-scale laboratory investigation of the microannulus behavior in the casing-cement interface. In Proceedings of the 54th US Rock Mechanics / Geomechanics Symposium (ARMA), ARMA 20-1325.

Nedmag, B. V. (2018). Winningsplan 2018. November. NLOG.nl

Nghiem, L.X. and Li, Y.-K., "Phase-Equilibrium Calculations for Reservoir Engineering and Compositional Simulation", Second International Forum on Reservoir Simulation, Alpbach, Austria, September 4-8, 1989.

Nowamooz, A., Lemieux, J.M., Molson, J., and Therrien, R., 2015. Numerical investigation of methane and formation fluid leakage along the casing of a decommissioned shale gas well. Water Resour. Res. 51 (6), 4592–4622.

Peng, D.Y. and Robinson, D.B., "A New Two-Constant Equation of State", Ind. Eng. Chem. Fundamen., Vol. 15, (1976), pp. 59-64.

Reagan, M.T., Moridis, G.J., Keen, N.D., and Johnson, J.N., 2015. Numerical simulation of the environmental impact of hydraulic fracturing of tight/shale gas reservoirs on near surface groundwater: background, base cases, shallow reservoirs, short-term gas, and water transport. Water Resour. Res. 51 (4), 2543–2573.

Rice, A.K., McCray, J.E., and Singha, K., 2018. Methane leakage from hydrocarbon wellbores into overlying groundwater: numerical investigation of the multiphase flow processes governing migration. Water Resour. Res. 54, 2959–2975.

Rowe, A.M. and Chou, J.C.S., "Pressure-Volume-Temperature-Concentration Relation of Aqueous NaCl Solutions", J. Chem. Eng. Data, Vol. 15, (1970), pp. 61-66. Bachu, S., 2017. Analysis of gas leakage occurrence along wells in Alberta, Canada, from a GHG perspective – Gas migration outside well casing. Int. J. Greenh. Gas Control 61, 146-154.

Schout, G., Griffioen, J., Hassanizadeh, S.M., Cardon de Lichtbuer, G., and Hartog, N., 2019. Occurrence and fate of methane leakage from cut and buried abandoned gas wells in the Netherlands. Sci. Total Environ. 659, 773–782.

SGS Horizon BV, 2016. Independent Review of Groningen Subsurface Modelling, Update for Winningsplan 2016 with Opinion Letter. https://www.nam.nl/over-nam/onderzoeksrapporten.html

Shi, S., Belhaj, H. & Bera, A. Capillary pressure and relative permeability correlations for transition zones of carbonate reservoirs. J Petrol Explor Prod Technol 8, 767–784 (2018).

Tao, Q., Bryant, S.L., 2014. Well permeability estimation and CO2 leakage rates. Int. J. Greenhouse Gas Control 22, 77–87.

Thomas, G.W. and Thurnau, D.H., "Reservoir Simulation Using an Adaptive-Implicit Method", SPEJ, Vol. 23, (October 1983), pp. 759-768.

TNO-GDN, 2022. Breda Formation. In: Stratigraphic Nomenclature of the Netherlands, TNO – Geological Survey of the Netherlands. Accessed on 03-02-2022 from http://www.dinoloket.nl/en/stratigraphic-nomenclature/breda-formation.

van Elk, J., Landmann,, A.J., van Eijs, R., 2021. Reservoir Pressure and Subsidence Groningen Field update for Production Profile GTS – raming 2021. https://www.nam.nl/over-nam/onderzoeksrapporten.html

Wilke, C.R. and Chang, P., "Correlation of Diffusion Coefficients in Dilute Solution", AIChE Journal, Vol. 1, (June 1955), pp. 264-270.

E Ground movement

E.1 Subsidence calculation sensitivities

The incremental subsidence after shut-in was calculated for all scenarios defined above (Figure E-1). The scenarios show very little variation for the production period. The sensitivities show the same qualitative behaviour with a limited variation in the maximum additional subsidence expected (9 – 13 cm for the NW position and 4 – 7 cm for the West position).

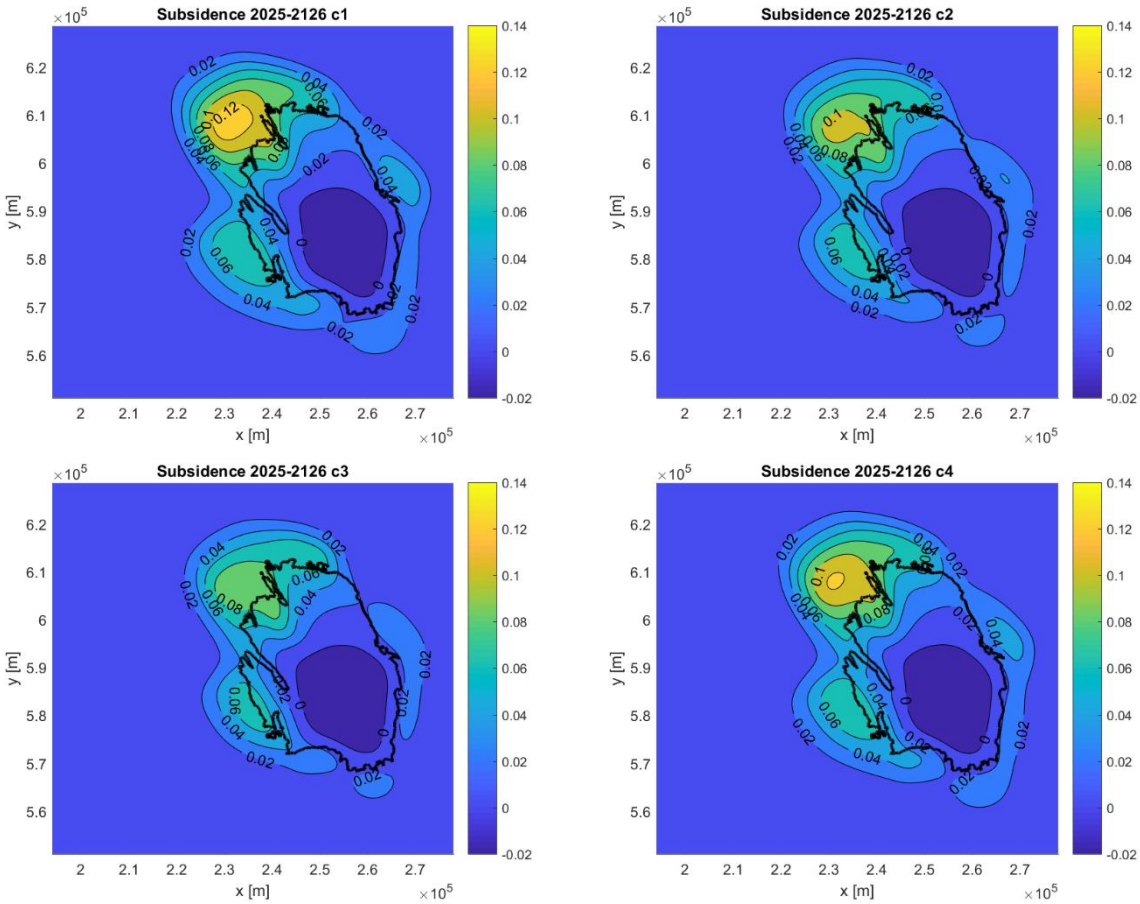

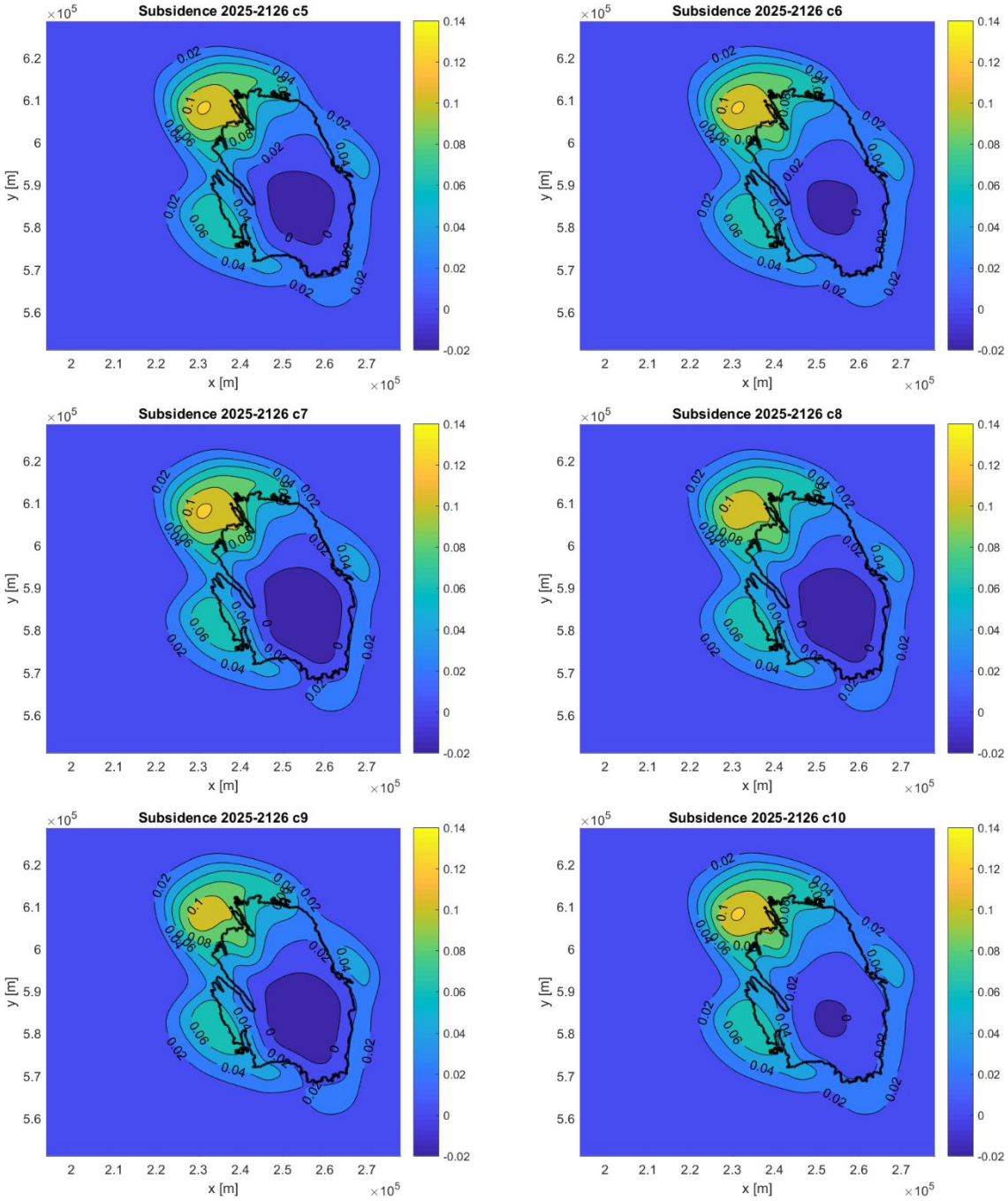
Subsidence 2025-2126 c5
Subsidence 2025-2126 c6
Subsidence 2025-2126 c7
Subsidence 2025-2126 c8
Subsidence 2025-2126 c9
Subsidence 2025-2126 c10
x [m]
y [m]
×10^5

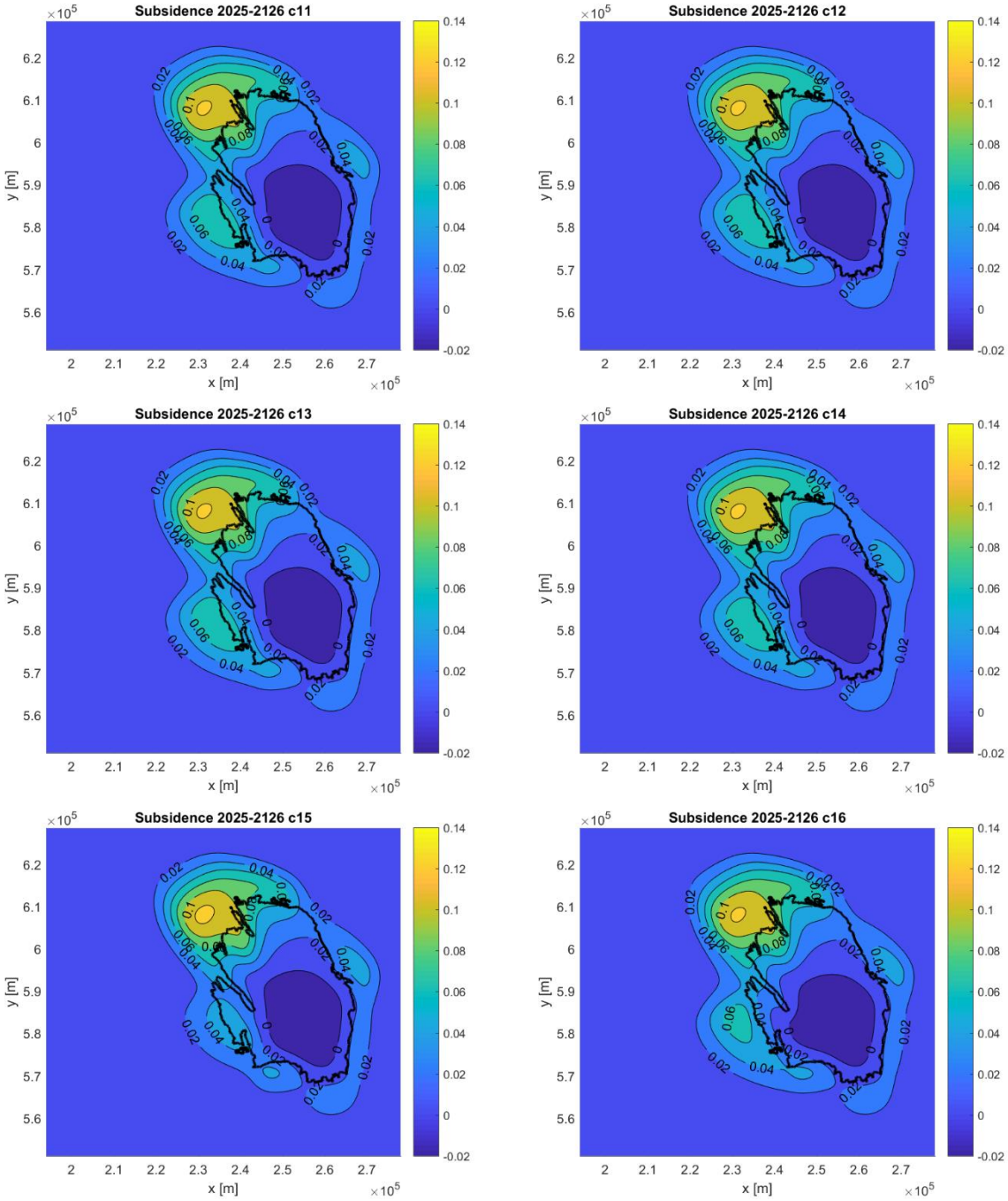
Subsidence 2025-2126 c11
Subsidence 2025-2126 c12
Subsidence 2025-2126 c13
Subsidence 2025-2126 c14
Subsidence 2025-2126 c15
Subsidence 2025-2126 c16
x [m]
y [m]
×10^5

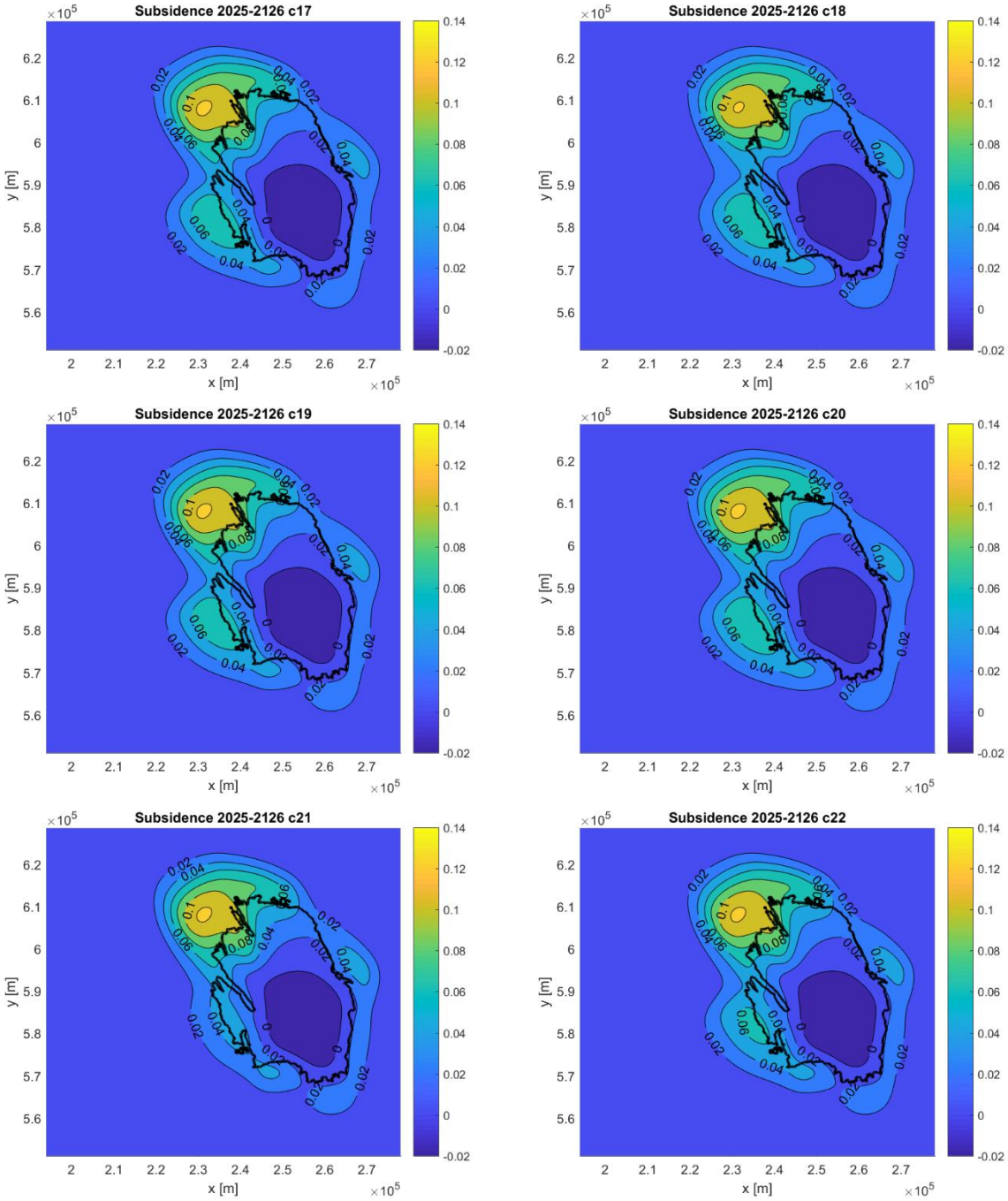
Subsidence 2025-2126 c17
Subsidence 2025-2126 c18
Subsidence 2025-2126 c19
Subsidence 2025-2126 c20
Subsidence 2025-2126 c21
Subsidence 2025-2126 c22
x [m]
y [m]
×10^5

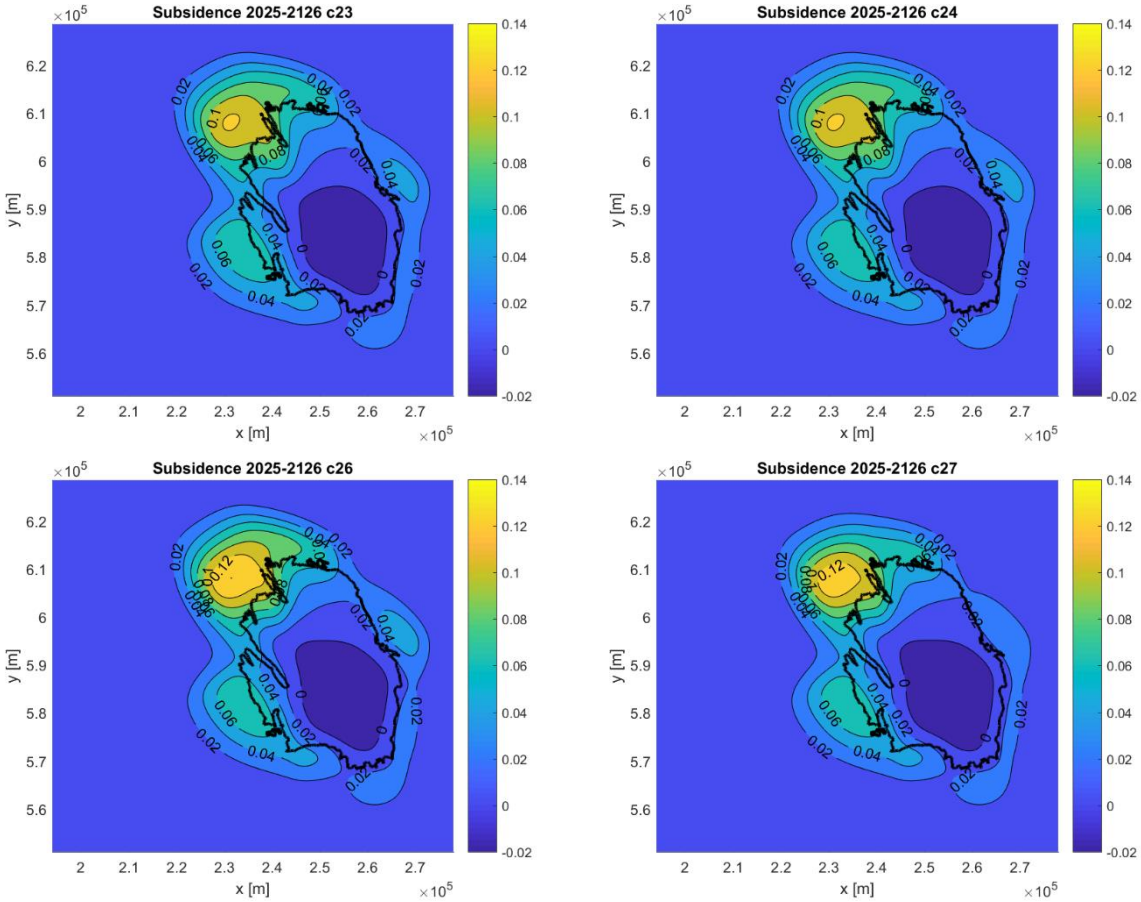
Subsidence 2025-2126 c23
Subsidence 2025-2126 c24
Subsidence 2025-2126 c26
Subsidence 2025-2126 c27
x [m]
y [m]
×10^5

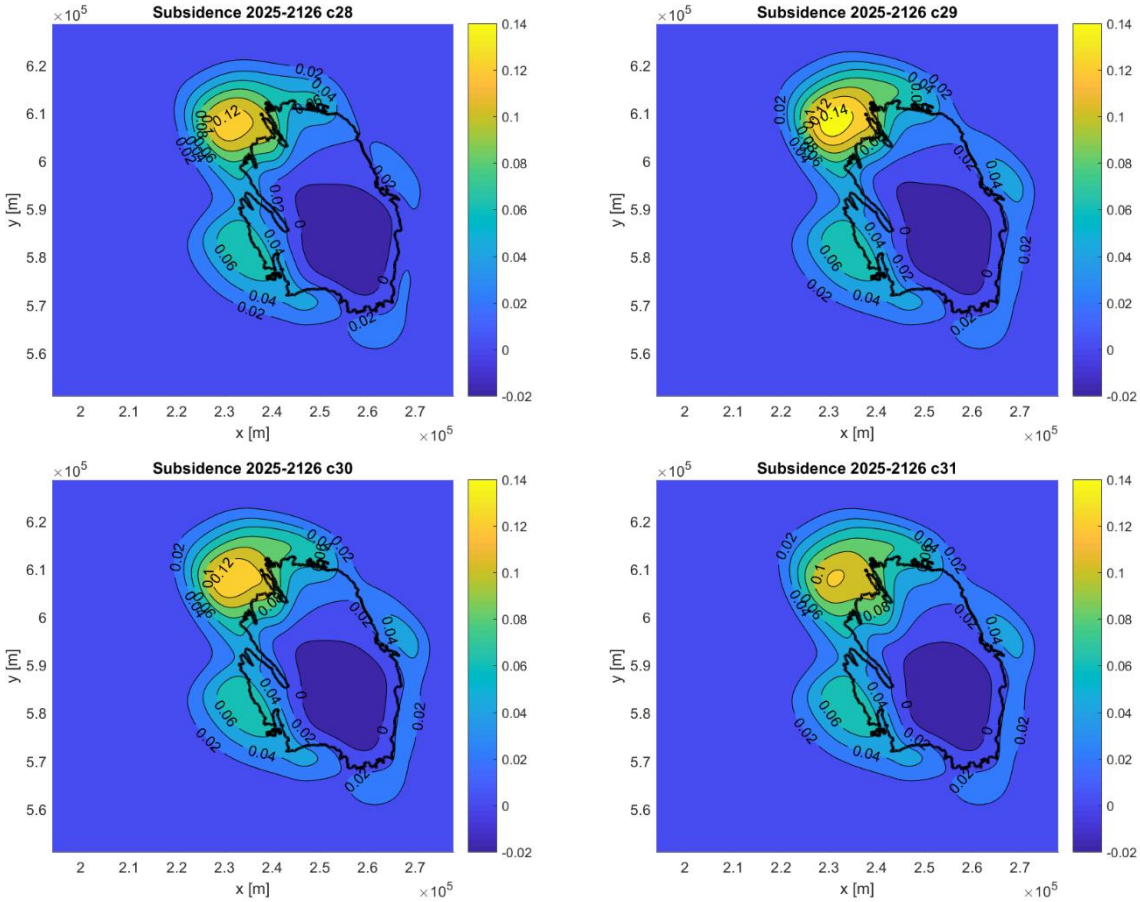

Figure E-1 Additional subsidence 2025 – 2125 for the base case and all sensitivity runs

E.2 Reactivation in uniaxially deforming parts of a reservoir

In this Appendix subsection we detail the formulas required for reactivation analysis in uniaxially deforming parts of the reservoir. Uniaxial deformation implies that there is no lateral displacement. In addition, the total vertical stress, controlled by the weight of the overlying subsurface strata, is constant. This means zero vertical stress change and zero horizontal strains:

$$\Delta\sigma_z = 0;\ \varepsilon_x = \varepsilon_y = 0 \qquad \text{Eq. 7}$$

With Hooke's law including poro-elasticity becomes (Fjaer et al [2008], with the the Lamé parameters $\lambda = \frac{2G\nu}{1-2\nu}$ and $\varepsilon_{vol} = \varepsilon_z$; G and ν are shear modulus and Poisson ratio) the compaction and the change in horizontal stresses can be calculated as a function of the pressure change ΔP_f. The compaction per unit of reservoir thickness is the vertical strain, and we have

$$\varepsilon_z = -\frac{1-2\nu}{1-\nu}\frac{1}{2G}\alpha\Delta P_f$$
$$\Delta\sigma_x = \Delta\sigma_y = \frac{1-2\nu}{1-\nu}\alpha\Delta P_f \qquad \text{Eq. 8}$$

The parameter α is the Biot coefficient. For reactivation, the Terzaghi effective stress is used (Fjaer et al [2008], p. 76): $\sigma' = \sigma - \Delta P_f \mathbf{I}$. This results in the changes of effective stresses horizontal and vertical in the reservoir as

$$\Delta\sigma_h' = -\left(1 - \frac{\alpha[1-2\nu]}{1-\nu}\right)\Delta P_f$$
$$\Delta\sigma_z' = -\Delta P_f \qquad \text{Eq. 9}$$

Both the horizontal and the vertical effective stresses increase upon depletion – i.e. negative pressure change. Whether destabilization takes place is determined by examining the movement of shear stress and the effective normal stress with respect to the Mohr-Coulomb failure envelope. We calculate the normal effective stress $\Delta\sigma'$ and the shear stress on a fault $\Delta\tau$ with dip θ, with the equations for the change in principal effective stresses due to pressure change:

$$\frac{\Delta\sigma'}{\Delta P_f} = -1 + \frac{1}{2}\frac{\alpha[1-2\nu]}{1-\nu} - \frac{1}{2}\frac{\alpha[1-2\nu]}{1-\nu}\cos(2\theta)$$
$$\frac{\Delta\tau}{\Delta P_f} = -\frac{1}{2}\frac{\alpha[1-2\nu]}{1-\nu}\sin(2\theta) \qquad \text{Eq. 10}$$

Movement of the stress in the direction of destabilization happens when the slope of the increase in the Mohr diagram is larger than the friction coefficient μ. The slope is given by $\frac{\Delta\tau}{\Delta\sigma'}$. Depletion causes a stress development in the direction of destabilization when this number is larger than μ.

For a fault with the most critical dip angle θ, we have $\cos(2\theta) = \frac{-\mu}{\sqrt{1+\mu^2}}$ and $\sin(2\theta) = \frac{1}{\sqrt{1+\mu^2}}$. The slope of the stress path of the most critical fault orientation is then calculated as

$$\frac{\Delta\tau_c}{\Delta\sigma_c{}'} = \frac{\alpha[1-2\nu]}{2\sqrt{1+\mu^2}[1-\nu] - \alpha[1-2\nu]\left[\sqrt{1+\mu^2}+\mu\right]} \qquad \text{Eq. 11}$$

Clearly, whether destabilization happens depends on the Biot coefficient α, the Poisson ratio ν and the friction coefficient μ itself. For every pair of Biot coefficient α and Poisson ratio ν we can calculate the friction coefficient at which the slope is neutral, i.e. equal to μ. For every point in the (ν, α) plane, the friction coefficient must be larger than the indicated value to ensure stabilization upon depletion. Critical movement is reached earlier (neutral coefficients are larger) if the Poisson ratio is smaller or the Biot coefficient is larger.

When the stress path is critical, an important question is how much pressure change is required to reach the Mohr-Coulomb failure line. This pressure change can be assessed if both the original distance to the failure line and the rate of movement toward it are known.

For the stress at a fault that is most critically oriented we can calculate the stress distance to failure in the Mohr diagram to be

$$d\sigma_f = \frac{1}{\sqrt{1+\mu^2}}\left[C + \frac{\mu}{2}(\sigma_v' + \sigma_h')\right] - \frac{1}{2}(\sigma_v' - \sigma_h') \qquad \text{Eq. 12}$$

With a change in pressure the distance also changes:

$$\begin{aligned}\Delta d\sigma_f &= \frac{1}{\sqrt{1+\mu^2}}\left[\frac{\mu}{2}(\Delta\sigma_v' + \Delta\sigma_h')\right] - \frac{1}{2}(\Delta\sigma_v' - \Delta\sigma_h') \\ &= \Delta P_f\left\{\frac{1}{\sqrt{1+\mu^2}}\left[\frac{\mu}{2}\left(-2 + \frac{\alpha[1-2\nu]}{1-\nu}\right)\right] + \frac{1}{2}\frac{\alpha[1-2\nu]}{1-\nu}\right\} \qquad \text{Eq. 13} \\ \frac{\Delta d\sigma_f}{\Delta P_f} &= \frac{\mu}{2\sqrt{1+\mu^2}}\left(-2 + \frac{\alpha[1-2\nu]}{1-\nu}\right) + \frac{1}{2}\frac{\alpha[1-2\nu]}{1-\nu}\end{aligned}$$

E.3 References

Bonson, C.G., Childs, C., Walsh, J.J., Schopfer, M.P.J., Carboni, V., 2007. Geometric and kinematic controls on the internal structure of a large normal fault in massive limestones: the Maghlaq Fault, Malta. Journal of Structural Geology 29, 336–354

Fjaer, E., Holt, R. M., Horsrud, P., & Raaen, A. M. (2008). *Petroleum related rock mechanics*. Elsevier.

Schroot, B.M. and Schüttenhelm, R.T.E., 2003. Expressions of shallow gas in the Netherlands North Sea. Netherlands Journal of Geosciences 82 (1), 91-105

Tartakovsky, 2007. Probabilistic risk analysis in subsurface hydrology. Geophysical Research Letters 34, 5. doi.org/10.1029/2007GL029245

Tartakovsky, 2013. Assessment and management of risk in subsurface hydrology: A review and perspective. Advances in Water Resources 51, 247-260.

Ten Veen, J. H., Van Gessel, S. F., & Den Dulk, M. (2012). Thin-and thick-skinned salt tectonics in the Netherlands; A quantitative approach. Geologie En Mijnbouw/Netherlands Journal of Geosciences, 91(4), 447–464. https://doi.org/10.1017/S0016774600000330